Copyright

By

Francisco Javier Brenes
2005

The Dissertation Committee for Francisco Javier Brenes certifies that this is the approved version of the following dissertation:

Anchorage of Grouted Vertical Duct Connections for Precast Bent Caps

Committee:

Sharon L. Wood, Supervisor

Michael E. Kreger, Co-Supervisor

James O. Jirsa

Oguzhan Bayrak

Eric B. Becker

Anchorage of Grouted Vertical Duct Connections for Precast Bent Caps

by

Francisco Javier Brenes, B.S.C.E., M.S.C.E.

Dissertation

Presented to the Faculty of the Graduate School of

The University of Texas at Austin

in Partial Fulfillment

of the Requirements

for the Degree of

Doctor of Philosophy

The University of Texas at Austin

December 2005

Dedication

To my parents and Ivania.

Acknowledgements

I would like to thank my research supervisors, Drs. Sharon Wood and Michael Kreger, for their support, meticulous criticism, and constant encouragement. Other faculty members of the School of Civil Engineering have generously shared their knowledge and have influenced me in numerous ways: thanks in particular to Drs. John Breen, James Jirsa, and Oguzhan Bayrak. My colleagues in the Doctoral program and in the Master's program have been excellent companions and friends. Special thanks to Jorge Varela, Liang Yu, Juan Felipe Beltrán, Michael Brown, Taichiro Okasaki, Sungjin Bae, Alfredo Castro, Juan José Icaza, and Jeff Diephus.

The financial support from the Texas Department of Transportation that made this research possible is greatly appreciated. I would like to thank the project director, Lloyd Wolf, and Michael Hyzak for their active involvement.

A number of undergraduate research assistants participated in the execution of the experimental program. I am sincerely grateful to them for their constant effort and commitment to the project. I would like to thank Austin Payne, Michael Stonaker, Josh Verastique, Vanessa Rosales, and Ryan Hindman.

I am grateful to the laboratory technicians and administrative staff at the Ferguson Structural Engineering Laboratory for assisting me in my research activities. Special thanks to Blake Stasney, Mike Bell, Dennis Fillip, Mike Wason, Eric Schell, and Hortensia Peoples.

I would like to acknowledge the significant donations of material used in the experimental program. Special thanks to Mark Aument of Degussa Building Systems for donating the grout material and to Giovanni Silvestri of VSL and Joe Harrison of GTI for donating duct materials.

Finally, I would like to thank Ivania Quesada-Lobo for her relentless patience and support, sensible advice, and for being always at my side.

Francisco J. Brenes

July 24, 2005

Anchorage of Grouted Vertical Duct Connections for Precast Bent Caps

Publication No. _____

Francisco Javier Brenes, Ph.D.

The University of Texas at Austin, 2005

Supervisors: Sharon L. Wood and Michael E. Kreger

In the last decade, the need to reduce traffic disruption at construction sites has led to innovations in bridge prefabrication. In Texas, most of these recent innovations have involved prefabrication of bent cap elements. Bent cap-to-column connections currently being used incorporate either corrugated galvanized steel or plastic ducts that are precast in the bent cap element to serve as sleeves to house connectors. Designers and contractors prefer this type of precast connection over other types because the volume of grout that is required to complete the cap-to-column connection is minimized.

This research intends to reduce some of the uncertainties that currently surround the design of grouted vertical duct connections. The main test parameters that influence connection performance are identified. These

parameters include bar coating, duct material, embedment depth, number of connectors, bar eccentricity, and transverse reinforcement.

The experimental program examines the behavior and failure modes of grouted vertical duct connections. Results from thirty-two large-scale pullout tests are reported, and the effects of the studied parameters on connection behavior are evaluated. A simple phenomenological bond-slip model is presented that can be used to estimate the observed behavior.

The development of the anchorage design provisions considers the stress in the connectors at service load levels. Design provisions are developed for connectors that experience: (1) compression or low tension, and (2) significant tension. Design provisions applicable to connectors that experience compression or low levels of tension are based on limiting serviceability stresses related to widespread splitting in the connection specimens. Connectors that experience significant tension and may be expected to yield are designed using anchorage provisions based on experimental average peak bond strengths. Observed pullout modes of failure are precluded by incorporating adequate levels of safety in the development of the design recommendations.

Table of Contents

List of Tables……xvi

List of Figures…….….xvii

CHAPTER 1 Introduction……1

1.1 Perspective……...1

1.2 Previous Research at The University of Texas at Austin……4

1.3 Challenges and Needs……..6

1.4 Objectives……....8

1.5 Scope……....9

1.6 Literature Survey……...10

1.6.1. Grouted Vertical Duct Connections…….….11

1.6.2. Precast Bent Caps…….....….15

1.6.3. Anchorage of Reinforcing Bars…….….....18

1.6.3.1 Mechanics of Bond……..18

1.6.3.2 Bond Stress……..…22

1.6.3.3 Anchorage of Bars in Grout…….……....25

1.6.3.4 Code Provisions in Development Length……28

1.7 References……..……31

CHAPTER 2 Current Use and Constraints……..……...….55

2.1 Precast Bent Cap Analysis and Design Procedures……...56

2.1.1 Selection of Trial Bent Configuration……..….56

2.1.2 Analysis and Design of Bent……...……..57

2.1.3 Determination of Connection Actions……..58

2.1.4 Selection of Connection Type…….…..59

2.1.5 Selection of Connector Configuration……..60

2.1.6 Analysis of Connector Configuration……...60

2.1.7 Determination of Connector Type and Embedment…….61

2.1.8 Selection of Transverse Reinforcement……....62

2.2 Current Precast Bent Cap Construction…….62

2.2.1 Lake Ray Hubbard Bridge Project……62

2.2.2 Lake Belton Bridge Project……...…65

2.2.3 Dallas High Five Project……..….67

2.3 Limitations and Need for Research……68

2.4 References……..69

CHAPTER 3 Overview of Experimental Program……...……83

3.1 Introduction……..…..83

3.2 Test Parameters……..……83

3.2.1 Bar Coating……...…84

3.2.2 Duct Material……85

3.2.3 Embedment Depth……...…….86

3.2.4 Group Effects……86

3.2.4.1 Number of Connectors……..…….…….87

3.2.4.2 Duct Clear Spacing…….87

3.2.5 Bar Eccentricity……..…..87

3.2.6 Transverse Reinforcement……..…..88

3.2.7 Other Parameters…….…..88

3.2.7.1 Connector Type……..…….88

3.2.7.2 Connector Diameter……..…..89

3.3.7.3 Ratio of Duct Diameter to Connector Diameter……..…89

3.2.7.4 Grout Type……..90

3.2.7.5 Strength of Concrete……..….90

3.3 Specimen Fabrication…….……91

3.4 Materials……96

3.4.1 Steel……..96

3.4.2 Plastics……..97

3.4.3 Concrete……..…..98

3.4.4 Grout……...……..98

3.5 Testing Program Overview……..……100

3.6 References……101

CHAPTER 4 Experimental Setup……123

4.1 Introduction……..123

4.2 Test Setup……..…123

4.3 Instrumentation……126

4.4 Test Method……...…..129

CHAPTER 5 Experimental Setup……140

5.1 Introduction……..140

5.2 Observed Failure Modes……..……141

5.2.1 Galvanized Steel Duct Specimens……..142

5.2.2 Polyethylene Duct Specimens…….....143

5.2.3 Polypropylene Duct Specimens……..143

5.3 Visual Observations of Crack Development……....144

5.3.1 Galvanized Steel Duct Specimens……..145

5.3.2 Polyethylene Duct Specimens…….....146

5.3.3 Polypropylene Duct Specimens……..147

5.4 Stress-End Slip Diagrams….…….…..148

5.4.1 Galvanized Steel Duct Specimens……..149

5.4.2 Polyethylene Duct Specimens…….....151

5.4.3 Polypropylene Duct Specimens……..153

5.5 Strain Distribution Diagrams……...……....154

5.5.1 Galvanized Steel Duct Specimens……..155

5.5.2 Polyethylene Duct Specimens…….....157

5.5.3 Polypropylene Duct Specimens……..159

5.6 Stress Distribution Diagrams……...……160

5.6.1 Galvanized Steel Duct Specimens……..161

5.6.2 Polyethylene Duct Specimens…….....164

5.6.3 Polypropylene Duct Specimens……..166

5.7 Stress-Slip Relative to Grout Diagrams…….…..167

5.7.1 Galvanized Steel Duct Specimens……..169

5.7.2 Polyethylene Duct Specimens…….....172

5.7.3 Polypropylene Duct Specimens……..174

5.8 Strain Measurements in the Ducts…….……..176

5.8.1 Galvanized Steel Duct Specimens……..177

5.8.2 Polyethylene Duct Specimens…….....180

5.8.3 Polypropylene Duct Specimens……..182

5.9 Specimen Autopsies……...…..184

5.9.1 Galvanized Steel Duct Specimens……..185

5.9.2 Polyethylene Duct Specimens…….....185

5.9.3 Polypropylene Duct Specimens……..185

5.10 Summary……..186

CHAPTER 6 Evaluation of Test Results……..…235

6.1 Introduction……..235

6.2 Effect of Test Parameters on Behavior……..…..237

6.2.1 Bar Coating…….....237

6.2.2 Duct Material……..238

6.2.3 Embedment Depth……..241

6.2.4 Number of Connectors……..……..242

6.2.5 Duct Clear Spacing…….....243

6.2.6 Bar Eccentricity……..244

6.2.7 Transverse Reinforcement……...…...245

6.3 Development of a Phenomenological Model……..246

6.3.1 Theory of Bond Mechanism……...246

6.3.2 Bond Stress-Slip Model……..248

6.4 References……..…..254

CHAPTER 7 Design Recommendations…….……..…286

7.1 Introduction……..286

7.2 Anchorage Design Provisions……..287

7.2.1 Design Provisions for Connectors Experiencing Compression or Low Tension……..……...…….289

7.2.2 Design Provisions for Connectors Experiencing Significant Tension……...…….……296

7.3 Comparison of Anchorage Design Provisions with Experimental Data…….……...…301

7.3.1 Connectors Experiencing Compression or Low Tension……...301

7.3.2 Connectors Experiencing Significant Tension……....302

7.4 Connection Design……...……305

7.5 Guidelines for Application of the Anchorage Design Provisions…...….305

7.6 Model Code Provisions……307

CHAPTER 8 Summary and Conclusions……328

8.1 Summary……..…328

8.1.1 Experimental Program ……...……329

8.1.2 Identification of Main Test Parameters……..329

8.1.3 Design Recommendations……..329

8.2 Conclusions……..330

8.3 Suggestions for Further Research……331

APPENDIX A Bonding Strain Gages to Plastic……..……334

APPENDIX B Stress-Strain Model for Connectors……...…337

APPENDIX C Concrete and Grout Strength Data.……...…342

C.1 Concrete Strength……...……..342

C.2 Grout Strength……..342

BIBLIOGRAPHY……....……..…366

Vita……....……..…372

List of Tables

Table 1.1 Advantages and Disadvantages of Bent Cap Types…….……...….35
Table 3.1 Duct Dimensions…….……103
Table 3.2 Ideal Combinations of Connectors and Ducts…….....103
Table 3.3 TxDOT Grout Performance Specification…….....104
Table 3.4 Connector Strengths…….105
Table 3.5 TxDOT Class C Concrete Mixture Design……..105
Table 3.6 Grout Operations Temperature and Efflux Time Data.……...106
Table 3.7 Average Grout Compressive Strengths for the Tests……..106
Table 3.8 Tabular Synopsis of Testing Program…….…107
Table 5.1 Test Matrix and Selected Test results…….188
Table 5.2 Autopsy Data on Galvanized Steel Duct Specimens……...191
Table 5.3 Autopsy Data on Polyethylene Duct Specimens…….192
Table 5.4 Autopsy Data on Polypropylene Duct Specimens……...…193
Table 6.1 Designations Used to Identify Test Specimens……...255
Table 6.2 Average Bond Strength of Broad Test Categories……...257
Table 6.3 Values of Model Parameters used in Basic Bond-Slip Curves.....258
Table 6.4 Group Effect Modification Factor – Comparison with Test Data…...259
Table 7.1 Connector Stress at Occurrence of Widespread Splitting……....315
Table 7.2 Values of $u_{ws}/\sqrt{f'_c}$ for a Series of Connector Configurations……..…..317
Table 7.3 Average Plug Bond Strength …….....318
Table 7.4 Embedment Length Required for a Range of Concrete and Grout Compressive Strengths (#11 Bar, Compression or Low Tension, γ = 1.0)……..318
Table 7.5 Normalized Average Values of $u_{max}/\sqrt{f'_c}$ for Single-connector Tests……...….319
Table 7.6 Comparison of Values of $u_{max}/\sqrt{f'_c}$ modified by the Group Effect Factor with Experimental Values……..…320
Table 7.7 Development Length Required for a Range of Concrete and Grout Compressive Strengths (#11 Bar, Significant Tension, γ = 1.0)…….....321
Table B.1 Parameters for Stress-Strain Idealized Model…….339
Table C.1 Concrete Compressive Strengths for Beam Specimens and Age of Testing……..344
Table C.2 Grout Compressive Strengths for Beam Specimens and Age of testing……...345

List of Figures

Figure 1.1 Typical Prefabricated Pretensioned Girders Used by TxDOT…...…..36
Figure 1.2 Precast Concrete Partial-Depth Deck Panels Used by TxDOT……37
Figure 1.3 Red Fish Bay Project Precast Bent Caps……..37
Figure 1.4 US 290 Ramp E-3 Project Precast Bent Cap……....38
Figure 1.5 Pierce Elevated Project Precast Bent Caps……...…38
Figure 1.6 Connection Types Developed by TxDOT Research Project 1748…...39
Figure 1.7 Test of Single Bar Embedded in Grouted Vertical Duct (Research Project 1748)……..……...……..…40
Figure 1.8 Test of Column-Bent Cap Specimen with Grouted Vertical Ducts (Research Project 1748)……40
Figure 1.9 Full-Scale Multi-Column Bent of Phase Three (Research Project 1748)……....41
Figure 1.10 Lake Ray Hubbard Bridge Project……41
Figure 1.11 Lake Belton Bridge Project……...…42
Figure 1.12 Dallas High Five Project……...…42
Figure 1.13 Detail to Join Wall Panels Vertically Using Large Conduit…….....43
Figure 1.14 Precast Beam-Column Connections Used in New Zealand……...…43
Figure 1.15 Flexural Failure Mechanisms for Precast Connection Using Grouted Ducts…….……44
Figure 1.16 Test of Connector Embedded $10d_b$……45
Figure 1.17 Detail of NMB Mechanical Splice System……..…..45
Figure 1.18 Pullout Failure of Generic Grout-Filled Splice Sleeve……...46
Figure 1.19 Precast Crossheads Used in the Getty Center People-Mover System Project…….…46
Figure 1.20 Wolf River Precast Bent Cap Connection…….…47
Figure 1.21 Beaufort and Morehead Railroad Trestle Bridge Bent Caps……..47
Figure 1.22 Forces between Deformed Bars and Surrounding Concrete……..48
Figure 1.23 Effect of Confinement on Bond - Failure Modes……...49
Figure 1.24 Influence of Transverse Reinforcement on Bond Stress-Slip Relationship……50
Figure 1.25 Influence of Transverse Pressure on Bond Resistance……...50
Figure 1.26 Effect of Transverse Reinforcement on Splice Strength……....51
Figure 1.27 Bond Stress Distribution……...…52
Figure 1.28 Bond Deterioration Mechanisms under Monotonic Loading…….53
Figure 1.29 Basic Failure Modes for Grouted Connector……54
Figure 1.30 Influence Area for Single Straight Connector……....54

Figure 2.1 Connection Detail for Single-line Grout Pocket on Pile (Embedded Option)……..……72
Figure 2.2 Connection Detail for Double-line Grout Pocket on Column (Surface-flush Option)…….73
Figure 2.3 Connection Detail for Grouted Vertical Ducts on Column (Surface-flush Option)…….……74
Figure 2.4 Connection Detail for Bolted Connection on Column (Surface-flush Option with Plate-and-Leveling Nut Option)……..75
Figure 2.5 Design Flowchart for Precast Bent Cap System…….....76
Figure 2.6 Lake Ray Hubbard Bridge Construction Site……..….77
Figure 2.7 Bent Cap Connection Zone under Construction……...77
Figure 2.8 Bent Cap Placement Operations……..….78
Figure 2.9 Construction of the Lake Belton Bridge……...78
Figure 2.10 Bent Cap Reinforcement Scheme……...……79
Figure 2.11 Bent Cap Connection Zone Detail……..……79
Figure 2.12 Bent Cap Placement Operation with Barge-mounted Crane……..80
Figure 2.13 Aerial View of Dallas High Five Interchange Construction Site……...…80
Figure 2.14 Tall Single Column Bent……..……..81
Figure 2.15 Placement of Bent Cap Reinforcement and Ducts…….....81
Figure 2.16 Detail of Bent Cap Cross Section……..…82
Figure 3.1 Epoxy-coated and Uncoated Deformed Bars…….108
Figure 3.2 Corrugated Galvanized Steel Duct…….108
Figure 3.3 Corrugated High-density Polyethylene Duct…….109
Figure 3.4 Corrugated Polypropylene Duct…….....109
Figure 3.5 Improper Alignment of Reinforcing Bars that Project from Bridge Column at Lake Belton Bridge Project……..…110
Figure 3.6 Headed Connector……..110
Figure 3.7 Connections with a Large Number of Connectors Require Larger Construction Tolerances (Lake Belton Bridge)…….111
Figure 3.8 Lake Ray Hubbard Bridge Project – Connection Area Dimensions……....111
Figure 3.9 Lake Ray Hubbard Bridge Project – Placement of Connectors Relative to Pier Section…….…112
Figure 3.10 Test Specimen Dimensions…….….113
Figure 3.11 Lake Ray Hubbard Bridge Project – Bent Cap Reinforcement at Connection Zones……..114
Figure 3.12 Test Specimen Reinforcement Scheme……115

Figure 3.13 Spirals Used as Transverse Reinforcement……...…….…..116
Figure 3.14 Test Specimen Formwork…….116
Figure 3.15 Vertical Alignment of Ducts during Concrete Placement……...….117
Figure 3.16 Specimen Casting with Aid of Crane-operated Hopper……...117
Figure 3.17 Concrete Finishing Operations…….…118
Figure 3.18 Preparation of Concrete Cylinders……..….118
Figure 3.19 Beam Specimens after Formwork Removal…….....119
Figure 3.20 Precast Bent Cap Placement over Bridge Pier and Connectors
(Lake Ray Hubbard Bridge)……..…….119
Figure 3.21 Positioning and Vertical Alignment of Connectors in
Preparation for Grouting Procedures…….120
Figure 3.22 Formwork to Hold Connectors Aligned and in Place during
Grouting…….....120
Figure 3.23 Mortar Mixer (2.5 ft^3 capacity) Used to Mix Grout…….121
Figure 3.24 Flow Cone Test to Measure the Fluid Consistency of the
Grout……..…121
Figure 3.25 Gravity Tremie-tube Technique to Fill Ducts with Grout……122
Figure 3.26 Preparation of Grout Cubes……..……122
Figure 4.1 Expected Applied Loads on a Precast Bent Cap Connection…….132
Figure 4.2 Test Setup……..…….132
Figure 4.3 Test Connector Arrangements……133
Figure 4.4 Surface Preparations on a Connector for Bonding a Strain Gage…..133
Figure 4.5 Layers of Waterproofing Protection on Gage Installations
Bonded to Metal Surfaces……..…134
Figure 4.6 Two Completed Strain Gage Installations……..134
Figure 4.7 Typical Strain Gage Locations on Connectors and Ducts……..……135
Figure 4.8 Strain Gage Orientations on Galvanized Steel Duct……..135
Figure 4.9 Completed Gage Installations on HD Polyethylene Duct……..…136
Figure 4.10 Completed Strain Gage Installations on Galvanized Steel
Ducts……..…136
Figure 4.11 Schematic of Test Setup and Instrumentation……..137
Figure 4.12 Instrumentation to Measure Lead Connector Displacement and
Relative Displacement between Grout and Concrete……..138
Figure 4.13 Instrumentation to Measure End Connector Displacement and
Beam Deflection……...…138
Figure 4.14 Marking of Crack Formations during a Test……....139
Figure 5.1 Pullout Failure Modes – Relationship between Connector End
Slip and Grout Displacement……...…194

Figure 5.2 Pullout Failure Modes for Galvanized Steel Duct Connections…....195
Figure 5.3 Pullout Failure Modes for Polyethylene Duct Connections……...195
Figure 5.4 Pullout Failure Mode for Polypropylene Duct Connections
(Tests No. 30 and No. 32)……196
Figure 5.5 Widespread Splitting in Test No. 10……..196
Figure 5.6 Cracking Pattern at Failure in Test No. 10…….....197
Figure 5.7 Widespread Splitting Cracks in Test No. 13…….….197
Figure 5.8 Double Connector Test with 1-D Duct Spacing (Test No 13)…...…198
Figure 5.9 Widespread Splitting Cracks in Test No. 23…….….198
Figure 5.10 Double Connector Test with 2-D Duct Spacing (Test No. 23)…....199
Figure 5.11 Splitting Cracks in Test No. 9…….…...……..199
Figure 5.12 Test No. 9 at Failure Load……....200
Figure 5.13 Widespread Radial Splitting in Test No. 14…….…....200
Figure 5.14 Test No. 14 at Failure Load……..201
Figure 5.15 Widespread Radial Splitting in Test No. 28……...…..201
Figure 5.16 V-shaped Crack Formations in Test No. 28…….202
Figure 5.17 V-shaped Crack Formations in Test No. 32…….…202
Figure 5.18 Measured Lead and End Connector Displacements (Test No. 3)....203
Figure 5.19 Stress vs. End Slip Diagram for Epoxy-coated Connector in
Galvanized Steel Duct Embedded 12d_b (Test No. 4)…….203
Figure 5.20 Stress vs. End Slip Diagram for Uncoated Connector in
Galvanized Steel Duct Embedded 12d_b (Test No. 10)……..….204
Figure 5.21 Stress vs. End Slip Diagram for Double-connector Test in
Galvanized Steel Duct Embedded at 16d_b (Test No. 13)……..….204
Figure 5.22 Stress vs. End Slip Diagram for Double-connector Test in
Galvanized Steel Duct Embedded at 12d_b (Test No. 17)…….…..205
Figure 5.23 Widespread Radial Splitting Pattern in Test No. 17 at 45 ksi…..…205
Figure 5.24 Stress vs. End Slip Diagram for Test No. 23……....206
Figure 5.25 Stress vs. End Slip Diagrams for Single Connectors in
Polyethylene Ducts Embedded at 8, 12, and 16d_b…….....206
Figure 5.26 Stress vs. End Slip Diagrams for Test No. 9……....207
Figure 5.27 Stress vs. End Slip Diagram for Double-connector Test in
Polyethylene Duct Embedded at 16d_b with 1-D Duct Spacing
(Test No. 14)……....207
Figure 5.28 Stress vs. End Slip Diagram for Double-connector Test in
Polyethylene Duct Embedded at 16d_b with 2-D Duct Spacing
(Test No. 24)……....208
Figure 5.29 Stress vs. End Slip for Single Connectors in Polypropylene

Ducts Embedded at 8 and 12d_b……208
Figure 5.30 Stress vs. End Slip for Test No. 28…….....209
Figure 5.31 Stress vs. End Slip for Test No. 32…….....209
Figure 5.32 Strain Distribution along Connector Length (Test No. 3)……210
Figure 5.33 Strain Distribution along Connector Length (Test No. 4)……210
Figure 5.34 Strain Distribution along Connector Length (Test No. 13, Left Bar)……..….211
Figure 5.35 Strain Distribution along Connector Length (Test No. 17, Left Bar)……..….211
Figure 5.36 Strain Distribution along Connector Length (Test No. 7)……..…..212
Figure 5.37 Strain Distribution along Connector Length (Test No. 22)……..212
Figure 5.38 Distribution along Connector Length (Test No. 14, Left Bar)…….213
Figure 5.39 Strain Distribution along Connector Length (Test No. 24, Left Bar)……...…213
Figure 5.40 Strain Distribution along Connector Length (Test No. 30)……..….214
Figure 5.41 Strain Distribution along Connector Length (Test No. 28, Right Bar)……...……..…214
Figure 5.42 Strain Distribution along Connector Length (Test No. 32, Right Bar)……...……..215
Figure 5.43 Stress Distribution along Connector Length (Test No. 3)……...….215
Figure 5.44 Stress Distribution along Connector Length (Test No. 4)……....216
Figure 5.45 Stress Distribution along Connector Length (Test No. 13, Left Bar)……..……..…216
Figure 5.46 Stress Distribution along Connector Length (Test No. 17, Left Bar)……..….217
Figure 5.47 Stress Distribution along Connector Length (Test No. 7)……....217
Figure 5.48 Stress Distribution along Connector Length (Test No. 22)……..218
Figure 5.49 Stress Distribution along Connector Length (Test No. 14, Left Bar)……...…218
Figure 5.50 Stress Distribution along Connector Length (Test No. 24, Left Bar)……...…219
Figure 5.51 Stress Distribution along Connector Length (Test No. 30)……..219
Figure 5.52 Stress Distribution along Connector Length (Test No. 28, Right Bar)…….……....220
Figure 5.53 Stress Distribution along Connector Length (Test No. 32, Right Bar)……...……..220
Figure 5.54 Stress vs. Connector Slip Relative to Grout (Test No. 3)……..…221
Figure 5.55 Stress vs. Connector Slip Relative to Grout (Test No. 4)……221

Figure 5.56 Stress vs. Connector Slip Relative to Grout (Test No. 13, Left connector)…….……....222
Figure 5.57 Stress vs. Connector Slip Relative to Grout (Test No. 17, Left Connector)…….……...222
Figure 5.58 Stress vs. Connector Slip Relative to Grout (Test No. 7)……..…223
Figure 5.59 Stress vs. Connector Slip Relative to Grout (Test No. 22)……...223
Figure 5.60 Stress vs. Connector Slip Relative to Grout (Test No. 14, Left Connector)……224
Figure 5.61 Stress vs. Connector Slip Relative to Grout (Test No. 24, Left Connector)…….……..….224
Figure 5.62 Stress vs. Connector Slip Relative to Grout (Test No. 30)……...225
Figure 5.63 Stress vs. Connector Slip Relative to Grout (Test No. 28, Right Connector)……...……...225
Figure 5.64 Stress vs. Connector Slip Relative to Grout (Test No. 32, Right Connector)…….....226
Figure 5.65 Stress vs. Duct Strain (Test No. 3)……...……226
Figure 5.66 Stress vs. Duct Strain (Test No. 4)……..….227
Figure 5.67 Stress vs. Duct Strain (Test No. 13, Left Connector)……..…..227
Figure 5.68 Stress vs. Duct Strain (Test No. 17, Left Connector)……..….228
Figure 5.69 Stress vs. Duct Strain (Test No. 7)……...…228
Figure 5.70 Stress vs. Duct Strain (Test No. 22)……..…229
Figure 5.71 Stress vs. Duct Strain (Test No. 14, Left Connector)……..…..229
Figure 5.72 Stress vs. Duct Strain (Test No. 24, Left Connector)……...230
Figure 5.73 Stress vs. Duct Strain (Test No. 30)…….....230
Figure 5.74 Stress vs. Duct Strain (Test No. 28, Right Connector)…….231
Figure 5.75 Stress vs. Duct Strain (Test No. 32, Right Connector)…….....231
Figure 5.76 Autopsy on Galvanized Steel Duct Specimen (Test No. 4)…….232
Figure 5.77 Autopsy on Galvanized Steel Duct Specimen (Test No. 23, Left Connector)……..……..…232
Figure 5.78 Autopsy on Polyethylene Duct Specimen (Test No. 7)……233
Figure 5.79 Autopsy on Polyethylene Duct Specimen (Test No. 8)……....233
Figure 5.80 Autopsy on Polypropylene Duct Specimen (Test No. 28)……...…234
Figure 5.81 Autopsy on Polypropylene Duct Specimen (Test No. 32)……..….234
Figure 6.1 Effect of Bar Coating ($8d_b$ Embedment)……....260
Figure 6.2 Effect of Bar Coating ($12d_b$ Embedment)…….….260
Figure 6.3 Effect of Bar Coating on Stress Distribution along Connector ($12d_b$)……....261
Figure 6.4 Effect of Duct Material (Single Connectors, $8d_b$ Embedment)……..261

Figure 6.5 Effect of Duct Material on Stress Distribution along Connector (Single Connectors, $8d_b$ Embedment)……..……....262
Figure 6.6 Effect of Duct Material (Single Connectors, $12d_b$ Embedment)...….262
Figure 6.7a Effect of Duct Material on Stress Distribution along Connector (Single Connectors, $12d_b$ Embedment, and Applied Load 20 ksi)……..……...263
Figure 6.7b Effect of Duct Material on Stress Distribution along Connector (Single Connectors, $12d_b$ Embedment, and Applied Load 40 ksi)…….263
Figure 6.7c Effect of Duct Material on Stress Distribution along Connector (Single Connectors, $12d_b$ Embedment, and Applied Load 60 ksi)…….……..264
Figure 6.8 Effect of Duct Material at $12d_b$ (Double-Connector Tests)……264
Figure 6.9 Effect of Duct Material at $16d_b$ (Double-Connector Tests)……....265
Figure 6.10 Effect of Duct Material at $16d_b$ (Triple-Connector Tests)……265
Figure 6.11 Effect of Embedment Depth (Single Connectors in Steel Duct)…..266
Figure 6.12 Effect of Embedment Depth (Double-Connector Tests, Steel Ducts)…….……..266
Figure 6.13 Effect of Embedment Depth (Single Connectors in Polyethylene Duct)…….....267
Figure 6.14 Effect of Embedment Depth (Double-Connector Tests, Polyethylene Duct)……..267
Figure 6.15 Effect of Embedment Depth (Single Connectors in Polypropylene Duct)……....268
Figure 6.16 Effect of Number of Connectors (Steel Ducts, $12d_b$ Embedment)...268
Figure 6.17 Effect of Number of Connectors (Steel Ducts, $16d_b$ Embedment)...269
Figure 6.18 Effect of Number of Connectors on Stress Distribution along Connectors (Steel Ducts, $16d_b$ Embedment)……269
Figure 6.19 Effect of Number of Connectors (Polyethylene Ducts, $12d_b$ Embedment)…….……....270
Figure 6.20 Effect of Number of Connectors (Polyethylene Ducts, $16d_b$ Embedment)……..……...270
Figure 6.21 Effect of Number of Connectors on Stress Distribution along Connectors (Polyethylene Ducts, $16d_b$ Embedment)…….……..271
Figure 6.22 Effect of Number of Connectors (Polypropylene Ducts, $16d_b$ Embedment)……...……..271
Figure 6.23 Effect of Number of Connectors on Stress Distribution along Connectors (Polypropylene Ducts, $16d_b$ Embedment)……272

Figure 6.24 Effect of Duct Spacing (Steel Ducts, $12d_b$ Embedment)……..…272
Figure 6.25 Effect of Duct Spacing (Polyethylene Ducts, $16d_b$ Embedment).…273
Figure 6.26 Effect of Connector Eccentricity ($8d_b$ Embedment)…….273
Figure 6.27 Effect of Connector Eccentricity ($12d_b$ Embedment)……...…274
Figure 6.28 Effect of Bar Eccentricity on Stress Distribution along Connector ($12d_b$ Embedment)……..274
Figure 6.29 Effect of Transverse Reinforcement (Steel Ducts, $16d_b$ Embedment)...……..…275
Figure 6.30 Effect of Transverse Reinforcement (Single Connectors in Polyethylene Duct)…….....275
Figure 6.31 Effect of Transverse Reinforcement (Double-Connector Tests in Polyethylene Ducts, $16d_b$ Embedment)…….……..276
Figure 6.32 Theory of Bond Mechanism…….277
Figure 6.33 Bond Stress – Slip Model…….…278
Figure 6.34 Effect of Embedment Depth on Average Peak Bond Strength…....278
Figure 6.35 Effect of Duct Material on Average Peak Bond Strength……....279
Figure 6.36 Idealized Curve for Single Connectors in Galvanized Steel Ducts……279
Figure 6.37 Idealized Curve for Single Connectors in Polyethylene Ducts……....280
Figure 6.38 Idealized Curve for Single Connectors in Polypropylene Ducts…..280
Figure 6.39 Idealized Curve for Single Connectors in Specimens without Ducts……281
Figure 6.40 Idealized Curve for Two Connectors in Galvanized Steel Ducts….281
Figure 6.41 Idealized Curve for Two Connectors in Polyethylene Ducts…...…282
Figure 6.42 Idealized Curves for Two and Three Connectors in Polypropylene Ducts……..……..…282
Figure 6.43 Idealized Curve for Three Connectors in Galvanized Steel Ducts...283
Figure 6.44 Concrete Cone-shaped Break-out…….…283
Figure 6.45 Projected Failure Surface for Individual Connector, A_{No}……284
Figure 6.46 Comparison of Idealized Curves with Group Effect Modification Factor for Two Connectors in Galvanized Steel Ducts……..….284
Figure 6.47 Comparison of Idealized Curves with Group Effect Modification Factor for Two Connectors in Polyethylene Ducts……...……..285
Figure 6.48 Comparison of Idealized Curves with Group Effect Modification Factor for Three Connectors in Galvanized Steel Ducts……..……...285
Figure 7.1 Connector Stress Ratios for Galvanized Steel Duct Specimens…….322
Figure 7.2 Connector Stress Ratios for Polyethylene Duct Specimens……...323

Figure 7.3 Connector Stress Ratios for Polypropylene Duct Specimens…….324
Figure 7.4 Influence of Duct Material on Connector Stress at Widespread Splitting in the Concrete……..…325
Figure 7.5 Influence of Embedment Depth on Connector Stress at Widespread Splitting in the Concrete (Galvanized Steel Ducts)……..…325
Figure 7.6 Influence of Embedment Depth on Connector Stress at Widespread Splitting in the Concrete (Polyethylene Ducts)……...326
Figure 7.7 Influence of Embedment Depth on Connector Stress at Widespread Splitting in the Concrete (Polypropylene Ducts)……....326
Figure 7.8 Influence of Embedment Depth on Plug Bond Strength……....327
Figure B.1 Stress-Strain Idealized Model……340
Figure B.2 Stress-Strain Curves for Epoxy-coated Connectors……...340
Figure B.3 Stress-Strain Curves for Uncoated Type I Connectors……..341
Figure B.4 Stress-Strain Curves for Uncoated Type II Connectors…….341
Figure C.1 Concrete Compressive Strengths for Beam Specimens…….347
Figure C.2 Equipment used during Grout Operations…….348
Figure C.3 Emptying of Grout Bags for Mixing……..348
Figure C.4 Grout Strength – Trial Batches……..349
Figure C.5 Grout Strength – Beam Specimens 1 through 4……349
Figure C.6 Grout Strength – Beam Specimens 5 through 8……350
Figure C.7 Grout Strength – Beam Specimens 9 through 12……..350

CHAPTER 1
Introduction

1.1 PERSPECTIVE

A significant fraction of the nation's bridge infrastructure is approaching the end of its service life. According to the FHWA [1.1], approximately 30% of bridges in the U.S. are obsolete and need to be replaced. Moreover, urban congestion is increasing, and with a growing population, the need for new bridge construction will continue as traffic patterns and volumes change. Direct and indirect costs related to traffic control and disruption, work-zone safety, and environmental impact have become a major concern to the public and to government agencies. Efficient bridge designs and new construction methods that address these concerns are needed. Improved efficiency in design and construction can reduce the associated costs and produce, at the same time, bridges that are of a higher quality and that have lower life-cycle costs.

The bridge construction process, typical also for other structures, comprises several stages. These construction stages follow a logical order and involve the construction of foundations, followed by the bridge substructure (generally columns and bent caps), and then the superstructure (girders and deck). The construction process consists of many time-consuming tasks such as formwork erection and removal, steel reinforcement and concrete placement, and concrete curing time. Use of prefabricated elements and systems allows moving part of the construction, such as fabrication of components (including girders and bent caps), away from the bridge site and its traffic. The obvious result is a shorter schedule for construction in the field. Accelerated bridge construction translates

into fewer delays to motorists driving through work sites. Reduced congestion and delay time for motorists is also related to a decrease in fatalities and injuries due to vehicular accidents.

Very often, bridge construction sites demand that workers operate close to moving traffic, over water, near power lines, or at high elevations. Prefabrication allows workers to operate off-site in a safer and controlled environment while performing activities such as formwork erection and removal, and steel reinforcement and concrete placement. Prefabricated elements constructed off-site can then be transported to the bridge site and quickly erected in place. The quality of the prefabricated elements is typically higher than that achieved by conventional cast-in-place construction and a controlled off-site environment creates plant-like conditions, which lead to better quality control, more thorough inspection, and improved monitoring of concrete curing.

The Texas Department of Transportation (TxDOT) has used prefabricated bridge elements for many years. Prefabricated pretensioned girders (Figure 1.1) have long been used in bridge construction, as have precast concrete partial-depth deck panels (Figure 1.2). In recent years, the need to reduce traffic disruption at work sites has lead to additional prefabricated bridge innovations. Most of these recent innovations have involved prefabrication of the substructure elements. In the 1990s, TxDOT undertook a number of bridge projects involving precast bent caps. These projects were: the Red Fish Bay Project in Port Aransas (Figure 1.3), the US 290 Ramp E-3 Project in Austin (Figure 1.4), and the Pierce Elevated Project in downtown Houston (Figure 1.5).

The use of precast bent caps in the Redfish Bay Project, completed in 1994 by TxDOT, was requested by the contractor to minimize concrete operations over water [1.2, 1.3]. Connections involved large voids or pockets preformed into the caps to house connectors (Figure 1.3). U-shaped, epoxy-coated #9 dowels

were grouted into embedded sleeves that were cast in trestle piles. Precast caps were then lowered over the dowels, and concrete was cast inside the voids to complete the connections. Construction time for the project was reduced by one third compared with the estimated construction time for cast-in-place bent caps.

Another TxDOT project completed in 1994 was the US 290 Ramp E-3 Project in Austin (Figure 1.4). Originally conceptualized as cast-in-place construction, the bent cap design for this ramp was changed to precast when it was found that estimated closure time of the ramp to traffic due to construction would be reduced from weeks to only hours [1.3]. The cap was cast adjacent to the erection site. Two vertical sleeves made of corrugated steel duct were formed on each end of the cap. Dywidag threaded bars that protruded from the columns below passed through the entire cross section to be anchored and post-tensioned at the top. Grout was then poured into the sleeves to complete the connection.

The use of prefabricated bent caps in the Pierce Elevated Project in downtown Houston expedited construction remarkably and allowed the project to be completed in just 95 days instead of the estimated 548 days needed for conventional cast-in-place construction [1.3, 1.4]. This replacement project, completed in 1997, made use of the existing columns of the replaced structure. After removal of the original deteriorated superstructure and bent caps, post-tensioning bars were epoxied into the top of the columns. The new precast caps, which contained preformed sleeves made of corrugated steel duct, were then lowered into position (Figure 1.5). Bars were anchored through plates at the top of the cap, and sleeves were filled with grout.

Recognizing the benefits of precast bent caps, TxDOT initiated research project 1748, "Development of a Precast Bent Cap System," [1.5] with the Center for Transportation Research at the University of Texas at Austin. This research,

completed in 2001, produced a series of connection types, a design methodology, and constructible connection details for the different connection types.

Since the completion of research project 1748, TxDOT has initiated new bridge projects that incorporate the use of precast bent caps. Grouted vertical ducts were used in the cap-to-column connections of these bridges. Contractors and TxDOT engineers have a preference for this type of precast connection because the volume of grout needed to complete the connections is minimized. Many uncertainties regarding the details and configuration of the connections were recognized during the design and construction of these bridges. Concern among TxDOT engineers involved in the design of the new bridge projects led to this investigation on the behavior of grouted vertical duct connections.

1.2 PREVIOUS RESEARCH AT THE UNIVERSITY OF TEXAS AT AUSTIN

The success of the Red Fish Bay and Pierce Elevated projects encouraged TxDOT engineers to initiate formal development of a precast bent cap system and sponsor research project 1748, "Development of a Precast Bent Cap System" [1.5]. An Industry Review Committee was formed, which included representatives from the precast and construction industries, as well as TxDOT engineers. Researchers, together with the Industry Review Committee, developed three main connection types: grout pockets, grouted vertical ducts, and bolted connections (Figure 1.6). Grout pocket connections derive their name from the fact that they incorporate precast voids or pockets formed in the bent cap to accommodate connectors. Grouted vertical duct connections incorporate corrugated ducts to serve as sleeves to house the connectors. Bolted connections are similar to grouted vertical duct connections, but the connectors run through the entire depth of the cap and are anchored by bearing at the top. In all connection types, pockets or sleeves are filled with grout. Advantages and

disadvantages of these connection types were identified and a summary of these is shown in Table 1.1.

Many uncertainties existed regarding design, detailing, behavior, and durability of the developed connection types. A three-phase experimental program was conducted to investigate and refine connection details. The first phase of testing consisted of 32 pull-out tests of headed and straight bars embedded in grout pockets and grouted vertical ducts. Of the 32 tests, 24 involved reinforcing bars embedded in grouted pockets (14 single-bar tests, and 10 double-bar tests). The remaining tests were single-bar tests embedded in grouted vertical ducts. The variables of embedment depth, grout type, and connector type (straight versus headed connector) were explored in connector tests involving grouted vertical ducts; all connectors were #11 epoxy-coated bars, and only corrugated galvanized steel ducts were used. A photograph of one of the grouted vertical duct tests is shown in Figure 1.7. The first phase of testing served to develop anchorage design provisions for straight or headed bars embedded in grout pockets or ducts. Information about grout performance and placement techniques was also obtained. The following expressions were provided for required development length:

grout pocket connections,

$$l_d = \frac{0.022 d_b f_y}{\sqrt{f'_c}} \tag{1-1}$$

grouted vertical duct connections,

$$l_d = \frac{0.024 d_b f_y}{\sqrt{f'_c}} \tag{1-2}$$

where l_d is the required development length (in.), d_b is the nominal diameter of the connector (in.), f_y is the specified yield strength of the connector (psi), and f'_c is the specified compressive strength of the concrete (psi).

The second phase of testing involved full-scale single column and bent cap specimens representing the three developed connection types. Connectors used were #9 bars. Figure 1.8 shows a photograph of the column and bent cap specimen with the grouted vertical duct connection. The full-scale tests confirmed the adequacy of the anchorage design provisions developed after the first phase of testing; they also served to evaluate constructability issues of a precast bent cap system.

The third phase of testing involved the construction of two multi-column bents in the field by a contractor that included all three of the connection types (Figure 1.9). All connectors used were #9 bars. The main purpose of this phase was to assess the constructability of the different connection types in the field. Behavior of connections was also examined. The researchers made observations on use of plans by the contractor, construction tolerances, setting of the caps, and grouting practices. The development of a grout performance specification was an important product of research project 1748, and the third phase of testing made use of this new development. The grout performance specification was part of a larger specification document on precast bent cap connections developed by the research team and TxDOT engineers.

A comprehensive design methodology for a precast bent cap system was also developed, and a summary is presented in Chapter 2 of this document. The investigation concluded that the three connection types studied were acceptable connection alternatives for a precast bent cap system.

1.3 CHALLENGES AND NEEDS

In the years following the completion of research project 1748, TxDOT undertook new bridge construction projects that incorporated the use of precast bent caps, such as the Lake Ray Hubbard Bridge Project (Figure 1.10), the Lake

Belton Bridge Project (Figure 1.11), and the Dallas High Five Project (Figure 1.12). Throughout these projects, precast bent caps proved again to be a very efficient construction system. Grouted vertical duct connections were employed in all of the new bridge projects. This type of connection was singled out as the connection of choice by contractors and TxDOT engineers primarily because of the reduced volume of grout (compared with grout pockets) needed to complete the connections.

TxDOT engineers involved in the design and construction of the new bridge projects were concerned about the precast bent cap connection details being used. Many uncertainties about the behavior of grouted vertical duct connections arose because engineers designing the connections used large connectors, such as #11 bars, in large numbers, and placed very close to each other. Contractor-driven construction modifications intending to increase bridge durability, like replacing galvanized steel ducts with plastic ducts in the connections, raised additional concerns regarding the performance of the connections.

Very limited information is available regarding connectors embedded in grouted vertical ducts. TxDOT research project 1748 [1.5] mainly addressed the behavior of grout pocket connections, and the small number of tests involving grouted vertical ducts were mostly limited to single-connector tests, and connectors housed inside galvanized steel ducts. The full-scale column-bent cap specimens, which comprised multiple-connectors, contained #9 bars that generally were not spaced very close to each other. Information available elsewhere, as will be discussed later in Section 1.6, regarding the behavior of grouted vertical duct connections is scarce. The evolution of grouted vertical duct connections as the preferred connection type in precast bent cap systems,

demonstrated by the new TxDOT bridges, has revealed the need for additional research on the behavior of these connections.

1.4 OBJECTIVES

Conscious of the continuing need for efficient bridge construction systems, the Texas Department of Transportation initiated research project 0-4176, "Development of Precast Bridge Construction Systems," through the Center for Transportation Research at the University of Texas at Austin. The initial problem statement for this project contemplated the development of a largely precast bridge system that could be assembled and open to traffic in days or weeks instead of the months or years required for conventional cast-in-place construction. The start of project 0-4176 coincided with a TxDOT implementation study on precast bent cap connections. The implementation study, related to finalized research project 1748, was following closely the construction of the Lake Ray Hubbard Bridge. It became very clear at the inception of project 0-4176 that uncertainties in behavior of grouted vertical duct connections, which arose during the construction of the Lake Ray Hubbard Bridge, needed to be addressed and resolved through laboratory testing. Moreover, the design of the Lake Belton Bridge was almost complete, and additional uncertainties about the behavior of the conceived bent cap connections were emerging.

The demonstrated need for broad laboratory testing of grouted vertical duct connections prompted TxDOT engineers and the researchers participating in this investigation to pursue this matter. As a result, the research direction of project 0-4176 concentrated on examining the behavior of precast bent cap connections constructed using grouted vertical ducts in the laboratory. The main objectives of this research project are to:

1. Understand the behavior of grouted vertical duct connections constructed using a variety of duct materials
2. Develop simple models to represent the observed connector behavior
3. Develop simple design expressions for grouted vertical connectors
4. Recommend practical details for connecting precast bent caps to columns and piles using grouted vertical duct connection

1.5 SCOPE

The research conducted during Project 0-4176 is documented in eight chapters and three appendices. In Chapter 2, the current design and construction practices concerning precast bent cap connections using grouted vertical ducts are presented. Uncertainties that evolved during the construction of the new bridge projects are also described.

Chapter 3 presents an overview of the experimental program developed to examine the behavior of grouted vertical duct connections. Main parameters that affect the behavior of these connections, such as bar coating, duct material, embedment depth, and connector group effects are described. The design and fabrication processes of the test specimens are also detailed. The experimental setup and instrumentation used during the tests are then described in Chapter 4.

In Chapter 5, the presentation of the test results is divided into groups, based on the duct material used in the test specimens. The measured response is presented in terms of observed crack patterns, stress-displacement behavior of the connectors, stress distribution along the connectors, and duct response during loading. Pull-out failure modes are also identified. The pull-out modes of failure of the connection specimens are verified through forensic examination.

Chapter 6 consists of an analysis of the data collected during the experimental investigations, presented in Chapter 5. The observed effects of the parameters that influence connection behavior are discussed. A simple phenomenological bond model is developed that explains connection behavior.

Recommendations for design of grouted vertical duct connections are presented in Chapter 7. Equations for anchorage of connectors are developed based on gathered experimental data. Practical details for connecting precast bent caps to columns and piles using grouted vertical duct connections are suggested.

Chapter 8 provides a summary and conclusions of the research, as well as suggestions for further research. Appendix A presents information on bonding of strain gages to plastic duct. Appendix B describes the model used to convert the measured strains along the connectors to stresses. Concrete and Grout Strength Data are included in Appendix C.

There are limitations on the scope of research of this project that deserve to be mentioned. All of the connections in this investigation were tested monotonically; consequently, the design recommendations are not intended to apply to seismic or dynamic applications. Additional tests taking this into consideration should determine if the results contained within this document can be extended to such cases. It is also possible that the design recommendations developed in this study may not be applicable to bent caps of unusual proportions or with connection configurations very different than those contemplated in this research.

1.6 LITERATURE SURVEY

The literature survey conducted for this investigation covers three main areas: (1) grouted vertical duct connections, (2) precast bent caps, and (3) anchorage of reinforcing bars. In (1), the limited literature found regarding

behavior and design of grouted vertical duct connections is detailed; some of the information found is related to building applications. Bridge projects that have used precast bent caps as part of the construction system are described in (2); mention is made if the connections used involved grouted vertical ducts. In (3), the review of anchorage of reinforcing bars focuses on the mechanics of bond, results from experimental studies on bar anchorage in concrete and in grout, and code provisions for development length.

1.6.1 Grouted Vertical Duct Connections

Precast connections identified in this investigation as grouted vertical duct connections incorporate ducts made of steel or plastic, such as those used in post-tensioning applications. Ducts serve as sleeves to house connectors, which are then filled with grout. There is limited information available regarding this type of precast connection; most of the literature found either relates to building applications or has partial relevance to the connections studied in this investigation.

As is typical in the detailing of precast connections, the principal intention when designing and detailing grouted vertical duct connections is to obtain a precast structure that emulates the behavior of a cast-in-place structure. The differences between an emulative precast structure and a cast-in-place structure lie in the areas of field connections and assembly of prefabricated elements, while the analysis and design procedures remain the same for both. ACI Committee 550 has prepared a report that serves as a practical guide to detail unions between precast elements to emulate cast-in-place structure behavior [1.6]. This document provides advice regarding detailing of joints and splices between precast components of a building structure. These include wall systems, frame systems, and floor diaphragms. The report provides a series of connection details that

generally involve the use of mechanical splices, such as proprietary threaded coupler devices. Details for joining wall panels using lapped splices inside a large conduit or duct are also presented; the conduit is filled with grout to complete the connection. One of these details is shown in Figure 1.13. The lap splice shown in the detail is required to conform to ACI 318-05 [1.7] lap length requirements.

Park [1.8] has presented a perspective on the design and construction of buildings in New Zealand incorporating precast concrete elements in floors, moment resisting frames, and structural walls. Multi-story buildings have been built in that country using a framing system of precast beams that pass through the column elements. The longitudinal column bars from the column below pass through vertical holes preformed in the precast beam element and protrude above. The voids in the precast beam element are formed using corrugated steel ducts, which are filled with grout after the column bars have passed through. Figure 1.14 shows the construction of beam-column connections using this framing system. Columns can be precast or cast-in-place; if they are precast, mechanical splices or corrugated metal ducts are incorporated in the column end section. Tests of subassemblies of this construction system conducted by Restrepo et al. [1.9] exhibited excellent ductility and stiffness. No significant differences in behavior compared to monolithic concrete construction were reported.

Stanton et al. [1.10] reported test results and a design methodology for eight moment resisting precast beam-column connections. Two of the connection specimens used #6 dowel bars that were either partially or fully grouted in ducts. The bars were embedded $24d_b$. In both connection tests, bars yielded and very ductile behavior was observed. Debonding of the bars did not lead to any noticeable improvement in performance. Figure 1.15 shows flexural failure mechanisms for the type of connection tested: (1) yielding of the beam top reinforcement, (2) yielding of the dowels at the joint, (3) crushing of concrete at

edge of column, (4) bond failure leading to pull-out before yielding of the connector, and (5) yielding of the dowel along the debonded length. To obtain ductile system behavior, mechanism (1) is the preferred failure mode, followed by mechanisms (2) and (5).

The PCI Design Handbook [1.11] presents design provisions for reinforcing bars embedded in grout-filled flexible metallic conduit. The conduit must have sufficient concrete cover around its periphery for adequate confinement; a minimum cover of 3 in. is required. Additional requirements also include: (1) minimum duct thickness of 0.023 in., (2) minimum clearance around the bar of 0.375 in., and (3) strength of the grout equal or higher than concrete strength, with a minimum strength of 5000 psi. Development length information is provided in a tabular form for different bar sizes. Values in the table were obtained from a design equation that appeared in the previous edition [1.12] of the manual. The equation provides the embedment depth needed to develop yielding of the connector:

$$l_e = \frac{0.04 A_b f_y}{\sqrt{f'_c}} \geq 12 \text{ in.} \tag{1-3}$$

where l_e is the required embedment length (in.), A_b is the area of the bar (in^2), f_y is the specified yield strength of the bar (psi), and f'_c is the specified compressive strength of the concrete (psi). Use of the equation is restricted to #8 and smaller uncoated bars. The origins of the design equation and test data supporting its development are not stated in the source, but it is likely that the equation was based on the development length provisions of ACI 318-71 [1.13].

Tests underway at California State University in Sacramento are investigating the applicability of a precast bent cap system using grouted ducts in seismic regions. The first phases of testing have examined the cyclic behavior of

single epoxy-coated #9 bars embedded in galvanized steel ducts [1.14, 1.15]. Connectors embedded $10d_b$ achieved yielding before failure by pull-out, while connectors embedded $16d_b$ failed by fracture. Figure 1.16 shows a photograph of a test involving a connector embedded $10d_b$. No significant bond degradation due to tension cycles was reported when bars were anchored to achieve yield and the strength of the grout was at least 1000 psi greater than the strength of the concrete. The preliminary results indicate that grouted vertical duct connections are a viable alternative for use in precast bent cap systems in seismic regions.

VSL International Ltd. has conducted a series of investigations [1.16, 1.17] to compare the bond characteristics of tendons with corrugated galvanized steel duct and PT-PLUS plastic ducts. Although tendons would not be used in grouted vertical duct connections as the connectors, the research has some relevance with regard to the bond properties of post-tensioning ducts. Results of tendon pull-out tests on shallow slab-like concrete specimens [1.16] indicated that multi-strand tendons placed inside plastic ducts exhibited reductions in capacity and stiffness, compared to corrugated steel duct specimens. Based on test data, development lengths on the order of 30 to 40 duct diameters were estimated for plastic ducts used in stressing applications. In a subsequent study involving similar pull-out tests and accompanying bond-length tests [1.17], reductions in stiffness and capacity were also observed for tendon specimens using plastic ducts. Bond-length tests indicated that the development length required for plastic ducts was approximately 50% longer than that required for corrugated steel ducts.

Partially related to grouted vertical duct connections, mechanical splice devices are available for use in the connections of precast elements. One of these systems is the NMB grouted sleeve coupler [1.18] shown in Figure 1.17. Embedment depths as short as $7d_b$ can be used with these devices. Coupling

devices like these must be manufactured for compliance to code specified standards.

Einea et al. [1.19] tested a series of generic grout-filled reinforcing bar splices monotonically in tension utilizing standard steel pipe as the sleeve material (Figure 1.18). Four different types of splice specimens were tested using both lap splice and butt splice arrangements, and with different steel pipe end details. Details included welding steel rings on the ends of pipes to mobilize confinement action in the grout. Tests involved #5, #6, and #9 bars with embedment varied between 5 and $11d_b$. Most specimens failed at an axial stress higher than the bar specified yield strength. High bond strengths were obtained due to the confined grout around the bars. However, the tests did not evaluate the bond between the steel pipe sleeve and concrete.

1.6.2 Precast Bent Caps

Several bridges have been built that incorporate precast bent caps connected using grouted vertical ducts. The Lake Ray Hubbard Bridge, the Lake Belton Bridge, and the Dallas High Five Project are innovative bridges that make use of these connections. These TxDOT projects will be discussed in detail later in Chapter 2 of this dissertation.

The Getty Center People-Mover System, completed in 1995 in Los Angeles, California, was built using precast concrete crossheads with grouted vertical duct connections [1.20]. Use of precast crosshead elements provided the contractor an efficient construction system in an environmentally sensitive site along steep hillsides (Figure 1.19). The columns of the tram system were cast-in-place and included a double reinforcing bar template to ensure adequate alignment of the vertical reinforcement that projected from the tops of the columns into the precast crosshead elements. The connection configuration

typically consisted of 16 reinforcing bars, as large as #11's, in a 3'-0" diameter circular pattern. The protruding column bars were housed inside 1.5-in. diameter corrugated sleeves cast into the crossheads; high-strength grout was then poured into the sleeves to complete the connections. The sleeve diameter was restricted to 1.5 in. so that it would not interfere with the crosshead reinforcing. Construction of the crosshead elements also made use of templates in the formwork that aligned and maintained the corrugated sleeves at the proper location. Although clearances were extremely tight, all crossheads aligned correctly when erected in the field.

The use of precast substructure and superstructure elements in the replacement bridge on Route 57 over the Wolf River in Moscow, Tennessee, facilitated rapid construction and made possible erection of the bridge from the top down without putting any equipment on the surrounding wetlands [1.21]. Bent cap connections consisted of grouted connectors placed inside corrugated metal ducts. The connection detail used in the bent caps is shown in Figure 1.20. A cylindrical recess 24 in. in diameter and 12 in. deep was formed at the bottom of the precast caps. One 4-in. diameter corrugated duct was also provided in the cap to accommodate a 1.5 in. diameter high-strength connector that passed through the joint into the pipe section. The void surrounding the connector was filled with concrete (pipe section) and grout (cap section). The contractor worked closely with engineers at the Tennessee Department of Transportation to develop a prototype connection adequate for the high seismic demands of the site.

A number of bridge projects have incorporated the use of precast bent caps built with connections other than grouted vertical duct connections that also take advantage of the expedited construction and enhanced durability offered by precast systems. Three of these bridge projects (the Red Fish Bay Project, the

Ramp E-3 Project, and the Pierce Elevated Project) were described in detail in Section 1.1.

A more recent project built in Texas that incorporates the use of precast bent caps is the Dallas/Fort Worth Airport People-Mover System [1.22]. Scheduled to be completed in 2005, the project incorporates precast segments of columns and inverted-T bent caps that are joined together by post-tensioning. This construction system was selected by the owner because it reduces construction time substantially and minimizes disruption to airport operations. Column segments and bent caps are fabricated well in advance at an adjacent precasting yard; they are then transported and erected during night operations. After the cap is in place, multi-strand post-tensioning tendons are threaded through ducts down the column around a bend that occurs in the base below grade; tendons are then stressed and grout is placed inside the ducts.

Precast bent caps were used in the Beaufort and Morehead Railroad Trestle Bridge Project in North Carolina. Pier caps were cast upside down with protruding top pile reinforcement (Figure 1.21). As caps were placed into position, top pile reinforcement was positioned inside steel pipe piles, and concrete was then pumped into the pipes to make the moment connections between caps and piles [1.23]. Through the use of precast bent caps, improved constructability and minimized traffic disruption were achieved. Trestles were replaced while serving rail traffic, with individual spans replaced between scheduled trains [1.24].

The Florida Department of Transportation (FDOT) conducted a study in 1996 regarding the feasibility of using precast substructures in bridges [1.25]. The study analyzed different column and bent cap arrangements, taking into account site requirements, speed of construction, methods of connection, and shape, weight, and size of precast elements. Multi-column and hammerhead caps were

considered, with solid and voided cross sections. Proposed methods of connection between caps and columns were mechanical couplers, post-tensioning, and grouted pockets. An industry review board composed of engineers, contractors, and fabricators evaluated a series of precast column and bent cap arrangements. For bent caps over multiple columns or piles, the board recommended using solid rectangle or inverted-U sections; while for hammerhead caps, both precast cantilever sections joined by post-tensioning and voided sections were considered as most desirable.

1.6.3 Anchorage of Reinforcing Bars

A brief overview of anchorage of reinforcing bars is presented emphasizing bond of straight, deformed reinforcing bars. The mechanics of bond and how bond stresses are utilized to achieve development of reinforcement are discussed. Results from a suite of experimental studies on anchorage of bars in concrete and grout are also presented. Emphasis was given to tests of confined specimens due to their relevancy to grouted vertical duct connections. Review of development length design provisions focuses on the requirements of ACI 318-05 [1.7] and the AASHTO LRFD Specifications [1.26].

1.6.3.1 Mechanics of Bond

Bond refers to the interaction between reinforcing steel and the surrounding concrete that allows transfer of tensile stresses between the steel and concrete. Lutz and Gergely [1.27] have shown that bond between reinforcing bars and concrete is made up of three components: (1) chemical adhesion, (2) friction, and (3) mechanical interlocking of bar lugs (ribs) with the surrounding concrete. In the case of deformed bars, bond stresses are transferred mainly by mechanical interlock. The effect of chemical adhesion is small, and friction does not occur until there is slip between the reinforcing bar and the concrete.

The resultant force exerted by a steel rib on the concrete is inclined at an angle α to the axis of the bar (Figure 1.22b). This angle corresponds roughly to the angle of inclination of the face of the rib. The resultant force can be divided into a parallel component and a normal component, relative to the axis of the bar (Figure 1.22d). The parallel component is usually called the bond stress, while the normal or radial component is termed the splitting stress. Radial components of the bond forces are resisted by tensile stress rings in the concrete surrounding the bar (Figure 1.22e). When a ring is stressed to rupture, it breaks and longitudinal (splitting) cracks appear on the concrete surface.

The formation of cracks around deformed bars acting in tension was studied by Goto [1.28]. Test specimens consisted of single deformed bars embedded concentrically in long concrete prisms. Cracking in the concrete was indicated by dye from special injecting holes provided in the specimens. Lateral cracks (called primary cracks) formed first at a few locations along the length of the specimens. Small internal cracks (such as those shown in Fig. 1.22), which did not appear at the concrete surface, were seen around the bars along the entire length of the specimens. Cracks like these began to form shortly after the formation of primary cracks. The angles of these inclined cracks were in the range of 45 to 80 deg relative to the bar axis. The inclination of these internal cracks matches the general orientation of the compressive forces exerted by the faces of the ribs on the concrete. Longitudinal cracks (in the direction of the bar axis) formed at higher stresses, and usually started at the locations of primary cracks.

Slip of a deformed bar occurs as a result of both the wedging action of the steel ribs pushing the concrete away (splitting), and due to the crushing of concrete keys by the ribs (pullout). In the absence of confinement, deformed bars fail in bond by splitting, which depends primarily on the force on the concrete and not so much on the bar stress and the bar perimeter (Figure 1.23a). If confinement

is provided, usually by the use of stirrups and/or a large concrete cover, bond failure occurs by shear failure of the concrete keys between the steel ribs (Figure 1.23b), and the ultimate load per unit length depends increasingly on the bar perimeter [1.27]. After adhesion is lost and ribs begin to bear on the concrete, slip occurs by progressive crushing of the porous concrete paste structure in front of the rib. The compacted crushed concrete creates a wedge that becomes lodged in front of the rib and moves along with it. This, in effect produces a rib with a face angle of 30 to 40 deg [1.27]. Thus, the angle at which the steel rib bears on the concrete, α, changes as load acting on the reinforcing bar increases. As a result, radial splitting stresses tend to increase at a rate greater than the parallel bond stresses as tensile load in the bar rises.

The splitting resistance of concrete can be enhanced if confinement stresses are superimposed onto the tensile ring stresses around the reinforcing bar. Confinement can be classified as either active or passive. Compressive stress fields induced by applied loads, reactions, and prestressing are considered to be active confinement. In contrast, passive confinement refers to compressive stress fields that are generated by forces in the mild reinforcement surrounding the anchorage zone of the bar. Surrounding reinforcement may involve spirals, stirrups, or straight bars perpendicular to the axis of the bar being anchored. Passive confinement is engaged only after crack deformations in the concrete ring develop that induce tension forces in the surrounding steel. Now acting as transverse reinforcement, the surrounding steel restricts the propagation and widening of splitting cracks that originate at the interface of the anchored bar and the concrete. Growth of splitting cracks is restrained more effectively when transverse reinforcement is placed close to the surface of the bar.

Eligehausen et al. [1.29] tested both monotonically and cyclically a series of specimens built to represent the confined region of a beam-column joint. Single

bars were embedded in concrete a short length of $5d_b$. Different quantities and arrangements of transverse reinforcement, that included straight bars and stirrups, were used in most specimens. Alternately, transverse pressure was also applied to some specimens to represent the influence of column compressive forces on the joint. For specimens involving transverse reinforcement, test results showed small differences in bond behavior when the quantity or total area of transverse steel was varied (Figure 1.24). Pullout modes of failure were characteristic of these specimens; results indicated that there exists an upper limit on the quantity of transverse reinforcement after which there is no improvement in bond behavior. Improvement in bond resistance was observed as transverse pressure increased (Figure 1.25). The ratio between the added bond resistance and applied pressure decreased significantly with increasing pressure.

The influence of transverse reinforcement on bar anchorage was also investigated by Astrova et al. [1.30]. Spirals and an array of meshes of straight bars were used as the transverse reinforcement in rectangular concrete block specimens. Test results of specimens using mesh reinforcement showed an increase in bond strength; while specimens using spirals as transverse reinforcement did not produce a similar increase. As observed in the studies conducted by Eligehausen et al. [1.29], increasing the quantity of transverse reinforcement beyond a certain point failed to yield any further increase in bond strength.

Tepfers [1.31] conducted a series of tests on lapped splices in beam specimens with varying arrangements and quantities of transverse reinforcement. Confinement effects provided by stirrups and spirals were investigated. In the case of stirrups, the splice strength improved at an increasing rate as the stirrup diameter increased (Figure 1.26a). Similar data obtained for the specimens containing spiral reinforcement are shown in Figure 1.26b. Data points shown in

this figure inside parenthesis indicate that failure of the splice had not been achieved when the test was stopped.

The influence of normal (transverse) pressure on bond strength has been studied by Untrauer and Henry [1.32]. Test specimens consisted of #6 and #9 bars embedded in 6-in. concrete cubes, and the lateral pressure applied ranged from 0 to 2370 psi. Results showed that bond strength increases approximately in proportion to the product of the square root of the normal pressure and the square root of the compressive strength of the concrete. The equation developed using regression analysis of test data is:

$$u_{ult} = (18.0 + 0.45\sqrt{f_n})\sqrt{f'_c} \qquad (1\text{-}4)$$

where u_{ult} is the ultimate bond strength (psi), f_n is the applied normal pressure (psi), and f'_c is the specified compressive strength of the concrete (psi). The slip at ultimate bond stress was found to increase with corresponding increases in normal pressure. However, restraint provided to the test specimens by the loading plates was not evaluated and may have contributed to the observed improvement in bond strength.

1.6.3.2 Bond Stress

The distribution of bond stress along the length of a deformed bar embedded in concrete and subjected to axial tension is assumed to be similar to the diagram shown in Figure 1.27. At first, when the pull on the bar is small, high stresses develop near the loaded end of the bar; some slip of the bar occurs as adhesion between the bar and the concrete in this region breaks down and as steel ribs begin to crush part of the concrete between the ribs. Failure can occur at this early stage if concrete surrounding the bar is unconfined. If some degree of confinement is present, a rise in load tends to shift the bond stress diagram deeper

along the bar engaging additional ribs to resist the additional load. In some instances, especially when the level of confinement is low around the loaded end of the bar, bond resistance near the surface can be reduced to zero due to extensive cracking and cone breakouts formed in the concrete. As load is increased to maximum levels, shifting of the bond stress diagram continues as bond stress peaks move deeper along the confined region of the bar. Failure occurs when there is no capacity left provided by the interlocking of the steel ribs and the concrete.

The distribution and magnitude of bond stresses along a bar are difficult to establish quantitatively. One problem is the progressive shifting of the bond distribution along the bar as bond deterioration occurs near the loaded end. Moreover, it is difficult to verify which ribs are actually transferring loads and what share of the load is being resisted by each rib. In spite of this, some assessment of bond stress is required in order to be able to estimate the length of embedment required to anchor bars effectively in concrete. As a way to deal with the complexities of actual bond stress conditions around reinforcing bars, investigators have resorted to the use of a nominal or average bond stress, u, determined by dividing the force in the bar, P, by the nominal bar perimeter $(\pi * d_b)$, and the embedment length (l_e). The equation follows:

$$u = \frac{P}{\pi \, d_b \, l_e} \tag{1-5}$$

Numerous experimental studies have been conducted to investigate the parameters that influence the anchorage of reinforcement. Conventional bond tests have consisted of a concrete block from which a reinforcing bar is pulled; in some test arrangements the block was modeled to be part of a beam or a joint. Orangun, Jirsa, and Breen [1.34] evaluated the results of several studies on

development length and lap splice length that were conducted in the United States and Europe. Variations in the average bond stress, *u*, obtained in the tests were plotted versus a set of test parameters that have been known to affect the strength of anchored bars. Studied parameters included the effect of embedment length, cover, bar spacing, bar diameter, concrete strength, and transverse reinforcement. Data from the tests were analyzed using a nonlinear regression analysis with the aim of developing a simple equation that could be integrated into code design provisions. The resulting empirical equation was modified to determine development length rather than average bond strength for practical design purposes.

Viwathanatepa et al. [1.35] investigated the bond deterioration of anchored bars. Specimens consisted of blocks of well-confined concrete constructed to represent a beam-column joint of a moment resisting frame. Concentrically placed single bars (with bonded lengths between 15 and $27d_b$) were tested monotonically and cyclically. Strain gages were installed along the bars at 1.5-in. spacing. The bond stress distribution along the bars was estimated by averaging calculated bond stress values between gage locations. Bond distribution diagrams similar to those shown in Figure 1.27 were observed. Three different concrete regions were identified and classified according to different bond behavior (Figure 1.28a). Ultimate peak bond strengths were found to be around 1.0, 2.1, and 4.0 ksi for unconfined, confined and pushed-end regions, respectively. The bond deterioration mechanism under monotonic loading is shown in Figures 1.28b and 1.28c for the unconfined and confined regions. In the unconfined region, the inclined internal cracks that form at the roots of the steel ribs propagate as load is applied until they reach the concrete surface; the failure mode is that of a cone-shaped concrete formation that breaks loose from the rest. The initial behavior exhibited by confined regions is similar to that of unconfined

regions, but the presence of transverse reinforcement controls the propagation of inclined cracks. In the confined region, bond deterioration results from bearing failure, inelastic deformations of the concrete "strut" and reductions in the effective shearing area of the concrete (keys).

1.6.3.3 Anchorage of Bars in Grout

Grouted anchors are a type of adhesive anchor commonly used in repair and rehabilitation applications because they provide a practical and economical method for adding new concrete sections or steel members to an existing concrete structure. In spite of their frequent use, a very small number of studies were found in the literature that examined the anchorage of connectors in grout. Moreover, most of the literature concentrates on the behavior of headed connectors, and very limited information and test data are available regarding the anchorage of straight deformed bars.

Darwin and Zavaregh [1.36] examined the anchorage of reinforcing bars grouted into holes drilled in existing concrete. Tests involved #5 and #8 bars embedded in concrete blocks; most bars had a 3-in. cover. Epoxy-coated and uncoated bars were used. Embedment depths ranged between 6 and $19d_b$, and the drilled holes were typically 0.25 in. larger than the bar diameter. Six types of grout were examined, including two cement-based grouts. No transverse reinforcement was provided to aid in confinement. Most specimens exhibited a splitting failure, accompanied by the formation of a shallow angle concrete cone. Results showed that the bond strength provided by most grouts is not sensitive to either hole diameter or drilling method. Bond strength improved with increases in embedment length, bar size, and cover. No significant differences in bond strength were observed due to epoxy-coating.

Cook et al. [1.37] have reported on the behavior of single adhesive anchors under tensile load. Although the study concentrated on epoxy, polyester, and vinylester adhesives, results from the study are relevant to grouted anchors because methods of analysis and design are similar. Investigators analyzed data from a worldwide database using regression analysis; and then used the results to evaluate a series of design concepts and models. Design models were based on failure modes observed in tests and included concrete cone models, bond models, combined cone/concrete models, and two-interface bond models. Statistical analysis indicated that a model based on uniform bond stress provided the best fit to the data. Cook [1.38] later reported on the applicability of the Uniform Bond Stress (UBS) model that was developed earlier [1.37] for post-installed grouted anchors. Anchors included threaded rods with and without a hex nut at the end, and also straight #4 deformed bars. Embedment depths were typically between 6 and $7d_b$. All straight anchors exhibited bond failure at the grout-anchor interface, accompanied by a shallow concrete cone formation at the face. Performance of grouted anchors was considered comparable to that of cast-in-place anchors.

Miltenberger [1.39] has proposed a rational procedure for strength design of grouted connectors (fasteners) that uses both the Concrete Capacity Design (CCD) model and the Uniform Bond Stress (UBS) model. Design equations that describe potential failure modes were developed along with modification factors that account for edge effects, group effects, and concrete cracking. The design of a group of connectors is limited by the strength of the connector that carries the largest load; structural analysis must be performed to identify that connector. After calculating the load demand or required capacity using the appropriate load factors, the nominal capacity of the connector is determined, plus applicable modification factors, for all potential failure modes. Basic tensile failure modes are shown in Figure 1.29. Finally, a check on the interaction between tension and

shear is performed. The mean bond strength and standard deviation determined from standardized tests on a specific grout anchor system are used to calculate the characteristic bond stress, τ', used for design. The characteristic bond stress corresponds to the 5% fractile, a statistical term meaning 90% confidence that there is 95% probability of the actual strength exceeding the nominal strength. For straight grouted connectors, the applicable nominal tensile strength equations corresponding to possible failure modes are:

connector yield,

$$N_s = f_y A_e \tag{1-6}$$

$$\phi N_n = \phi N_s \tag{1-7}$$

adhesive bond strength,

$$N_a = \tau'_a \pi d h_{ef} \tag{1-8}$$

$$\phi N_n = \phi \psi_g \psi_e \psi_{cr} N_a \tag{1-9}$$

plug bond strength,

$$N_o = \tau'_o \pi d_o h_{ef} \tag{1-10}$$

$$\phi N_n = \phi \psi_g \psi_e \psi_{cr} N_o \tag{1-11}$$

$$\psi_g = \frac{A_N}{n A_{No_o}} \leq 1.0 \qquad \psi_e = 0.7 + 0.0375 \frac{c}{d} \leq 1.0$$

where: N_n = nominal tensile strength (lb)

N_s = basic anchor tensile strength (lb)

N_a = basic adhesive bond strength to steel (lb)

N_o = basic plug bond strength to steel (lb)

ϕ = capacity reduction factor, taken as 0.75

f_y = connector specified yield strength (psi)

A_e = effective connector area (in^2)

τ'_a = characteristic bond strength (psi)

τ'_o=characteristic bond strength calculated at grout-concrete interface (psi)

d = connector diameter (in.)

d_o = hole diameter (in.)

h_{ef} = embedment depth (in.)

ψ_g = modification factor for group effects

ψ_e = modification factor for side effects

ψ_{cr} = modification factor to account for cracking, taken as 0.5

A_N = projected failure surface for group of connectors (in^2)

A_{No} = projected failure surface for one connector (in^2), (see Figure 1.30)

n = number of connectors

c = shortest edge distance (in.)

The smallest nominal capacity of Equations 1-7, 1-9, and 1-11 for the most heavily loaded fastener controls the capacity of the connector group.

1.6.3.4 Code Provisions on Development Length

The ACI 318-05 Building Code Requirements for Structural Concrete [1.7] contains design provisions for calculating the required development length of deformed straight bars. The equation follows:

$$l_d = \left(\frac{3}{40} \frac{f_y}{\sqrt{f'_c}} \frac{\psi_t \psi_e \psi_s \lambda}{\left(\frac{c + K_{tr}}{d_b} \right)} \right) \geq 12\,in. \tag{1-12}$$

$$\left(\frac{c + K_{tr}}{d_b} \right) \leq 2.5 \qquad\qquad K_{tr} = \left(\frac{A_{tr} f_{yt}}{1500 sn} \right)$$

where: l_d = development length of bar (in.)

d_b = bar diameter (in.)

f_y = specified yield strength of the connector (psi)

f'_c = specified compressive strength of concrete (psi)

ψ_t = reinforcement location factor

ψ_e = coating factor

ψ_s = reinforcement size factor (0.8 for #6 and smaller bars, 1.0 otherwise)

λ = lightweight aggregate concrete factor

c = spacing or cover dimension measured from center of connector (in.)

K_{tr} = transverse reinforcement index

A_{tr} = Area of transverse reinforcement (in^2)

f_{yt} = specified yield strength of transverse reinforcement (psi)

s = maximum spacing of transverse reinforcement within l_d (in.)

n = number of bars being developed along the plane of splitting

Equation 1-12 is based on the work performed by Orangun et al. [1.34]. A factor of 1.25 multiplying f_y is embedded in the equation to satisfy ductility requirements; the ACI equation also incorporates a strength reduction factor, ϕ, equal to 0.9 to account for deviations in material properties. The limit on the term $(c + K_{tr})/d_b$ of 2.5 is to safeguard against pullout type failures. For values above 2.5, ACI 318-05 states that a pullout failure is expected and an increase in cover or transverse reinforcement is unlikely to increase anchorage capacity.

In the AASHTO LRFD Bridge Design Specification [1.26], three design equations are provided for deformed bars developed in tension:

#11 and smaller bars,

$$l_{db} = \left(\frac{1.25 A_b f_y}{\sqrt{f'_c}} \right) \geq \{0.4 d_b f_y \ , 12 in. \ \} \tag{1-13}$$

#14 bars,

$$l_{db} = \left(\frac{2.70 f_y}{\sqrt{f'_c}} \right) \geq 12 in. \tag{1-14}$$

#18 bars,

$$l_{db} = \left(\frac{3.5 f_y}{\sqrt{f'_c}} \right) \geq 12 in. \tag{1-15}$$

where: l_{db} = basic development length (in.)

A_b = area of reinforcing bar (in^2)

f_y = specified yield strength of steel reinforcement (ksi)

f'_c = specified concrete compressive strength (ksi)

d_b = diameter of bar (in.)

In order to obtain the required development length for design, l_d, the basic development length, l_{db}, obtained in Equations 1-13 to 1-15, is multiplied by a series of modification factors:

- Top bars with more than 12 in. of concrete below x 1.4
- Cover $\leq d_b$ or clear spacing $\leq 2d_b$ x 2.0
- Lightweight aggregate, f_{ct} is specified x $\left(\frac{0.22\sqrt{f'_c}}{f_{ct}} \right) \geq 1.0$
- For all-lightweight concrete, f_{ct} is not specified x 1.3
- For sand-lightweight concrete, f_{ct} is not specified x 1.2
- Epoxy-coated bars (cover less than 3db) x 1.5
- All other epoxy-coated bars x 1.2
- Bar spacing ≥ 6 in. and clear cover ≥ 3 in. x 0.8
- Spiral provided with diameter ≥ 0.25 in. and pitch ≤ 4 in. x 0.75

Equation 1-13 is basically the same design equation provided in the ACI 318-71 Building Code [1.13] for calculating development length. The differences lie in unit conversion from (psi) to (ksi) and minor rounding of coefficients. As in Equation 1-12, a factor of 1.25 is embedded in the AASHTO equations multiplying f_y to satisfy ductility requirements.

1.7 REFERENCES

1.1. U.S. Department of Transportation, 2002 Study of the Nation's Highways, Bridges, and Transit: Conditions and Performance, (FHWA), 2003.

1.2. Wolf, L. M., and Friedman, N. K., "Redfish Bay and Morris & Cummings Cut: Innovations on Bridge Construction and Durability," Technical Quarterly, V. 9, No. 2, Texas Department of Transportation, Austin, TX, October 1994.

1.3. Medlock, R., Hyzak, M., Wolf, L., "Innovative Prefabrication in Texas Bridges," *Proceedings of Texas Section, American Society of Civil Engineers, Spring Meeting 2002*, American Society of Civil Engineers, Texas Section, Austin, TX, March 2002.

1.4. Wigington, N., "Pierce Elevated Draws Rave Reviews," Transportation News, Texas Department of Transportation, Houston, TX, March 1997.

1.5. Matsumoto, E. E., Waggoner, M. C., Sumen, G., Kreger, M. E., Wood, S. L., and Breen, J. E., "Development of a Precast Bent Cap System," Research Report 1748-2, Center for Transportation Research, University of Texas at Austin, January 2001.

1.6. ACI Committee 550, "Emulating Cast-in-Place Detailing in Precast Concrete Structures," *ACI 550.1R-01*, American Concrete Institute, Farmington Hills, MI, 2001.

1.7. ACI Committee 318, "Building Code Requirements for Structural Concrete and Commentary," *ACI 318-05/ACI 318R-05*, American Concrete Institute, Farmington Hills, MI, 2005.

1.8. Park, R., "A Perspective on the Seismic Design of Precast Concrete Structures in New Zealand," PCI JOURNAL, V. 40, No. 3, May-June 1995.

1.9. Restrepo, J. I., Park, R., and Buchanan, A. H., "The Seismic Behavior of Connections Between Precast Concrete Elements," Research Report No. 93-3, Department of Civil Engineering, University of Canterbury, Christchurch, April 1993.

1.10. Stanton, J. F., Anderson, R. G., Dolan, C. W., and McCleary, D. E., "Moment Resistant Connections and Simple Connections," Research Project No. 1/4, Precast/Prestressed Concrete Institute, Chicago, IL, 1986.

1.11. *PCI Design Handbook-Precast and Prestressed Concrete*, 5th edition, Precast/Prestressed Concrete Institute, Chicago, IL, 1999.

1.12. *PCI Design Handbook-Precast and Prestressed Concrete*, 4th edition, Precast/Prestressed Concrete Institute, Chicago, IL, 1992.

1.13. ACI Committee 318, "Building Code Requirements for Reinforced Concrete," *ACI 318-71*, American Concrete Institute, Detroit, MI, 1971.

1.14. Mandawe, J., Mislinski, S., and Matsumoto, E. E., "Reinforcement Anchorage in Grouted Duct Connections for a Precast Bent Cap System in Seismic Regions," *PCI/Federal Highway Administration/National Concrete Bridge Council Concrete Bridge Conference Proceedings*, Nashville, TN, October, 2002.

1.15. Matsumoto, E. E., "Development of a Precast Bent Cap System for Seismic Regions," *Lake Belton Bridge-Precast Concrete Bent Cap Demonstration Workshop*, *FHWA/AASHTO/TxDOT*, Temple, TX, July 2003.

1.16. Ganz, H. R., "PT-Plus Plastic Duct System," Report No. 241 e, VSL International Ltd, Berne, May 1991.

1.17. Marti, P., "Pull-out Tests with PT-Plus Plastic Ducts," Report No. 92.205-1, VSL International Ltd., Berne, June 1993.

1.18. *NMB Splice-Sleeve Systems-Product Brochure*, Splice Sleeve North America, Inc., Ontario, California.

1.19. Einea, A., Yamane, T., and Tadros, M. K., "Grout-Filled Pipe Splices for Precast Concrete Construction," PCI JOURNAL, V. 40, No. 1, Jan-Feb 1995.

1.20. Josten, M. G., Painter, W. L., and Guarre, J. S., "Precast Prestressed Concrete Structure Provides Solution for Getty Center Tram Guideway," PCI JOURNAL, V. 40, No. 3, May-June 1995.

1.21. "Bridges: Precast Concrete Bridges Aid Environment, Seismic Design," Precast/Prestressed Concrete Institute website http://www.pci.org/markets/markets.cfm?path=bridges&id=wolf_river.cfm

1.22. Nicholas, D. G., Solis, P. M., and Brown, D. K., "Airport on the Move," Civil Engineering Magazine, American Society of Civil Engineers, September 2001.

1.23. "Prefabricated Bridge Elements and Systems: Beaufort and Morehead Railroad Trestle Bridge Project Photos," Federal Highway Administration website http://www.fhwa.dot.gov/bridge/prefab/beauphot.htm.

1.24. "Prefabricated Bridge Elements and Systems-Substructures: Bent Caps," Federal Highway Administration website http://www.fhwa.dot.gov/bridge/prefab/bentcaps.htm

1.25. LoBuono, Armstrong, and Associates, "Development of Precast Bridge Substructures," Report for the Florida Department of Transportation, May 1996.

1.26. Association of State Highway and Transportation Officials (AASHTO), *AASHTO LRFD Bridge Design Specifications*, 3rd ed., AASHTO, Washington, D.C., 2004.

1.27. Lutz, L. A., and Gergely, P., "Mechanics of Bond and Slip of Deformed Bars in Concrete," Journal of the American Concrete Institute, *Proceedings* V. 64, No. 11, November 1967.

1.28. Goto, Y., "Cracks Formed in Concrete around Deformed Tension Bars," Journal of the American Concrete Institute, *Proceedings* V. 68, No. 4, April 1971.

1.29. Eligehausen, R., Popov, E. P., and Bertero, V. V., "Local Bond Stress-Slip Relationship of Deformed Bars Under Generalized Excitations," Report No. UCB/EERC-83/23, Earthquake Engineering Research Center, University of California, Berkeley, CA, October 1983.

1.30. Astrova, T. I., Dmitriev, S. A., and Mulin, N. M., "The Anchorage of Deformed Reinforcing Bars in Ordinary and Prestressed Reinforced Concrete," Transactions of the Scientific-Research Institute of Concrete and Reinforced Concrete of the Academy of Building and Architecture, issue 23, Moscow, 1961.

1.31. Tepfers, R, "A Theory of Bond Applied to Overlapped Tensile Reinforcement Splices for Deformed Bars," Publication No. 73:2, Division of Concrete Structures, Chalmers University of Technology, Göteborg, 1973.

1.32. Untrauer, R. E., and Henry, R. L., "Influence of Normal Pressure on Bond Strength," Journal of the American Concrete institute, Proceedings V. 62, No. 5, May 1965.

1.33. Ferguson, P. M., Breen, J. E., and Jirsa, J. O., *Reinforced Concrete Fundamentals*, 5th edition, John Wiley & Sons, Inc., New York, 1988.

1.34. Orangun, C. O., Jirsa, J. O., and Breen, J. E., "Reevaluation of Test Data on Development Length and Splices," Journal of the American Concrete Institute, *Proceedings* V. 74, No. 3, March 1977.

1.35. Viwathanatepa, S., Popov, E. P., and Bertero, V. V., "Effects of Generalized Loadings on Bond of Reinforcing Bars in Confined Concrete Blocks," Report No. UCB/EERC-79/22, Earthquake Engineering Research Center, University of California, Berkeley, CA, August 1979.

1.36. Darwin. D., and Zavaregh, S. S., "Bond Strength of Grouted Reinforcing Bars," *ACI Structural Journal*, V. 93, No. 4, July-August 1996.

1.37. Cook, R. A., Kunz, J., Fuchs, W., and Konz, R. C., "Behavior and Design of Single Adhesive Anchors Under Tensile Load in Uncracked Concrete," *ACI Structural Journal*, V. 95, No. 1, January-February 1998.

1.38. Cook, R. A., "Grouted and Adhesive Anchor Tests of Master Builders Products," Structures and Materials Research Report No. 98-4, UF Project No. 4910 4504 640 12, University of Florida, December 1998.

1.39. Miltenberger, M., "Capacity Design of Grouted Anchors," *16th International Conference on Structural Mechanics in Reactor Technology (SMiRT 16) Transactions*, Washington D. C., August 2001.

Table 1.1 Advantages and Disadvantages of Bent Cap Connection Types [1.5]

Grout Pockets	**Grouted Vertical Ducts**	**Bolted Connection**
+ simple grouting operations	+ stay-in-place ducts	+ stay-in-place ducts
+ large construction tolerances	+ smaller volume of grout needed	+ optional post-tensioning
- potential congestion of cap reinforcement	+ minimal interference with cap reinforcement	+ minimal interference with cap reinforcement
- large exposed top surface	+ more limited exposed top surface	- exposed cap top anchorage needs to be protected

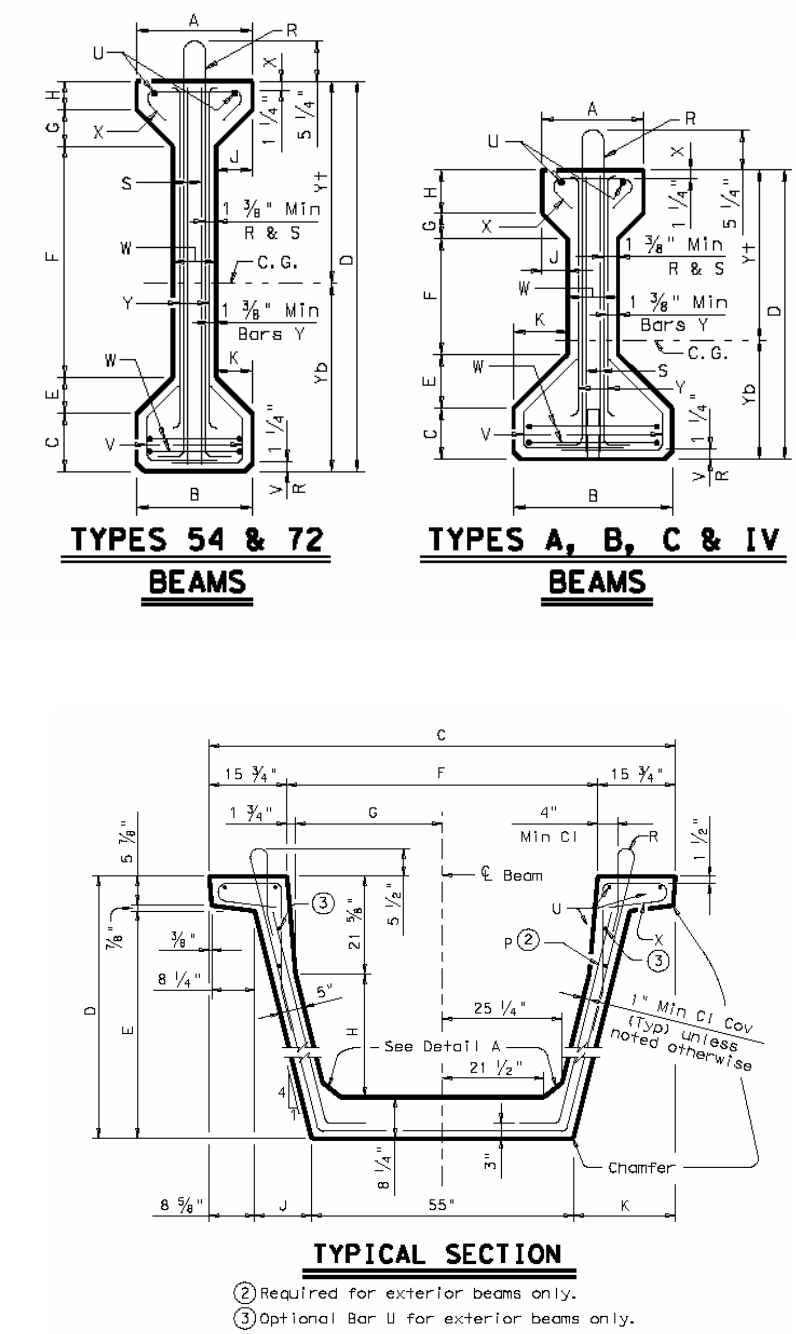

Figure 1.1 Typical Prefabricated Pretensioned Girders Used by TxDOT

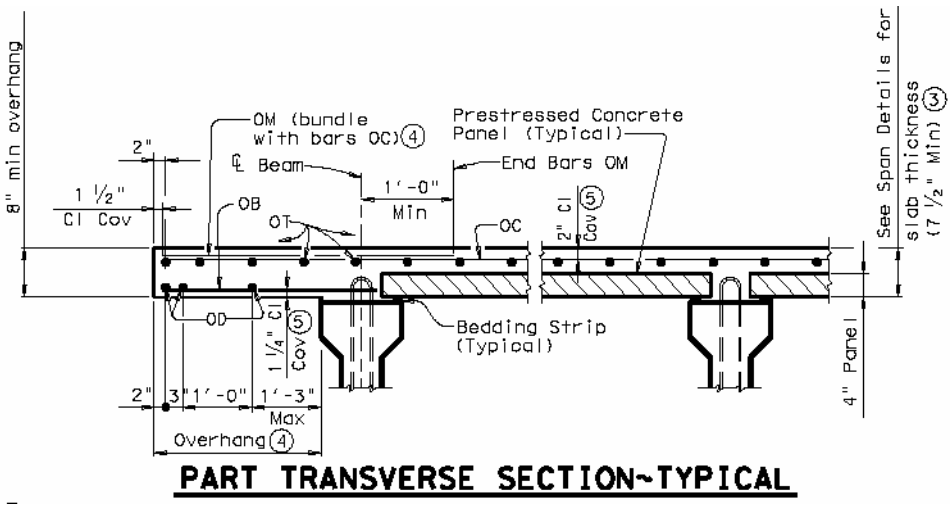

Figure 1.2 Precast Concrete Partial-Depth Deck Panels Used by TxDOT

Figure 1.3 Red Fish Bay Project Precast Bent Caps

Figure 1.4 US 290 Ramp E-3 Project Precast Bent Cap

Figure 1.5 Pierce Elevated Project Precast Bent Caps

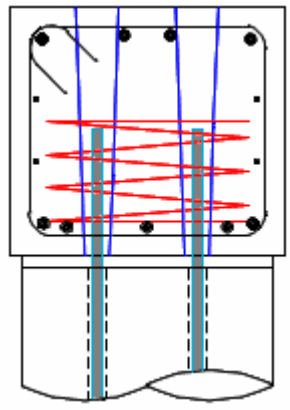

A. Grout Pocket Connection

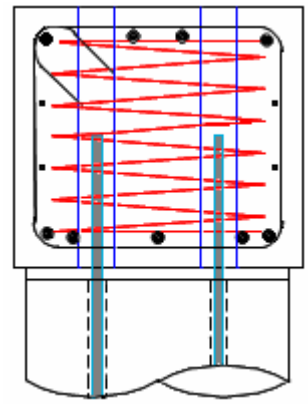

B. Grouted Vertical Duct Connection

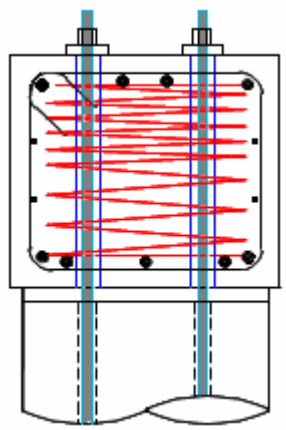

C. Bolted Connection

Figure 1.6 Connection Types Developed by TxDOT Research Project 1748 [1.5]

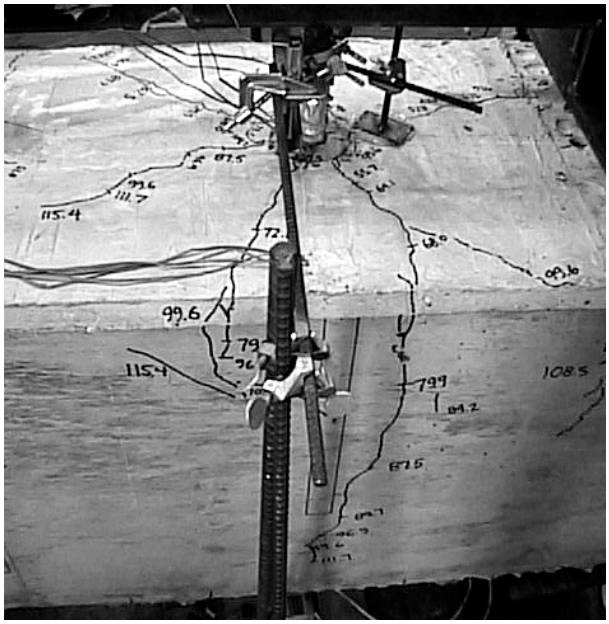

Figure 1.7 Test of Single Bar Embedded in Grouted Vertical Duct (Research Project 1748) [1.5]

Figure 1.8 Test of Column-Bent Cap Specimen with Grouted Vertical Ducts (Research Project 1748) [1.5]

Figure 1.9 Full-Scale Multi-Column Bent of Phase Three (Research Project 1748) [1.5]

Figure 1.10 Lake Ray Hubbard Bridge Project

Figure 1.11 Lake Belton Bridge Project

Figure 1.12 Dallas High Five Project

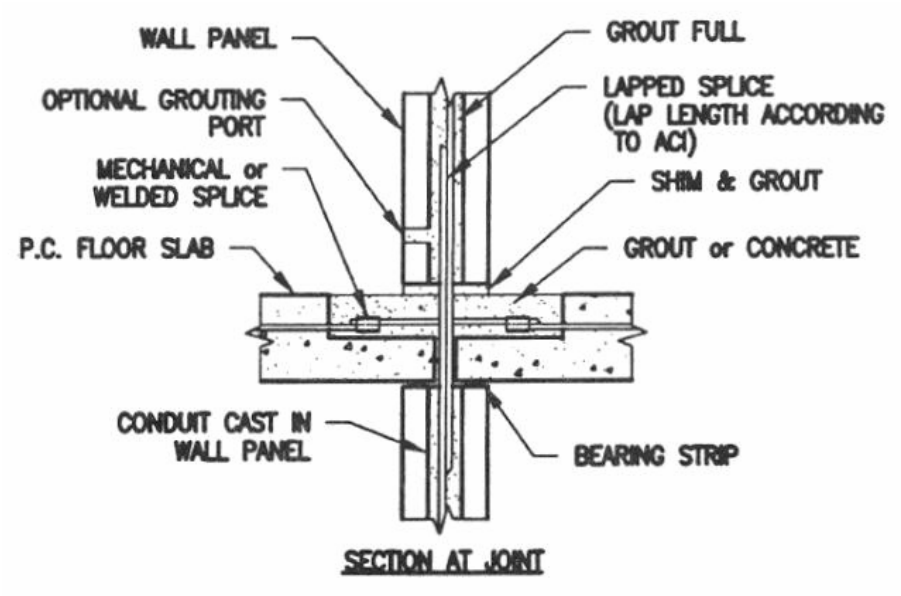

Figure 1.13 Detail to Join Wall Panels Vertically Using Large Conduit [1.6]

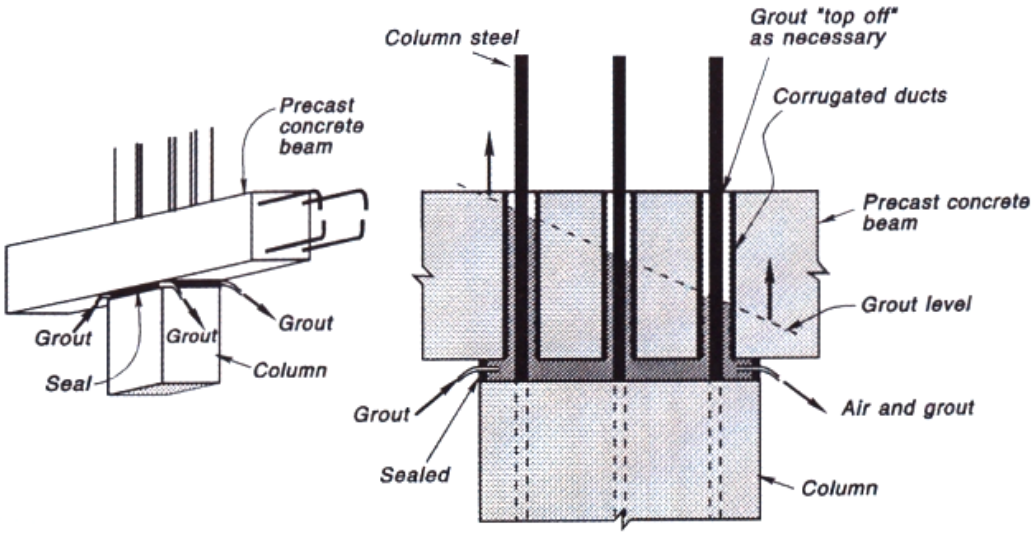

Figure 1.14 Precast Beam-Column Connections Used in New Zealand [1.8]

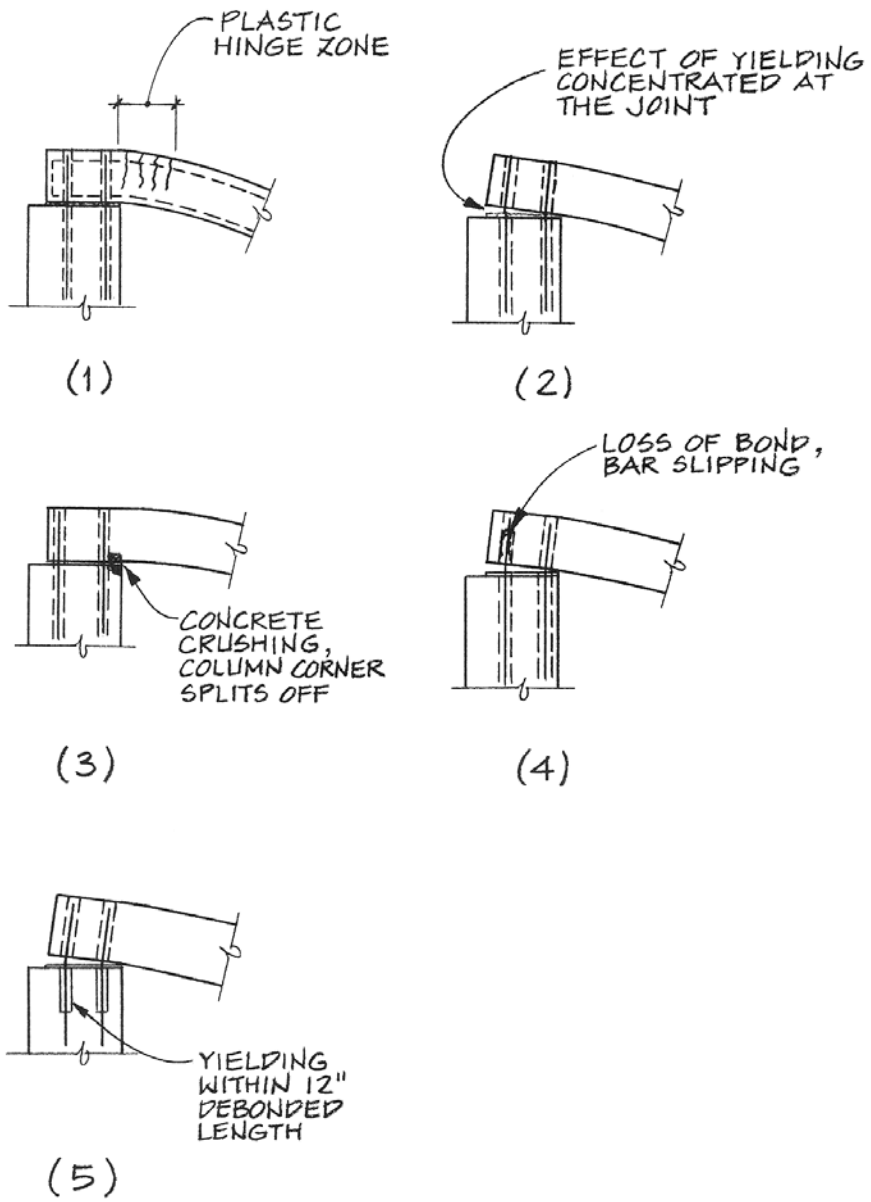

Figure 1.15 Flexural Failure Mechanisms for Precast Connection Using Grouted Ducts [1.10]

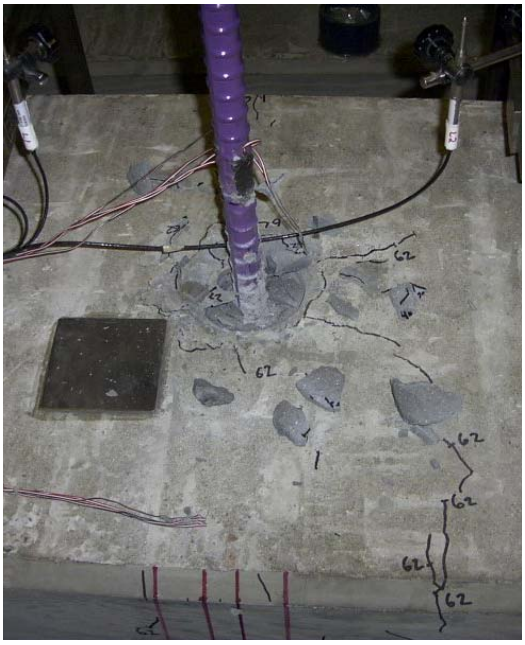

Figure 1.16 Test of Connector Embedded 10d_b [1.14]

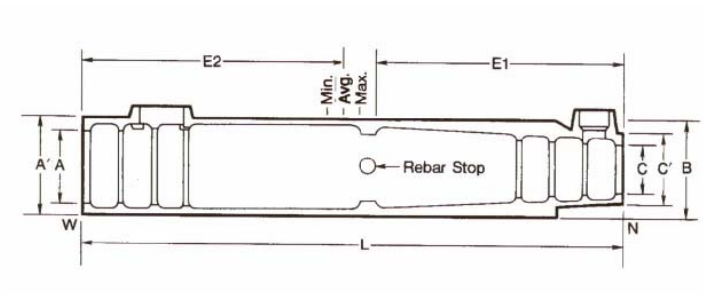

Figure 1.17 Detail of NMB Mechanical Splice System [1.17]

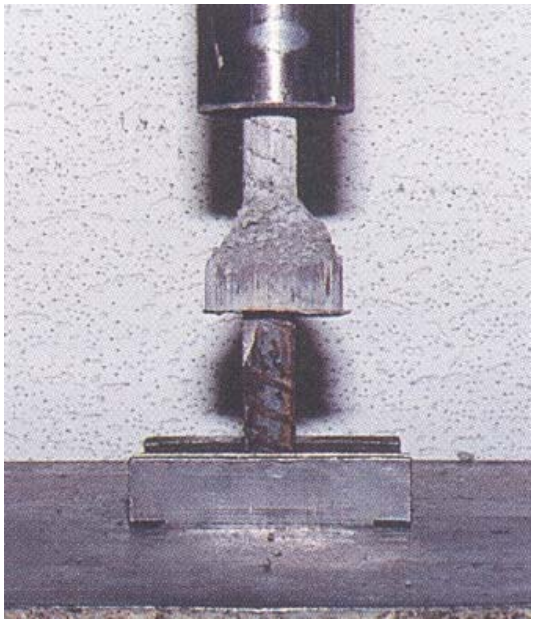

Figure 1.18 Pullout Failure of Generic Grout-Filled Splice Sleeve [1.18]

Figure 1.19 Precast Crossheads Used in the Getty Center People-Mover System Project [1.19]

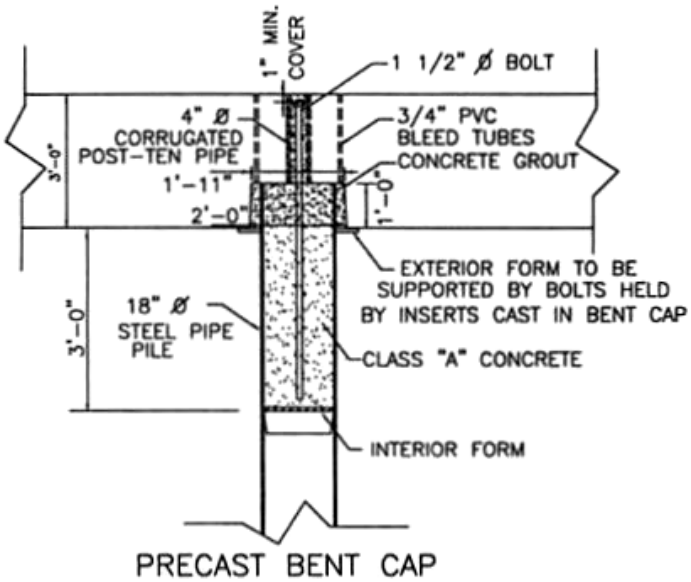

Figure 1.20 Wolf River Precast Bent Cap Connection [1.20]

Figure 1.21 Beaufort and Morehead Railroad Trestle Bridge Bent Caps [1.23]

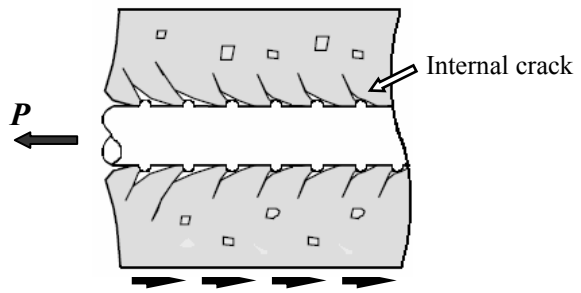

A. Tension acting on Reinforced Concrete

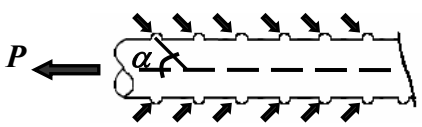

B. Bond Force on Bar

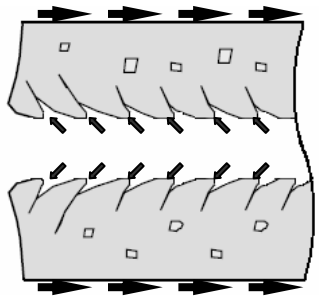

C. Reaction on Concrete

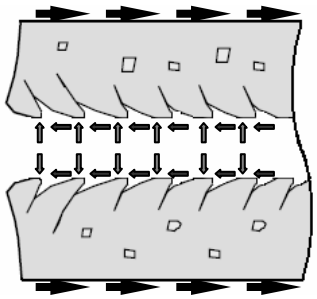

D. Parallel and Radial Components of Bond

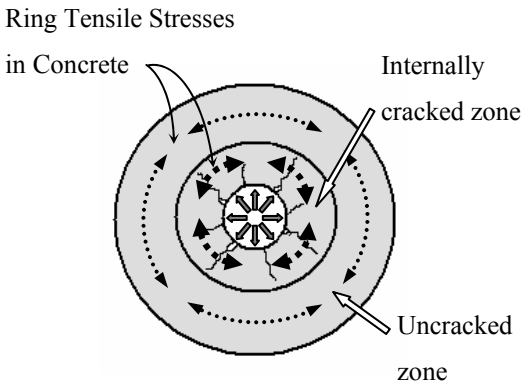

E. Cross Section

1.22 Forces between Deformed Bars and Surrounding Concrete

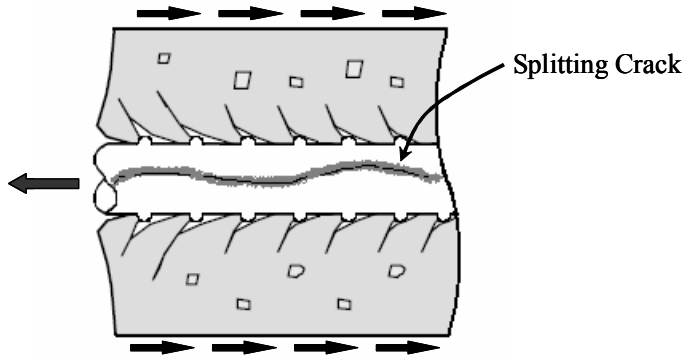

A. Bond Failure by Splitting

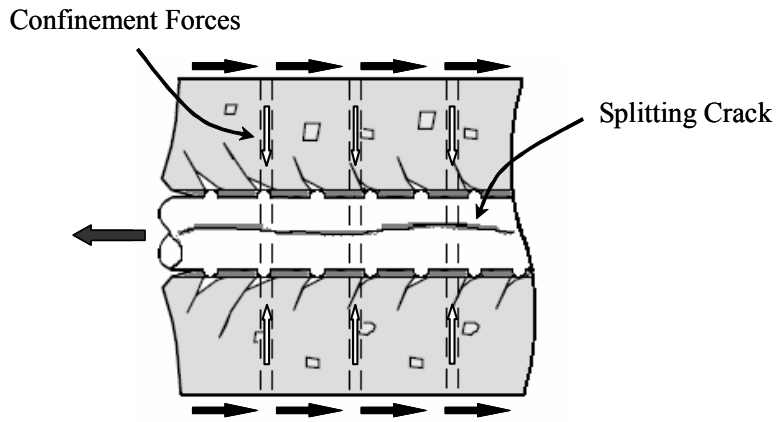

B. Bond Failure by Shearing of the Concrete Keys in Between Ribs (Pullout)

Figure 1.23 Effect of Confinement on Bond - Failure Modes

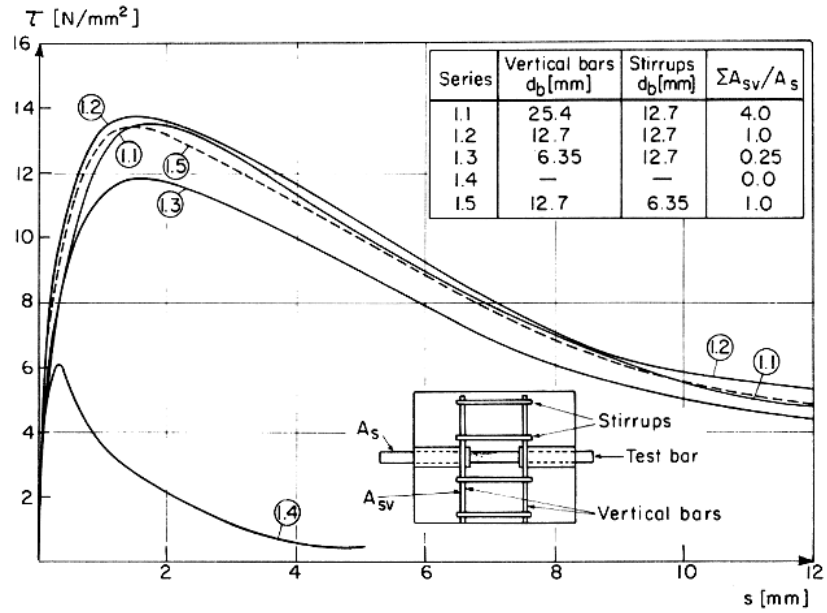

Figure 1.24 Influence of Transverse Reinforcement on Bond Stress-Slip Relationship [1.28]

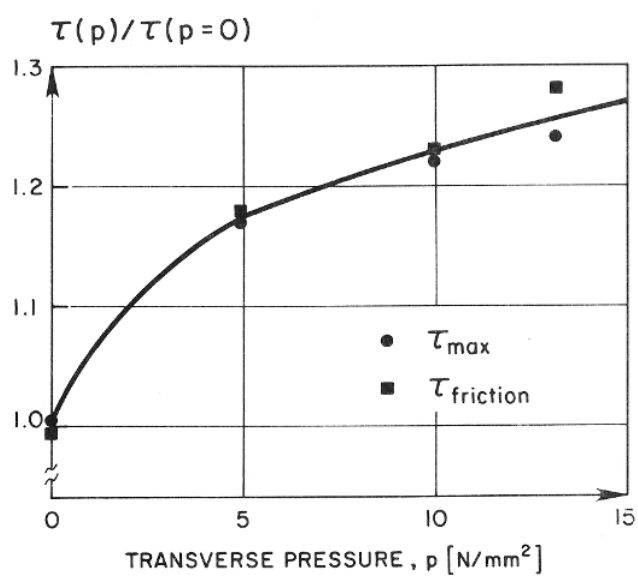

Figure 1.25 Influence of Transverse Pressure on Bond Resistance [1.28]

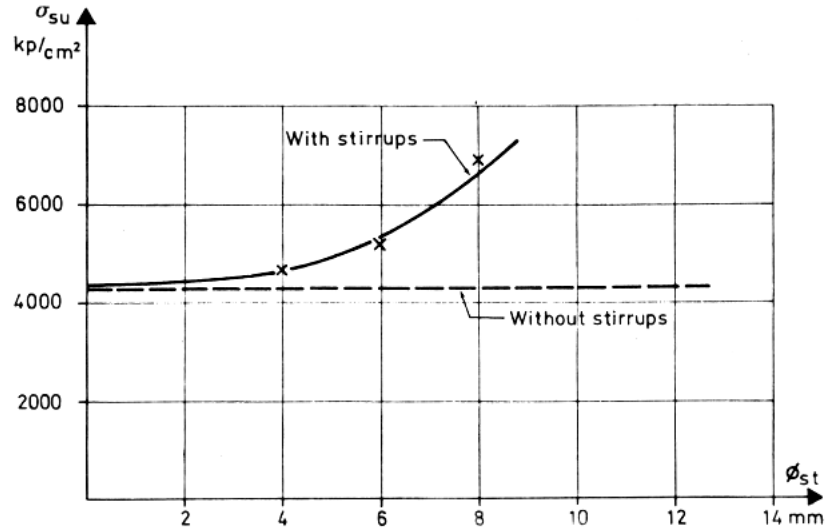

A. Splice Strength as a Function of Stirrup Diameter

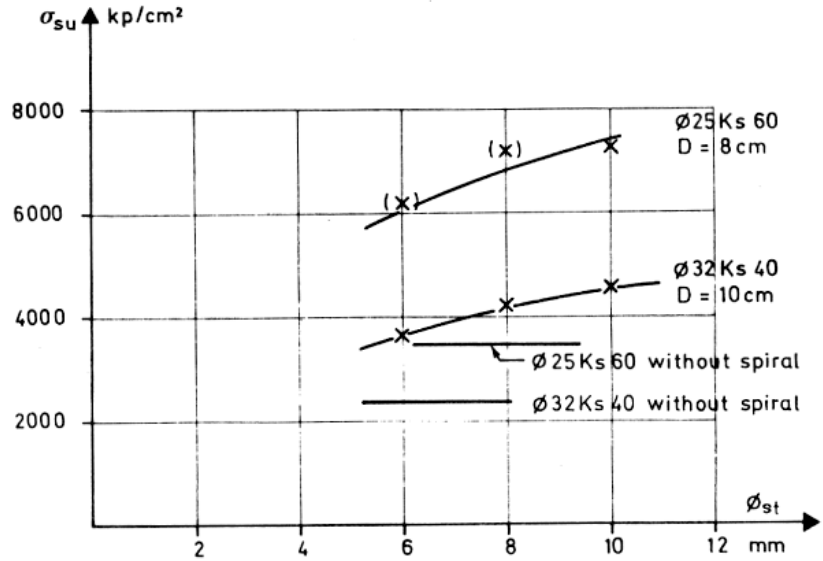

B. Splice Strength as a Function of Spiral Diameter

Figure 1.26 Effect of Transverse Reinforcement on Splice Strength [1.30]

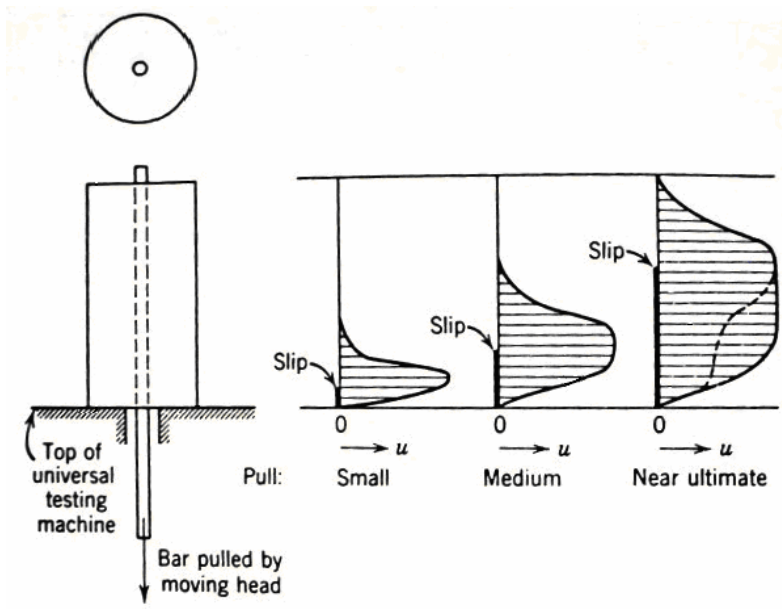

Figure 1.27 Bond Stress Distribution [1.33]

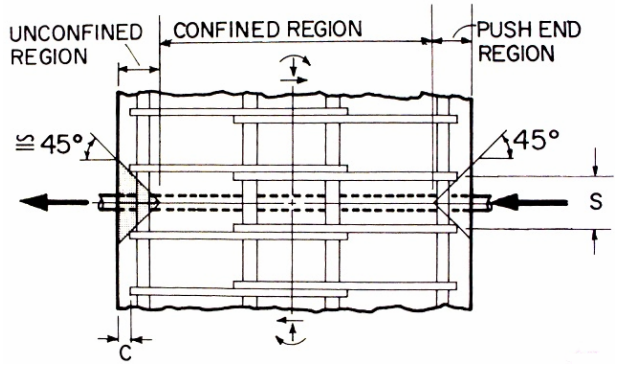

A. Regions in Concrete Block Specimen

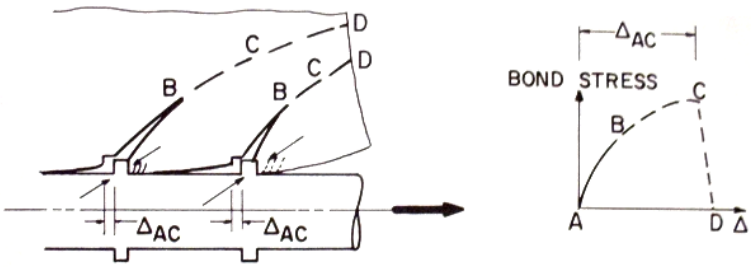

B. Mechanism of Bond Resistance in Unconfined Region

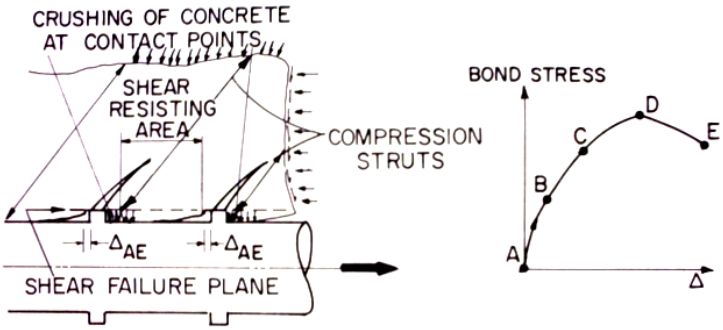

C. Mechanism of Bond Resistance in Confined Region

Figure 1.28 Bond Deterioration Mechanisms under Monotonic Loading [1.34]

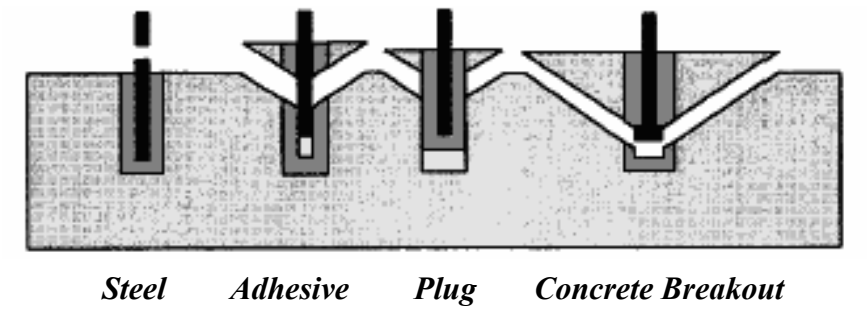

Figure 1.29 Basic Failure Modes for Grouted Connector [1.39]

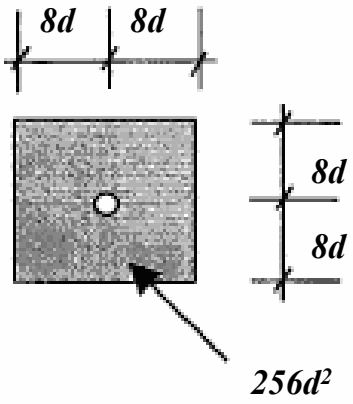

Figure 1.30 Influence Area for Single Straight Connector [1.39]

CHAPTER 2
Current Use and Constraints

The advantages of precast bent cap systems over conventional construction were discussed in Chapter 1 by reviewing several innovative bridge projects that have incorporated this technology. Prefabrication has provided efficiency by accelerating the construction schedule for bridges, and has allowed workers to operate more safely over water and in congested urban areas. The fact that contractor requests to use precast bent caps have produced these innovative projects is also evidence that these systems enhance bridge constructability and economy.

The connection details produced by research project 1748, "Development of a Precast Bent Cap System" [2.1], some of which are shown in Figures 2.1 through 2.4, were very important to the development of precast bent cap technology. Experimental results led to a systematic methodology for design of precast bent cap connections, which included design provisions for bars anchored in grouted ducts, grout pockets, and bolted connections. In addition, a comprehensive specification for precast bent cap connections was also developed that addresses material properties, placement of caps, construction tolerances, and grouting methods.

In the last five years, a series of bridge projects in Texas have incorporated the design and construction recommendations of research project 1748. The design and construction aspects of the Lake Ray Hubbard Bridge, the Lake Belton Bridge, and the Dallas High Five projects are described in this Chapter. Throughout these projects, precast bent caps proved again to be a very efficient construction system. Grouted vertical ducts were used in the cap-to-column connections of these new bridges. This type of connection was singled out as the

connection of choice by contractors and TxDOT engineers primarily because of the reduced volume of grout needed to complete the connections. The limited exposed grout surface of grouted vertical duct connections was also desired for durability purposes.

However, many uncertainties about the behavior of grouted vertical duct connections arose as engineers designing the connections selected large connectors, such as #11 bars, in large numbers, and then configured them very close to each other. Contractor-driven construction modifications intending to increase bridge durability, like replacing galvanized steel ducts with plastic ducts in the connections, raised additional concerns regarding the performance of the connections. Connection configurations and details used in practice were becoming more complex and had evolved from those developed by research project 1748. Concern among TxDOT engineers involved in the design and construction of the new bridge projects, led to this investigation on the behavior of grouted vertical duct connections.

2.1 PRECAST BENT CAP ANALYSIS AND DESIGN PROCEDURES

Research project 1748 [2.1] produced a design methodology for a precast bent cap system. This design procedure, shown in flow chart format in Figure 2.5, is currently used by TxDOT to design precast bent cap systems. This section summarizes the procedure.

2.1.1 Selection of Trial Bent Configuration

Short span bridges (with a span less than 120 ft) comprise more than 90% of the bridges in Texas [2.2], and are ideal candidates for concrete construction, which produces economical, durable, and aesthetically pleasing structures. Following standard practice, TxDOT normally selects multi-column and trestle pile bents for short-span bridges. While these bent configurations do not have a

reputation for being the most visually attractive, they provide advantages like structural redundancy and standardization. Typical bent caps used by TxDOT are rectangular or inverted-T in cross-section; while column sections are either round, rectangular, or square.

The majority of the bridges in Texas cross over small streams in rural areas where aesthetics is not usually considered a priority. However, for bridges located in urban or in recreational areas, TxDOT is normally incorporating aesthetics in their design. Projects like the Lake Ray Hubbard Bridge and the Lake Belton Bridge show that precast bent cap systems are very versatile in that they can be integrated to very different bent configurations, and also be at the heart of the aesthetics treatment of a bridge.

The process of selection of a trial bent configuration includes the selection of the cap type (cross-section), as well as the number, spacing, and size of columns or piles. Consideration is given to the characteristics of the superstructure system, such as span lengths and girder type. The weight of precast cap elements is usually high, and bent cap dimensions may be limited by crane capacities.

2.1.2 Analysis and Design of Bent

TxDOT currently designs bridges according to the AASHTO LRFD Bridge Design Specifications [2.3]. Dead and live loads, longitudinal forces (thermal effects, joint closing, braking), centrifugal forces, forces due to water flow (flood), wind and other lateral loads are considered at both the service and factored load levels. The design methodology does not consider seismic forces.

Differences in design for cast-in-place and precast bents concentrate on frame analysis and connection design. The effect of anchorage of connectors in a grouted connection, presence of a grouted bedding layer, and optional embedment

of the column (or pile) in the cap were investigated [2.1], and no significant differences in structural behavior versus that of a cast-in-place connection were noted. Connections of a precast bent cap system are considered to have a stiffness between that provided by a cast-in-place system (rigid) and a pinned (no rotational restraint) connection. The rotational stiffness of the connections is affected by the number and location of the connectors; a small number of connectors or a design configuration where connectors are located deep in the center of the joint results in a smaller rotational stiffness. Multi-column bents loaded in the transverse direction exhibited beam deflections within approximately 30 percent of a frame analysis assuming rigid connections [2.1]. Tests also showed that rotational stiffness depends not only on connector configuration, but also on the level of loading, and load history. The procedure suggests a simple approach where the bent is analyzed for the two limiting cases of pinned and rigid connection at the top of the column. The design of the connections is then based on the worst-case response of this frame analysis.

Caps and columns are usually considered separately in design. Bent caps are typically designed using in-house analysis programs that assume pinned connections at the top of the columns [2.4]. The forces in the columns in the transverse direction (relative to the bridge) are determined by the frame analysis that is also used to design the connections. In the longitudinal direction, columns are usually analyzed as having a pinned connection at the top.

2.1.3 Determination of Connection Actions

The forces acting on the connections are determined by frame analysis of the bent, considering the connection at the top of the columns to be capable of resisting moments. The load combination that controls the design consists of the most severe combination of simultaneous transverse and longitudinal actions. The

factored loads acting on the connections are multiplied by a factor of 1.3, according to Section 1.3.3 of the AASHTO LRFD Specifications, to satisfy ductility requirements.

2.1.4 Selection of Connection Type

The selection of the connection type is based on a series of factors, such as economics, constructability, and durability. Recent implementation of precast bent cap connections has demonstrated that grouted vertical ducts have evolved as the preferred connection type. The cost-savings offered by the reduced volume of grout used in grouted ducts compared with grout pockets, outweighs the benefits of having a simpler grouting operation. Bolted connections share the advantages provided by grouted vertical ducts and add the option of post-tensioning, which may be beneficial in some bridge applications that demand superior connection capacity to transfer large moments, or that demand a higher degree of redundancy in the connection.

The decision to embed columns (or piles) into the cap is also considered at this stage. Placing the cap surface-flush over the column simplifies the setting operations and allows for inspection of the bedding layer after the grouting operations. Embedment of the column in the cap enhances the durability of the connection by restricting the path of moisture, and also improves to some extent the rotational stiffness of the connection. Column embedment depths of 3 to 5 in. are recommended to accommodate vertical construction tolerances and to protect against corrosion in aggressive environments.

In the case of grouted vertical duct connections, the designer has the option of not continuing the ducts all the way to the top of the cap. This alleviates some of the concerns about exposure of the grout surface to the atmosphere leading to durability problems. However, in order to inspect that the grout has

filled the entire height of the ducts, it may be necessary to extend a few of the ducts all the way to the top of the cap or have grout ports at the top.

2.1.5 Selection of Connector Configuration

A trial connector configuration is selected based on spacing and minimum connection reinforcement requirements. Connector and duct spacing are normally maximized to facilitate constructability and to limit splitting stresses in the concrete. Whenever possible, connectors are positioned away from the center of the joint for maximum eccentricity to resist moments.

The number, size, and yield strength of the connectors are determined by the magnitude of the loads to be resisted. As the number of connectors increase, spacing becomes more critical for construction and anchorage. Minimum clear connector spacing in grout pockets is $2d_b$. For grouted vertical ducts, a minimum clear spacing of one duct diameter is generally specified. The selection of the duct diameter must facilitate the placement of the bent cap in the field. It is recommended that duct diameters be 2 to 3 times the bar diameter and provide a horizontal tolerance of at least 1 in., although a horizontal tolerance of 1.5 in. is considered preferable.

Reinforcement crossing the joint must be at least 0.7% of the gross area of the column, or 1.0% of the gross area of the pile. To provide redundancy, a minimum of four connectors are provided in columns, while a minimum of three connectors are provided in trestle piles.

2.1.6 Analysis of Connector Configuration

The selected trial configuration is analyzed by evaluating strength and serviceability requirements. Checks at the strength limit state involve comparing the results obtained from the frame analysis (factored axial loads and moments acting in both the transverse and longitudinal directions) described in Section

2.1.3, with a design interaction diagram. Shear friction at the bedding layer and joint shear are also evaluated using the AASHTO LRFD Specification.

Checks at the service limit may include potential opening at the bedding layer, cracking in the connection region at the cap top, and deflections of the bent. The possibility of an opening at the bedding layer is conservatively estimated by establishing the location of the neutral axis for service-level load combinations; if the section analysis indicates that one or more connectors experience tension, then there is a potential for an opening to form. In cases where durability is a primary concern, such as in aggressive environments, the designer has the following options: (1) embedding the column (or pile) in the cap, (2) use of epoxy-coated connectors, (3) use of an external sealant, (4) use of water stops, and (5) post-tensioning if the connection is bolted. Control of concrete cracking in the connection area follows the AASHTO LRFD [2.3, Section 5.7.3.4] provisions.

2.1.7 Determination of Connector Type and Embedment

Uncoated straight reinforcing bars are normally selected for bridges situated in non-corrosive environments [2.4]; while epoxy-coated connectors are used in coastal and aggressive environments. The designer also has the option of using headed anchors to provide redundancy in the connection if the bond transfer mechanism is in question due to poor grouting operations, dynamic loads, or close connector spacing. However, constructability is impaired by the larger dimension of the head if the connectors are to be housed inside ducts. In the case of bolted connections, a large number of high-strength threaded rod systems are available that can be post-tensioned. Hooked bars or U-shaped bars can be used in grout pocket connections.

The embedment depth of connectors housed inside grout pockets and grouted vertical ducts is determined by design equations (shown in Section 1.2),

with the premise of ensuring a ductile mode of failure (yielding of the connector). There are also provisions for calculating the development length of headed bars in grout pockets. Results of this investigation will present new anchorage design provisions that take into account duct material and connector group effects.

2.1.8 Selection of Transverse Reinforcement

Transverse reinforcement in the form of spirals is specified around the connector group through the entire depth of the cap. Results of this investigation will show that the confining effect provided is insignificant in terms of improvements in strength and ductility. Spirals do however have the potential to control splitting cracks in the connection region and prevent deterioration of the joint; and designers are encouraged to use them.

2.2 CURRENT PRECAST BENT CAP CONSTRUCTION

A series of bridges have been completed in the last five years by TxDOT that have incorporated precast bent caps as part of their structure. In two of these bridges, the use of precast caps was requested by project contractors. The design and construction aspects of the Lake Ray Hubbard Bridge, the Lake Belton Bridge, and the Dallas High Five projects are described in Sections 2.2.1 to 2.2.3.

2.2.1 Lake Ray Hubbard Bridge Project

In the year 2000, TxDOT began replacement of the narrow two-lane crossing of SH 66 over Lake Ray Hubbard. The replacement of the 40 year-old bridge was necessary because it had become a congested route for commuters living in the suburbs east of Dallas [2.5]. The new crossing consists of a pair of bridges with conventional multi-column bents that support prestressed I-girders. Bridge lengths are 10,280 ft for the westbound structure, and 4,360 ft for the eastbound structure, and typical span lengths are 100 ft. The project called for

phased construction, which allowed the original structure to remain operational as the westbound replacement bridge was being built next to it. Traffic was then shifted to the completed westbound bridge, as construction of the eastbound bridge ensued following the removal of the original structure.

Three-column bents supported on drilled shaft foundations make up the substructure system of the replacement bridge. At the initial stages of the project, all substructure elements were constructed using cast-in-place concrete. However, before beginning construction of the eastbound bridge, the contractor asked TxDOT for permission to use precast bent caps in order to accelerate construction, avoid the difficulties of handling formwork and materials over water, and to minimize exposure of the workers to power lines that were located very close to the site [2.5, 2.6]. Figure 2.6 shows a photograph of the construction site. A first precast bent cap design by TxDOT involved a grout void or pocket connection detail. Although this detail facilitated construction tolerances, the amount of grout needed for completing the connections was cost prohibitive. TxDOT then designed a connection detail that would utilize grouted vertical ducts instead of grout pockets. This change in design led to a 60% reduction in the volume of grout needed [2.6].

The selected precast bent cap connection detail consisted of six #11 straight reinforcing bars, each housed inside a 4-in. diameter duct. Spiral reinforcement was provided around the connector group to control cracking and enhance ductility. Clear spacing between ducts was 4 in. (or one duct-diameter spacing) in the longitudinal direction of the cap. A photograph of a bent cap connection zone under construction is shown in Figure 2.7. The contractor asked TxDOT for authorization to use plastic (polyethylene) ducts instead of the galvanized steel ducts that were specified in the design plans. The change in duct material was approved by TxDOT based on information supplied by the duct

manufacturer regarding bond properties of the plastic ducts in prestressing applications. While there may be similarities between a reinforcing bar grouted in a duct and a grouted tendon, test data are required to assess the behavior of reinforcing bars grouted in plastic ducts. Because such test data were not available at the time, TxDOT designed the connections conservatively, assuming a reduction in bond strength [2.7]. The use of plastic ducts instead of galvanized steel ducts was considered beneficial to the bridge because of the enhanced durability. Constructability also improved because plastic is easier to cut in the field and is safer for workers to handle (no sharp edges).

Drilled shaft and column construction were conducted while bent caps were being constructed at a casting yard setup at the eastern end of the bridge. Templates were used at the top of the columns during casting to position the connectors properly to match the sleeves formed in the bent cap element. Bent caps were loaded onto barges and transported for erection. Figure 2.8 shows a bent cap being hoisted for placement on top of the columns. Friction collars were placed on the columns to provide temporary support for the cap during the placement and grading operations. Grout was pumped from the bedding layer into each connection; three vents were provided in the forms of the bedding layer to ensure a successful grouting operation. Flow of grout up the ducts was monitored from the top.

The decision to precast the caps shortened the construction schedule by approximately six months. Most of the time saved was related to bent cap curing time, which was removed from the critical path [2.8]. The safety of the workers was improved because most of the work associated with the construction of the caps was performed in a controlled environment on the ground instead of over water.

2.2.2 Lake Belton Bridge Project

The replacement of the 50-year old two-lane crossing of SH 36 over Lake Belton began in the fall of 2002. The original 3,840 ft-long structure had numerous problems, which included a deteriorated superstructure, a narrow width of only 26 ft, and railing damage. The new twin bridge structure incorporates two additional lanes of traffic, increasing the total roadway width to 84 ft. Prestressed U-beams make up the superstructure of the bridges; typical span lengths are 120 ft. The substructure of each bridge consists of twin, cast-in-place, round columns that support a massive hammerhead bent cap. Figure 2.9 shows a photograph of the bridge in an advanced stage of construction. A total of 62 identical caps were precast for this project.

Surface elevations fluctuate significantly in Lake Belton because it is a flood-control reservoir. The bridge needed to be constructed nearly 50 ft over the normal lake elevation to allow for these water level fluctuations [2.6, 2.9]. The lake is also a source of drinking water for the population of Waco, and environmental concerns favored precast instead of cast-in-place construction. TxDOT decided not to precast the columns of these bridges due to concerns about the performance of the column joints underwater. However, precasting of the bent caps was considered advantageous due to the large number of identical caps needed, the high construction elevations demanded by the site, and the higher quality control provided by prefabrication.

Lake Belton is a body of water that is used extensively for recreation. In the substructure design, the bridge incorporated aesthetics by emulating a single-pylon structure, with a stylized bent cap at the top. The caps vary in depth from 5’-6” at the middle to 3’-0” at the edge of the cantilevers. At the top, the caps measure 5’-6” in width, while at the bottom, the width reduces to 5’0”. Figure 2.10 shows a cross section of the cap including reinforcement arrangements.

Each of the two connection zones (one for each column) involved the anchorage of fourteen #11 Grade 60 reinforcing bars in 4.5 in. diameter galvanized steel ducts (Figure 2.11). The connectors were embedded 4'-2" into the cap, and the ducts that housed them did not extend to the top of the cap. Discontinuing the ducts prevented interference with the negative moment reinforcement in the cap and also having to expose a large grout surface to the atmosphere. Two of the connectors (those closest to the sides of the cap) and their associated ducts extended all the way to the top of the cap. These connectors were plate anchored at the top to provide provisional support to the cap until grouting of the connections. The ducts that extended the full height of the cap aided in the inspection of the grout filling the ducts. Injection and vent ports for grout were provided in each duct to ensure adequate grouting and venting of the connections.

Each of the precast caps had a weight of approximately 75 kips, and they were transported by truck from a precasting yard located 140 miles south of the construction site. After arriving at the site, caps were mounted on a barge with an integrated the crane used for lifting and placing the caps (Figure 2.12). A 2-in. thick bedding layer was formed between the cap and the columns that included dry-pack grout placed in the periphery of the connection zones. The bedding layer and the ducts were then filled with grout that was pumped at high pressure from below.

The bent configuration selected posed many potential design problems for a precast bent cap connection. There was a question of how much tension would be developed in the connectors due to unbalanced moments. Although post-tensioning was an option, the top portion of the cap was congested with negative moment longitudinal reinforcement making it very difficult to provide suitable anchorage regions [2.6]. Analysis showed that the connectors could experience

low levels of tension (around 7 ksi) under some load combinations, but not to the point where post-tensioning was considered necessary [2.9].

2.2.3 Dallas High Five Project

The Dallas High Five Interchange project (shown in Figure 2.13 under construction) at the intersection of Interstate Highway 635 and U.S. 75 was begun in 2001; at $260 million, it is the largest single contract ever awarded by TxDOT. The original design of the ramp structures involved cast-in-place construction, and included in the superstructure a combination of post-tensioned segmental trapezoidal beams and U-beams supported on single column bents. The giant interchange comprises five stacked levels of roadway and ramps, which required workers to erect formwork, and place steel rebar and concrete as high as 80 ft in the air (Figure 2.14). Shortly after the beginning of the project, the contractor requested using precast bent caps to speed up construction and reduce lane closures. Precasting the caps on the ground allowed working crews to operate in a safe and controlled environment.

Caps were fabricated on the construction site (Figure 2.15). A typical detail of the inverted-T cap cross section is shown in Figure 2.16. A total of 18 - #11 bars (approximately 60% of the longitudinal reinforcing steel in the column) extended beyond the column and were grouted in the corrugated steel ducts provided in the caps. Ducts were located in the stem and in both ledges of each cap. Column bars that were anchored in the ledge regions of the cap had a short embedment length of around 18 in. ($13d_b$ for a #11 bar). Connections (bedding layer and ducts) were pressure grouted from the ground. Four threaded bars anchored at the top of the cap provided support during grouting operations. Except for those ducts housing the erection bolts, all other ducts were terminated before reaching the top surface of the cap.

Original estimates of construction time for the project indicated that completion would be achieved in 2007. At the time of this writing, the project seems to be ahead of schedule.

2.3 LIMITATIONS AND NEED FOR RESEARCH

Section 2.2 presented the design and construction aspects of three innovative TxDOT bridges that have incorporated precast bent caps with grouted vertical ducts. It is clear that many uncertainties arose regarding the behavior of grouted vertical duct connections during the design and construction phases of these bridges. The connection configurations and details that are currently being used have evolved from those developed by research project 1748 [2.1]. Recommendations for design were based on the anchorage of single epoxy-coated connectors embedded in galvanized steel ducts. In light of current experience with construction of precast bent caps, these recommendations need to be re-evaluated and extended to take into account the effects of multiple closely-spaced connectors, duct material, and other design features on connection behavior.

As a general trend, designers select large diameter connectors, such as #11 reinforcing bars, to minimize the number of connectors crossing the cap to column joint. Often, these connectors are placed very close to each other (duct clear spacing of one duct diameter or less) in order to avoid interference with cap reinforcement or due to restrictions imposed by the column section below on the embedment location of the connectors. Information about the interaction (group effects) between closely-spaced connectors is needed in order to evaluate anchorage strength.

Contractor-driven construction modifications aimed to increase bridge durability, like replacing galvanized steel ducts with plastic ducts in the connections, raised additional concerns regarding the performance of the

connections. Motivation for the use of plastic ducts stems in part from research conducted at the University of Texas at Austin [2.10]. Long-term exposure tests of post-tensioned beams revealed serious durability problems associated with galvanized steel ducts. Forensic investigation of beams subjected to conditions representing aggressive environments indicated that the presence of grout voids was detrimental to the durability of the ducts; bleed water voids were observed in ducts even after high-quality grouting procedures. Use of galvanized steel ducts in aggressive environments was strongly discouraged. The use of plastic ducts instead of galvanized steel ducts requires investigation of the bond between the duct and the grout, and the concrete. The confinement provided by the duct to the grout, potentially an essential mechanism of resistance to grouted vertical duct connections, is dependent on the stiffness of the duct material. Tests must be performed in order to establish required anchorage lengths for connectors embedded inside plastic ducts.

Demand for precast bent caps is expected to increase as TxDOT continues to incorporate rapid construction techniques as an option to conventional construction in upcoming projects. Precast bent cap technology is reaching the levels of maturity necessary for implementation in a standardized format in new bridge designs, and contractors now have an option of selecting a precast bent cap alternative over conventional cast-in-place construction. Design recommendations developed through experimental investigation and updated to reflect current construction practices are necessary to clarify the uncertainties that are causing concern to those involved in the design and construction of these systems.

2.4 REFERENCES

2.1. Matsumoto, E.E., Waggoner, M.C., Sumen, G., Kreger, M.E., Wood, S.L., and Breen, J.E., "Development of a Precast Bent Cap System," Research

Report 1748-2, Center for Transportation Research, University of Texas at Austin, January 2001.

2.2. Holt, J., and Medlock, R., "Standardized Concrete Bridges in Texas," Post-Tensioning Institute (PTI)/National Concrete Bridge Council Concrete Bridge Conference Proceedings, Charlotte, NC, May 2004.

2.3. Association of State Highway and Transportation Officials (AASHTO), *AASHTO LRFD Bridge Design Specifications*, 3rd ed., AASHTO, Washington, D.C., 2004.

2.4. Wolf, L. M., and Hyzak, M. D., "Design of Precast Bent Cap to Column Connections," *Post-Tensioning Institute (PTI)/National Concrete Bridge Council Concrete Bridge Conference Proceedings*, Charlotte, NC, May 2004.

2.5. Medlock, R., Hyzak, M., Wolf, L., "Innovative Prefabrication in Texas Bridges," *Proceedings of Texas Section, American Society of Civil Engineers, Spring Meeting 2002*, American Society of Civil Engineers, Texas Section, Austin, TX, March 2002.

2.6. Freeby, G., Hyzak, M., Medlock, R. D., Ozuna, K., Vogel, J., and Wolf, L., "Design and Construction of Precast Bent Caps at TxDOT," *82nd TRB (Transportation Research Board) Annual Meeting*, Washington, D. C., January 2003.

2.7. Hyzak, M., "Lake Ray Hubbard Bridge: Structural Design," Lake Ray Hubbard Bridge-Precast Concrete Bent Cap Demonstration Workshop, FHWA/AASHTO/TxDOT, Mesquite, TX, March 2002.

2.8. Friggle, T., "State Highway 66 Lake Ray Hubbard Bridge Construction with Precast Bent Caps," *Lake Ray Hubbard Bridge-Precast Concrete Bent Cap Demonstration Workshop*, *FHWA/AASHTO/TxDOT*, Mesquite, TX, March 2002.

2.9. Hyzak, M., "Lake Belton: Precast Bent Cap Design," Lake Belton Bridge-Precast Concrete Bent Cap Demonstration Workshop, FHWA/AASHTO/TxDOT, Temple, TX, July 2003.

2.10. Salas, R. M., Kotys, A. L., West, J. S., Shocker, A. J., Breen, J. E., and Kreger, M. E., "Long-Term Post-Tensioned Beam Exposure Test

Specimens: Final Evaluation," Research Report 0-1405-7, Center for Transportation Research, University of Texas at Austin, August 2003.

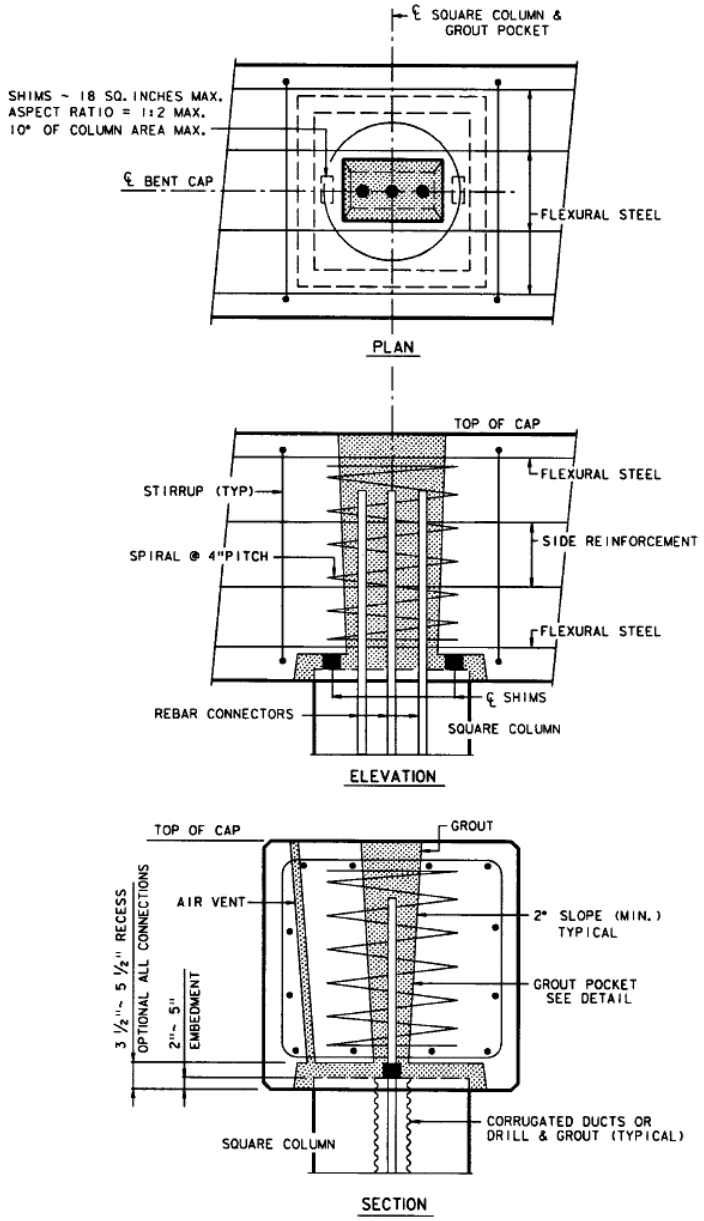

Figure 2.1 Connection Detail for Single-line Grout Pocket on Pile (Embedded Option) [2.1]

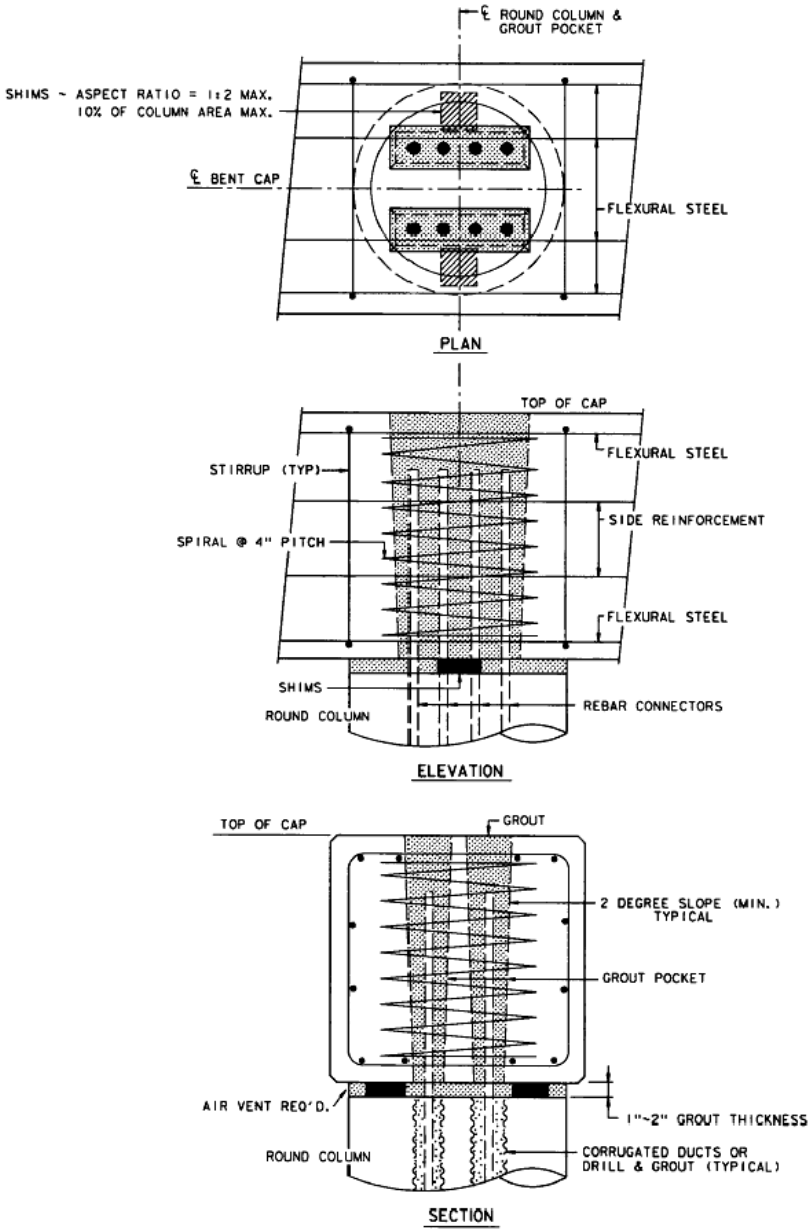

Figure 2.2 Connection Detail for Double-line Grout Pocket on Column (Surface-flush Option) [2.1]

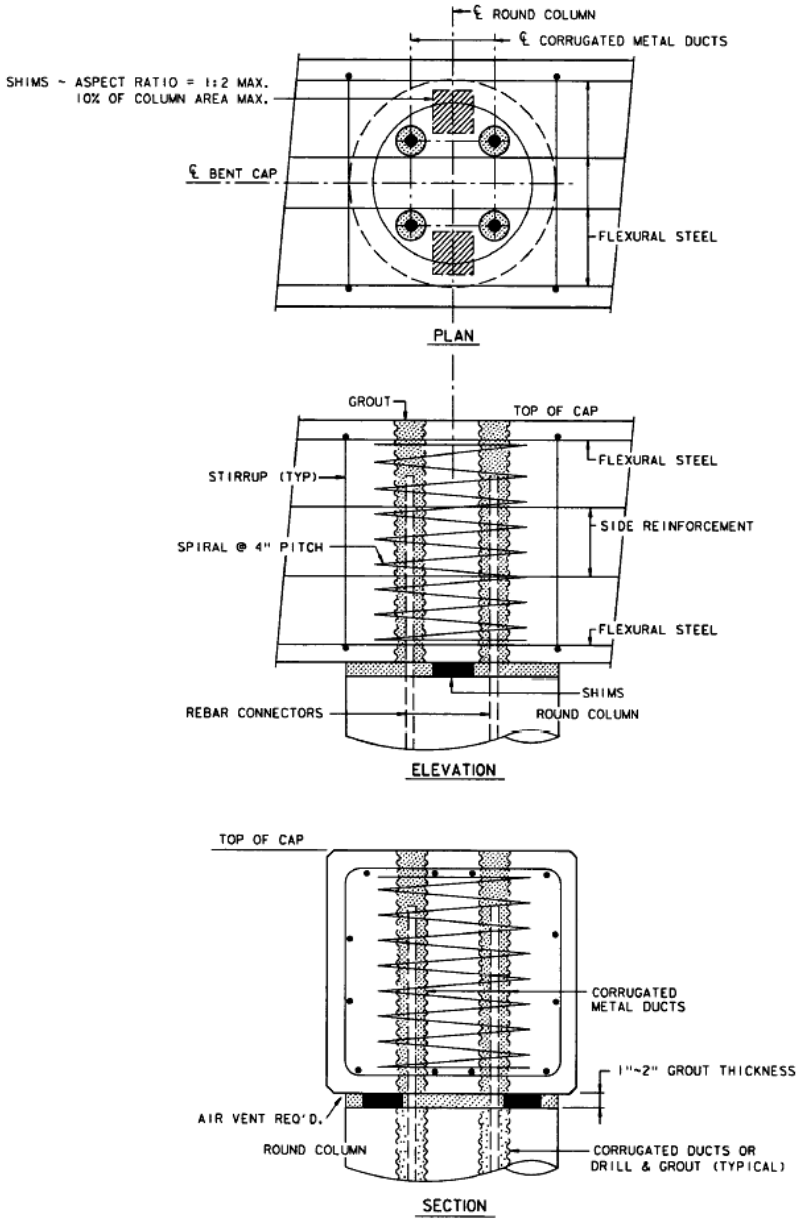

Figure 2.3 Connection Detail for Grouted Vertical Ducts on Column (Surface-flush Option) [2.1]

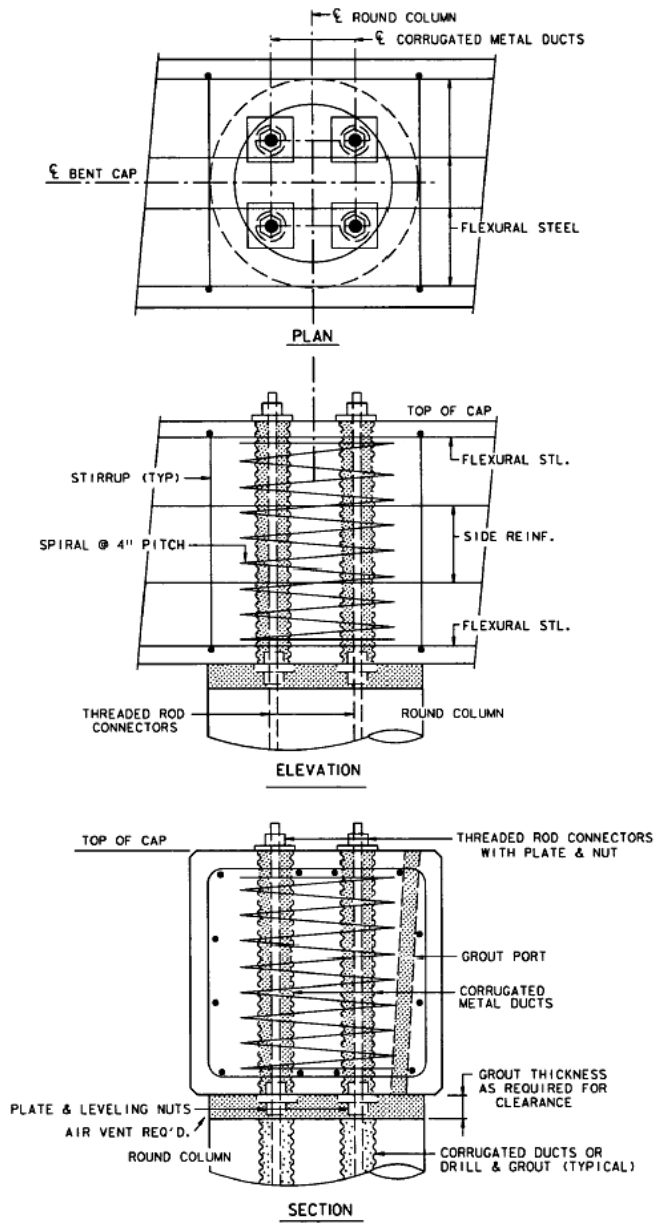

Figure 2.4 Connection Detail for Bolted Connection on Column (Surface-flush Option with Plate-and-Leveling Nut Option) [2.1]

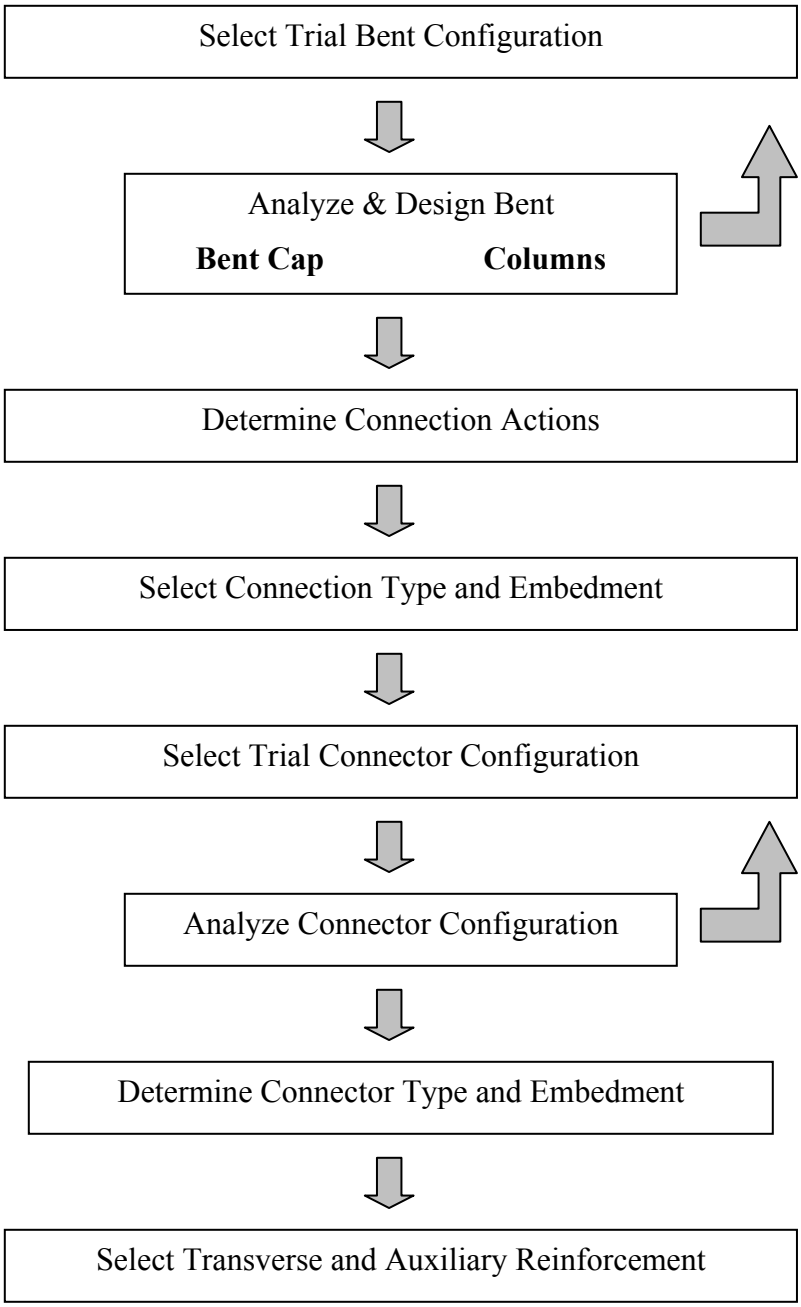

Figure 2.5 Design Flowchart for Precast Bent Cap System [2.1]

Figure 2.6 Lake Ray Hubbard Bridge Construction Site [2.8]

Figure 2.7 Bent Cap Connection Zone under Construction

Figure 2.8 Bent Cap Placement Operations

Figure 2.9 Construction of the Lake Belton Bridge

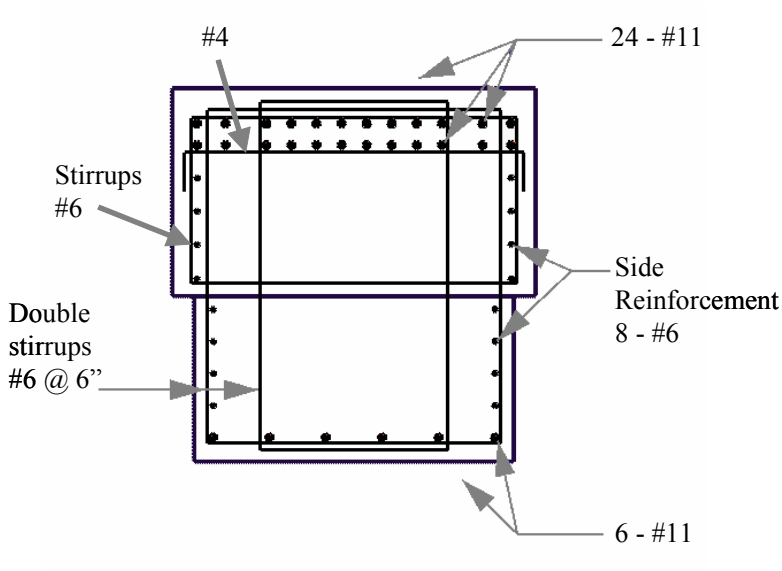

Figure 2.10 Bent Cap Reinforcement Scheme [2.9]

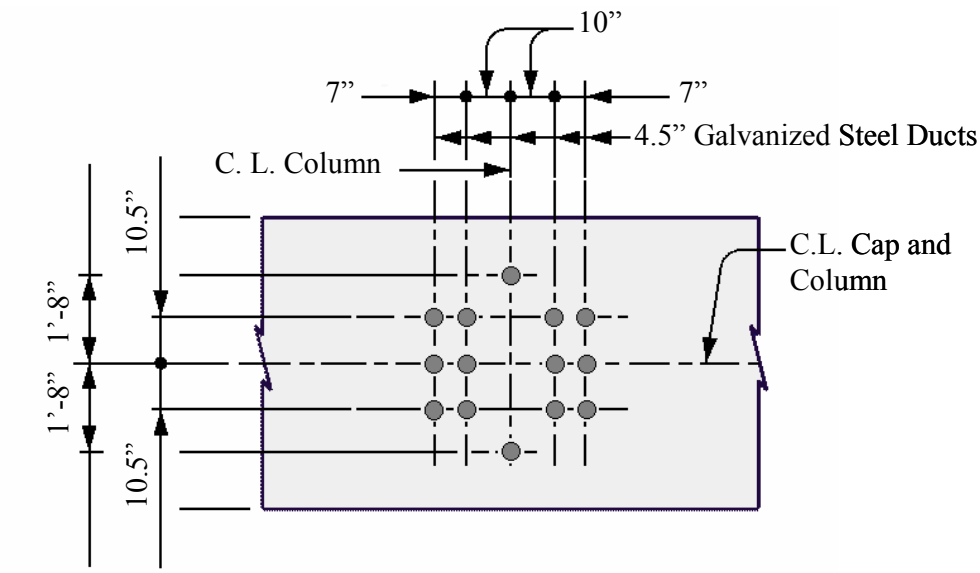

Figure 2.11 Bent Cap Connection Zone Detail [2.9]

Figure 2.12 Bent Cap Placement Operation with Barge-mounted Crane

Figure 2.13 Aerial View of Dallas High Five Interchange Construction Site

Figure 2.14 Tall Single Column Bent

Figure 2.15 Placement of Bent Cap Reinforcement and Ducts

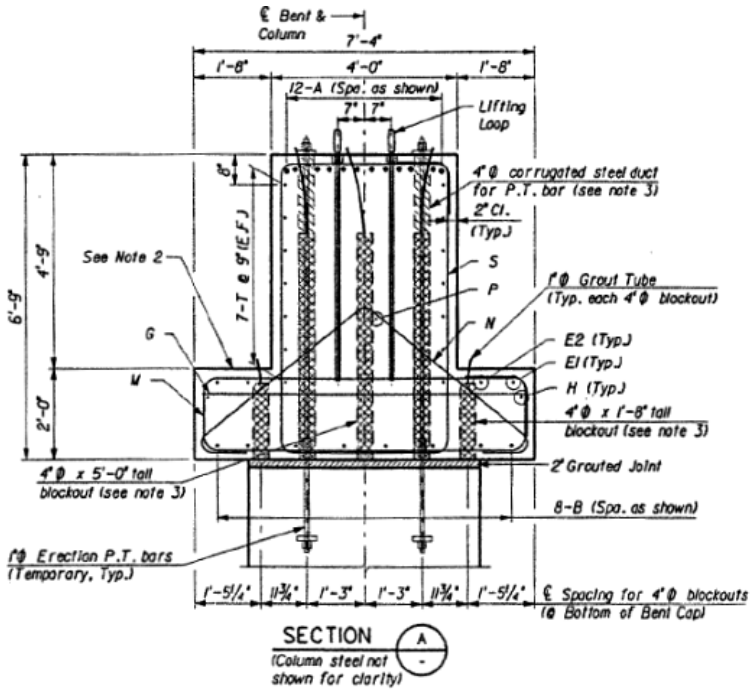

Figure 2.16 Detail of Bent Cap Cross Section

CHAPTER 3
Overview of Experimental Program

3.1 INTRODUCTION

An experimental program was developed to examine the behavior of precast bent cap connections constructed using grouted vertical ducts. A number of parameters that affect the behavior of these connections were identified, and will be described in the following section. The limitation on the number of tests that could be performed did not allow for an experimental investigation of all parameters originally considered. Thus, the most important of these parameters were selected for investigation, based on their expected influence on behavior of the bent cap system and on current design configurations and probable future use.

The materials and dimensions of the test specimens correspond to those that have been used in actual bent cap connections. Some aspects of constructability of these connections related to grouting procedures were also investigated during the experimental program.

3.2 TEST PARAMETERS

The use of grouted vertical duct connections in precast bent cap systems provides a large number of options to the designer. Many connector configurations are possible, sometimes involving closely-spaced ducts. In order to obtain a connection that is more resistant to corrosion, the designer also has the option of using epoxy-coated connectors and/or plastic ducts. The design flexibility inherent in these connections led to a substantial number of parameters that were studied in the experimental program. Unfortunately, as mentioned in Chapter 1, little is known about the behavior of grouted vertical duct connections,

and even less about the influence of these different parameters on connection performance. An ambitious testing program was developed to collect as much data as possible and obtain a better understanding about the behavior of these connections. Based on issues that were raised by TxDOT during construction of precast bent caps and during conversations with engineers that were designing them, a list of parameters to be studied was created. Due to the size of test specimens, the practical limitation on the number of tests that could be conducted during this investigation led to reducing the list of main parameters that were investigated experimentally. Identification of the main parameters was based on three considerations: uncertainty associated with each parameter, their expected impact on behavior and durability of the bent cap, and their relation to current and future design practices.

Although none of the main parameters had been studied previously in the laboratory, some parameters were expected to have a greater influence on the bent cap behavior than others. For instance, duct material and group effects were expected to impact connection behavior more than connector diameter and the ratio of duct diameter to connector diameter.

3.2.1 Bar Coating

Ordinarily, ACI 318-05 [3.1] requires that the development length of epoxy-coated reinforcing bars be increased from 20 to 50 percent relative to uncoated bars due to a lack of adhesion and reduced friction between the bar and the concrete. The smaller increase of 20% can be used when the cover and spacing between bars is large, thereby precluding a splitting failure. The AASHTO LRFD Bridge Design Specification [3.2] uses the same modification factors. To explore the effect of coating on connector behavior, comparison tests were conducted using both epoxy-coated bars, and uncoated bars (Figure 3.1).

3.2.2 Duct Material

The duct material that is typically used in grouted vertical duct connections is the same as is used for post-tensioning applications. The ducts are inexpensive and readily available, they form a stay-in-place sleeve in the bent cap to house the connectors, and they come in a variety of sizes and corrugation patterns. Typically, these ducts are made of galvanized steel or from plastic materials like polyethylene or polypropylene. The main functions of the duct are to serve as a sleeve for the connector and to permit the transfer of forces within the connection. From a structural point of view, the galvanized steel duct was expected to perform better than the plastic ducts, due to adhesion and enhanced friction or mechanical interlock between the duct and both the surrounding concrete and the grout. Previous research conducted by Matsumoto et al. [3.3], only explored the use of galvanized steel ducts. Since that research was conducted, there has been an increased interest in the use of plastic duct materials to inhibit corrosion in the connection.

A large portion of the testing program dealt with comparing the performance of connections configured with different duct materials. Three different duct types were selected for the investigation. The first type was made of a corrugated galvanized strip steel material conforming to ASTM A653 with a 26-gauge thickness (Figure 3.2). The other two duct types were made from different plastic materials: one was made of high-density polyethylene (Figure 3.3), and the other was made of polypropylene (Figure 3.4). Because the bond transfer mechanism between the plastic duct and the concrete/grout depends mainly on friction and mechanical interlock, the influence of the rib pattern on behavior can be of great consequence. For the plastic duct types considered, the duct made of polypropylene had a smaller spacing between corrugations. It was important to determine how the corrugation pattern, and not only the material, affects the

performance of a connection. For all duct types, only one duct size of 4-in. nominal diameter was used. Table 3.1 summarizes the geometries of the three duct types used.

3.2.3 Embedment Depth

The capacity and failure mode of a connector are largely determined by the length of embedment. In general, deep embedment depths will produce a ductile mode of failure, while reduced ductility and low capacities are expected from shallow embedment depths. A main objective of this investigation was to correlate connection performance with variation in the embedment depth of the connectors, given a particular connection configuration. The configuration includes parameters such as duct material, number of connectors, clear spacing of ducts, and arrangement of the ducts. The embedment depth parameter was thus logically linked in a special way to all of the other parameters under investigation.

Initially, shallow embedment depths were explored in single-connector tests in order to establish the different failure modes characteristic of these types of connections. As testing progressed, and tests involved more than one connector, the embedment depth was increased, and other modes of failure were observed. The three different embedment depths selected were 8, 12, and 16 times the connector diameter ($8d_b$, $12d_b$, and $16d_b$).

3.2.4 Group Effects

Tests involving single connectors are acceptable to obtain general information about modes of failure, and for studying the effects of changes in parameters like bar coating or duct material. However, actual connections are normally constructed using more than one connector, and it is likely that in a precast bent cap connection consisting of several connectors, at least two of these could experience some degree of tension at the same time. Moreover, the

arrangement of connectors in actual connection designs is such that the spacing between them is relatively small, and some level of interaction between them is expected. To investigate this, several tests were conducted with groups of either two or three connectors.

3.2.4.1 Number of Connectors

Tests consisting of multiple connectors had either two or three bars acting in tension simultaneously. Typically, these tests had connectors embedded at $12d_b$ and $16d_b$.

3.2.4.2 Duct Clear Spacing

Precast bent cap connections are currently being designed in Texas using grouted vertical ducts with connectors positioned in close proximity to each other, frequently having a clear spacing between the ducts equal to one duct diameter. To explore the effect of close proximity of the connectors, duct clear spacing from one to two duct diameters was examined. For the 4-in. nominal diameter of the ducts used, this meant center-to-center distances between the connectors of 8 and 12 in. (or approximately $5.7d_b$ and $8.5d_b$ for #11 bars).

3.2.5 Bar Eccentricity

The eccentric placement of connectors inside the duct was considered a main parameter for this investigation after observations of final bent cap placements in the field showed that connectors often made contact with the sides of the ducts. This issue caused concern to the engineers working on the Lake Belton Bridge Project. This situation can occur due to improper alignment of the connectors extending out of the column section, out-of-straightness of the reinforcing bars, or lack of a suitable connector template. A photograph of one of the connections at the Lake Belton Bridge (Figure 3.5), illustrates this situation.

3.2.6 Transverse Reinforcement

Anchorage tests have shown that transverse reinforcement can increase the bond strength between reinforcing bars and surrounding concrete [3.4-3.6]. In the case of a connector acting in tension, transverse reinforcement can increase bond strength by containing radial splitting and sustaining friction between the connector and the concrete. Confinement in a grouted vertical duct connection can have many sources. It can be a local passive form of confinement, like the type a duct provides to the connector and grout system, or it can be a global passive form of confinement like that provided by bent cap reinforcement. Active confinement can also be present in the form of a large compression field near the connection caused by a column or beam reaction. The effect of providing transverse reinforcement in the form of spirals around individual ducts was explored to study local confinement effects. In a similar fashion, the contrasting effect of providing a large round spiral around the entire connection was also evaluated.

3.2.7 Other Parameters

Some parameters that were not considered in this experimental program and that may influence the behavior of grouted vertical duct connections are described below.

3.2.7.1 Connector Type

The connector type may influence the behavior of a grouted vertical duct connection significantly. For example, a shallower embedment depth can be used with a headed connector (Figure 3.6) compared with a straight connector. Headed connectors are seldom considered for use in these connections for two reasons: (1) unit costs are higher; and (2) the enlarged head reduces construction tolerances and may interfere with the inside surfaces of the ducts. Furthermore, although the use of headed connectors at a shallow embedment may increase the connection

capacity substantially, tests conducted during a previous precast bent cap research project [3.3] concluded that their use at a deep embedment does not produce significant increases in capacity.

3.2.7.2 Connector Diameter

The connectors that are normally used in grouted vertical duct connections are large-diameter reinforcing bars, typically #11 bars. This is because the designer typically selects a reinforcement configuration that has a small number of connectors in order to minimize the amount of grout used in the connection and the interference of the vertical ducts with the reinforcement in the bent cap. It is expected that bars as small as #9 may be used in these connections, and it is possible that bars as large as #14 may be used for some large bridge applications. In this investigation, only #11 reinforcing bars were used as connectors. Differences in bond behavior may be observed for connectors with different diameters, but given the small range of connector diameters that will probably be used in these connections; the differences in behavior are anticipated to be small.

3.2.7.3 Ratio of Duct Diameter to Connector Diameter

The selection of the diameter of the ducts used in a particular grouted vertical duct connection is controlled by construction tolerances and by interference with bent cap reinforcement. An efficient design would use the smallest-diameter duct that would accommodate the connector to reduce the amount of grout needed in the connection and minimize reinforcement congestion. However, the selection of the duct diameter must also allow for adequate tolerance to facilitate the placement of the bent cap in the field. A previous research project conducted by Matsumoto et. al. [3.3] recommended that duct diameters be 2 to 3 times the bar diameter and provide a horizontal tolerance of at least 1 in., although a horizontal tolerance of 1.5 in. was considered

preferable. Recent implementation of grouted vertical duct connections in the field has demonstrated that a clearance of at least 1 in. may be sufficient for jobs with a small number of connectors per connection, but that a 1.5-in. tolerance should be used when the number of connectors is large, such as the Lake Belton Bridge (Figure 3.7). Connections consisting of four or six connectors would be classified as having a small number of connectors. Given the range of bar diameters used in grouted vertical duct connections, and with allowance for these minimal horizontal tolerances, it is expected that the ratio of duct diameter to connector diameter will vary between 2.66 and 3.15, as illustrated in Table 3.2. During this investigation, the value was maintained at 2.84, because only #11 reinforcing bars were used as connectors, and the duct size of 4 in. was used for all tests. Small differences in bond behavior are expected with variations of this parameter, similar to the case of connectors with different diameters.

3.2.7.4 Grout Type

The choice of grout type could have a significant influence on the behavior of grouted vertical duct connections. However, the grouts that are typically used in actual connections must satisfy the TxDOT standard grout specification (Table 3.3), which establishes the minimum requirements for precast bent cap connections. Only one type of grout, Masterflow 928, was used during this experimental program. This grout satisfies the TxDOT grout specification, and it was assumed that grouts with similar characteristics would produce similar behavior in bent cap connections.

3.2.7.5 Strength of Concrete

The construction of precast bent cap elements with high-strength concrete can be beneficial to the performance of grouted vertical duct connections. However, it is expected that the capacity of the connections would not increase

substantially with an increase in the concrete compressive strength. One reason is that the formation of radial splitting cracks around the connectors, which limit the load transfer mechanism in these connections, depends not on the compressive properties, but on the tensile strength of the concrete. Because the tensile strength of concrete is related approximately to the square root of the compressive strength, the benefits of added strength are reduced. As a note of caution, to improve the performance of the connection and avoid an undesired failure mode, any increase in concrete strength should be accompanied by a corresponding increase in grout strength.

3.3 SPECIMEN FABRICATION

The test specimens were designed with dimensions representative of actual dimensions within bent cap connection zones, and to provide an efficient means of testing connectors. Because only the connection area of a typical bent cap element was needed for the experiments, there was no need to build an entire bent cap specimen. Instead, the test specimen consisted of a block beam that included a series of connection zones. This was an effective specimen design, because the use of space in the laboratory and material were minimized. It also meant that each test specimen could be used for more than one test, because each contained multiple connection zones. A set of block beams could also be cast simultaneously to minimize the number of casting operations.

Test specimens used on a previous bent cap research project conducted by Matsumoto et. al. [3.3], and bent cap elements being designed and constructed for the Lake Ray Hubbard Bridge, served as a benchmark for establishing the dimensions of the test specimens. The bent cap test specimens tested by Matsumoto, had a width of 2’-9” and a height of 2’-6”, with a side clear concrete cover to the ducts between 7.5 in. and 9 in. The bent caps used in the Lake Ray

Hubbard Bridge, shown in Figure 3.8, are a clear example of typical bent cap dimensions. In this case, the bent caps, which were supported on 3'-0" diameter columns, had a width of 3'-3", and a height of 3'-3". Based on the connection configuration, the clear cover between the side of the bent caps and the vertical ducts was 9.5 in. The size of the piers in this bridge is typical for a multi-column bridge, and TxDOT seldom uses columns smaller than 3'-0" diameter in its bridges.

The dimension of clear concrete side cover to the ducts is an important parameter for the design of the test specimens. A value for this side cover dimension corresponding to a lower bound for what could be expected in an actual connection was considered appropriate. The reasoning for this stemmed from the assumption that increases in side cover to the ducts would lead to enhanced bond strength due to better confinement of the connection and reduced potential for concrete splitting. The dimensions of the test specimens also needed to take into account the general connector configurations that were going to be examined during the tests. One aspect of connection details that was causing concern among designers was the close proximity of connectors in the field. Bridge engineers were designing the connections with a clear distance of one duct diameter between the ducts to satisfy the required number of connectors needed to resist connection forces and to accommodate space limitations of the circular pier section below the cap. An example of this can be seen in the design of the Lake Ray Hubbard Bridge (Figure 3.9). Because this detail was typical of normal practice in current designs, the specimens were constructed with a clear spacing of one duct diameter between the ducts. A square, four-duct pattern was selected as the standard for the experimental program, although a triangular arrangement was also used in the last series of tests. Constraints inherent in the test setup prevented the use of a clear spacing between the ducts in the transverse direction

less than 5.5 in., which for a 4-in. diameter duct, meant that the clear spacing between ducts in the transverse direction could not be less than 1.375-duct diameters.

After processing and evaluating the requirements for dimensions of the test specimens, a square cross-section of 2'-6" was selected (Figure 3.10). This resulted in a clear concrete side cover to the ducts of 8.25 in., which is a realistic lower bound to what could be expected in an actual connection. A depth of 2'-6" was considered adequate because large-diameter connectors, like #11 reinforcing bars, could be embedded as deep as 18 d_b, which was considered sufficient during the initial planning of the testing program. The size of the connection area was somewhat smaller than that usually encountered in prototype bent caps, but deemed adequate for the purposes of the investigation.

The overall length of the beam specimens depended on the number of connection zones provided. Originally, the beam specimens were designed with three connection zones, but lifting limits on some laboratory equipment forced the specimens to have only two connection zones. The overall design length of the cap beam specimens was then 12'-0", and each had a weight of approximately 11 kip.

Reinforcement in the test specimens was designed to resist the anticipated loads during tests and prevent premature shear or bending failure of the concrete beam; failure modes during the testing should only be related to anchorage failure or fracture of the connectors. Nonetheless, some consideration was also given to providing the connection regions of the specimens with a realistic reinforcement scheme, like that used in the Lake Ray Hubbard Bridge bent caps (Figure 3.11). To minimize the influence of the bent cap reinforcement on the connection behavior, stirrups were not placed in the immediate vicinity of the connection, and beam longitudinal reinforcement was not allowed to pass through the central

portion of the connections. The beam specimen reinforcement schematic is shown in Figure 3.12. Longitudinal reinforcement consisted of 6-#8 reinforcing bars at both the top and bottom of the beam. Stirrups were #4 open stirrups at 6-in. spacing. Some specimens included transverse reinforcement around the ducts. Spiral reinforcement is shown in Figure 3.13. Large (group of ducts) spirals had a diameter of 24 in. and a pitch of 6 in.; whereas the small (individual duct) spirals had a diameter of 7.5 in. and a pitch of approximately 1.5 in. Bar diameters were 0.375 in. for the large spirals, and 0.25 in. for the small spirals.

Test specimens were constructed two at a time. Two sets of formwork, shown in Figure 3.14, were used to fabricate all the test specimens. After reinforcing cages were placed inside the formwork, ducts were ready to be placed. Ducts were sealed with duct tape at both ends to prevent penetration of concrete during casting. Duct locations were carefully laid out, and ducts were held in place by small, round, plywood block-outs at both ends to maintain proper alignment during concrete placement (Figure 3.15). Proper positioning and vertical alignment of ducts in the formwork was important because it ensured that the connector would be within tolerance to fit in the space allocated in the test setup. Three sets of anchor rods were also positioned in each specimen: one at mid-length and one at each end to be used to connect the beam to the test setup. Additionally, one lifting insert was placed at each end of the beam.

The specimens were constructed using a normal weight concrete mixture, with a target slump of 4 in. that was mixed in a truck typically in 8-yd^3 batches. The maximum coarse aggregate size was 0.75 in. Concrete was dumped from the truck into a crane-operated hopper (Figure 3.16). Concrete was placed in the formwork in three lifts, with internal vibration after each lift. Concrete at the top surface of each beam was then leveled using 2X4 wood spreaders and finished using steel trowels (Figure 3.17).

A series of 6 in. by 12 in. concrete cylinders was prepared for each batch of concrete using standard procedures. Cylinders were cured in the lab in the same environment as the beam specimens (Figure 3.18). The entire concrete placement operation frequently lasted about one hour. Specimens were covered with large plastic sheets before initial set of the concrete. After initial set, wet burlap was placed between the concrete and plastic sheets and kept moist for three days.

Three or four days after concrete placement, the forms were untied and removed, and the beams were left to gain strength for approximately two weeks (Figure 3.19). It is worth noting that at this point, a precast concrete bent cap in the field would be prepared to be hoisted and positioned into its final position on top of a bridge pier, as shown in Figure 3.20, followed by grouting operations to complete the connection. In contrast, the test specimens used in this investigation do not have accompanying piers to complete the connections. Instead, beams were moved to the testing area where they were set on neoprene pads and leveling shims on three concrete support blocks.

Individual connectors were then positioned within the ducts. The required embedment depth was measured from the top of the beam to the bottom of the connector and each connector was carefully aligned (Figure 3.21). The ducts were then filled with grout. Most of the connection zones had a square four-duct configuration, but usually, connectors were only placed in one or two of these ducts. However, all ducts were filled with grout.

The formwork required for filling the ducts with grout was simple. The bottom of the connection area was sealed with a square plywood panel, held firmly in position by a jacking device from below. At the top of the specimens, connectors were restrained and positioned using a combination of clamps, small shims, and wood craftwork, as shown in Figure 3.22. Vertical alignment of the connectors was checked using surveying equipment.

Only one beam was grouted at a time because the quantity of grout needed for two beams exceeded the volume capacity of the mechanical mortar mixer available in the laboratory (Figure 3.23). Grout was mixed for five minutes, and was then dumped through a 0.25-in. sieve into buckets, which were then taken to the top of the beam for placement of grout inside the ducts. Fluid consistency of the grout was also measured using a flow cone (Figure 3.24), and the temperatures of the mixing water, air, and grout after mixing were recorded. Grout was placed using a gravity tremie-tube method. Grout was poured from buckets into large funnels, which had a 0.625 in. clear plastic hose that extended from the base of the funnel to the bottom of the duct (Figure 3.25). Ducts were thus filled from the bottom up, in a continuous, uninterrupted fashion to avoid the inclusion of air in the grout. A series of 2-in. grout cubes were also prepared using standard procedures for each grouting operation (Figure 3.26). After the ducts were filled, and the grout was beginning to show signs of hardening, normally two to three hours after placement, a curing compound was applied on top of the grout surface, and wet cloth rags were then applied and kept moist for 24 hours.

Three days after grouting, grout formwork was removed and the specimen was brushed, and washed to remove dirt and grout chunks. At this point, fabrication of each specimen was complete. Generally, the grout achieved sufficient strength for testing of connections ten days after the grouting procedure.

3.4 MATERIALS

3.4.1 Steel

Grade 60 deformed bars, conforming to ASTM A615, were used for the connectors as well as reinforcement within the specimens. In the case of the connectors, both epoxy-coated and uncoated bars were used. The yield strength and deformation pattern differed for both types of bar. Moreover, after an initial

set of tests, a discovery was made that there were two kinds of uncoated bars in the connector batch, which had different yield strengths. The deformation patterns of these two uncoated types were very similar, which lead to this fact going unnoticed at the start of the investigation. Still, in all cases it was possible to identify which type of uncoated bar was being used in each test. Yield and fracture strengths for the connectors, based on laboratory testing, are listed in Table 3.4.

Other kinds of steel reinforcement consisted of plain bars to form spirals. Grade 60 plain bars of 0.375-in. diameter were used for the large spirals that confined the entire four-duct connection zone, while smaller 0.25-in. diameter bars were used to confine individual ducts.

The corrugated galvanized strip steel duct used conformed to ASTM A653, and was of 26-gauge wall thickness (Table 3.1). A duct with a larger wall thickness of 24-gauge was available for testing, but due to the limitation on the number of tests, only the steel duct of 26-gauge wall thickness was used in the tests. It is expected that the use of steel ducts with thicker walls would lead to similar, if not better, behavior.

3.4.2 Plastics

As mentioned in Section 3.2.2, the plastic duct material used in grouted vertical duct connections is that same material that is used in post-tensioning applications. The PTI Specification for Grouting of Post-Tensioned Structures [3.7] specifies that corrugated polyethylene and polypropylene ducts shall comply with fib technical bulletin 7: “Corrugated Plastic Ducts for Internal Bonded Post-Tensioning” [3.8]. This bulletin identifies material properties and requirements that have to meet a series of international standards. Because corrugated plastic ducts are a recent innovation, products still differ widely in material properties

and geometric patterns. As a result, they have not reached the level of standardization of corrugated galvanized steel ducts.

Two kinds of plastic duct were used in this investigation: one was made of high-density polyethylene, and the other was made of polypropylene. All ducts had a 4-in. nominal diameter. Corrugations for both types of ducts were circular and intermittent, as shown in Figures 3.3 and 3.4. The duct made of polypropylene had an additional corrugation pattern in the longitudinal direction, designed to improve bond properties. Because the two plastic duct types have equal wall thickness, and because the tensile properties for both materials are similar, differences in behavior were expected to be due to variation in corrugation patterns. The geometries of the plastic ducts used are summarized in Table 3.1.

3.4.3 Concrete

Concrete that was used to fabricate the test specimens was the standard TxDOT Class C mixture, with a minimum compressive strength at 28 days of 3600 psi. Maximum coarse aggregate size was 0.75 in. Table 3.5 displays the mixture design. The measured slump was 4 in. on average, which proved to be satisfactory during the concrete placement operations. Strength control was accomplished by testing standard 6 by 12 in. cylinders at 3, 7, 14, and 28 days after casting. Cylinders were also tested on days that the specimens were tested. The average compressive strength at 28 days for the different batches of concrete was 5100 psi. Additional concrete strength data are included in Appendix C.

3.4.4 Grout

The only type of grout used in the experiments was Masterflow 928 (MF 928). This is a high precision, non-shrink natural aggregate grout and meets the ASTM C 1107 Standard Specification, Grades B and C. More importantly, it also

satisfies the TxDOT Grout Performance Specification, which is summarized in Table 3.3. MF 928 had been used in a previous research project investigating precast bent cap systems [3.3], and proved to be a very reliable material.

On a hot summer day prior to grouting of the first specimen, a series of trial batches were prepared, where the equipment to be used during the actual grouting procedures was tested; these included the mortar mixer, flow cone, funnels, and plastic hoses. These trial batches helped in determining the optimal amount of water to be added per bag of material to obtain the fluidity necessary in the grout to complete the connections within the established working time of the mixture.

For the grouting operations, the water amounts used varied between 1.27 to 1.37 gallons (10.45 to 11.25 lb) of water per 55 lb bag of grout material, which were within the fluid consistency range provided by the manufacturer that would produce an efflux time of 25 to 35 sec using the ASTM C 939 flow cone standard test. Water amounts were adjusted depending on the temperature at the time of grouting. Efflux times measured using the flow cone were generally inconsistent, when compared with the amount of water in the mix or the air temperature, and were always higher than 35 sec. Table 3.6 summarizes temperature data and flow cone results for the grouting operations conducted. Even when the efflux times were high, no re-mixing or tempering of the grout was made. Strength control was accomplished by testing the ASTM C 109 standard 2-in. cubes at 1, 3, 7, and 28 days, as well as on test days. Following standard practice, strength data obtained from the cube tests were multiplied by a factor of 0.8 to obtain the modified grout compressive strength. Table 3.7 shows grout compressive strength data averaged for all grouting operations. Additional grout strength data, such as mix water amounts and temperatures, are included in Appendix C.

3.5 TESTING PROGRAM OVERVIEW

The aim of the experimental program was to gain a better understanding of how different configuration parameters affect the behavior of precast bent cap connections constructed using grouted vertical ducts. Previous tests of grouted vertical duct connections [3.3] had examined only epoxy-coated connectors placed inside steel galvanized ducts. This test configuration was examined early in the testing program.

The experimental program included the construction of twelve beam specimens, built two at a time. The program was thus divided into six series of tests, with each pair of specimens representing one series. The initial series concentrated on testing single connectors at shallow embedment of 8 and $12d_b$, primarily to establish failure modes of connectors, and as a preliminary exploration into the effect of duct material on connector capacity. As testing progressed into later series, multiple bars were tested, and the embedment depth of connectors was increased. The effect of bar coating was a parameter that was studied early in the program. Because the reduction in bond strength was less noticeable as embedment was increased, the parameter of bar coating was taken out of the test matrix for subsequent test series.

The second test series concentrated mainly on the parameter of duct material. It is worth noting that through the first four test series, only two types of duct were included for investigation; at this time, only galvanized steel ducts and high-density polyethylene were considered. In this series, four single connector tests at $12d_b$ embedment were performed. The first had a polyethylene duct, the second a galvanized steel duct, and the last two had no-duct at all. For the no-duct condition, a corrugated steel duct was cast in the beam so that it could be easily removed. The grout was then poured into the void left by the duct and bonded directly to the concrete.

The third series was the first to explore the effect of multiple connectors. This series focused on double connector tests at $16d_b$, placed either inside polyethylene or steel ducts, with and without global spiral reinforcement. This test series was critical and defined to a great extent the tests that followed.

The fourth and the fifth series, continued the investigation of group effects, and included respectively the parameters of bar eccentricity and local spiral reinforcement around individual plastic ducts.

A third type of duct material, polypropylene was included for investigation during the sixth and last series of testing. The inclusion of this third duct type resulted in a comparison of behavior between two types of plastic duct. This last series further explored the effect of multiple bars a step further by simultaneously testing three bars arranged in a triangular pattern. A tabular synopsis of the testing program is presented in Table 3.8.

3.6 REFERENCES

3.1. ACI Committee 318, "Building Code Requirements for Structural Concrete and Commentary," *ACI 318-05/ACI 318R-05*, American Concrete Institute, Farmington Hills, MI., 2005.

3.2. Association of State Highway and Transportation Officials (AASHTO), *AASHTO LRFD Bridge Design Specifications*, 3rd ed., AASHTO, Washington, D.C., 2004.

3.3. Matsumoto, E.E., Waggoner, M.C., Sumen, G., Kreger, M.E., Wood, S.L., and Breen, J.E., "Development of a Precast Bent Cap System," Research Report 1748-2, Center for Transportation Research, University of Texas at Austin, January 2001.

3.4. Eligehausen, R., Popov, E. P., and Bertero, V. V., "Local Bond Stress-Slip Relationship of Deformed Bars Under Generalized Excitations," Report No. UCB/EERC-83/23, Earthquake Engineering Research Center, University of California, Berkeley, CA, October 1983.

3.5. Astrova, T. I., Dmitriev, S. A., and Mulin, N. M., "The Anchorage of Deformed Reinforcing Bars in Ordinary and Prestressed Reinforced Concrete," Transactions of the Scientific-Research Institute of Concrete and Reinforced Concrete of the Academy of Building and Architecture, issue 23, Moscow, 1961.

3.6. Tepfers, R, "A Theory of Bond Applied to Overlapped Tensile Reinforcement Splices for Deformed Bars," Publication No. 73:2, Division of Concrete Structures, Chalmers University of Technology, Göteborg, 1973.

3.7. PTI Committee on Grouting Specifications, "Specification for Grouting of Post-Tensioned Structures," Post-Tensioning Institute, First Edition, 2001.

3.8. Task Group 9.6 Plastic Ducts of fib Commission 9, "Corrugated Plastic Ducts for Internal Bonded Post-Tensioning," *Bulletin no. 7*, International Federation for Structural Concrete ***fib***, Lausanne, Switzerland, 2000.

Table 3.1 Duct Dimensions

	Galvanized Steel	Polypropylene	HD Polyethylene
Internal Diameter (in.)	3.97	3.94	3.94
Wall Thickness (in.)	0.018	0.118	0.118
Corrugation Height (in.)	0.12	0.20	0.20
Rib Spacing (in.)	0.85	1.55	2.36

Table 3.2 Ideal Combinations of Connectors and Ducts

Bar Size	**#9**	**#10**	**#11**	**#14**
Bar Diameter (in.), d_b	1.128	1.270	1.410	1.693
Minimum duct diameter, d_b + 2"	3.128	3.270	3.410	3.693
Target duct diameter, d_b + 3"	4.128	4.270	4.410	4.693
Selected Duct Diameter, D	3.5"	4"	4"	4.5"
D/d_b	**3.10**	**3.15**	**2.84**	**2.66**

Table 3.3 TxDOT Grout Performance Specification

Property	Values	
Mechanical	**Age**	**Compressive strength (psi)**
Compressive strength	1 day	2500
(ASTM C-109, 2-in. cubes)	3 days	4000
	7 days	5000
	28 days	5800
Compatibility		
Expansion requirements	Grade B or C – expansion per ASTM C 1107	
(ASTM C 827 & ASTM C 1090)		
Modulus of elasticity	$3.0\text{-}5.0 \times 10^{6}$ psi	
(ASTM C-469)		
Coefficient of thermal expansion	$3.0\text{-}10.0 \times 10^{-6}$ /ºF	
(ASTM C-531)		
Constructability		
Flowability	Fluid consistency efflux time: 20-30 seconds	
(ASTM C-939;		
CRD-C 611 Flow Cone)		
Set Time (ASTM C-191)		
Initial	3-5 hr	
Final	5-8 hr	
Work Time	30 min @ 80ºF	
Durability		
Freeze Thaw (ASTM C-666)	300 cycles, RDF 90%	
Sulfate Resistance	Expansion at 26 weeks < 0.1%	
(ASTM C-1012)		

Table 3.4 Connector Strengths

Bar Type	Yield Strength (ksi)	Fracture Strength (ksi)
#11 Epoxy-coated	68	102
#11 Uncoated Type I	75	106
#11 Uncoated Type II	59	95

Table 3.5 TxDOT Class C Concrete Mixture Design

	Cement	Coarse Agg. (0.75-in.)	Fine Agg.	Water	Retarder (oz.)
lb/yd^3	564	1882	1191	250	24

Table 3.6 Grout Operations Temperature and Efflux Time Data

Grout Operation	Water (lb/bag)	Air Temperature (deg F)	Efflux Time (sec)	Comments
1	11.25	85	44	Minimal clumps
2	11.25	86	65	No clumps
3	11.25	81	77	No clumps
4	11.00	69	60	Few clumps
5	10.75	70	81	Few clumps
6	10.75	70	83	Few clumps
7	11.25	66	56	Minimal clumps
8	11.00	76	86	Few clumps
9	11.00	91	68	Minimal clumps
10	10.45	85	101	Few clumps
11	10.45	76	96	Low workability
12	11.00	67	81	Low workability

Table 3.7 Average Grout Compressive Strengths for the Tests

Age (days)	Modified Grout Compressive Strength (ksi)
1	3.1
3	4.0
7	5.0
28	6.2

Table 3.8 Tabular Synopsis of Testing Program

Test Parameters	**Test Series**					
	1	**2**	**3**	**4**	**5**	**6**
Bar Coating	**X**	**X**				
Duct Material	**X**	**X**	**X**	**X**	**X**	**X**
Embedment Depth	**X**		**X**	**X**	**X**	**X**
Group Effects						
Number of Connectors			**X**	**X**		**X**
Duct Clear Spacing					**X**	
Bar Eccentricity				**X**		
Transverse Reinforcement			**X**		**X**	

X- Test Parameter directly under investigation

Figure 3.1 Epoxy-coated and Uncoated Deformed Bars

Figure 3.2 Corrugated Galvanized Steel Duct

Figure 3.3 Corrugated High-density Polyethylene Duct

Figure 3.4 Corrugated Polypropylene Duct

Figure 3.5 Improper Alignment of Reinforcing Bars that Project from Bridge Column at Lake Belton Bridge Project

Figure 3.6 Headed Connector

Figure 3.7 Connections with a Large Number of Connectors Require Larger Construction Tolerances (Lake Belton Bridge)

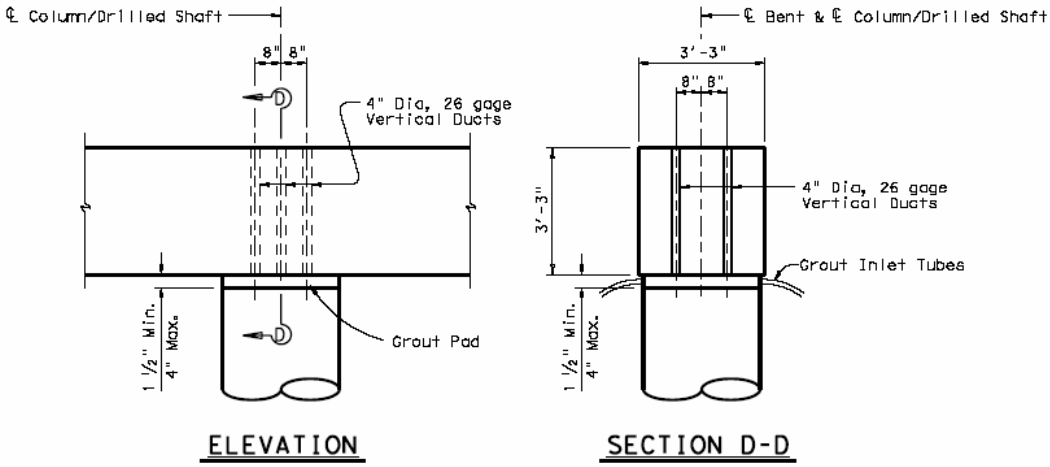

Figure 3.8 Lake Ray Hubbard Bridge Project – Connection Area Dimensions

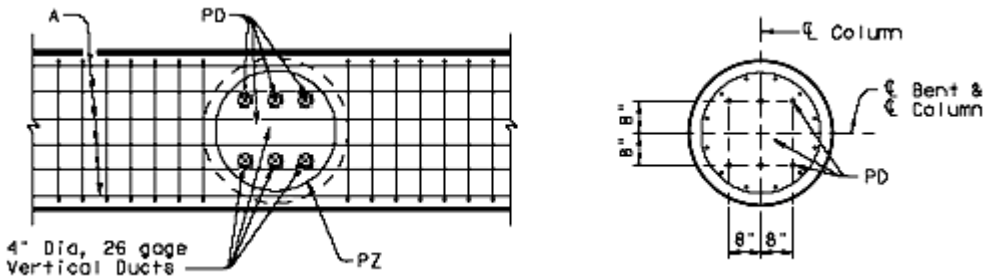

A. Connection Area (Plan) ***B. Pier/Column Section***

Figure 3.9 Lake Ray Hubbard Bridge Project – Placement of Connectors Relative to Pier Section

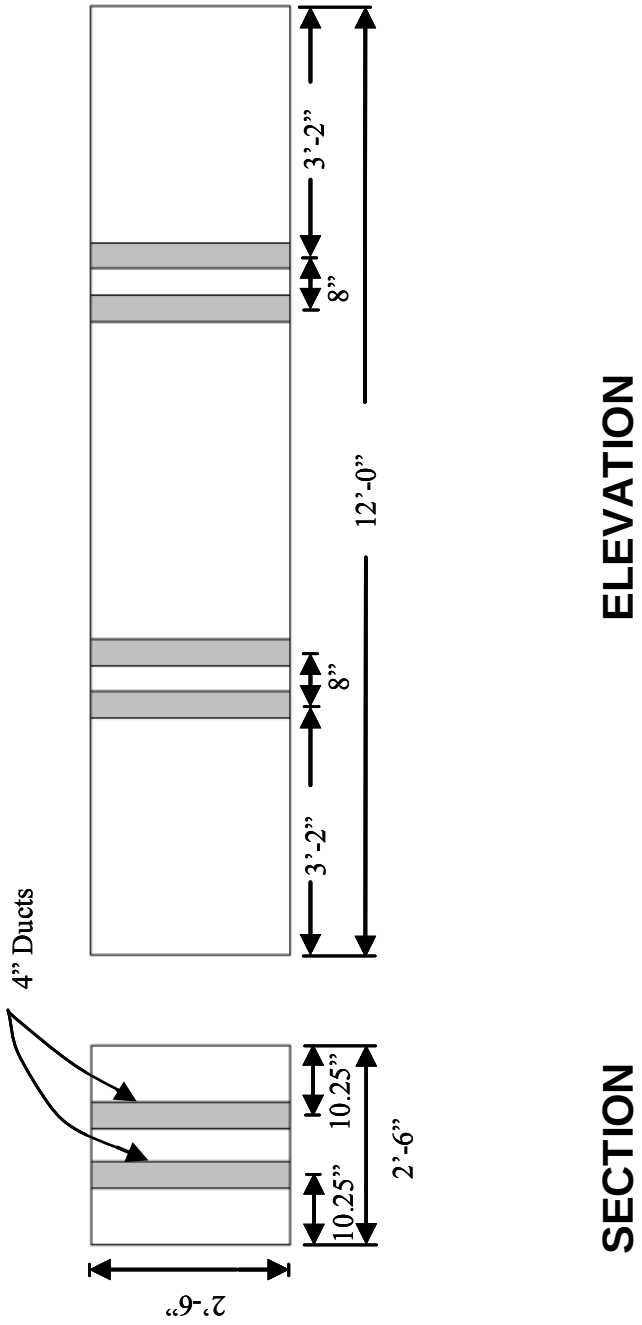

Figure 3.10 Test Specimen Dimensions

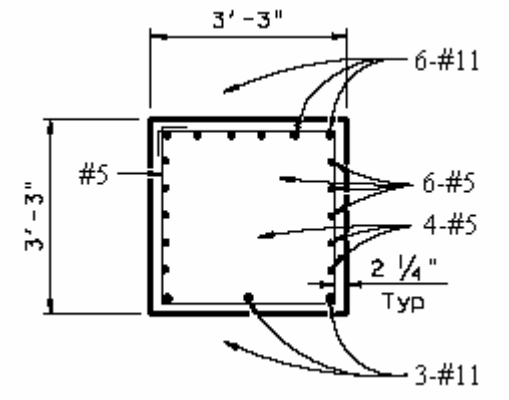

Figure 3.11 Lake Ray Hubbard Bridge Project – Bent Cap Reinforcement at Connection Zones

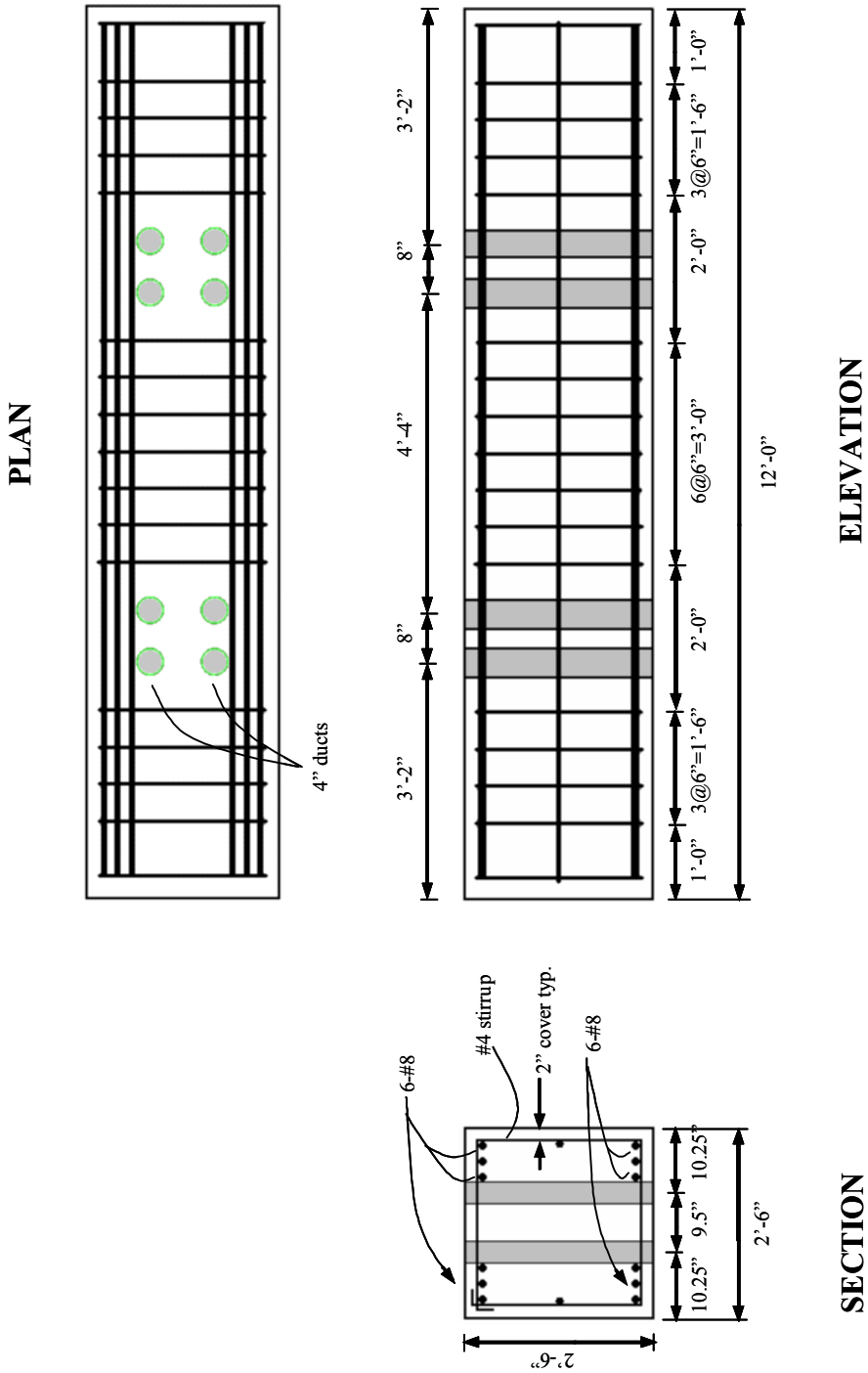

Figure 3.12 Test Specimen Reinforcement Scheme

A. Local Reinforcement *B. Global Reinforcement*

Figure 3.13 Spirals Used as Transverse Reinforcement

Figure 3.14 Test Specimen Formwork

Figure 3.15 Vertical Alignment of Ducts during Concrete Placement

Figure 3.16 Specimen Casting with Aid of Crane-operated Hopper

Figure 3.17 Concrete Finishing Operations

Figure 3.18 Preparation of Concrete Cylinders

Figure 3.19 Beam Specimens after Formwork Removal

Figure 3.20 Precast Bent Cap Placement over Bridge Pier and Connectors (Lake Ray Hubbard Bridge)

Figure 3.21 Positioning and Vertical Alignment of Connectors in Preparation for Grouting Procedures

Figure 3.22 Formwork to Hold Connectors Aligned and in Place during Grouting

Figure 3.23 Mortar Mixer (2.5 ft^3 capacity) Used to Mix Grout

Figure 3.24 Flow Cone Test to Measure the Fluid Consistency of the Grout

Figure 3.25 Gravity Tremie-tube Technique to Fill Ducts with Grout

Figure 3.26 Preparation of Grout Cubes

CHAPTER 4
Experimental Setup

4.1 INTRODUCTION

A precast bent cap must be designed to resist the axial forces, shears, and bending moments due to the applied loads (Figure 4.1). While it is possible to construct and test a bent cap in the laboratory under the design loads, it was decided to test the connectors under tensile loads to investigate the large number of parameters discussed in Chapter 3. The fundamental behavior of grouted vertical duct connections is centered on the bond transfer mechanism between the connector and the duct with the concrete. Thus, all of the actions that can occur simultaneously in a precast bent cap connection are resisted mainly by some degree of axial tension or compression in the connectors, and tension and compression in the surrounding concrete. Of these, the state of axial tension in the connectors is the one that is critical and that warrants investigation.

A large number of tests were required to study the different combinations of the many variables considered for investigation, therefore a simple and inexpensive test setup that could be used to pull single or multiple connectors was considered appropriate for this investigation. The design of the test setup influenced the choice of instrumentation used to monitor the specimens.

4.2 TEST SETUP

A photograph of the test setup selected is shown in Fig. 4.2. The testing frame consisted of back-to-back C15X40 steel channels, which supported 200-kip capacity center-hole hydraulic rams, load cells, and wedge and chuck assemblies. The channels were bolted together with a 2-in. gap between them. The

connectors, already embedded in the concrete specimens, extended between the channels. Three short wide-flange cross beams provided support for the channels, and transferred the loads to the concrete test specimen below. These crossbeams were bolted to both the back-to-back channels, and to the concrete beam for stability purposes. The concrete beam specimens rested on neoprene pads supported by three large concrete blocks, which provided space underneath the specimens for attaching the instrumentation needed to measure the connector end displacement and the beam deflection.

The test setup was arranged so that the bent cap connections were tested in an inverted position. Because the test specimens did not include a bridge pier element, forces acting in the connection were applied by pulling on the connectors. Tension forces in the connectors were then counteracted by reaction forces of the testing frame on the concrete beam specimens. A self-equilibrating force system was thus attained, which meant that attachment of the test setup to the laboratory floor was not required.

The test setup selected for conducting this investigation had these three main advantages: (1) it was simple and self-equilibrating, (2) it was versatile for testing various configurations of connectors with almost no modification, and (3) its testing frame was easy to mount and dismount from one test specimen to the next providing test speed and efficiency. Furthermore, the test setup could be used with confidence, because similar test assemblies have been used successfully in the past for bar pullout tests.

As described in the previous chapter, every beam specimen had two connection zones. Typically, each connection zone accommodated four ducts in a square configuration. The initial series of testing involved many single connector tests with shallow embedment. In order to maximize the number of tests per beam specimen, two single connectors were tested within the same connection zone,

with the test bars positioned in diagonally opposite corners. The results of these initial tests were later compared with the results of tests involving only a single connector per connection zone.

The interaction among multiple connectors was also an important experimental variable during the experiments. Connections containing two and three connectors were also tested. For tests involving two connectors, one set of back-to-back channels was used as the loading frame, because the connectors were oriented to represent a longitudinal moment (in the direction of the bridge) configuration. Double-connector tests representing a transverse moment configuration were not conducted because it was believed that the formation of splitting cracks for this configuration would cause smaller disturbances in the load transfer region than would the longitudinal moment arrangement. During the last phase of testing, three connectors were tested in a triangular configuration. A second set of back-to-back steel channels was used to apply load to the third bar. Figure 4.3 shows the configurations of the different connector arrangements used in the testing program.

The test setup proved to be a very efficient method of applying tensile loads during the experimental program. The only limitation was the minimum spacing of the connectors. The diameter of the hydraulic rams limited the minimum spacing of the connectors to 8 in., or a duct clear spacing of one duct diameter.

Although this test setup did not reproduce the typical state of stress expected in precast bent cap connections, it did produce a conservative load scenario where the connection experiences axial tension. In an actual connection, axial compression is expected to dominate. If tension is experienced by the connectors due to applied moments, the accompanying compression field in the connection provides a confinement effect, which would increase the capacity of

the connector. Additionally, the pier would provide additional confinement that would increase the connector capacity further.

4.3 INSTRUMENTATION

Three types of transducers were used during the tests: (1) load cells to measure applied load on the connectors, (2) strain gages to measure strains in the connectors, ducts, and spiral reinforcement, and (3) linear potentiometers to measure connector, grout, and beam displacements. It was important to obtain information about how load was distributed along the embedded portion of connectors and how much connectors slipped at different load stages. Measurements of strain in ducts and surrounding transverse reinforcement provided an indication of the degree of confinement provided at different load stages. Test data were acquired using a Hewlett Packard 3852A scanner and integrated LabView software, and all measuring devices were properly calibrated before the experiments began.

A 10,000-psi pressure transducer and two center-hole load cells were used to measure applied loads in the connectors. One load cell had a capacity of 200 kip, while the other had a capacity of 400 kip. The pressure transducer was used in all experiments, and load cells were used as needed, depending on the number of connectors. Correlation of data among these different load measuring devices was very good, with most discrepancies being smaller than 1 kip.

Two types of strain gages were used throughout the experiments. Strains in the connectors, transverse reinforcement, and galvanized steel ducts were measured using 5 mm long strain gages, which had a grid area of 7.5 mm^2, and a resistance of 120 ohm. Strain gages used to measure strains on the polyethylene and polypropylene ducts had a larger resistance and a larger grid area due to the poor thermal conductivity of these materials. Based on an excitation voltage of 2

volts, the gages selected for use on the plastic materials had a length of 6 mm, a grid area of 16.2 mm^2, and a resistance of 350 ohm. The strain gages also had a very flexible backing material, which is specially suited for plastic applications.

Surfaces of the materials were carefully prepared and cleaned before strain gages were applied. In the case of the connectors, a small portion of a bar lug had to be ground away to leave a flat surface, long enough to bond the gage and apply the water-proofing and protective coatings. Care was given to grind only the amount of metal necessary to achieve this flat surface. Figure 4.4 shows the surface preparation of the rebar. The adhesive used to bond gages to the metal surfaces was a cyanoacrylate-type adhesive, commonly used in structural experiments. The plastic surfaces had to be pre-treated with a poly-primer compound before bonding the gage using the same cyanoacrylate adhesive. After visually confirming that the bonding procedure was successful, a series of water-proofing and protective coatings was applied to the gages.

For the case of the strain gages bonded to metal surfaces, the first water-proofing coating consisted of an acrylic-based solvent. This solvent, once dry, forms a hard, but tough coating over the gage. Two coats of this solvent were applied within a 45-minute interval. This acrylic-based solvent was not used on the gages bonded to plastic materials because it could provide sufficient stiffness to constrain the gage. Therefore, a more flexible water-proofing coating was used over the gages installed on plastic materials. Two coats of a silicone rubber compound were applied over the gages, also within a 45-minute interval.

Additional coatings were the same for both metal and plastic surfaces. A second water-proofing coating consisting of a layer of butyl rubber was applied over the first coating, as shown in Figure 4.5. Then, a pad of neoprene rubber was placed over the butyl-rubber to give some mechanical protection to the gage, which was followed by application of aluminum foil tape to completely cover the

gage, as shown in Figure 4.6. Following these procedures, none of the gage installations were damaged due to moisture penetration or placement of concrete.

Strain gages were typically placed at 6 in. intervals along the embedded portion of each connector. Hence, the number of strain gages attached to each connector depended on the length of embedment. Figure 4.7 shows strain gage locations for a connector with an embedment depth of $12d_b$. Two diametrically-opposed strain gages were located at the lead end of the connector to monitor bar bending during tests. The stress distribution along the connector was determined based on the connector strain readings.

Strain gages were placed in two orientations on the galvanized metal ducts: in the circumferential direction and at an angle parallel to the seams of the duct (Figure 4.8). Strain gages were placed 4, 8, 13, and 18 in. from the top of the duct in the circumferential direction, and one gage was placed at 8 in. from the top of the duct parallel to the seams. On the plastic ducts all gages were placed in the circumferential direction at distances of 4, 8, 13, and 18 in. from the top of the duct. In a limited number of tests, one additional strain gage was placed 6 in. from the top of the duct to measure axial strain in the plastic duct. A polyethylene duct with complete strain gage installations is shown in Figure 4.9. The actual number of strain gages attached to a duct may be smaller if the embedment depth of the connector was shallow. Figure 4.10 shows a group of galvanized steel ducts with complete strain gage installations as they were being placed in the formwork.

Figure 4.11 illustrates the test setup with the instrumentation used to measure applied loads and displacements of the connectors, grout, and beam specimen. Load-displacement behavior of connectors was determined by measuring their lead and end displacements. The lead displacement was measured using two, 2-in. linear potentiometers placed on a stainless steel angle attached to the connector, as shown in Figure 4.12. Taking the average of the readings of two

linear potentiometers would correct for any tilt experienced by the connector during testing. The connector end displacement was measured with the help of a threaded rod that extended through the bottom of the specimen and was screwed into the end of the connector, and to which was attached a string-type linear potentiometer. The threaded rod was protected from the grout by copper sheathing.

Displacement of the concrete beam was also measured using a string-type linear potentiometer. This beam deflection was then subtracted from the experimental connector lead and end displacement values during the data analyses to obtain the actual connector displacements. Figure 4.13 shows the instrumentation placed underneath the beam specimen.

Relative displacements between the grout and concrete were measured using a 2-in. linear potentiometer that was mounted on a small metal stand epoxy-glued to the top of the concrete beam (see Figure 4.12). A small Plexiglas square was epoxy-glued to the top of the grout surface to serve as a smooth level surface for the tip of the linear potentiometers. Monitoring of the relative displacement between the grout and concrete was sometimes limited by the spreading and widening of radial cracks emanating from the ducts. However, the data were useful in acquiring information about slip of the connectors and about anchorage of the grout being confined by the duct.

4.4 TEST METHOD

After zeroing all electronic data channels, load was slowly applied to each connector using a 200-kip hydraulic ram located on top of the back-to-back channels. The hydraulic rams were actuated by a pneumatically-operated hydraulic pump. Application of pressure makes the piston of each ram move upward, which in turn presses upward on the chuck and wedge assembly causing

the wedges to grip and lift the connector. Typically, a load cell was placed between the ram and wedge-chuck assembly to measure the applied load; a pressure transducer was also connected to the hydraulic pump to measure the applied load.

At the initial stages of testing, load was applied in 2-kip increments until the first signs of cracking were observed. Beam specimens were frequently monitored for the presence of cracks both in the grout and in the concrete. Data channels were scanned continuously every 3 sec during testing. The applied load and connector lead displacements were plotted in real-time during the experiments to aid in assessment of cracking and bar yield. At intermediate load stages, when cracking became significant, load was applied in 1-kip increments. Throughout each test, crack patterns were marked on the specimen with an indication of the load at which they appeared, until capacity of the connection was reached. Loads recorded on the specimens, and in further data analyses correspond to the forces acting on individual connectors, and not the summation of the group. Photographs of specimens were also taken at different stages of loading to serve as documentation for each test. Figure 4.14 shows cracks for one test at an intermediate load stage.

Load was applied until failure of the connection occurred. In cases where the test involved more than one connector, forces on each connector were kept approximately equal because the loading mechanism was force-controlled. Although the majority of these multiple-connector tests failed as a group, there were some instances where one connector failed before the others. In these cases, the failure load was taken as the load acting on the connection when the first connector failed, even though the remaining connectors sometimes reached a higher load when reloaded.

The majority of the tests proceeded without any irregularity. Small noises were heard during some tests in the initial stages of loading, which corresponded to the wedge grip adjusting around the connector. Corresponding levels of slip were recorded. The application of load was interrupted during one test when a set of wedges was installed incorrectly and prevented the load from increasing beyond intermediate load levels. The specimen was immediately unloaded, and a new set of wedges was installed at a different location along the connector. Reloading proceeded until failure was achieved without any further irregularities.

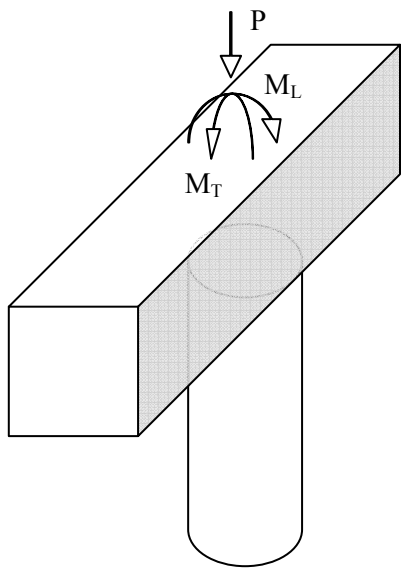

Figure 4.1 Expected Applied Loads on a Precast Bent Cap Connection

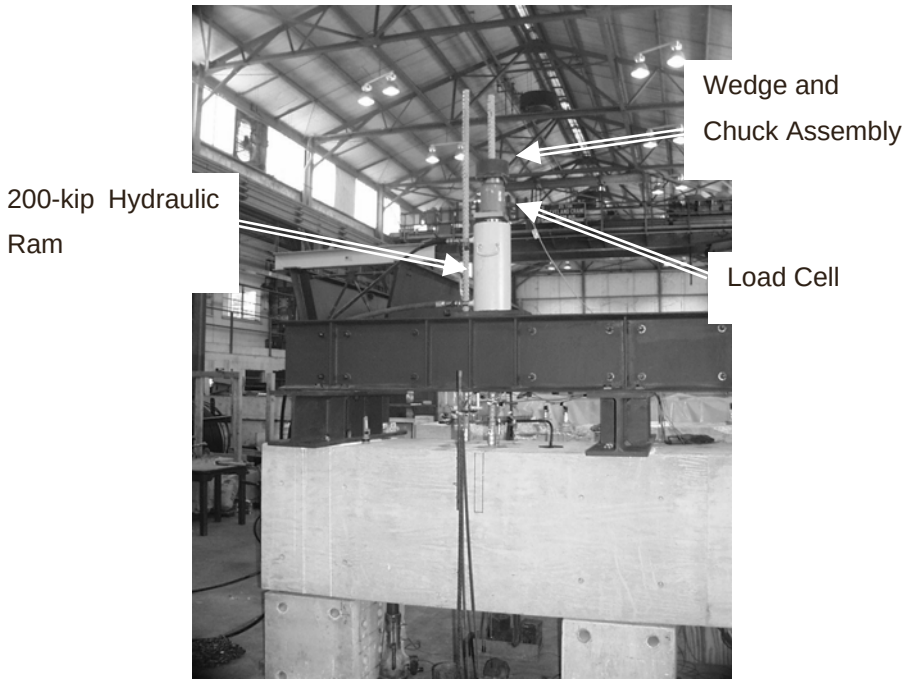

Figure 4.2 Test Setup

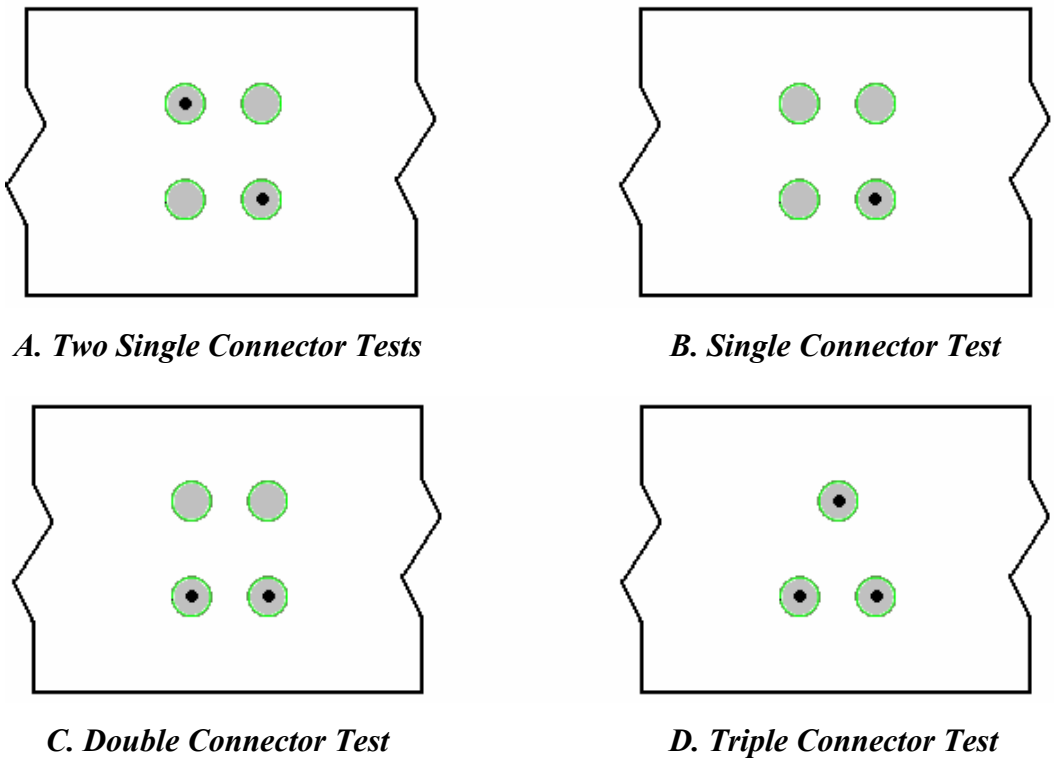

Figure 4.3 Test Connector Arrangements

Figure 4.4 Surface Preparations on a Connector for Bonding a Strain Gage

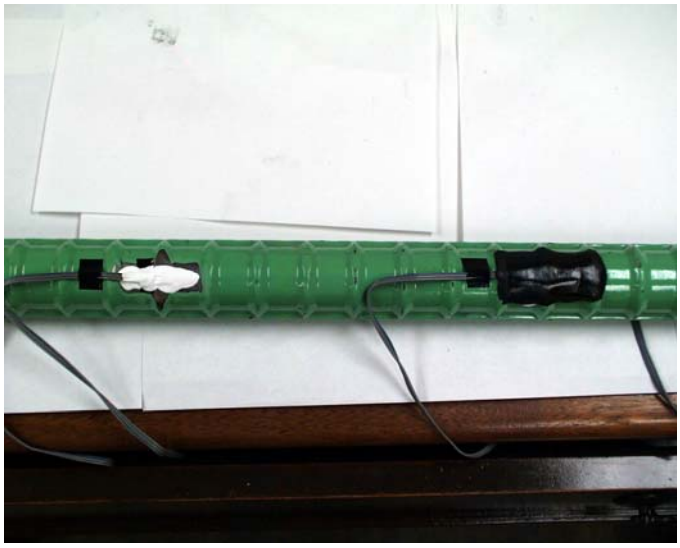

Figure 4.5 Layers of Waterproofing Protection on Gage Installations Bonded to Metal Surfaces

Figure 4.6 Two Completed Strain Gage Installations

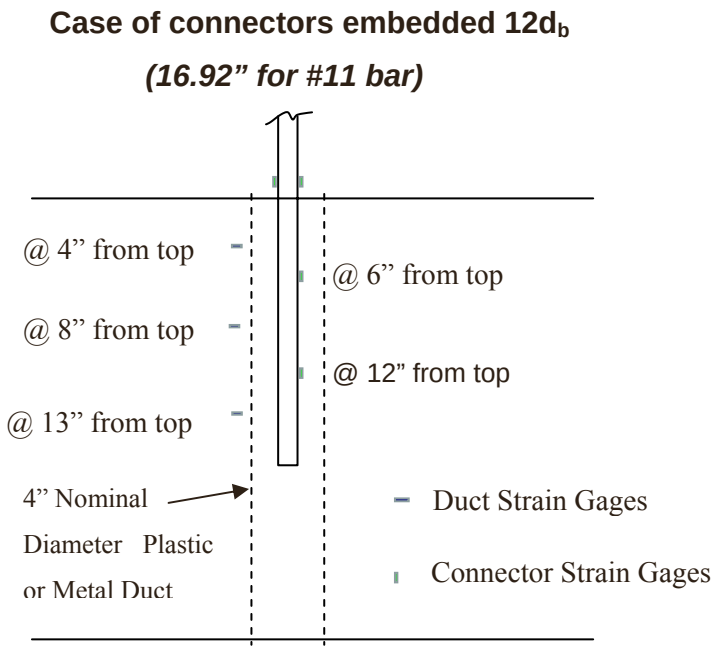

Figure 4.7 Typical Strain Gage Locations on Connectors and Ducts

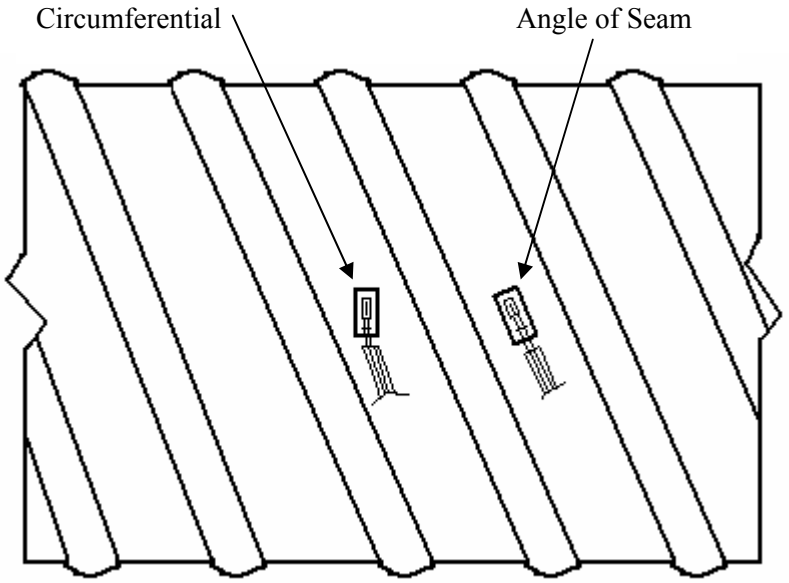

Figure 4.8 Strain Gage Orientations on Galvanized Steel Duct

Figure 4.9 Completed Gage Installations on HD Polyethylene Duct

Figure 4.10 Completed Strain Gage Installations on Galvanized Steel Ducts

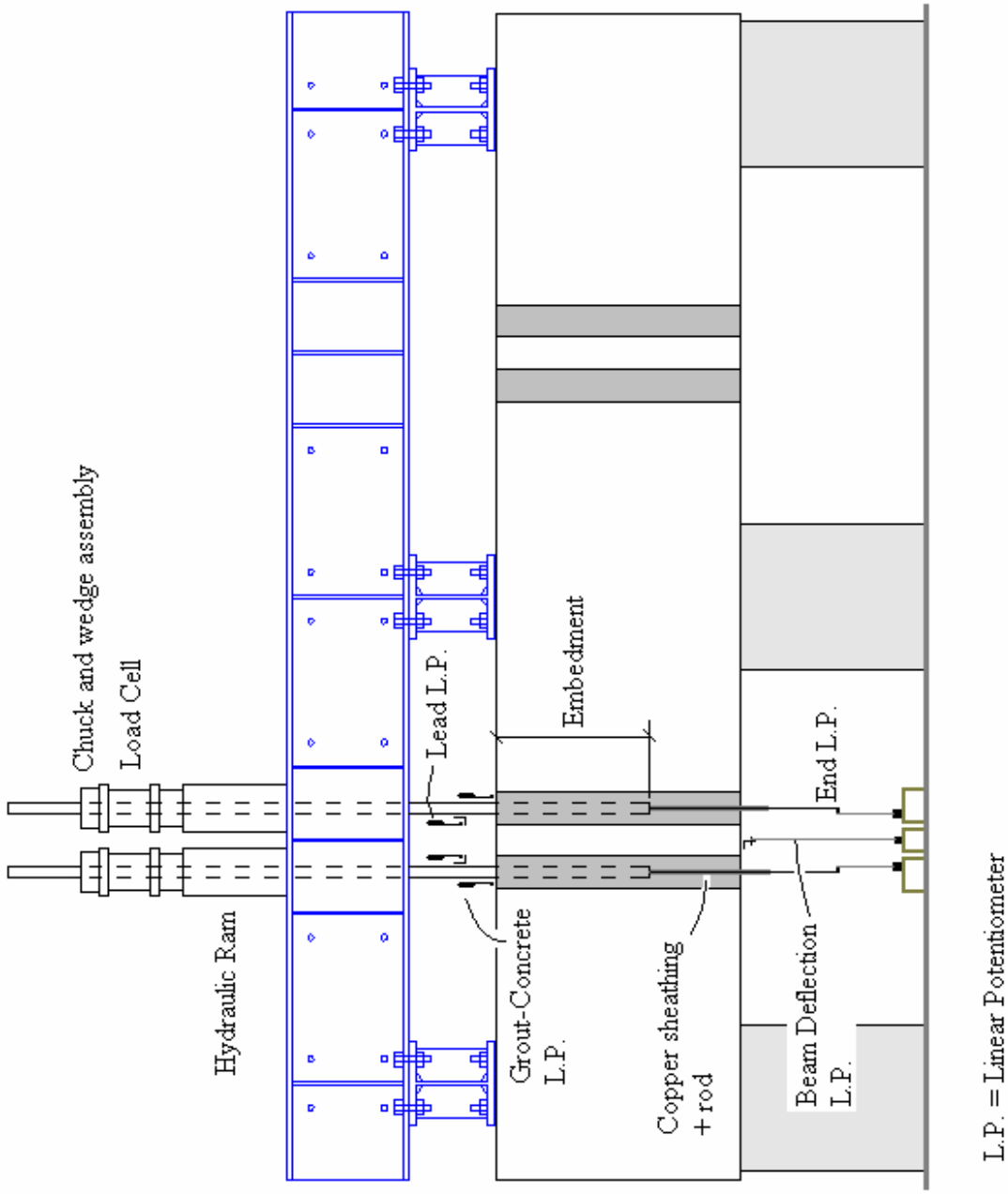

Figure 4.11 Schematic of Test Setup and Instrumentation

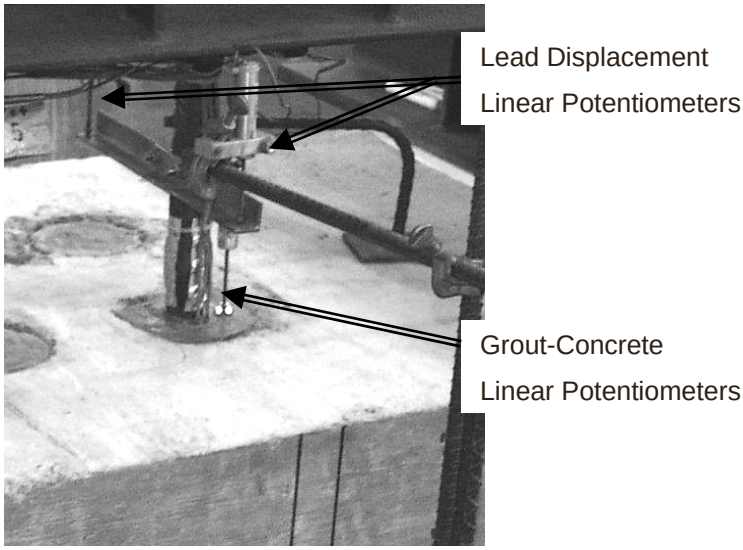

Figure 4.12 Instrumentation to Measure Lead Connector Displacement and Relative Displacement between Grout and Concrete

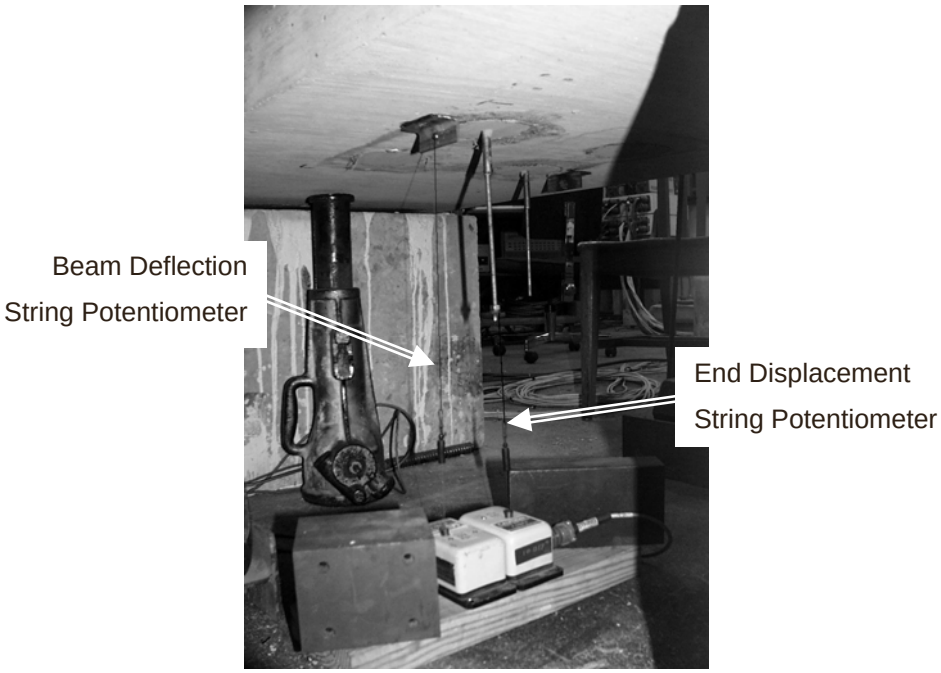

Figure 4.13 Instrumentation to Measure End Connector Displacement and Beam Deflection

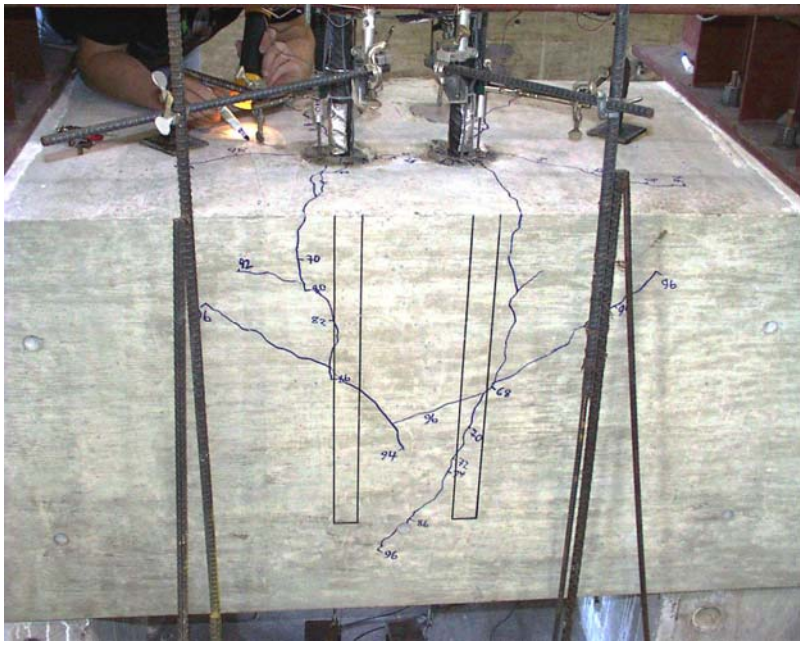

Figure 4.14 Marking of Crack Formations during a Test

CHAPTER 5
Measured Response

5.1 INTRODUCTION

The presentation of the test results is divided into three groups, determined by the duct material present in the connection test specimen. Besides connector embedment depth, the parameter of duct material affects most significantly the capacity of grouted vertical duct connections, and can determine to a great extent the mode of failure of the connection. The measured response is presented separately for specimens using galvanized steel ducts, polyethylene ducts, and polypropylene ducts.

All of the thirty-two connection specimens tested failed by pullout of the connectors. This type of failure, instead of a failure involving fracture of the connectors, was observed due to the relatively shallow embedment depths explored during the tests. A pure splitting type failure was not observed due to the presence of a massive amount of cap reinforcement and concrete cover around the ducts housing the connectors. Still, radial splitting cracks emanating from the duct surfaces developed during most of the tests, especially those involving more than one connector, but failure was mostly a pullout type accompanied by concrete cone breakouts. The different failure modes identified are described in the following section.

Table 5.1 shows the test matrix and selected test results for the testing program. The results for a representative set of tests of each duct material group are presented in detail. For the representative specimen connections, the measured response can be described as follows: (1) stress-end slip diagrams (Section 5.4), (2) strain distribution along the connector (Section 5.5), (3) stress distribution

along the connector (Section 5.6), (4) stress-slip of connector relative to grout diagrams (Section 5.7), and (5) strain measurements in the ducts (Section 5.8). In addition, results of visual observations of crack development (Section 5.3), such as radial splitting, are presented for the representative specimen connections.

End slip and strain values were obtained directly from experimental measurements. In (1), the stress was obtained directly by dividing the load measured during the tests by the respective connector cross-sectional area. To obtain the connector stress distribution in (3), the stress-strain relationships for the three kinds of connectors were needed. A simple mathematical model (Appendix B) was used, which was calibrated to tensile tests of actual connectors. Slight discrepancies between the real stress-strain curve for a given connector and the mathematical model used for converting strain to stress can lead to some error, mainly for converted stress values in the strain-hardening region.

Figure 5.1 shows the relationship between the grout displacement, δ_g, and the connector end displacement, δ_e. Three main scenarios of behavior are described in the figure: (1) δ_e equals δ_g, which suggests that the entire connector and the grout are pulling outward together as a unit (plug), (2) δ_e is smaller than δ_g, suggesting that the top portion of the grout is moving upward together with the lead end of the connector, while the end portion of the connector is moving upward a smaller amount, and (3) δ_e is greater than δ_g, implying that the connector, as a whole, is slipping out of the grout. The slip of the connector relative to the grout, δ_{srg}, corresponds to the difference between the measured end slip, δ_e, and the displacement of the grout relative to the concrete specimen, δ_g.

5.2 OBSERVED FAILURE MODES

Different pullout modes of failure were observed, where typically the bar and a portion of the grout would pullout together as a unit either out of the duct or

together with the duct out of the concrete. At deep embedment depths, connectors often reached their yield load, with pullout failure occurring at a much larger load.

The duct material affected significantly the capacity of the connection specimens, and determined to a great extent the pullout mode of failure. The presentation of the observed failure modes is presented separately for specimens using galvanized steel ducts, polyethylene ducts, and polypropylene ducts.

5.2.1 Galvanized Steel Duct Specimens

The pullout failure mode for connection specimens involving galvanized steel ducts was that of connector pullout together with a top segment of the grout and the duct. The length of the top segment of duct and grout being pulled out with the connector depended largely on the number of connectors per connection, and not so much on the connector embedment depth. This segment length was related to the depth of the cone-shaped concrete breakout zone that formed in the connection area at failure. The galvanized duct was very good at confining the grout and also at preventing slip of the grout. At failure, when the connector pulled out, a segment of the duct separated from the rest and moved upward with the connector; the seams of the duct opened at the location of a fracture surface that had formed in the grout. Figure 5.2 shows the mode of failure for the connections involving galvanized steel ducts. In single-connector tests, having connector embedment depths of 8 and 12d_b, the slit or tear in the duct occurred at depths between 2.5 and 4.5 inches. The slit or tear in the duct formed deeper when more than one connector was tested. When two connectors were tested, having embedment depths of 12 and 16 d_b, the slit in the duct occurred between 6.5 and 9.5 in. below the surface of the specimen. In the triple-connector Test No. 31, slits formed deeper in the duct, the shallowest at 14.5 inches below the surface.

5.2.2 Polyethylene Duct Specimens

The failure modes of connection specimens involving polyethylene ducts were characterized by the inability of the duct to provide sufficient anchorage to the grout. Three different pullout failure modes were observed in these connections: (1) pullout of connector with a top segment of the grout, (2) pullout of connector with a top segment of the grout and the duct, and (3) pullout of the connector and the grout out of the duct or plug failure. Figure 5.3 shows these different failure modes. The second pullout mode of failure could be regarded as an intermediate failure condition between the first and the third failure modes. The pullout failure mode of connector and grout slipping out of the duct normally included a top segment of the duct that separated from the rest and that remained attached to the grout. Also observed in this third failure mode, was the shearing of the ribs that formed in the grout at the location of the duct corrugations as the grout slipped out of the duct. Connector embedment depth and the number of connectors per connection influenced somewhat the type of pullout failure that occurred. Single connectors embedded 8 and 12 d_b generally exhibited pullout of the connector with a top segment of the grout. The prevailing failure mode observed in multiple connector tests and in tests of single connectors embedded $16d_b$ was that of pullout of the connector and the grout out of the duct. In tests involving more than one connector, different pullout failure modes were sometimes observed in the connectors.

5.2.3 Polypropylene Duct Specimens

The four connection tests that involved polypropylene ducts exhibited one main mode of failure: connector and grout pullout (plug) with a top segment of the duct attached. The polypropylene duct was generally good at preventing slip of the grout. The length of the top segment of the duct being pulled out with the

grout and the connector depended on the depth of the cone-shaped concrete breakout zone that formed in the connection area at failure. This top segment of the duct came out intact every time. The rest of the duct sometimes remained attached to the grout, with only the duct/grout ribs getting sheared off as the grout and connector pulled out. Figure 5.4 shows the mode of failure for the connections involving polypropylene ducts. No differences were seen in modes of failure of the connections as a result of variation in embedment depth or in the number of connectors.

5.3 VISUAL OBSERVATIONS OF CRACK DEVELOPMENT

During the initial stages of testing, load was applied in 2-kip increments until the first signs of cracking were observed. The beam specimens were frequently monitored for the appearance of cracks both in the grout and in the concrete. Throughout each test, crack formations were marked on the specimen with an indication of the load at which they appeared, until the capacity of the connection was reached. The loads recorded on the specimens during crack formation correspond to the forces acting on individual connectors, and not the summation of the group. Typically, radial cracks would first appear in the grout at an average load of 38 kip (25 ksi) for single connector tests, and at lower loads averaging 26 kip (17 ksi) for multiple connectors.

At intermediate load stages, when cracking in the form of radial splitting became significant, load was applied in 1-kip increments, until failure of the connection. The load level at the onset of splitting in the concrete depended mainly on the embedment depth of the connectors and the number of connectors, and was not sensitive to the strength of the concrete, as can be noticed in Table 5.1. The duct material had influence in the crack formation patterns observed during the tests.

5.3.1 Galvanized Steel Duct Specimens

Typical crack development in test specimens involving galvanized steel ducts is illustrated by discussing Test No. 10, a single-connector test, and Tests No. 13 and 23, two double-connector tests.

Test No. 10 consisted of an uncoated single-connector embedded at $12d_b$ (17 in.). The first signs of cracking occurred in the grout at a load of 26 kip (17 ksi), and as load increased, radial splitting cracks in the concrete started to emerge at loads around 68 kip (45 ksi). A widespread pattern of radial splitting can be seen in Figure 5.5, at an approximate load of 88 kip (58 ksi). The pattern of radial splitting in single connectors was generally axisymmetric, meaning cracks were usually spread equally in all directions. The cracks typically extended over a great part of the surface of the specimens. Figure 5.6 shows the crack pattern at the connection's failure load of 121 kip (80 ksi). The V-shaped cracks that formed on the loaded side of the specimen indicate that the connector, the grout, and the duct were working together as a system that was well anchored in the concrete. The orientations of these V-shaped diagonal cracks indicate the presence of inclined compression struts in the concrete, which are a main part of the resisting mechanism in the connections.

In multiple-connector tests, the cracking pattern was similar to that of single connectors. In Test No. 13, which consisted of two connectors embedded $16d_b$ (22.5 in.), the first signs of cracking occurred in the grout at a load of 24 kip (16 ksi). As loading continued, cracks began to emerge in the concrete and widespread radial splitting was observed at a load of 86 kip (57 ksi) as shown in Figure 5.7. Throughout the test, the cracking pattern of each connector mirrored that of the other. The close proximity of connectors with only a one-duct-diameter (1-D) clear spacing between the ducts caused extensive interaction between the

connectors. At failure, at a load of about 132 kip (87 ksi), both connectors failed together as a unit, as shown in Figure 5.8.

Test No. 23, also a double-connector test, consisted of connectors embedded $12d_b$ with a duct clear spacing of two duct-diameters (2-D). The increased duct clear spacing reduced the level of interaction between the connectors, producing a different cracking pattern for each connector (Figure 5.9). In this test, cracks first occurred in the grout at a load of about 19 kip (13 ksi), and widespread radial splitting was observed at a load of 74 kip (49 ksi). As loading approached failure, the connectors acted as a unit. Figure 5.10, shows the specimen's cracking pattern at failure, which included V-shaped crack formations.

5.3.2 Polyethylene Duct Specimens

The crack development in test specimens containing polyethylene ducts is illustrated by Test No. 9, a single-connector test, and Test No. 14, a double-connector test.

Test No. 9 consisted of an uncoated single-connector embedded at $12d_b$ (17 in.). The first signs of cracking occurred in the grout at a load of 20 kip (13 ksi). As loading continued, radial splitting cracks started to emerge in the concrete at loads around 64 kip (42 ksi). Figure 5.11 shows the cracking pattern at a load of 78 kip (51 ksi). The radial splitting cracks at this load level were not very numerous and affected a limited area of the connection surface. Figure 5.12 shows the crack pattern at the connection's failure load of 82 kip (54 ksi). V-shaped crack formations did not form on the loaded side of the specimen.

In Test No. 14, which consisted of two connectors embedded $16d_b$ (22.5 in.), the first signs of cracking occurred in the grout at a load of 27 kip (18 ksi). As loading continued, cracks began to emerge in the concrete and widespread

radial splitting was observed at a load of 75 kip (49 ksi), as shown in Figure 5.13. Throughout the test, the cracking pattern of each connector mirrored that of the other. The close proximity of connectors with only a one-duct-diameter (1-D) clear spacing between the ducts caused extensive interaction between the connectors. V-shaped crack formations were seen on the loaded side of the specimen as the connection was reaching its capacity. This meant that the force was being transferred effectively between the connector, the polyethylene duct, and the concrete. The connectors were embedded $16d_b$, which made possible the effective force transfer. At failure, at a load of about 97 kip (64 ksi), both connectors failed together as a unit, as shown in Figure 5.14. A horizontal side crack, which matched the depth of the top layer of bent cap longitudinal reinforcement, formed at this maximum load.

5.3.3 Polypropylene Duct Specimens

The crack development in test specimens involving polypropylene ducts is illustrated by Test No. 28, a double-connector test, and Test No. 32, a triple-connector test.

Test No. 28 consisted of two connectors embedded at $16d_b$ (22.5 in.). The first signs of cracking occurred in the grout at a load of 18 kip (12 ksi). Radial splitting cracks in the concrete started to emerge at loads around 66 kip (44 ksi). A widespread pattern of radial splitting can be seen in Figure 5.15, at an approximate load of 79 kip (53 ksi). Throughout the test, the cracking pattern of each connector mirrored that of the other. The close proximity of connectors with only a one-duct-diameter (1-D) clear spacing between the ducts caused significant interaction between the connectors. V-shaped crack formations were seen on the loaded side of the specimen, indicating again the transfer of forces from the

connector, through the duct, to the concrete (Figure 5.16). At the connection's failure load of 128 kip (85 ksi), both connectors failed by pullout simultaneously.

Test No. 32 involved three connectors arranged in a triangular pattern, embedded at $16d_b$ (22.5 in.). Cracking in the grout occurred at a load of 15 kip (10 ksi), while radial splitting cracks in the concrete started to develop at a load of 30 kip (20 ksi). V-shaped cracks, shown in Figure 5.17 started to form at a load of 75 kip (50 ksi). The failure load for this test was 101 kip (67 ksi).

5.4 STRESS-END SLIP DIAGRAMS

The load-displacement behavior of a structure is, in general, the most meaningful piece of information that can be recorded during a test. In this investigation, as has been mentioned before, the loads applied to the connectors were measured using load cells and a pressure transducer, while the connector displacements were measured using linear potentiometers. The lead displacement values were particularly useful to monitor bar yielding during a test. On the other hand, the measured connector end displacements can provide more useful information about the overall slip of the connectors inside the grout-duct system. Figure 5.18 shows values for both lead and end connector displacements for a representative test. The test portrayed in the figure is Test No. 3, which exhibited bar yielding. A yield plateau can be seen in the curve that depicted the lead displacement of the connector. Here, the values of displacement being recorded at the lead of the connector consisted of two components: (1) a slip component, where the connector was slipping out of the specimen as a whole (there are corresponding end slip values at the same load), and (2) a yielding component, where the portion of the connector at which the lead displacement values were being recorded was experiencing yield elongation. In the following presentation

of results, the end displacement (or end slip) is the displacement value that is of primary interest in order to examine the anchorage of connectors.

The load-displacement behavior of grouted vertical duct connections is presented using a series of stress-end slip diagrams obtained from representative tests of different duct materials. The load values are plotted as stress instead of force to make it easier to relate to the results. Constant stress lines corresponding to the yield strength, 0.6 times the yield strength, and 1.25 times the yield strength of the connectors are drawn in the diagrams.

5.4.1 Galvanized Steel Duct Specimens

The connector stress-end slip behavior for test specimens involving galvanized steel ducts will be illustrated by a set of representative tests consisting of one and two connectors.

Figure 5.19 shows the stress-end slip diagram for Test No. 4, which involved a single epoxy-coated connector embedded at $12d_b$. The connection specimen exhibited a very high initial stiffness, up to an applied stress of around 57 ksi. Radial splitting cracks in the concrete were seen in the specimen around this same load level, as indicated in Table 5.1. The effect of the concrete splitting is observable in the diagram as a slight softening in the stiffness of the connection after 57 ksi. The yield strength of this connector was 68 ksi. A yield plateau is not observed in the diagram, since the connector displacement being plotted in this diagram is the end displacement, and not the lead displacement. Yielding would be concentrated where the load is the highest; this happens mainly in the lead area of the connector. The stress-end slip diagram also shows that the connection could still resist additional load, even after the bar yielding event. After a load of about 77 ksi, the connection stiffness degraded progressively until the capacity of the

connection was reached at 88 ksi. The corresponding slip value at maximum load was 0.22 in.

The stress-end slip diagram for Test No. 10 is shown in Figure 5.20. Test No. 10 was a replicate test of Test No. 3; both tests involved single uncoated connectors embedded $12d_b$. At yield, the measured slip in Test No. 3 was 0.05 in., while the slip measured in Test No. 10 was 0.13 in. As seen in Figure 5.20, the stiffness of the connection specimen of Test No. 10, denoted by the slope of the stress-end slip diagram, was smaller than that of Test No. 3. The differences in stiffness and also in capacity can be attributed to weaker concrete and grout strengths present in Test No. 10.

Test No. 13 consisted of two uncoated connectors embedded at $16d_b$. The stress-end slip diagram for this test is shown in Figure 5.21. The connection exhibited very stable behavior, denoted by the high initial stiffness and ability to take additional load after yielding of the bars, up to the failure load. This kind of behavior was obtained due to the deep connector embedment provided. The diagram shows a softening of the connection stiffness as the load reached a stress of 63 ksi, which corresponded to a load of around 95 kip, when V-shaped cracks emerged on the loaded side of the specimen (Figure 5.8). The capacity of this connection was 87 ksi.

Figure 5.22 shows the stress-end slip diagram for Test No. 17, which involved two connectors embedded at $12d_b$ and a duct clear-spacing of one duct-diameter. Concrete splitting cracks started to emerge at a load of 50 kip (33 ksi), but a more widespread pattern of radial splitting developed at a load of 68 kip (45 ksi), as seen in Figure 5.23. At this stage, the connectors slipped, while the load remained unchanged, then the connection was able to resist additional load, but with a progressive reduction in stiffness. The maximum load attained by this

connection corresponded to 59 ksi, substantially below the connectors' yield strength.

Test No. 23 was a similar double-connector test, but with a duct clear-spacing of two duct diameters. The stress-end slip diagram of Test No. 23 is shown in Figure 5.24. The diagram shows a drop in load, accompanied by an increase in slip, when the connection reached 55 ksi (82 kip). Figure 5.9 showed that widespread radial splitting occurred at this load level. The shorter connector embedment of $12d_b$ in Tests No. 17 and 23 was not enough to anchor the bars as effectively as the deeper embedment of $16d_b$ did in Test No. 13. When radial splitting cracks developed in the concrete, the forces in the connectors redistributed to maintain anchorage. The maximum load attained by the connection of Test No. 23 was 68 ksi.

5.4.2 Polyethylene Duct Specimens

The connector stress-end slip behavior for test specimens involving polyethylene ducts will be illustrated by a set of representative tests consisting of one and two connectors.

Figure 5.25 shows the stress-end slip diagrams for Tests No. 5, 7, and 22. All three tests involved uncoated single connectors, but the embedment depths were different. Test No. 5 had a connector with an embedment depth of $8d_b$, while Tests No. 7 and 22 had connectors with embedment depths of $12d_b$ and $16d_b$, respectively. The connection capacities varied with the embedment depth. The stress-end slip curves for Test No. 5 and Test No. 7 are very similar in shape. Neither of these connections was able to resist a load equivalent to the yield strength of the connector. On the other hand, the stress-end slip diagram for Test No. 22 shows that the connector was able to resist loads larger than its yield strength, and that the connection had great ductility. The values of end slip at

maximum load for the three tests increased with relation to the embedment depth provided.

The stress-end slip diagram for Test No. 9 is shown in Figure 5.26. Test No. 9 was a replicate test of Test No. 7; both tests involved single uncoated connectors embedded $12d_b$. None of these connection specimens was able to resist a load equivalent to the yield strength of the connector. At maximum load, the measured slip in Test No. 9 was 0.22 in., while the slip measured in Test No. 7 was 0.26 in. The connection of Test No. 7 was able to resist a stress of 67 ksi, compared to the capacity of 54 ksi attained by the connection specimen of Test No. 9. The differences in capacity can be attributed to weaker concrete and grout strengths present in Test No. 9.

Figure 5.27 shows the stress-end slip diagram for Test No. 14, which consisted of two connectors embedded at $16d_b$, with a duct clear spacing of one duct-diameter. The connection specimen exhibited a very high initial stiffness up to applied stresses between 42 and 49 ksi. Radial splitting cracks in the concrete started to emerge in the specimen within this load range, as seen in Figure 5.13. As loading continued, the stiffness of the connection was reduced, and the connectors were able to resist additional loads. The connection failed at a stress of 64 ksi, which was lower than the connectors' yield strength. After reaching the maximum load, one of the connectors (right) started to pullout individually. The test continued, with only the specimen's right bar being pulled-out. Then, the bar on the left was reloaded individually, as seen in Figure 5.27. The bar reached a stress of 61 ksi, and failure by pullout followed.

Test No. 24 was a double-connector test similar to Test No. 14, but with a duct clear spacing of two duct-diameters. The stress-end slip behavior of Test No. 24, shown in Figure 5.28, was very similar to that of Test No. 14, with a slight stiffer response up to failure. When the stress applied was 65 ksi, the connection

showed signs of failure, and one of the bars (right) began to pullout. From this point, since the method of testing was force-controlled, the applied load was determined by the capacity of the failing connector. After pullout of the right connector, the test was resumed, this time with the load being applied only to the left connector. As seen in Figure 5.28, the connector was able to resist much larger forces on the order of 87 ksi, and behaved more like the single connector of Test No. 22. This is attributed to the increased clear spacing between ducts, and the reduced interaction between the two connectors.

5.4.3 Polypropylene Duct Specimens

The connector stress-end slip behavior for test specimens involving polypropylene ducts will be illustrated by a set of representative tests consisting of one, two, and three connectors.

Figure 5.29 shows the stress-end slip diagrams for Tests No. 29 and 30. Both tests involved uncoated single connectors, but the embedment depths were different. Test No. 29 had a connector with an embedment depth of $8d_b$, while Test No. 30 had a connector with an embedment depth of $12d_b$. While the connector in Test No. 30 was able to resist a load equivalent to its yield strength, the connector in Test No. 29 was only able to resist a load of approximately 0.6 times the yield strength. The stress-end slip curves for Test No. 29 and Test No. 30 are very similar in shape, with that of Test No. 29 showing perhaps a slightly lower initial stiffness. The noted jaggedness of the curves after the reached connection capacities can be attributed to imperfections in the loading method.

The stress-end slip diagram for Test No. 28 is shown in Figure 5.30. The connection exhibited very stable behavior up until it reached the maximum load of 85 ksi. At a load up to 59 ksi, when the connectors underwent yielding, the connection had already experienced significant radial splitting (see Figure 5.15),

yet no indication of reduction in the connection stiffness was observed. This stable behavior indicates that the polypropylene ducts were very effective at transferring the forces from the connectors and to the concrete.

The measured stress vs. end slip response of Test No. 32 is displayed in Figure 5.31. The fact that three connectors were being pulled out simultaneously caused radial concrete splitting to occur very early during the test at a connector stress of 20 ksi. The emergence of additional radial cracks did not cause a reduction in connection stiffness, even when a more widespread pattern of radial splitting was present at a connector stress of 47 ksi. However, when the applied stress reached 50 ksi, a drop in connection resistance, accompanied by an increase in slip, was observed (Figure 5.31). Figure 5.17 showed that at this same load, V-shaped cracks formed on the specimen's side that was loaded more heavily. The formation of these V-shaped cracks in the concrete instigated force redistribution along the length of the connectors to maintain anchorage. The capacity of the connection was 67 ksi, which was 8 ksi larger than the connectors' yield strength.

5.5 STRAIN DISTRIBUTION DIAGRAMS

The strain in the connectors was measured directly using strain gages. As mentioned in Section 4.3, strain was measured at the lead end of the connector, and at 6 in. intervals along the embedded portion of each connector. The results show the measured bar strain at the different gage locations, for a series of applied stress levels. The strain values shown in the results at the lead end of each connector correspond to the calculated average of the two lead gage readings.

The gages and the cyanoacrylate adhesive used in the experiments were not specially suited to measure post-yield strain measurements; therefore, several gage readings at strains above 10,000 $\mu\varepsilon$ were not reliable. These unreliable data points are shown in the plotted results with a dashed line. In a few occasions,

gages in the embedded portion of the connectors were damaged during a test. Strain readings at these bar locations are thus not available for subsequent levels of applied stress.

5.5.1 Galvanized Steel Duct Specimens

The strain distribution along the length of connectors housed inside galvanized steel ducts is illustrated by a representative set of tests consisting of one and two connectors.

Test No. 3 consisted of a single uncoated connector embedded at $12d_b$. The strain distribution along the length of the connector is shown in Figure 5.32. For applied stresses between 20 and 60 ksi, the strain readings show that the entire length of the connector was reacting to the applied load. The strain measured at a depth of 6 in. was approximately equal to the strain measured at the lead. Since the strain readings at a depth of 12 in. were small compared to the readings at the other gage locations, it is clear that at stress levels between 20 and 60 ksi, the applied load was being resisted mostly by the portion of the connector closest to the surface. The strain distribution corresponding to an applied stress of 80 ksi shows that the connector was experiencing post-yield strains at the lead, and even at a depth of 6 in. below the surface. These measured strains are corroborated given that the yield strength of the connector used in Test No. 3 was 75 ksi. Failure of the connector occurred at an applied stress level of 87 ksi. At this stress level, the dashed line in Figure 5.32 indicates that the measured strains in the connector at the lead and at 6 in. below the surface were not reliable. Furthermore, there is no strain reading available for the bar location 12 in. below the surface, since the gage suffered damage.

Figure 5.33 shows a similar strain distribution diagram, this time corresponding to Test No. 4. This test consisted of one epoxy-coated connector

embedded at $12d_b$. While the strain distribution diagram corresponding to Test No. 3 had an approximate trapezoidal shape for applied stress levels between 20 and 60 ksi, the diagram shown for Test No. 4 has a more dominant triangular shape. The connector portion located closest to the surface was not effective at resisting most of the applied load, and the load had to be resisted more uniformly along the entire length of the connector. This difference in the strain distribution patterns of Tests No. 3 and 4 can be attributed to the detrimental effect of the epoxy-coating on friction resistance. The strain distribution at 70 ksi shows that post-yield strains were recorded at the bar lead and at 6 in. below the surface of the specimen. These measured strains are corroborated since the yield strength of the connector used in Test No. 4 was 68 ksi. At an applied stress of 80 ksi, the recorded strain at the lead was unreliable, as shown by the dashed line. The failure load for this test corresponded to an applied stress of 88 ksi. Strain distribution data at this stress level were unreliable.

Figure 5.34 shows the strain distribution along the length of one of the connectors (left) tested in Test No. 13. Both of the connectors in this test had a similar strain distribution, hence only the results for one connector are shown. A first thing to notice by looking at the diagram in Figure 5.34 is that at a load level of 20 ksi, the gage located at a depth of 18 in. was recording a strain value close to zero. This means that at this stress level, the load was mainly being resisted by the top portion of the connector. As loading progressed, the gage located at a depth of 18 in. did begin to measure more significant strains. At a stress level of 60 ksi, the diagram shows that the bar was straining appreciably along its length. The strain recorded at a depth of 6 in. was approximately equal to the measured strain at the lead. At 80 ksi, 5 ksi above the connector's yield strength, the measured strains are in the post-yield range at the lead and at a depth of 6 in. At

failure, at an applied stress of 87 ksi, the recorded strain at the lead was unreliable, as shown by the dashed line.

The strain distribution diagram for one of the connectors tested in Test No. 17 is shown in Figure 5.35. The two connectors in this test behaved similarly, as in the case of Test No. 13, hence only the results for the left connector are presented. The embedment depth provided for the connectors in Test No. 17 was $12d_b$. As mentioned in Section 5.4.1, the connectors failed by pullout at an applied stress of 59 ksi. The strain distribution along the connector length is similar for stress levels of 20 and 40 ksi. The only difference lies in the overall magnitude of the measured strains. However, as the load increased, widespread radial splitting in the concrete occurred, as was shown in Figure 5.23, and the load was redistributed along the connector length, with more of the load being anchored deep at the end portion of the connector.

5.5.2 Polyethylene Duct Specimens

The strain distribution along the length of connectors housed inside polyethylene ducts is illustrated by a representative set of tests consisting of one and two connectors.

Test No. 7 consisted of a single connector embedded at $12d_b$. The strain distribution along the length of the connector is shown in Figure 5.36. Throughout the test, the strains recorded at the gage located 6 in. below the surface of the specimen were approximately equal than the ones recorded at the lead of the connector. Appreciable values of strain were also measured at the location 12 in. below the surface. The strain reading corresponding to a depth of 12 in. at failure was not available.

Figure 5.37 shows the strain distribution diagram for Test No. 22. Even at an applied stress as small as 20 ksi, a noticeable value of strain was recorded at a

depth of 18 in. below the surface. At stress levels equal and smaller than 60 ksi, the strains measured 6 in. below the surface of the specimen were approximately equal than the ones recorded at the lead end of the connector. A post-yield strain value was recorded at the lead of the connector when the applied stress was 80 ksi. At this load stage, the strain gage located at 6 in. below the surface indicated that the bar at this location was beginning to experience yield deformations as well. The connector failed at a load corresponding to 90 ksi. The strain record at a depth of 6 in. indicates that considerable yielding occurred in the connector as deep as 6 in. below the surface. The strain measured at the connector lead at this applied stress was unreliable.

The strain distribution diagram of Test No. 14 is shown in Figure 5.38. The results for the left connector are presented. Throughout the test, the strain values measured 6 in. below the surface were roughly equal to those measured at the lead. This is a phenomenon observed in all tests involving the polyethylene duct, and occurred independent of the embedment depth provided or the number of connectors. The diagram in Figure 5.38 shows that at stress levels of 60 and 64 ksi, the load was being redistributed along the length of the connector and the anchorage of the bar was essentially taking place very near the end portion of the connector.

For comparison purposes, a similar strain distribution diagram, corresponding to Test No. 24, is presented in Figure 5.39. The only difference between Test No. 14 and Test No. 24 was that the duct clear spacing in Test No. 24 was twice that of Test No. 14. The capacities of both tests were, nonetheless very similar. The stress-end slip diagram for Test No.24 was shown in Figure 5.28. The results presented here correspond to the left connector of Test No. 24 tested up to the connection failure load, and do not include the data obtained upon reloading of the connector. The strain distribution data for this connector, up to

the failure load, appear to be similar to that obtained for the connector of Test No. 22.

5.5.3 Polypropylene Duct Specimens

The strain distribution along the length of connectors placed inside polypropylene ducts is illustrated by a representative set of tests consisting of one, two, and three connectors.

Test No. 30 consisted of a single connector embedded at $12d_b$. The strain distribution along the length of the connector is shown in Figure 5.40. At applied stresses between 20 and 60 ksi, the strain readings corresponding to a depth of 6 in. were equivalent to the strain values measured at the lead. At a stress level of 68 ksi, post-yield strains were measured at a depth of 6 in. and at the lead. However, the strain value at the lead was unreliable, since it is suspected that, at this point, the gage installation was damaged. In general, for loads lower than the connector yield strength of 59 ksi, the strain distribution diagram has a trapezoidal shape, similar to that exhibited by Test No. 3, which involved galvanized steel ducts.

The strain distribution for one of the connectors of Test No. 28 is shown in Figure 5.41. Radial splitting in the concrete started to occur at a load of 66 kip (44 ksi), as was indicated in Figure 5.15. The strains measured along the length of the connector show that the strain recorded by the gage located 12 in. below the surface increased somewhat between applied stresses of 40 and 60 ksi. The change in the pattern of strain distribution indicates that due to extensive splitting in the concrete, the load along the connector was redistributed and more of it was being transferred deep into the end portion of the connector. An intermediate load step corresponding to an applied stress of 70 ksi shows that considerable yielding is occurring in the connector, even at 6 in. below the surface. Moreover, the strain

measured at a load corresponding to 80 ksi at a depth of 12 in. indicates that yielding was progressing along the length of the connector. The strain readings at the lead associated with the ultimate load stages were not reliable.

For comparison purposes, the strain distribution diagram for one of the three connectors of Test No. 32 is presented in Figure 5.42. In the case of Test No. 32, splitting in the concrete began at a low connector stress of 20 ksi. However a general widespread pattern of splitting did not develop until the load reached 46 ksi (70 kip). The event of significant concrete splitting and its effects on the pattern of strain distribution along the connector length can be seen in the diagram as the applied stress increased from 40 to 60 ksi. The load along the connector was redistributed and more of it was being transferred deep into the end portion of the connector. At failure, the strain measurements indicate that yielding in the connector extended to a depth of 12 in. below the surface.

5.6 STRESS DISTRIBUTION DIAGRAMS

The stress distribution diagrams for the same set of representative tests presented in Section 5.5 are shown in this section. Stress distribution diagrams provide a means of illustrating the load distribution along the connectors, especially at stresses larger than the yield strength of the connectors. Whereas connector strain was measured directly during the tests using strain gages, to obtain the values for stress, the strain values needed to be converted to stresses using a mathematical model. The mathematical model, presented in Appendix B of this dissertation, consisted of three different stress-strain relationships that corresponded to the three different kinds of connectors used. The model was calibrated to tensile tests of actual connectors. Still, slight discrepancies between the real stress-strain curve for a given connector and the mathematical model used

for converting strain to stress can lead to some error. The range for errors is larger for converted stresses in the strain-hardening region.

The results show the stress at the different connector locations, for a series of applied stress levels. The stress values shown in the results at the lead end of each connector correspond to the strains recorded by the strain gages. Sometimes, the converted stress values differed slightly with respect to the applied stress. The discrepancies in the readings can be attributed to signal noise during the tests. Because the gage installations were not specially suited to withstand large deformations, several gage readings at strains above 10,000 $\mu\varepsilon$ were not reliable. Consequently, the converted stress values are not reliable either, but are still shown and indicated by dashed lines. In a few occasions, gages in the embedded portion of the connectors were damaged during a test. Stress values are thus not available at those locations for subsequent levels of applied stress.

The stress distribution diagrams include an indication of the yield strength of the connector, represented by a horizontal dashed line. The figures also show the stress level at which radial concrete splitting started (first splitting) in the connection specimens.

5.6.1 Galvanized Steel Duct Specimens

The stress distribution along the length of connectors housed inside galvanized steel ducts is illustrated by a representative set of tests consisting of one and two connectors.

The stress distribution along the length of the connector of Test No. 3 is shown in Figure 5.43. As the applied stress level increased from 20 to 60 ksi, the stress in the connector at a depth of 12 in. increased in relation to the applied stress from a ratio of 30 percent to 50 percent. The stress in the connector at a depth of 6 in. was approximately equal to the applied stress at all load stages.

Since the stress at a depth of 12 in. was in all cases small compared to the stress near the lead portion of the connector, it is clear that the applied load was being resisted mostly by the portion of the connector closest to the surface. Considerable concrete splitting, which occurred at stresses higher than 66 ksi, did not cause a change in the stress distribution along the connector, as shown by the stress results for an applied stress of 80 ksi. At this load, the value of stress at the lead, obtained by conversion from the strain gage reading is 75 ksi, instead of the known stress level present of 80 ksi. As shown in Figure 5.32, the strain reading corresponding to this data point had a value in excess of 10,000 $\mu\varepsilon$; this particular strain gage was damaged, and the strain value recorded is deemed unreliable. The data points are thus shown in both the strain and stress distribution diagrams with a dashed line. Failure of the connector occurred at an applied stress level of 87 ksi. At this stress level, the dashed line in Figure 5.43 indicates that the stress values obtained at the lead and at 6 in. below the surface were not reliable. Moreover, there is no strain reading available at a depth of 12 in. below the surface, since the gage suffered damage, hence there is no converted stress value to show.

Figure 5.44 shows the stress distribution diagram for Test No. 4. As the applied stress level increased from 20 to 60 ksi, the stress in the connector at a depth of 12 in. increased in relation to the applied stress from a ratio of 36 percent to 66 percent. Additionally, for applied stress levels of 40 and 60 ksi, the ratio of stress in the connector at a depth of 6 in. to the applied stress increased from 79 percent to 89 percent. The stress values obtained at the lead of the connector diverged with respect to the known applied stresses. It is possible that the source for this error was signal noise during the test. In comparison to the results for Test No. 3, the stress at a depth of 12 in. was not small compared to the stress near the lead portion of the connector. This meant that the applied load was being resisted

more uniformly along the entire length of the connector. As mentioned in Section 5.5.1, this difference in behavior between Tests No. 3 and 4 can be attributed to the detrimental effect of the epoxy-coating on friction resistance. Concrete splitting, which occurred at stresses higher than 60 ksi, did not cause a change in the stress distribution along the connector, as shown by the stress results for an applied stress of 70 ksi. At an applied stress of 80 ksi, an erroneous stress value of 68 ksi was obtained at the lead; the strain reading from which it was determined was deemed unreliable. No reliable stress distribution information was available for an applied stress of 88 ksi.

The stress distribution along the length of one of the connectors tested in Test No. 13 is presented in Figure 5.45. At stresses smaller than 40 ksi, most of the applied load was being resisted by the top portion of the connector. This last statement can be verified by the low connector stresses observed at a depth of 18 in. below the surface. As loading increased from 40 to 60 ksi, the stress in the connector at a depth of 18 in. increased from 16 percent to 43 percent of the applied stress. At 60 ksi, the stress in the connector at a depth of 6 in. was approximately equal to the applied stress. The first concrete splitting cracks developed at a stress level of 38 ksi. However, as was shown in Figure 5.7, a widespread pattern of radial cracking developed until a load of 86 kip (57 ksi). Extensive cracking in the concrete caused the load to be redistributed down the connector. The pattern of stress distribution corresponding to an applied stress of 80 ksi was similar to that at 60 ksi; the ratio of the stress in the connector at a depth of 18 in. to the applied stress increased to 54 percent. At failure (87 ksi), the converted value of stress at the lead end of the connector was not reliable.

Figure 5.46 shows the stress distribution diagram for one of the connectors tested in Test No. 17. As the load was increased from a stress level of 20 to 40 ksi, the ratio of the stress in the connector at a depth of 12 in. to the applied stress

increased significantly. This ratio was 22 percent at 20 ksi, and 42 percent at 40 ksi. Although radial cracks in the concrete emerged at a stress level of 33 ksi, significant cracking did not occur until the stress increased to 45 ksi (Figure 5.23). After severe cracking, the load redistributed along the connector length, and a larger portion of the load was anchored deep at the end portion of the connector. The ratio of stress in the connector at a depth of 12 in. to the applied stress increased to 79 percent by the time the connection failed at 59 ksi.

5.6.2 Polyethylene Duct Specimens

The stress distribution along the length of connectors placed inside polyethylene ducts is illustrated by a representative set of tests consisting of one and two connectors.

The stress distribution along the length of the connector of Test No. 7 is shown in Figure 5.47. The data show that even at the low stress level of 20 ksi, a large share of the load was being resisted deep down in the connector. As the applied stress level increased from 20 to 60 ksi, the stress in the connector at a depth of 12 in. increased in relation to the applied stress from a ratio of 55 percent to a ratio of 82 percent. No reliable stress data were available at the failure stress of 67 ksi.

Figure 5.48 shows the stress distribution diagram for Test No. 22. The entire length of the connector was reacting to the applied load even at low stress levels. At a stress level of 20 ksi, a stress equal to 40 percent of the applied stress was measured at 12 in. below the surface. Six inches deeper, the stress in the connector was 23 percent of the applied stress. Following the initial splitting cracks that formed at 45 ksi, the expansion of radial splitting cracks in the concrete between applied stresses of 60 and 80 ksi triggered a progressive redistribution of the load down the connector. The results at 80 ksi show that the

connector was undergoing yielding as deep as 6 in. below the surface. At failure, the ratios of connector stress to applied stress were 71 percent for the 12 in. depth, and 53 percent for the 18 in. depth. The erroneous stress value at the lead was obtained from an unreliable strain reading. Throughout the test, the stress values obtained at the lead of the connector diverged with respect to the known applied stresses. As in Test No. 4, it is suspected that the source for this error was signal noise.

The stress distribution diagram of the left connector of Test No. 14 is shown in Figure 5.49. As the connector of Test No. 22, the entire length of the connector responded to the applied load even at low stress levels. At a stress level of 40 ksi, the stress in the connector 12 in. below the surface was 62 percent of the applied stress. Six inches below, the ratio of stress in the connector to applied stress was 31 percent. The development of radial splitting cracks in the concrete changed the pattern of stress distribution in the connector. A larger proportion of the load was now being resisted deeper down the connector. At 60 ksi and at a depth of 12 in., the connector stress to applied stress ratio was 76 percent; at 18 in., the ratio was 54 percent. As the connection reached its capacity, the stress in the connector 18 in. below the specimen's surface was 70 percent of the applied stress of 64 ksi.

The stress distribution diagram for the left connector of Test No. 24 is shown in Figure 5.50. The diagram includes the data up to the connection failure load, and does not include the data obtained upon reloading of the connector. The entire length of the connector reacted to the applied load even at low stress levels. At a stress level of 40 ksi, the stress in the connector 12 in. below the surface was 56 percent of the applied stress. Six inches below, the ratio of stress in the connector to applied stress was 31 percent. The development of radial splitting cracks in the concrete changed the pattern of stress distribution in the connector.

The share of the load that was being resisted deep down the connector increased. At 60 ksi and at a depth of 12 in., the connector stress to applied stress ratio increased to 75 percent; at 18 in., the ratio increased to 41 percent. As the connection reached its capacity, the stress in the connector 12 in. below the surface was 83 percent of the applied stress; while the stress at the 18 in. depth had only increased to 43 percent of the applied stress.

5.6.3 Polypropylene Duct Specimens

The stress distribution along the length of connectors housed inside polypropylene ducts is illustrated by a representative set of tests consisting of one, two, and three connectors.

The stress distribution along the length of the connector of Test No. 30 is shown in Figure 5.51. For stress levels between 20 and 60 ksi, the stress in the connector at a depth of 6 in. was equivalent to the applied stress. The percentage of the load that was being transferred down the connector, based on observed stress values at a depth of 12 in., varied from 51 percent at 20 ksi to 64 percent at failure. At the failure stress of 68 ksi, the incorrect stress obtained at the connector lead indicated that the strain gage reading at that location was not reliable.

The stress distribution for one of the connectors of Test No. 28 is shown in Figure 5.52. Radial splitting in the concrete started to occur at a load of 66 kip (44 ksi), as was indicated in Figure 5.15. The stress in the connector 12 in. below the surface increased substantially between applied stresses of 40 and 60 ksi. The ratio of stress in the connector to the applied stress rose from 60 percent to 83 percent. At a depth of 18 in., the ratio only rose from 23 to 32 percent. The change in the pattern of strain distribution indicates that due to extensive splitting in the concrete, the load along the connector was redistributed down into the connector. The data for an applied stress of 70 ksi show that yielding was

occurring in the connector at depths greater than 6 in. below the surface. At an applied stress of 85 ksi, the stress in the connector at a depth of 12 in. indicates that yielding had progressed down the length of the connector further. The stresses at the lead associated with the ultimate load stages, shown in the diagram with dashed lines, were obtained from unreliable strain gage readings.

Figure 5.53 shows the stress distribution diagram for one of the three connectors of Test No. 32. Although splitting in the concrete began at a low connector stress of 20 ksi, a general widespread pattern of splitting did not develop until the load reached 46 ksi (70 kip). After 46 ksi, the splitting cracks continued to grow, and at 50 ksi, V-shaped cracks (shown in Figure 5.17) also developed on the specimen's side that was loaded more heavily. The effect on the connector of extensive cracking in the concrete between the applied stresses of 40 and 60 ksi can be seen in the stress distribution diagram. The ratio of stress in the connector at a depth of 12 in. to applied stress increased from 62 to 90 percent. At 18 in., the ratio increased from 27 to 45 percent. At failure, the stress obtained at a depth of 12 in., indicates that yielding was progressing even to this depth.

5.7 STRESS-SLIP RELATIVE TO GROUT DIAGRAMS

As mentioned in Section 4.3, the relative displacement between the grout and the concrete specimen was monitored during the tests using a linear potentiometer. The grout displacement data were useful in acquiring information about the slip of the connectors and about the anchorage of the grout inside the ducts.

The data collected by the grout instrumentation were reliable until extensive cracking occurred in the connection specimens during the tests. The spreading and widening of radial cracks emanating from the ducts together with the development of cracks on the sides of the specimens led to the formation of

concrete breakouts. The breakouts involved a large area of the top surface of the specimens, and often disturbed the concrete zone beneath the epoxy-glued metal stands that supported the grout instrumentation. The accuracy of the grout displacement data was lost after cracking occurred underneath the instrumentation stands. Cracking caused an upward shift of the instrumentation, and the loss of the top concrete surface of the specimen as a reference point to measure grout displacement. The grout displacement data that are presented in the results exclude those portions of data that were considered unreliable due to extensive cracking in the specimen. Typically, grout displacement data were not available after connection failure.

Figure 5.1 showed the relationship between the grout displacement, δ_g, and the connector end displacement, δ_e. Three main scenarios of behavior were described in the figure: (1) δ_e equals δ_g, which suggests that the entire connector and the grout are pulling outward together as a unit (plug), (2) δ_e is smaller than δ_g, suggesting that the top portion of the grout is moving upward together with the lead end of the connector, while the end portion of the connector is moving upward a smaller amount, and (3) δ_e is greater than δ_g, implying that the connector, as a whole, is slipping out of the grout. The slip of the connector relative to the grout, δ_{srg}, was calculated and plotted, as the difference between δ_e and δ_g.

Whereas the connector end displacements provide general information about the overall slip of the connectors inside the grout-duct-concrete system, the stress-slip relative to grout diagrams provide more detailed information about the interaction between the connector and the grout.

A series of stress-slip relative to grout diagrams are presented in this section to illustrate the connector displacement relative to the grout for a

representative set of tests. The results are presented again in three groups, determined by the type of duct material.

The connector end displacement is plotted as well for comparison in the diagrams. Constant stress lines corresponding to the yield strength, 0.6 times the yield strength, and 1.25 times the yield strength of the connectors are also drawn in the diagrams.

5.7.1 Galvanized Steel Duct Specimens

The stress-slip relative to grout behavior of connectors placed inside galvanized steel ducts is illustrated by a set of representative tests consisting of one and two connectors.

For each of the representative tests, two curves are shown: (1) stress-end slip curve and (2) stress-slip relative to grout curve. The curve that displays the connector end slip is analogous to the curve displaying the slip of the connector relative to the grout. The first curve shows the displacement of the connector relative to the concrete specimen, while the second one shows the displacement of the connector relative to the grout. This, and ensuing, sections concentrate on examining the slip of the connector with respect to the grout.

It is possible to determine the relationship between the connector and the grout by examining the stress-slip relative to grout diagrams. If the direction of the curve is to the right, this means that the connector is slipping out of the grout. If the direction of the curve is to the left, this suggests that a portion of the grout near the lead of the connector has separated and is moving upward at a faster rate that the end of the connector. Then, if the direction of the curve is such that there is no increase or decrease of slip with a corresponding change in applied stress, this indicates that the connector and the grout are displacing upward together as a unit.

Figure 5.54 shows the stress-slip relative to grout diagram for Test No. 3. In general, the data reveal that the connector and the grout were displacing upward together up to an applied stress of around 66 ksi. This stress level coincided with the occurrence of splitting cracks in the concrete. The effect of proliferating splitting cracks in the concrete can be seen in the diagram as the connector's slip increased relative to the grout. At a stress level of 75 ksi, the connector experienced yielding. The formation of V-shaped cracks also occurred at a stress of 75 ksi, which caused additional slip of the connector relative to the grout. The data associated with applied stresses between 76 and 83 ksi show that the value of slip between the connector and the grout underwent a series of cycles, where the connector and the grout moved upward at different rates. The first cycle, where the relative slip between the connector and the grout decreased, can be attributed to yielding occurring in the connector at the lead and at a shallow depth beneath the surface. The connector elongation can subject the grout located near the surface to large strains, leading to a series of cracks that would allow the top surface of the grout to rise. Nonetheless, the overall slip between the connector and the grout at a stress of 83 ksi was almost equal to the observed value at 76 ksi. At a stress of 83 ksi, a horizontal crack began to form on the side of the specimen at a depth corresponding to the location of the beam's top longitudinal reinforcement. The formation of this horizontal crack, and its subsequent growth observed at 86 ksi led to additional slip of the connector relative to the grout.

Figure 5.55 shows the stress-slip relative to grout diagram for the epoxy-coated connector of Test No. 4. In general, the data show that the connector and the grout were moving upward together up to an applied stress of around 77 ksi. However, the data show that at stress levels between 30 and 58 ksi, the connector did slip temporarily relative to the grout. Splitting cracks in the concrete emerged

at an applied stress of 60 ksi. The data show that the connector was slipping relative to the grout when it began experiencing yielding at 68 ksi. Soon after yielding, the slip of the connector relative to the grout decreased, and at 75 ksi, both the connector and the grout were displacing upward together again at the same rate. At a stress of 77 ksi, V-shaped cracks formed on the side of the specimen; the connector slip relative to the grout then increased. At larger stresses of 85 and 88 ksi, the V-shaped cracking pattern intensified and the connector continued to slip relative to the grout. At a stress of 89 ksi, the connector failed by pullout and a concrete breakout formed at the specimen's surface. Grout displacement data were not available after failure.

The stress-slip relative to grout diagram for the left connector of Test No. 13 is shown in Figure 5.56. The connector and the grout were moving upward together until the applied stress was around 63 ksi. At this point during the test, the concrete underneath the grout instrumentation was affected significantly by radial splitting cracks. The data after this point were thus considered unreliable and are not shown. In spite of this, data for the other connector of Test No. 13 were available, and since the behavior of both connectors was very similar, it is possible to deduce that the grout displacement data for both connectors were similar. The data collected for the other connector show that at a stress of 63 ksi, the connector slipped with respect to the grout. V-shaped cracks formations were observed on the loaded side of the specimen at this stress level. The connector continued to slip relative to the grout until the yield strength of the connector was reached. Then both the connector and the grout slipped together at the same rate up to failure.

Figure 5.57 shows the stress-slip relative to grout diagram for the left connector of Test No. 17. The data show that the connector and the grout were moving upward together until the applied stress was around 33 ksi. At this stress

level, splitting cracks in the concrete were detected. Immediately after concrete splitting, the grout displaced upward an amount larger than the displacement measured at the connector end. Then both the connector and the grout continued to move upward together, at the same rate, until a widespread radial crack pattern developed around each connector at a stress of 45 ksi. At this stress level, the connector slipped relative to the grout. Later, at a stress of 48 ksi, V-shaped cracks formed on the side of the specimen, and the slip of the connector relative to the grout increased. At a stress of 57 ksi, a horizontal crack formed on the side of the specimen at a depth corresponding to the location of the beam's top longitudinal reinforcement. The slip of the connector relative to the grout kept increasing until failure of the connection.

5.7.2 Polyethylene Duct Specimens

The stress-slip relative to grout behavior of connectors placed inside polyethylene ducts is illustrated by a set of representative tests consisting of one and two connectors.

Figure 5.58 shows the stress-slip relative to grout diagram for Test No. 7. The diagram shows that the connector slipped temporarily a small amount relative to the grout between applied stresses of 8 and 33 ksi. The first splitting crack in the concrete was detected at a stress of 33 ksi. As splitting cracks continued to emerge around the connector, the connector and the grout displaced together until a stress of 53 ksi was reached. Then, the connector slipped relative to the grout as the stress approached 57 ksi. At this stress, a widespread pattern of splitting cracks developed. The connector and the grout now moved upward together as a unit until the applied stress was 63 ksi and a horizontal crack formed on the side of the specimen at a depth corresponding to the location of the beam's top

reinforcement. Following the formation of the crack, the slip of the connector relative to the grout increased until failure was reached.

The stress-slip relative to grout diagram for Test No. 22 is displayed in Figure 5.59. After an initial slip of the connector relative to the grout at low stress levels, the displacement of the grout increased in relation to the connector end displacement. At a stress of 45 ksi, when the first splitting cracks were detected in the concrete, the data show a sudden increase in displacement for the grout. For stresses between 45 and 62 ksi, the connector and the grout were displacing upward at the same rate. Then, when additional splitting cracks emerged at 63 ksi, another sudden increase in displacement was observed in the grout. For stresses between 63 ksi and 77 ksi, the connector and the grout moved upward together again as a unit. The bar experienced yielding at a stress of 76 ksi; this coincided with the development of a widespread pattern of radial splitting around the connector. At this stress, the connector slipped a small amount relative to the grout, but a subsequent increase in grout displacement followed. The increase in grout displacement can be attributed to the effect of yielding in a portion of the connector below the surface. When the stress reached 81 ksi, a horizontal crack formed on the side of the specimen at a depth corresponding to the location of the beam's top reinforcement. Further loading extended the length of the horizontal crack; the slip of the connector relative to the grout increased until failure was reached.

Figure 5.60 shows the stress-slip relative to grout diagram for the left connector of Test No. 14. In general, the data show that the connector and the grout were moving upward together until the applied stress was around 25 ksi. As loading progressed, the data show a series of sudden changes in grout displacement. At stresses between 33 and 50 ksi, the value of connector slip relative to the grout is negative, indicating that the top surface of the grout has

displaced a larger distance than the connector end. At a stress of 51 ksi, the first V-shaped cracks formed on the side of the specimen, and the connector slipped relative to the grout. As more V-shaped cracks developed, at 55 and 58 ksi, the slip of the connector relative to the grout increased.

The stress-slip relative to grout diagram for the left connector of Test No. 24 is shown in Figure 5.61. By and large, the connector and the grout were displacing at the same rate until the formation of V-shaped cracks on the loaded side of the specimen at a stress of 61 ksi. The connector slip with respect to the grout increased at this point. When another crack appeared on the side of the specimen at a stress of 64 ksi; the connector slip with respect to the grout increased even further. Shortly after this, the connection failed, but only the connector on the right pulled-out. The connector on the left was reloaded, but grout displacement data is not available for the latter portion of the test.

5.7.3 Polypropylene Duct Specimens

The stress-slip relative to grout behavior of connectors housed inside polypropylene ducts is illustrated by a set of representative tests consisting of one, two, and three connectors.

Figure 5.62 shows the stress-slip relative to grout diagram for Test No. 30. The diagram shows that after a sudden initial slip of the connector at a very low stress of 5 ksi, the connector and the grout displaced upward together as a unit. This was the case until the applied stress reached the yield strength of the connector. At this point, the data show that the top surface of the grout began to move upward, while the end of the connector continued to move but at a smaller rate. No grout displacement data were available for stresses above 66 ksi.

The stress-slip relative to grout diagram for the right connector of Test No. 28 is shown in Figure 5.63. At first loading, the connector showed signs of slip

relative to the grout. However, after a stress of 18 ksi, the general trend observed was that of the grout surface displacing upward relative to the end of the connector. This can be seen in the diagram, as the relative displacement of the connector end relative to the grout decreased and went from positive values to negative values. When the stress reached 53 ksi, a widespread pattern of radial splitting developed, and the connector and the grout now moved upward together as a unit. At a stress of 59 ksi, the connector experienced yielding. Shortly after, the connector slip relative to the grout increased; this was followed by an equal decrease in connector slip relative to the grout. V-shaped cracks formed on the side of the specimen when the stress reached 63 ksi. At this point, the grout surface continued to displace upward relative to the connector end, but at a decreasing rate as more V-shaped cracks formed on the side of the specimen at stresses of 67 and 74 ksi. At 79 ksi, V-shaped cracks formed on the unloaded side of the specimen, and failure of the connection was imminent; the relative displacement of the connector end relative to the grout increased until the connection failed.

Figure 5.64 shows the stress-slip relative to grout for the right connector of Test No. 32. The data show that the connector and the grout displaced together until the first splitting cracks emerged in the concrete at 20 ksi. Then, the grout temporarily displaced a small amount relative to the connector end. However, at a stress of 29 ksi, the connector and the grout were again moving upward at the same rate. When the stress reached 45 ksi, a widespread pattern of radial splitting developed around the connectors. The connector slipped relative to the grout a small amount. At a stress of 50 ksi, V-shaped cracks formed on the more heavily loaded side of the specimen, and a drop in connection resistance was recorded; a corresponding increase in connector slip relative to the grout was also recorded. Loading of the connection continued, and additional V-shaped crack formations

emerged on both sides of the specimen at stresses of 53 and 57 ksi. The rate of connector slip relative to the grout increased. At a stress of 59, the connector underwent yielding. Immediately after, the connector displacement relative to the grout increased, but a decrease was also observed shortly after. As has been mentioned before, this increase in grout displacement can be attributed to yield elongation occurring in the connector a short distance beneath the surface of the grout. When the stress reached 63 ksi, one of the connectors (third bar) showed signs of failure after a shallow horizontal crack developed on the less heavily loaded side of the specimen. At failure, some additional slip of the connector relative to the grout was observed.

5.8 STRAIN MEASUREMENTS IN THE DUCTS

As mentioned in Section 4.3, the strain in the ducts was monitored during the tests using strain gages. Measurements of strain in the ducts can provide an indication of the degree of confinement provided to the connector at different load stages. The duct gages were generally oriented in the circumferential direction to measure tensile stresses in the duct.

The function of the duct as part of the force resisting mechanism is to transfer the force applied on the connector to the surrounding concrete. This transfer of force includes enhancing the bond between the connector and the grout by providing confinement to the grout. The duct must also be able to resist the axial tension that is being transferred by friction between its surface and the grout and the concrete; the duct corrugation pattern plays a very important role here. The state of stress in the duct is therefore very complex, and may involve tensile stresses in many directions.

A series of stress-duct strain diagrams are presented in this section that show the strains in the duct at different depths for a representative set of tests. The results are presented once again in three groups determined by the duct type.

5.8.1 Galvanized Steel Duct Specimens

The stress-duct strain behavior of connectors placed inside galvanized steel ducts is illustrated by a set of representative tests consisting of one and two connectors.

Figure 5.65 shows the stress-duct strain diagram for Test No. 3. The strain readings in the duct increased slightly as loading began. Somewhat larger strains were observed at a depth of 4 in. than at other depths. At a stress of 47 ksi, the first splitting crack emerged in the concrete. Additional splitting cracks developed as the stress applied increased. As a result of splitting, the strain in the duct at a depth of 13 in. increased. The duct readings corresponding to the connector's yield strength of 75 ksi stayed constant for the most part. For stress values between 76 and 83 ksi, comparison of the duct strain data to the stress-slip relative to grout data for the connector (Figure 5.54) shows that increases in duct strain were observed for a corresponding increase in connector slip relative to the grout. The strains mobilized in the ducts show that they were confining the grout and the connector as the latter was slipping out of the grout. At maximum load, the strains in the duct down to a depth of 8 in. increased significantly. Comparison of strain data collected at a depth of 8 in. for both the strain gage oriented in the circumferential direction, and the one aligned with the duct seams, shows small differences. The gage aligned with the duct seams measured larger strains for stress values higher than 75 ksi.

The stress-duct strain diagram for Test No. 4 is shown in Figure 5.66. The strain readings in the duct increased slightly as loading began. A sudden increase

in strain was observed at a depth of 4 in. at a stress of 34 ksi, attributed to minor slip of the connector relative to the grout. At a stress of 60 ksi, the first splitting crack emerged in the concrete. Additional splitting cracks developed as the stress applied increased. As a result of splitting, the strain in the duct at a depth of 13 in. increased somewhat. Soon after the yield strength of the connector was reached, the strains in the duct at a depth of 4 in. decreased. This can be attributed to the development of horizontal cracks in the grout near the surface, and connector yield elongation. At a stress of 77 ksi, V-shaped cracks developed on the side of the specimen, and the slip of the connector relative to the grout increased (Figure 5.55). The connector slipping out of the grout incited the confining action of the ducts, demonstrated by an increase in the duct strain readings at all gage locations. Comparison of strain data collected at a depth of 8 in. for both the strain gage oriented in the circumferential direction, and the one aligned with the duct seams, shows small differences. The gage aligned with the duct seams measured larger strains for stress values higher than 85 ksi, the stress when an additional V-shaped crack formed on the side of the specimen.

Figure 5.67 shows the stress-duct strain diagram for the left connector of Test No. 13. The diagram shows small increases in duct strain at very low stresses. Many radial cracks in the grout were noticed at stresses between 13 and 16 ksi. The stress-slip relative to grout diagram for the same connector showed an increase in slip at these stresses (Figure 5.56). Splitting cracks in the concrete were detected at a stress of 38 ksi. Duct strains increased as splitting cracks continued to develop, especially at a depth 8 in. below the surface. The duct readings at 8 in. in the seam or spiral orientation between stresses of 53 and 66 ksi involved a series of cycles where the strain was increasing and decreasing alternately. The stress-slip relative to grout diagram for the connector (Figure 5.56) revealed that within this stress range, the upward displacement of the grout

was larger to that of the connector end. It is possible that horizontal cracks in the grout were forming at a depth of 8 in. and the duct was experiencing axial tension. This would explain the reductions in duct strain. When V-shaped cracks developed at a stress of 63 ksi, confining action at a depth of 13 in. was mobilized, indicated by the increase in the duct strain at this location. The connector was slipping out of the grout at this time. At a stress of 74 ksi, a significant number of cracks had developed on the side of the specimen. The connector then experienced yielding, and shortly after, the connector and the grout were displacing together upward confined by the steel duct. The strain readings at a depth of 8 in. show that a duct strain reversal occurred at a stress of 77 ksi. This reversal in duct strain can also be explained as the duct experiencing axial tension due to upward movement of the portion of grout located just above that particular gage location. With increased slip of the connector, increases in duct strain were observed at a depth of 13 in.; whereas increases in duct strain at a depth of 4 in. can be attributed to yield elongation as well as slip of the connector. Comparison of the circumferential and the seam oriented strain gage readings at 8 in. shows that, aside from the series of strain reversals observed in the spirally oriented gage, the strain values recorded up to the failure load were very similar.

The stress-duct strain diagram for the left connector of Test No. 17 is shown in Figure 5.68. The strain readings in the duct increased slightly as loading began. Somewhat larger strains were observed at a depth of 4 in. than at other depths. At a stress of 33 ksi, the first splitting crack emerged in the concrete. Additional splitting cracks developed as the stress applied increased. No significant increases in duct strain were observed until the stress reached 45 ksi. At this stress level, a widespread pattern of radial cracks surrounded the connectors (Figure 5.23). The duct readings increased a small amount, and then

continued to increase until the connection reached its capacity. At failure, the gages located 8 in. below the surface recorded the largest values of strain.

5.8.2 Polyethylene Duct Specimens

The stress-duct strain behavior of connectors housed inside polyethylene ducts is illustrated by a set of representative tests consisting of one and two connectors.

Figure 5.69 shows the stress-duct strain diagram for Test No. 7. As loading began, the strains recorded in the duct remained small; the gages located deeper in the duct recorded strains of negative value. At a stress of 33 ksi, the first splitting cracks were detected in the concrete. Additional splitting cracks developed as the stress applied increased. As a result of splitting, the strains in the duct gradually increased. The stress-slip relative to grout diagram for the connector showed that between stresses of 45 and 49 ksi, the grout was displacing upward at a faster rate relative to the connector end (Figure 5.58). The strain measured in the duct at a depth of 8 in. decreased after the stress reached 49 ksi. The decrease in strain is attributed to axial tension in the duct, which led to corresponding negative Poisson strains in the circumferential direction. At an applied stress of 57 ksi, extensive radial splitting has developed in the concrete; as the connector and the grout are moving upward together, increases in duct strain were observed at a depth of 4 and 13 in. below the surface. When the stress reached 63 ksi, a horizontal crack developed on the side of the specimen, and the connector slip relative to the grout increased (Figure 5.58). Increases in duct strain were then observed at all gage locations as loading continued. Shortly before failure, there was another strain reversal in the duct 8 in. below the surface; a strain reversal was also simultaneously recorded by the gage located 4 in. below

the surface. These strain reversals can also be attributed to Poisson effects related to axial tension in the duct.

The stress-duct strain diagram for Test No. 22 is shown in Figure 5.70. The strain increased very slowly in the duct during the beginning of the test. The gage located 4 in. below the surface experienced an increase in negative strain, but steadily the strain readings shifted to positive values when the connector slipped a small distance relative to the grout. When the stress applied was 45 ksi, the first splitting crack emerged in the concrete. At this point, all duct gages were measuring small, but positive increases in strain. Shortly after, at a stress of 57 ksi, a second splitting crack developed, and larger changes in duct strain were observed. When the stress reached 63 ksi, the stress-slip relative to grout diagram showed that the grout displacement increased relative to the connector end (Figure 5.59). As loading progressed, the negative strain readings in the duct at a depth of 4 in. indicate that at this depth the duct was experiencing significant axial tension. Soon after the yield strength of the connector was achieved, duct strains reversed at depths of 8 in. and 18 in. At a stress of 81 ksi, a horizontal crack formed on the side of the specimen. This crack extended at 83 ksi, and led to a steady increase in slip of the connector relative to the grout. Strain measurements in the duct indicate that the duct was experiencing axial tension along its entire length, caused by upward movement of the grout, possibly out of the duct.

Figure 5.71 shows the stress-duct strain diagram for the left connector of Test No. 14. As loading began, the strains recorded in the duct remained small. At a stress of 42 ksi, the first splitting cracks were detected in the concrete. Additional splitting cracks developed as the stress applied increased. As a result of splitting, the strains in the duct increased. When the stress reached 51 ksi, V-shaped cracks formed on the loaded side of the specimen. The duct strain values at a depth of 8 in. indicate that the duct was experiencing significant axial tension

at this depth. At a stress of 64 ksi, the connection failed, and the other connector involved pulled-out. As loading resumed, this time only the left connector, strains in the duct came close to their values before the connection failed. At a stress of 61 ksi, the left connector failed; the strain recorded by the gage at a depth of 8 in. increased as the bar was pulling out of the grout.

The stress-duct strain diagram for the left connector of Test No. 24 is shown in Figure 5.72. The first splitting cracks in the concrete were detected at a stress of 43 ksi, and splitting was widespread when the stress reached 58 ksi. Duct strain measurements increased at depths of 4, 8, and 13 inches. At 61 ksi, V-shaped cracks formed on the loaded side of the specimen and the connector slipped relative to the grout. Duct strain reversals were observed at depths of 8 and 13 in., indicating that the duct was experiencing significant axial tension at these locations just before failure. The strain in the duct at a depth of 18 in. increased as the connector's slip relative to the grout increased.

5.8.3 Polypropylene Duct Specimens

The stress-duct strain behavior of connectors placed inside polypropylene ducts is illustrated by a set of representative tests consisting of one, two, and three connectors.

Figure 5.73 shows the stress-duct strain diagram for Test No. 30. As loading began, the strains recorded in the duct remained small; two of the gages recorded strains of negative value. At a stress of 32 ksi, the first splitting crack was detected in the concrete. No appreciable change was seen in the strain measurements. At a stress of 42 ksi, the stress-slip relative to grout diagram showed a slight increase in grout displacement relative to the connector end (Figure 5.62). The strain in the ducts decreased and switched into negative values as loading progressed. After the stress reached the connector yield strength, the

gage located 4 in. below the surface recorded small increases in strain. The stress-slip relative to grout diagram also showed that the grout displacement was increasing in relation to the connector end (Figure 5.62). The upward movement of the grout coincided with significant axial tension in the duct, indicated by the strain readings at depths of 8 and 13 inches. At the failure stress of 65 ksi, and as the bar pulled out, increases in strain were observed in the duct at 4 and 13 inches. The gage at 8 in. continued to measure negative strains even after failure.

The stress-duct strain diagram for the right connector of Test No. 28 is shown in Figure 5.74. Radial splitting in the concrete first developed at a stress of 44 ksi. No appreciable changes were seen directly in the duct strain readings. The gage located at a depth of 4 in., followed by the one located at 8 in., recorded the largest strains, as splitting in the concrete continued. Yielding of the connector was a large event in the duct strain history. Shortly after yielding, V-shaped cracks developed on the loaded side of the specimen. After these successive events, strain increases were observed along the duct, except at a depth of 18 in.; here, the strain remained negative. At a stress of 81 ksi, the slip of the connector relative to the grout increased (Figure 5.63); the slip of the connector appeared to affect the gage readings at 8 and 13 in. in contrasting ways.

Figure 5.75 shows the stress-duct strain diagram for the right connector of Test No. 32. Radial splitting in the concrete first developed at a stress of 20 ksi. Strains in the duct remained small, except at 4 in. below the surface. As loading continued, and additional splitting cracks formed, increases in duct strain were eventually observed at the 8 in. depth. At a stress level of 50 ksi, a V-shaped crack formed on the side of the specimen. The connector slip relative to the grout increased (Figure 5.64). Strains increased in the duct at depths of 4, 8, and 13 in.; the gage located at a depth of 18 in. recorded negative strain values. At 59 ksi, the connector experienced yielding; the duct strains continued to increase at the

shallow depths, but a strain reversal was observed at a depth of 13 inches. This indicates that following the yielding event, the duct was experiencing significant axial strains at depths of 13 and 18 inches.

5.9 SPECIMEN AUTOPSIES

The connection specimens were loaded until only a small fraction of residual capacity was left. At this time, significant slip between the connector/grout/duct and the concrete had occurred. Testing the connectors in such manner would make a forensic investigation of the connection simpler, since a larger portion of the connector would be protruding above the concrete for careful examination. Sometimes, chipping of the concrete was necessary to reach deeper areas in the connectors in order to identify cracks in the grout and tears in the ducts. The specimen autopsies often involved cutting through the duct to examine crack formations in the grout. Most of the specimen examinations were conducted days after the test.

The pullout modes of failure of the connection specimens were verified through forensic examination. Many times, cracks in the grout or tears in the duct were visible directly after a test, which established the connection failure mode right away and eliminated the need for further exploration. Considering the manner in which the connection specimens were loaded after failure, it is possible that some of the damage observed in the connection specimen autopsies occurred following connection failure. The establishment of the mode of failure for a particular connection was not solely based on the forensic examinations, but the finding was also substantiated by data collected on duct strains and displacement of the connector relative to the grout.

5.9.1 Galvanized Steel Duct Specimens

The autopsies conducted on galvanized steel duct specimens generally involved determining the depth at which the duct opening or fracture occurred. Whenever the duct tear was not visible, chipping of the concrete around the duct was employed. Figure 5.76 and Figure 5.77 show pictures of the autopsies conducted on the connection specimens of Tests No. 4 and No. 23. The information gathered through the specimen autopsies on connections that contained galvanized steel duct is displayed in Table 5.2.

5.9.2 Polyethylene Duct Specimens

Three pullout modes of failure were observed in connections containing polyethylene ducts. The failure modes were themselves related by the fact that the polyethylene duct was not very effective in preventing the grout and the connector from slipping. The autopsies conducted on these connection specimens often involved determining the depth at which fractures in the grout occurred. The duct was frequently cut using a small saw to peek inside and find cracks in the grout. Whenever cracks in the grout were not visible, chipping of the concrete around the duct was employed to explore deeper. Figure 5.78 and Figure 5.79 show pictures of the autopsies conducted on the connection specimens of Tests No. 7 and No. 8. Table 5.3 displays the information gathered through the specimen autopsies on connections that contained polyethylene duct.

5.9.3 Polypropylene Duct Specimens

The autopsies conducted on connection specimens containing polypropylene ducts generally involved determining the depth at which fractures in the grout occurred. The duct was frequently cut using a small saw to peek inside of it and find cracks in the grout. Whenever cracks in the grout were not visible, chipping of the concrete around the duct was employed to explore deeper.

Figure 5.80 and Figure 5.81 show pictures of the autopsies conducted on the connection specimens of Tests No. 28 and No. 32. Table 5.4 displays the information gathered through the specimen autopsies on connections that contained polypropylene duct.

5.10 SUMMARY

The aim of the experimental program was to gain a better understanding of how different configuration parameters affect the behavior of precast bent cap connections using grouted vertical ducts.

The presentation of the test results was divided into three groups, determined by the duct material present in the connection test specimen: galvanized steel duct specimens, polyethylene duct specimens, and polypropylene specimens. Every connection specimen tested failed by pullout of the connectors. Different pullout failure modes were identified for the three connection groups.

Results of representative sets of tests involving each duct material were presented in detail. The presentation of the measured response included: stress-end slip diagrams, strain distribution along the connector, stress distribution along the connector, stress-slip of connector relative to grout diagrams, and stress-duct strain diagrams.

Larger connection capacities were recorded for connection specimens containing galvanized steel ducts. Connections containing polypropylene ducts generally performed better than connections containing polyethylene ducts. The capacities of the connections dropped significantly as the number of connectors per connection being tested increased. During loading, and as the stress applied approached the connection capacity, higher ratios of stress in the connector relative to applied stress were recorded along the connectors in specimens containing polyethylene ducts.

Slip of the grout relative to the connector end occurred frequently in connection specimens with polyethylene and polypropylene ducts. This was an indication of problems with the ducts in anchoring the grout. The duct strain measurements in the polyethylene and polypropylene ducts were characterized by a combination of circumferential tensile strains and axial tensile strains. Typically positive duct strain values were recorded when the primary action was slip of the connector relative to the grout. Negative duct strain values were recorded when the primary action was slip of the connector/grout out of the duct.

The pullout modes of failure of the connection specimens were verified through forensic examination. The establishment of the mode of failure for a particular connection was not solely based on the forensic examinations, but the assessment was also substantiated by data collected on duct strains and displacement of the connector relative to the grout.

Table 5.1 Test Matrix and Selected Test Results

Series	Test	Bars	Coating	Duct	Transverse Reinforcement	l_e (d_b)	f_g (ksi)	f'_c (ksi)	f_y (ksi)	f_{max} (ksi)	$Slip_{max}$ (in.)	f_{split} (ksi)
1	1	1-#11	No	Steel	G-spiral	8	5.0	5.4	-	58	0.20	46
	2	1-#11	Yes	Steel	G-spiral	8	6.1	5.4	-	55	0.09	48
	3	1-#11	No	Steel	G-spiral	12	6.4	5.4	75	87	0.19	47
	4	1-#11	Yes	Steel	G-spiral	12	6.4	5.4	68	88	0.22	60
	5	1-#11	No	PE	G-spiral	8	4.7	5.5	-	48	0.16	37
	6	1-#11	Yes	PE	G-spiral	8	5.5	5.5	-	40	0.14	30
	7	1-#11	No	PE	G-spiral	12	5.9	5.5	-	67	0.26	33
	8	1-#11	Yes	PE	G-spiral	12	5.8	5.5	-	65	0.17	36
2	9	1-#11	No	PE	G-spiral	12	5.1	4.5	-	54	0.22	42
	10	1-#11	No	Steel	G-spiral	12	5.6	4.5	75	80	0.26	45
	11	1-#11	Yes	None	G-spiral	12	5.1	4.6	-	68	0.13	45
	12	1-#11	No	None	G-spiral	12	5.1	4.6	-	67	0.18	42

Table 5.1 (continued) Test Matrix and Selected Test Results

Series	Test	Bars[A]	Bar Ecc.	Duct[B]	Transverse Reinforcement	l_e (d_b)	f_g (ksi)	f'_c (ksi)	f_y (ksi)	f_{max} (ksi)	$Slip_{max}$ (in.)	f_{split} (ksi)
3	13	2-#11	No	Steel	G-spiral	16	5.2	4.7	75	87	0.25	38
	14	2-#11	No	PE	G-spiral	16	5.3	4.7	-	64	0.27	42
	15	2-#11	No	Steel	None	16	5.4	4.7	75	86	0.24	39
	16	2-#11	No	PE	None	16	5.4	4.7	-	59	0.35	42
4	17	2-#11	No	Steel	G-spiral	12	4.8	5.2	-	59	0.19	33
	18	2-#11	No	PE	G-spiral	12	4.9	5.3	-	44	0.27	24
	19	1-#11	Yes	Steel	G-spiral	8	5.1	5.5	-	49	0.14	41
	20	1-#11	Yes	PE	G-spiral	8	5.1	5.5	-	40	0.19	31
	21	1-#11	Yes	Steel	G-spiral	12	5.4	5.5	59	74	0.12	36
	22	1-#11	No	PE	G-spiral	16	5.4	5.5	76	90	0.42	45

[A] All bars in series 3 and 4 were uncoated.

[B] In series 3 and 4, clear duct spacing for double-connector tests was 1 duct-diameter.

Table 5.1 (continued) Test Matrix and Selected Test Results

Series	Test	Bars[A]	Duct Spg.	Duct	Transverse Reinforcement	l_e (d_b)	f_g (ksi)	f'_c (ksi)	f_y (ksi)	f_{max} (ksi)	$Slip_{max}$ (in.)	f_{split} (ksi)
5	23	2-#11	2-D	Steel	G-spiral	12	6.0	6.1	59	68	0.21	48
	24	2-#11	2-D	PE	G-spiral	16	6.3	6.1	-	65	0.18	43
	25	1-#11	-	PE	I-spiral	8	6.5	6.1	-	34	0.12	34
	26	2-#11	1-D	PE	I-spiral	16	6.5	6.1	-	62	0.18	39
	27	1-#11	-	PE	I-spiral	12	6.5	6.1	-	63	0.15	49
6	28	2-#11	1-D	PP	G-spiral	16	6.8	6.1	59	85	0.20	44
	29	1-#11	-	PP	G-spiral	8	7.1	6.1	-	40	0.05	39
	30	1-#11	-	PP	G-spiral	12	7.1	6.1	59	68	0.08	32
	31	3-#11	1-D	Steel	None	16	5.8	6.1	59	73	0.13	23
	32	3-#11	1-D	PP	G-spiral	16	5.8	6.1	59	67	0.21	20

[A] All bars in series 5 and 6 were uncoated.

Table 5.2 Autopsy Data on Galvanized Steel Duct Specimens

Test	Bars	Coating	l_e (d_b)	f_{max} (ksi)	Pullout Failure Mode (duct opening or fracture)
1	1-#11	No	8	58	Duct opening at 3 in.
2	1-#11	Yes	8	55	Duct opening at 4.5 in.
3	1-#11	No	12	87	Two duct openings: 4 and 5.5 in.
4	1-#11	Yes	12	88	Duct opening at 4 in.
10	1-#11	No	12	80	Two duct openings: 3 and 4.5 in.
13	2-#11	No	16	87	Not enough data available (probably similar to Test No. 15)
15	2-#11	No	16	86	Left Bar: Duct opening at 6.5 in., Right Bar: Duct Opening at 8.5 in.
17	2-#11	No	12	60	Left Bar: Duct opening at 8.5 in., Right Bar: Duct Opening at 8.5 in.
19	1-#11	No	8	49	Duct opening at 2.5 in.
21	1-#11	No	12	74	Duct fracture at 4.5 in.
23	2-#11	No	12	68	Left Bar: Duct opening at 9.5 in., Right Bar: Duct Opening at 8.5 in.
31	3-#11	No	16	73	Left Bar: Duct opening at 18 in., Right Bar: Duct Opening at 14.5 in., Third Bar: Duct Opening at 18 in.

Table 5.3 Autopsy Data on Polyethylene Duct Specimens

Test	Bars	Coating	l_e (d_b)	f_{max} (ksi)	Pullout Failure Mode[A]	Comments
5	1-#11	No	8	48	(1)	Grout fracture at 2.5 in.
6	1-#11	Yes	8	40	(2)	Grout fracture at 4.5 in.
7	1-#11	No	12	67	(1)	Grout fracture at 2.5 in.
8	1-#11	Yes	12	65	(3)	Plug failure mode
9	1-#11	No	12	54	(1)	Grout fracture at 2.5 in.
14	2-#11	No	16	64	(1), (3)	Left Bar: Grout fracture at 4.5 in.
16	2-#11	No	16	59	(2), (3)	Left Bar: Grout fracture at 9 in.
18	2-#11	No	12	44	(3), (3)	Plug failure mode
20	1-#11	No	8	40	(1)	Grout fracture at 1.0 in.
22	1-#11	No	16	90	(3)	Plug failure mode
24	2-#11	No	16	68	(3), (1)	Right Bar: Grout fracture at 2.5 in.
25	1-#11	No	8	34	(3)	Plug failure mode
26	2-#11	No	16	62	(2), (3)	Left Bar: Grout fracture at 7.5 in.
27	1-#11	No	12	63	(1)	Grout fracture at 4.5 in.

[A] Pullout Failure Modes: (1) pullout of connector with top segment of grout, (2) pullout of connector with top segment of grout and duct, (3) pullout of connector and grout out of the duct (plug failure mode).

Table 5.4 Autopsy Data on Polypropylene Duct Specimens

Test	Bars	Coating	l_e (d_b)	f_{max} (ksi)	Plug Pullout Failure Mode
28	2-#11	No	16	85	Slip of grout out of duct with top duct segment attached (both bars)
29	1-#11	No	8	40	Slip of grout out of duct with top duct segment attached
30	1-#11	No	12	68	Slip of grout and duct out of the concrete
32	3-#11	No	16	67	Slip of grout and duct out of the concrete (three bars) Left Bar: Grout fracture at 22 in., Right Bar: Grout fracture at 17 in., Third Bar: Grout fracture at 17 in.

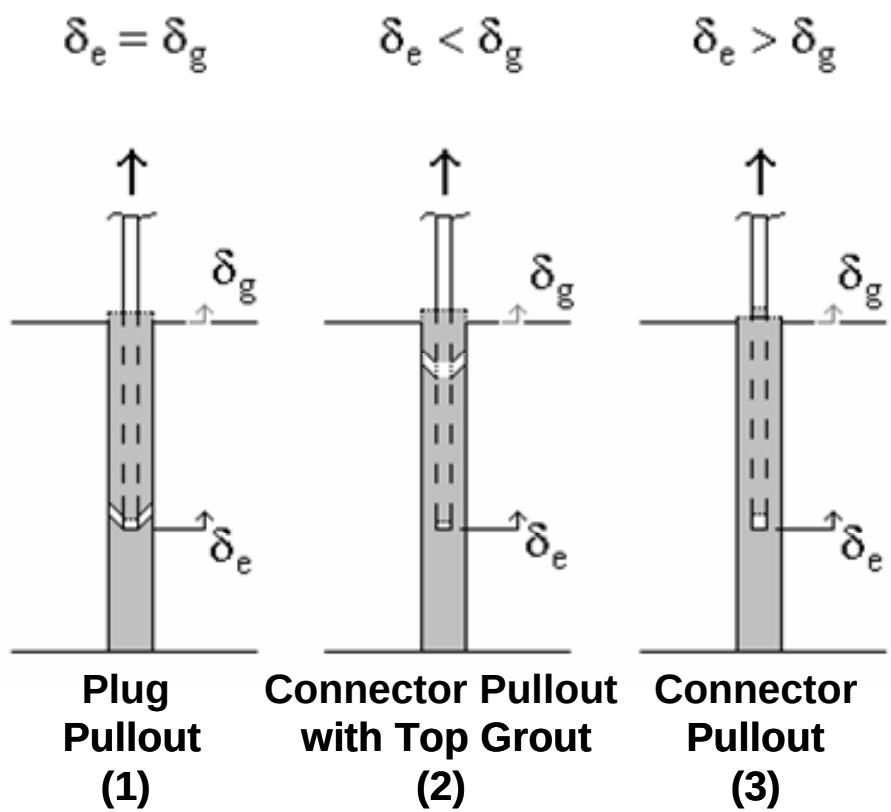

Figure 5.1 Pullout Failure Modes - Relationship between Connector End Slip and Grout Displacement

A. Single Connector ***B. Multiple Connectors***

Figure 5.2 Pullout Failure Modes for Galvanized Steel Duct Connections

(1) ***(2)*** ***(3)***

Figure 5.3 Pullout Failure Modes for Polyethylene Duct Connections

Figure 5.4 Pullout Failure Mode for Polypropylene Duct Connections (Tests No. 30 and No. 32)

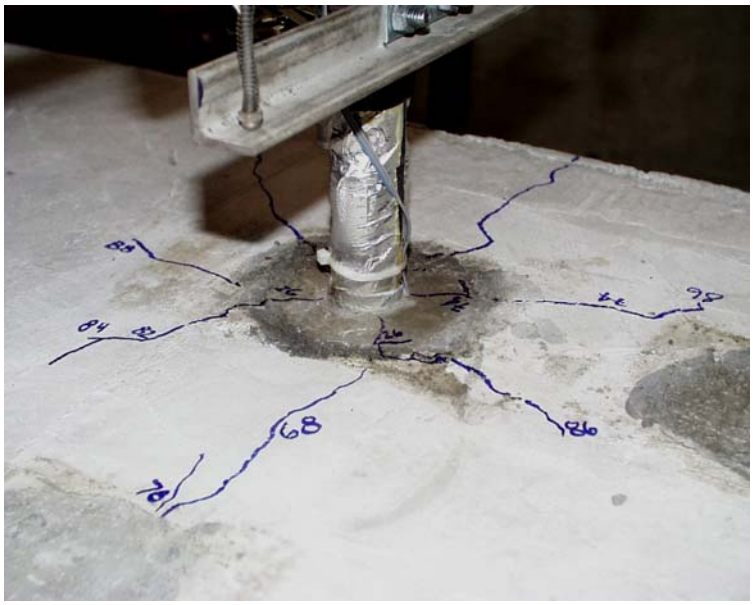

Figure 5.5 Widespread Splitting in Test No. 10

Figure 5.6 Cracking Pattern at Failure in Test No. 10

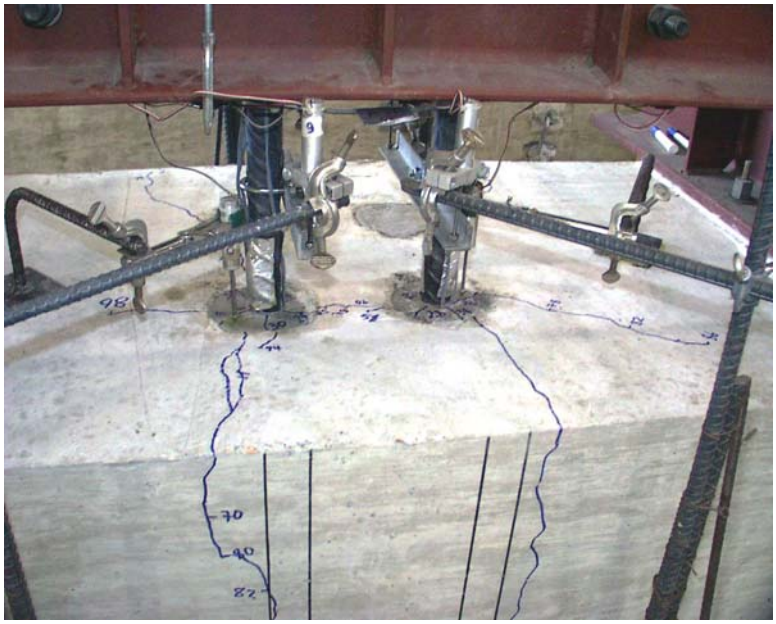

Figure 5.7 Widespread Splitting Cracks in Test No. 13

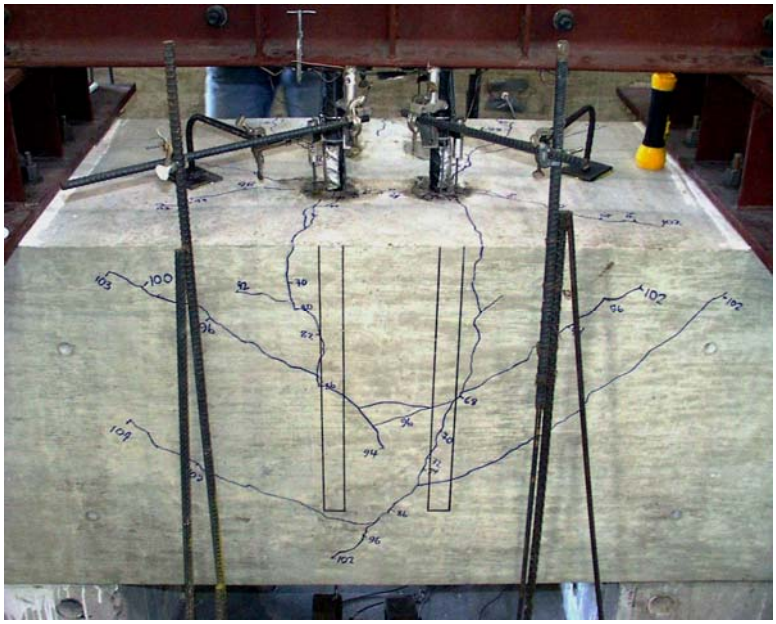

Figure 5.8 Double Connector Test with 1-D Duct Spacing (Test No. 13)

Figure 5.9 Widespread Splitting Cracks in Test No. 23

Figure 5.10 Double Connector Test with 2-D Duct Spacing (Test No. 23)

Figure 5.11 Splitting Cracks in Test No. 9

Figure 5.12 Test No. 9 at Failure Load

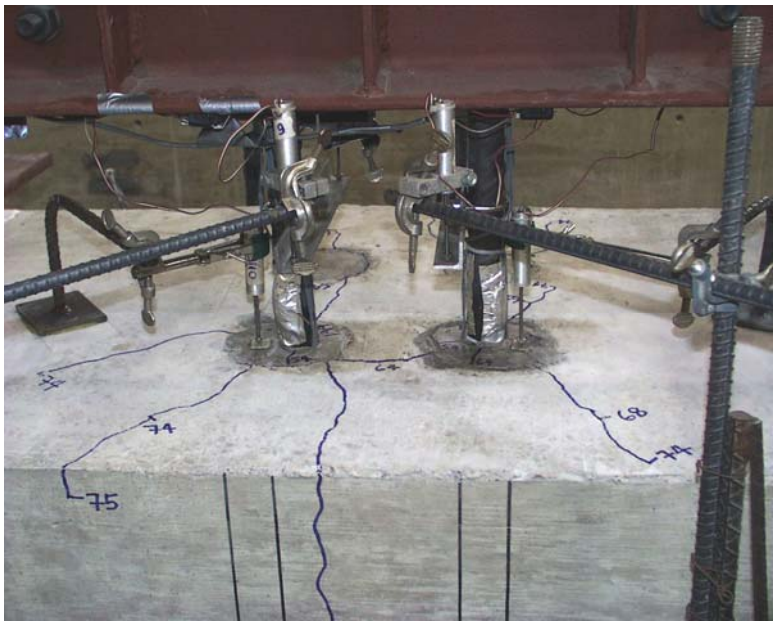

Figure 5.13 Widespread Radial Splitting in Test No. 14

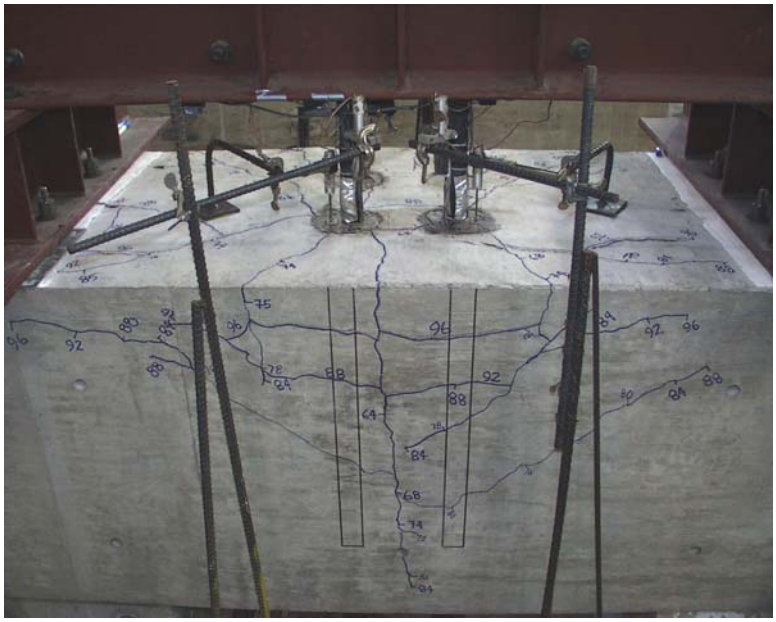

Figure 5.14 Test No. 14 at Failure Load

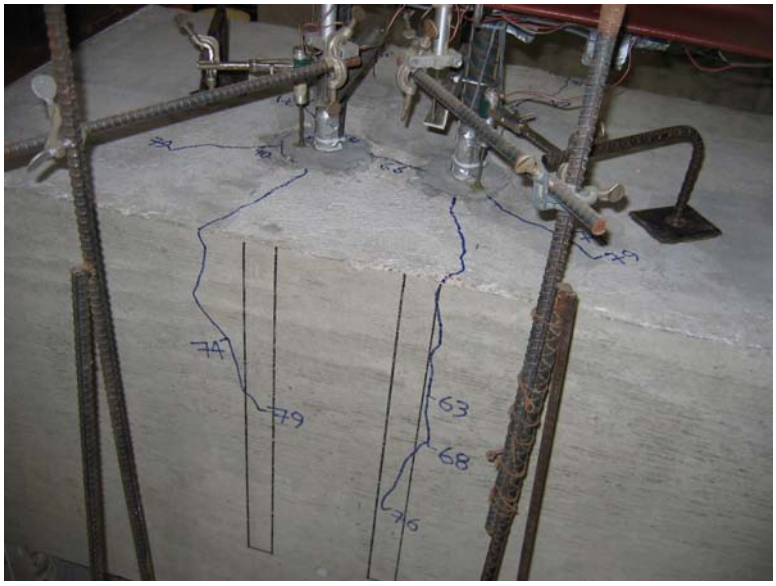

Figure 5.15 Widespread Radial Splitting in Test No. 28

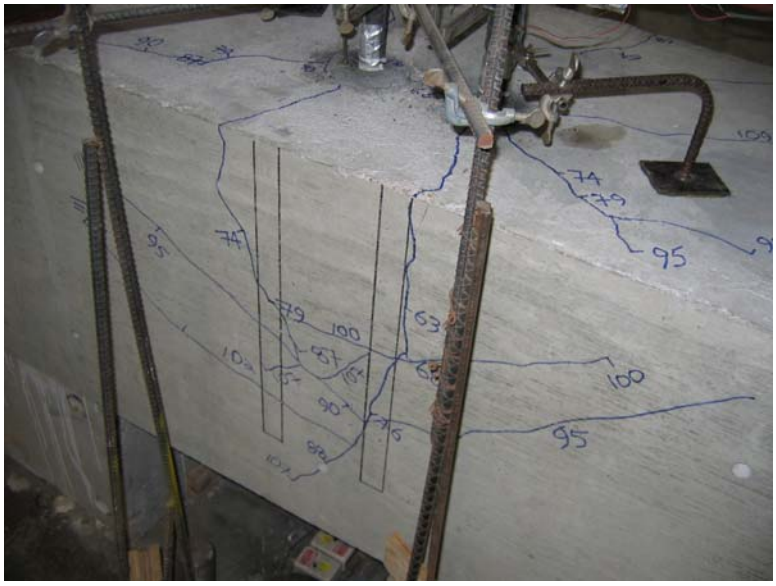

Figure 5.16 V-shaped Crack Formations in Test No. 28

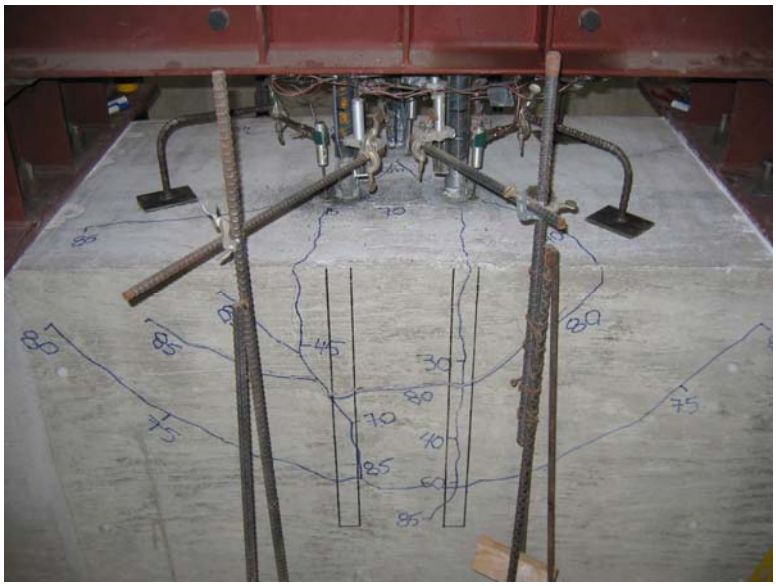

Figure 5.17 V-shaped Crack Formations in Test No. 32

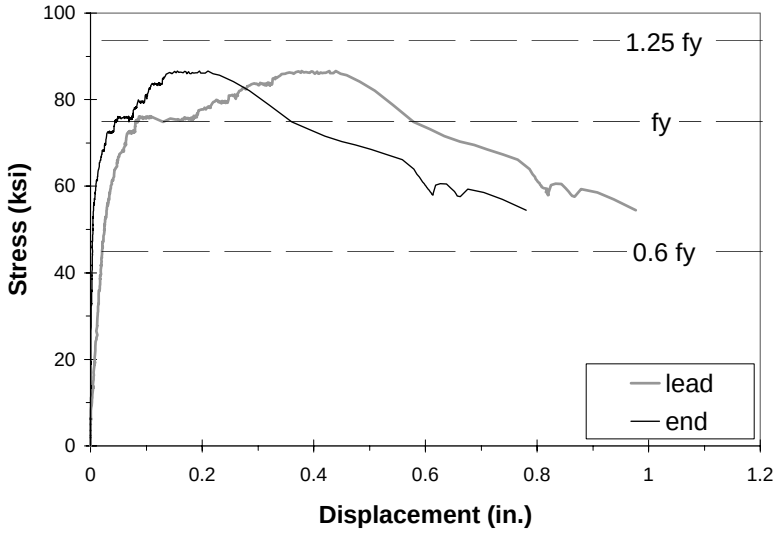

Figure 5.18 Measured Lead and End Connector Displacements (Test No. 3)

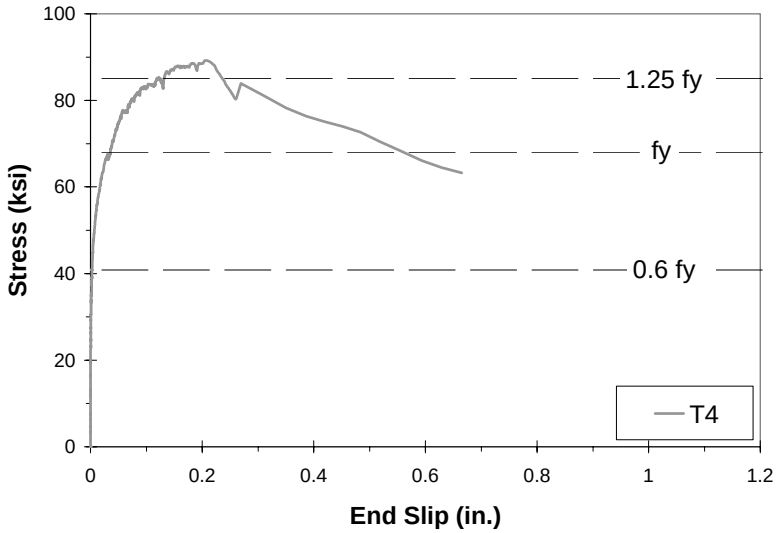

Figure 5.19 Stress vs. End Slip Diagram for Epoxy-coated Connector in Galvanized Steel Duct Embedded 12d_b (Test No. 4)

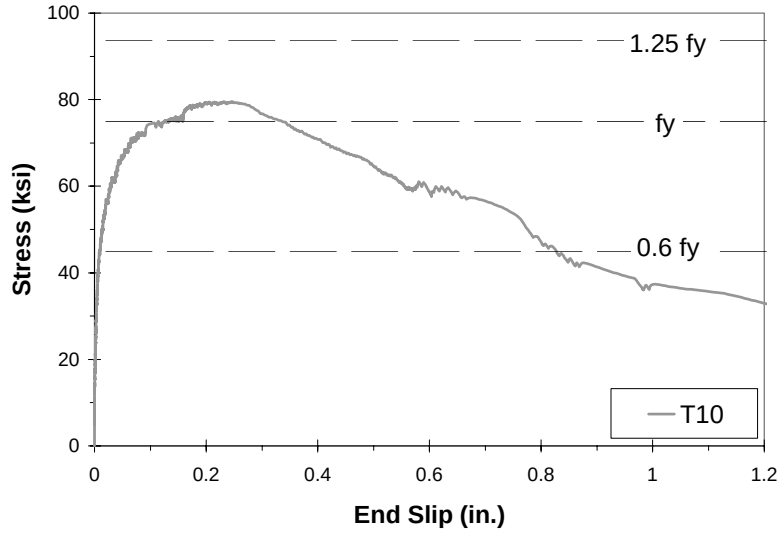

Figure 5.20 Stress vs. End Slip Diagram for Uncoated Connector in Galvanized Steel Duct Embedded 12d_b (Test No. 10)

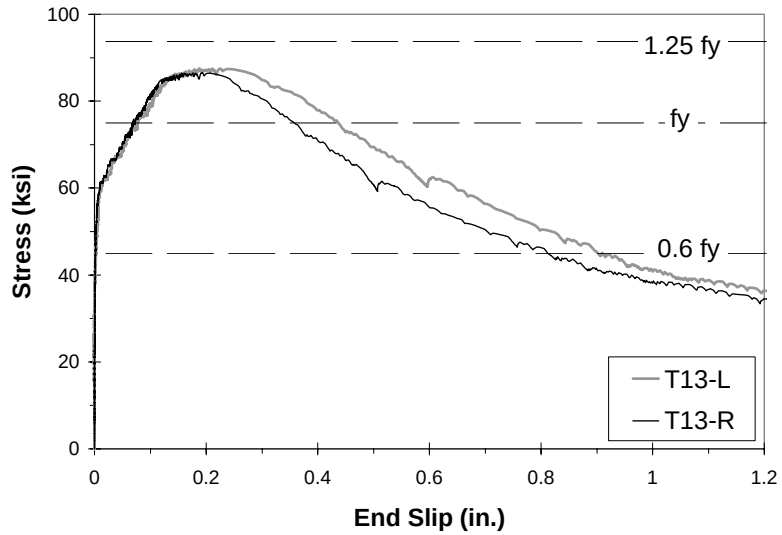

Figure 5.21 Stress vs. End Slip Diagram for Double-connector Test in Galvanized Steel Duct Embedded at 16d_b (Test No. 13)

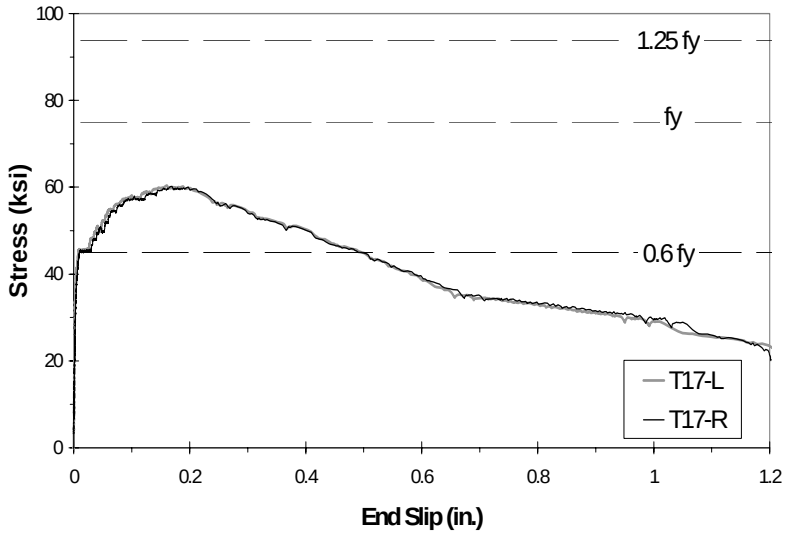

Figure 5.22 Stress vs. End Slip Diagram for Double-connector Test in Galvanized Steel Duct Embedded at 12d_b (Test No. 17)

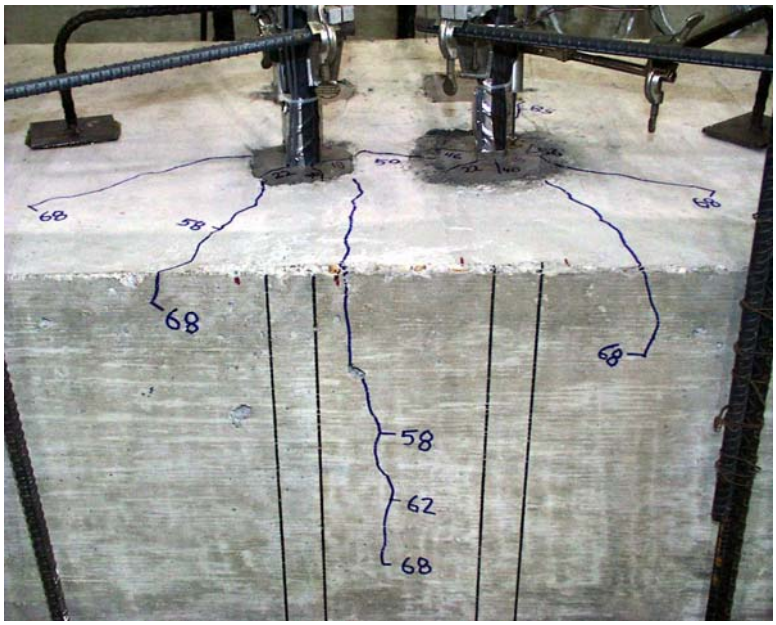

Figure 5.23 Widespread Radial Splitting Pattern in Test No. 17 at 45 ksi

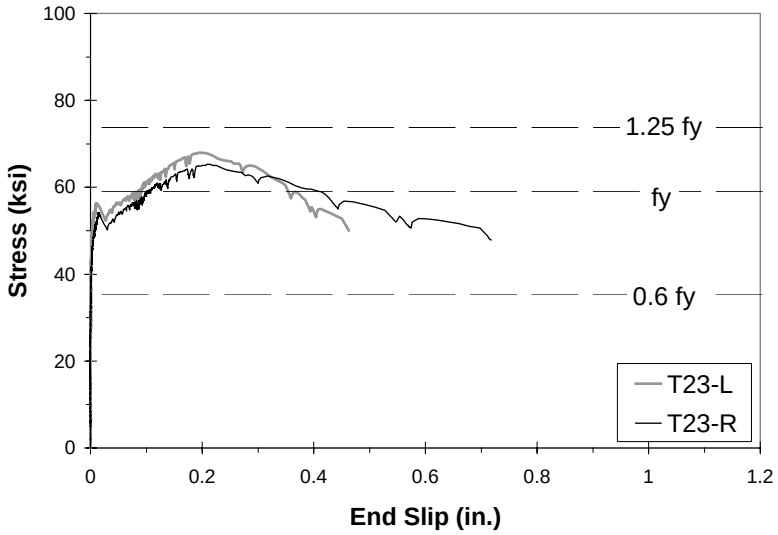

Figure 5.24 Stress vs. End Slip Diagram for Test No. 23

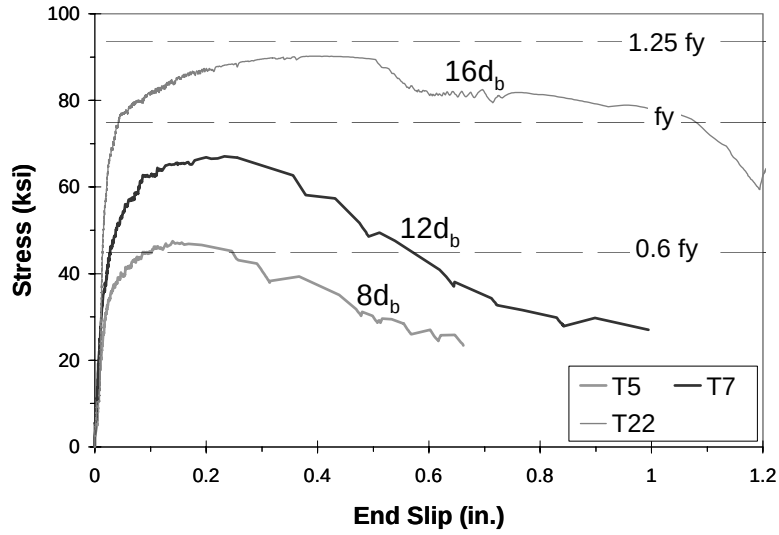

Figure 5.25 Stress vs. End Slip Diagrams for Single Connectors in Polyethylene Ducts Embedded at 8, 12, and 16d_b

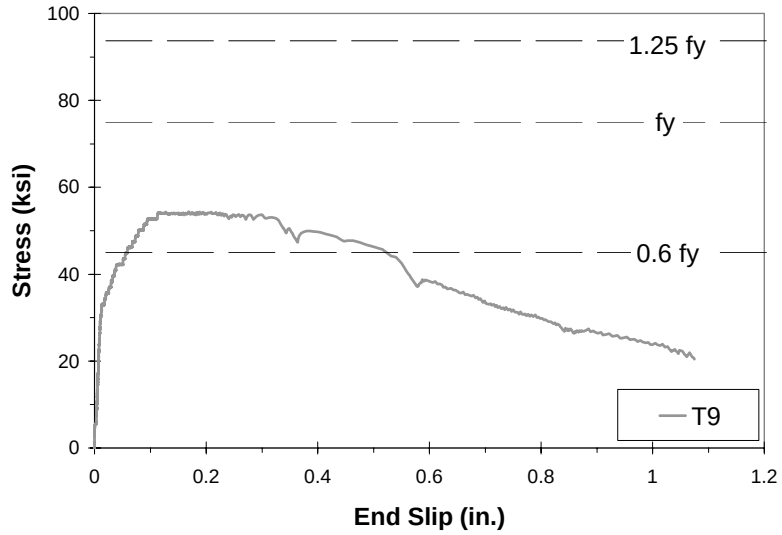

Figure 5.26 Stress vs. End Slip Diagrams for Test No. 9

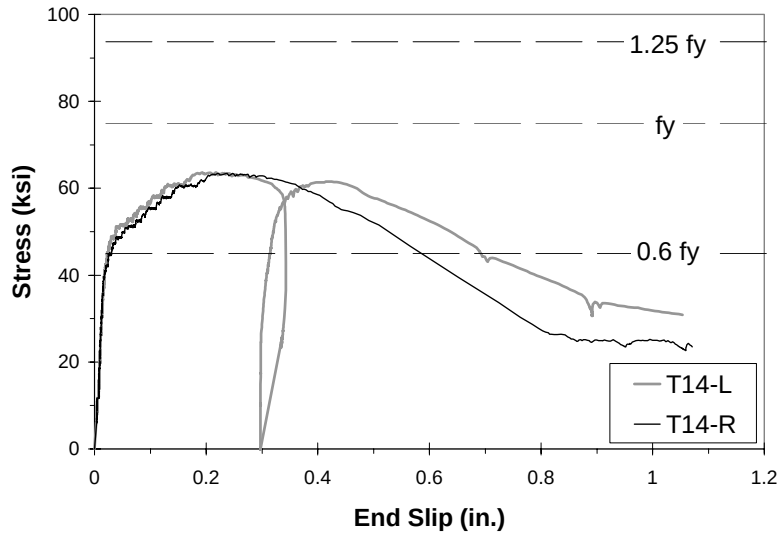

Figure 5.27 Stress vs. End Slip Diagram for Double-connector Test in Polyethylene Duct Embedded at 16d_b with 1-D Duct Spacing (Test No. 14)

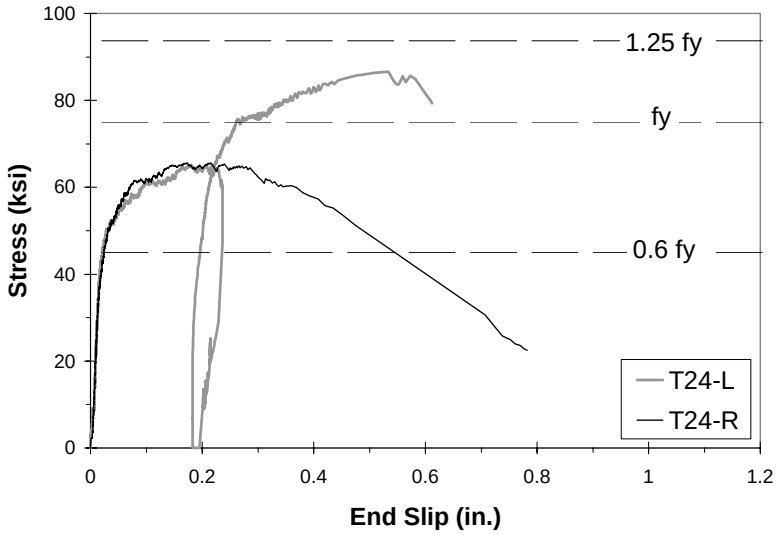

Figure 5.28 Stress vs. End Slip Diagram for Double-connector Test in Polyethylene Duct Embedded at 16d_b with 2-D Duct Spacing (Test No. 24)

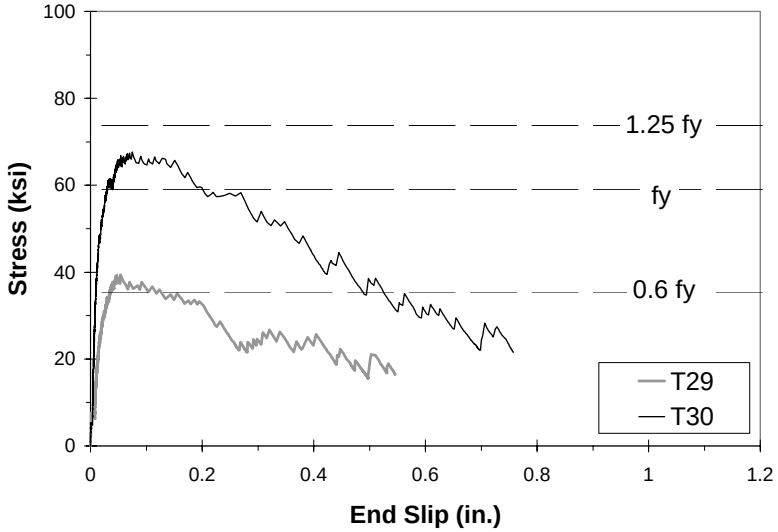

Figure 5.29 Stress vs. End Slip for Single Connectors in Polypropylene Ducts Embedded at 8 and 12d_b

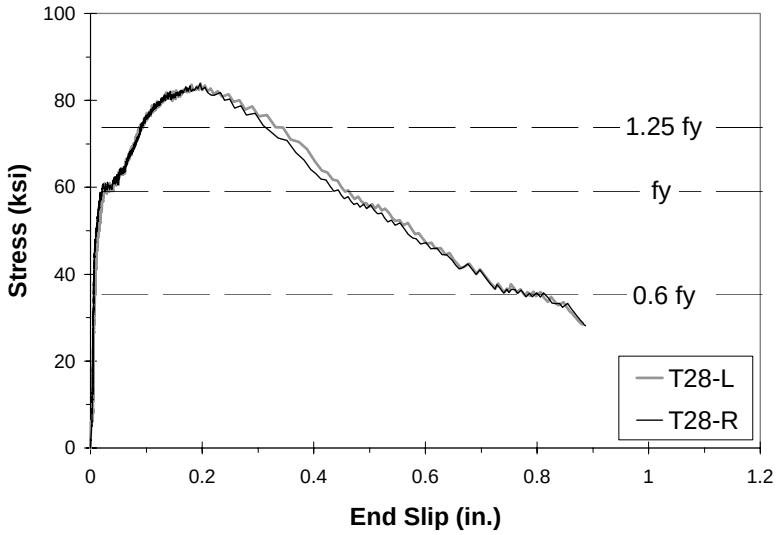

Figure 5.30 Stress vs. End Slip for Test No. 28

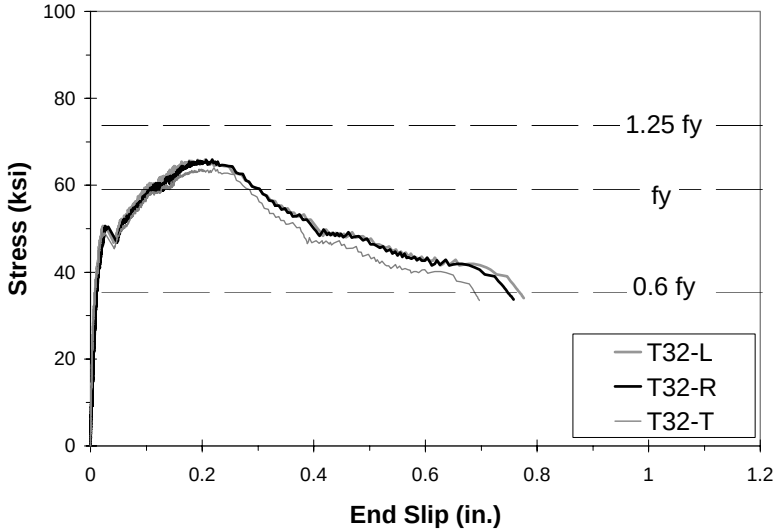

Figure 5.31 Stress vs. End Slip for Test No. 32

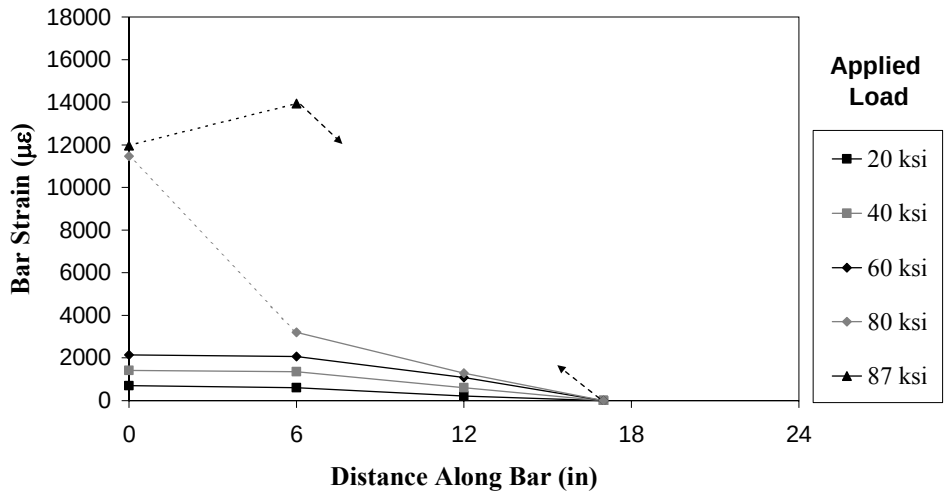

Figure 5.32 Strain Distribution along Connector Length (Test No. 3)

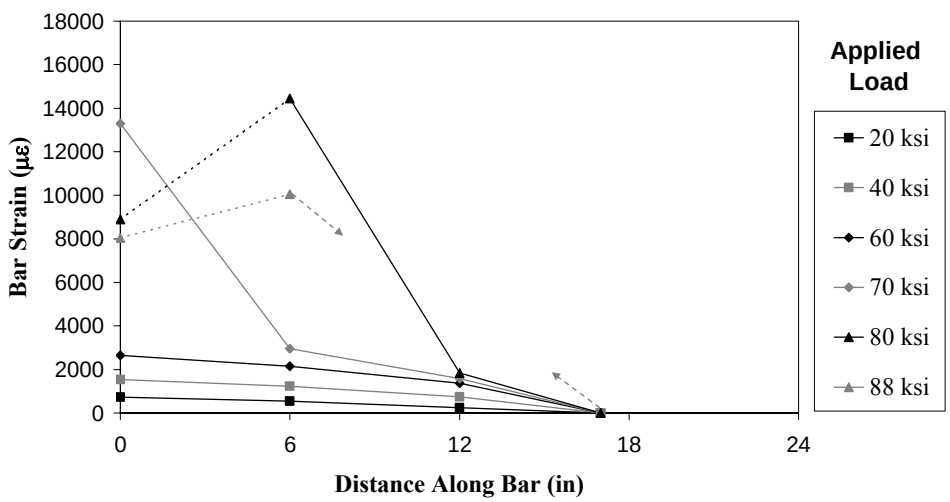

Figure 5.33 Strain Distribution along Connector Length (Test No. 4)

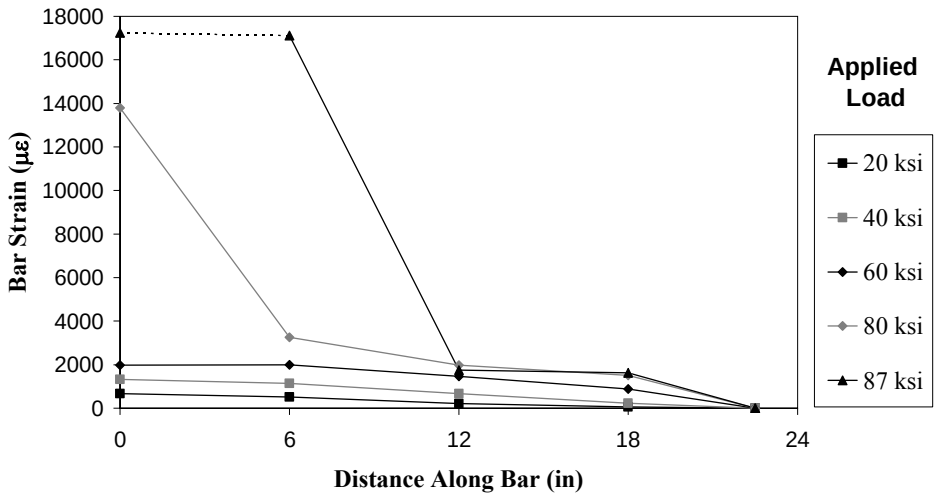

Figure 5.34 Strain Distribution along Connector Length (Test No. 13, Left Bar)

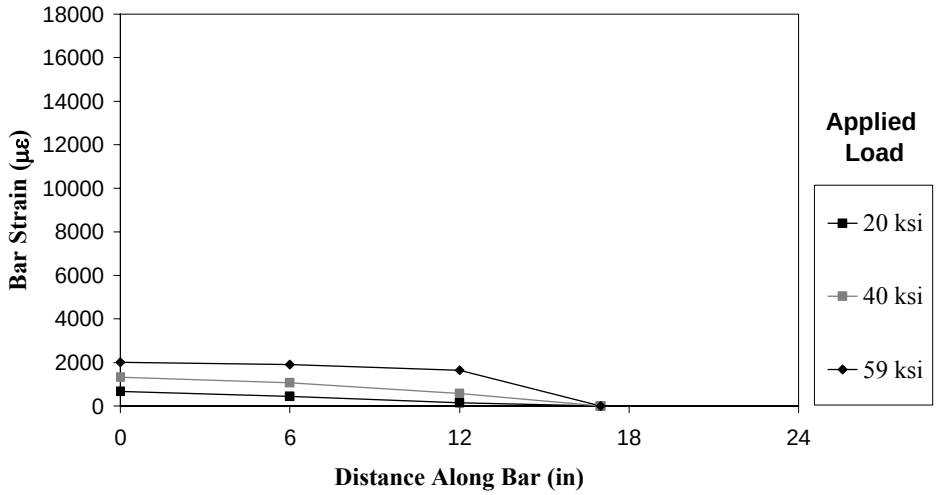

Figure 5.35 Strain Distribution along Connector Length (Test No. 17, Left Bar)

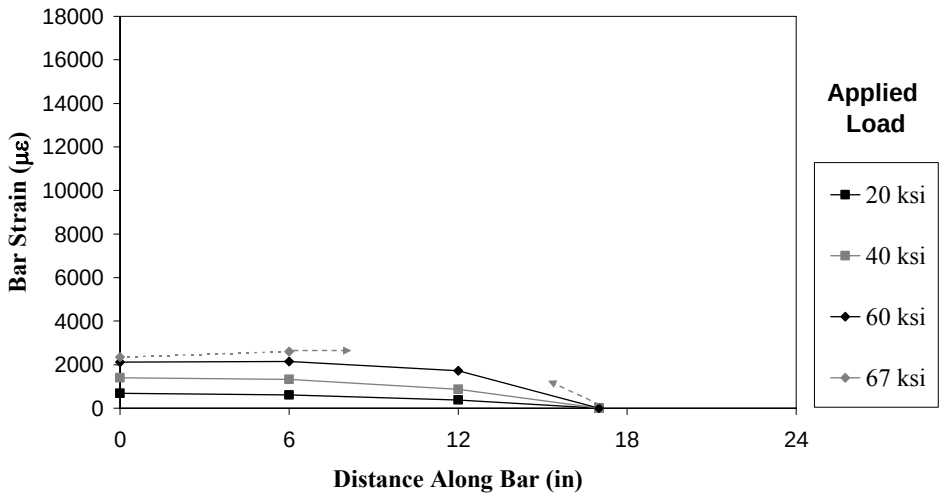

Figure 5.36 Strain Distribution along Connector Length (Test No. 7)

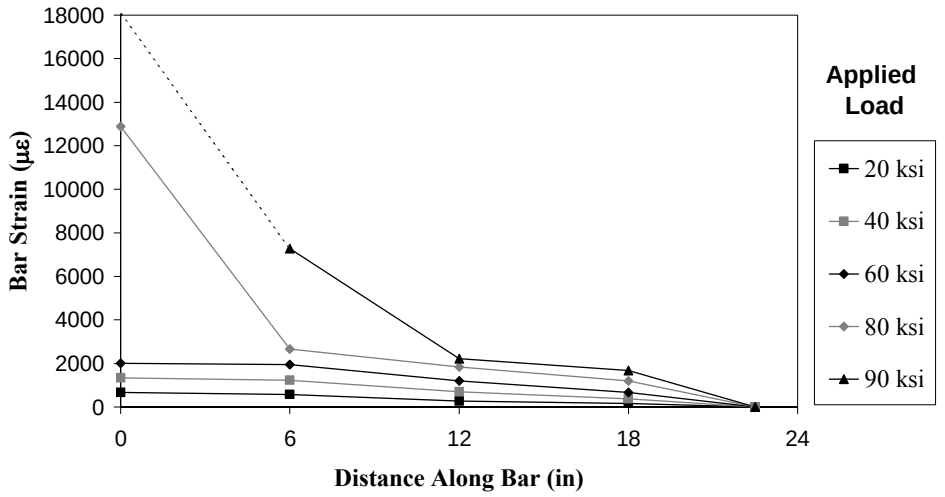

Figure 5.37 Strain Distribution along Connector Length (Test No. 22)

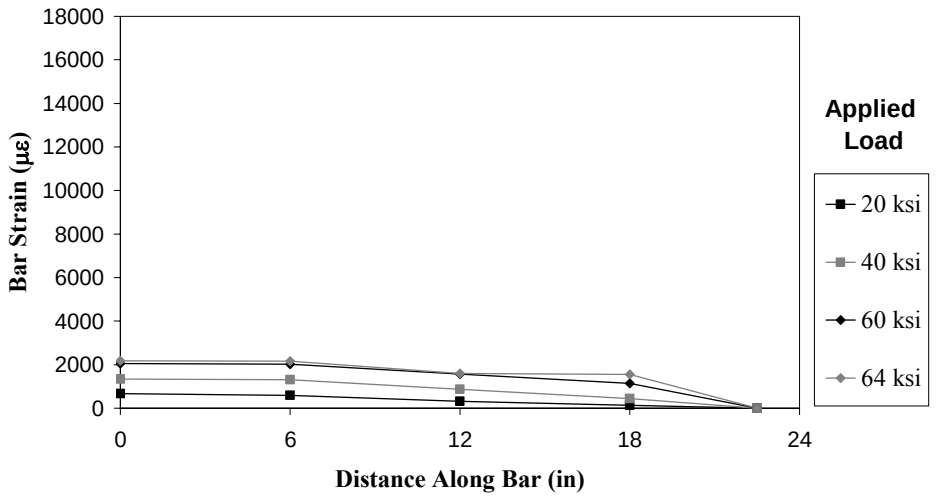

Figure 5.38 Strain Distribution along Connector Length (Test No. 14, Left Bar)

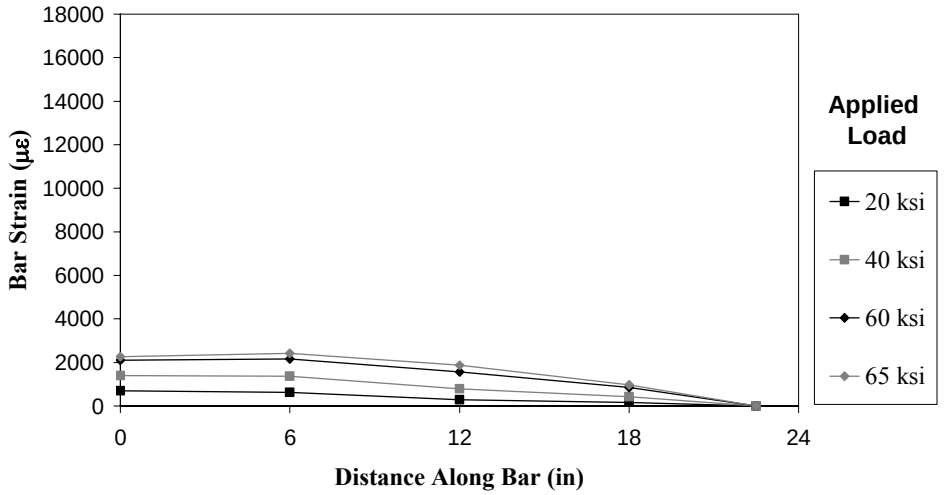

Figure 5.39 Strain Distribution along Connector Length (Test No. 24, Left Bar)

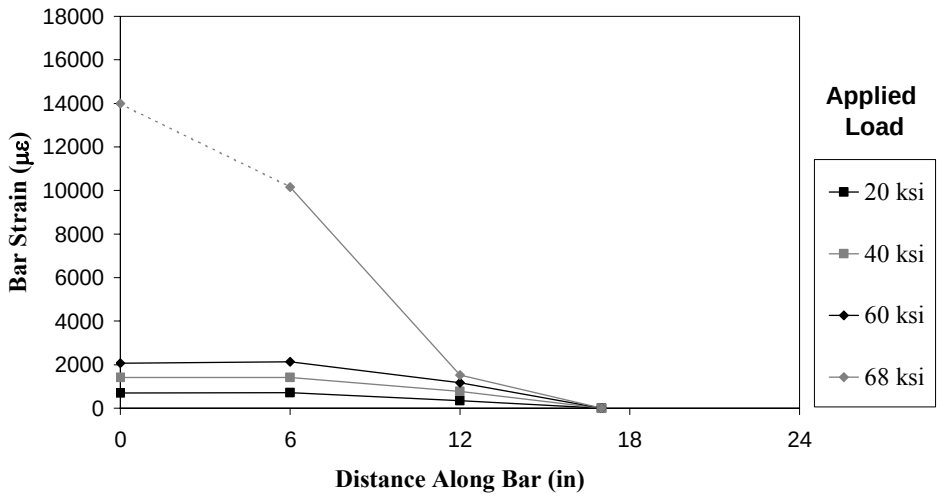

Figure 5.40 Strain Distribution along Connector Length (Test No. 30)

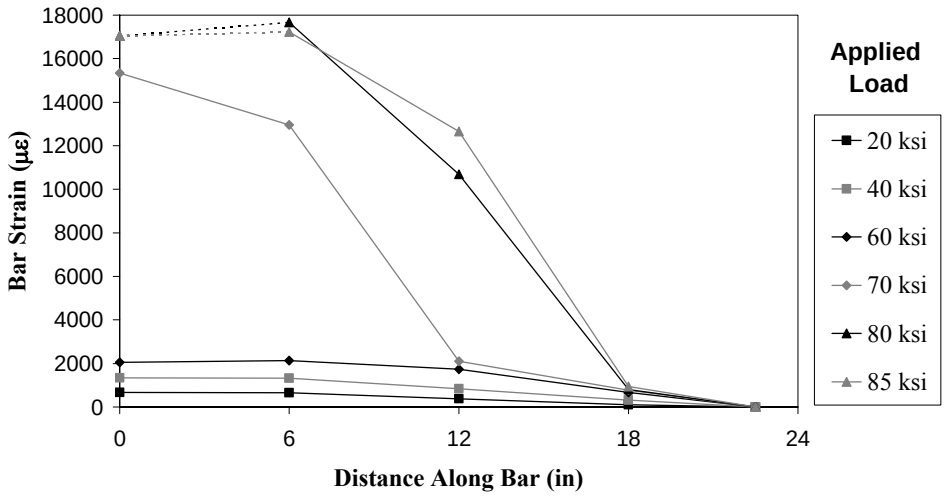

Figure 5.41 Strain Distribution along Connector Length (Test No. 28, Right Bar)

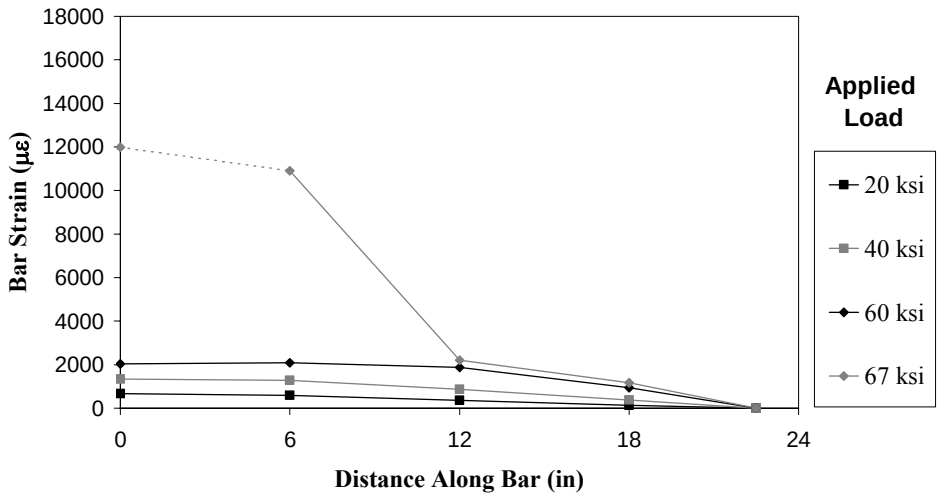

Figure 5.42 Strain Distribution along Connector Length (Test No. 32, Right Bar)

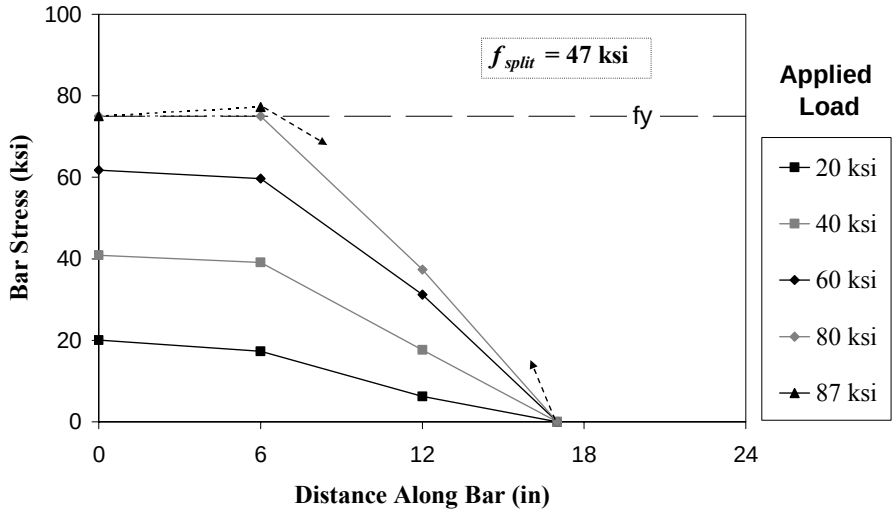

Figure 5.43 Stress Distribution along Connector Length (Test No. 3)

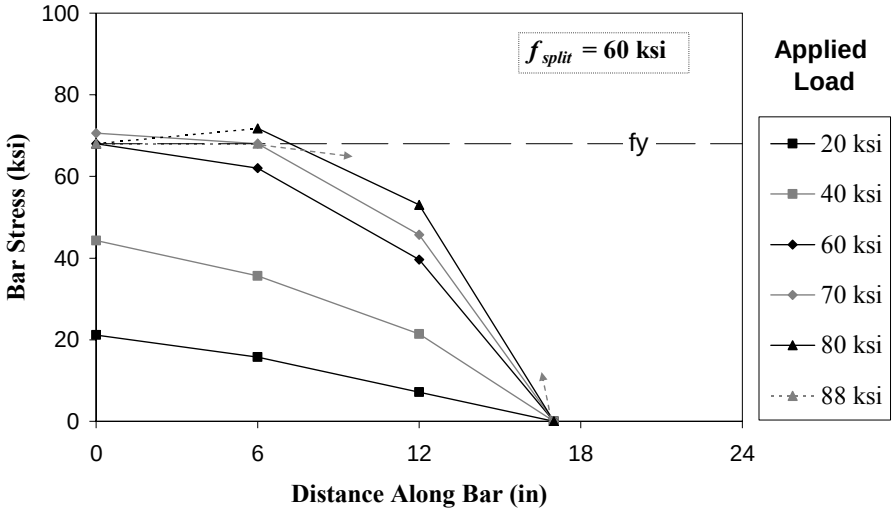

Figure 5.44 Stress Distribution along Connector Length (Test No. 4)

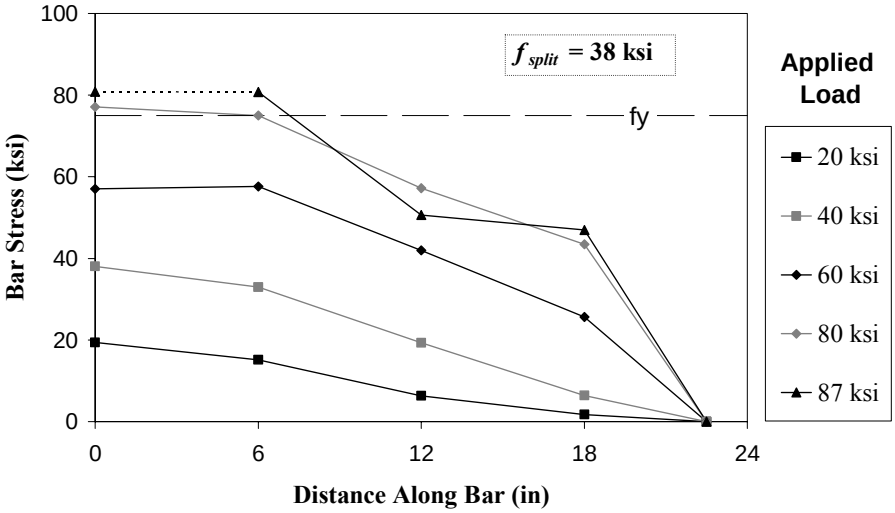

Figure 5.45 Stress Distribution along Connector Length (Test No. 13, Left Bar)

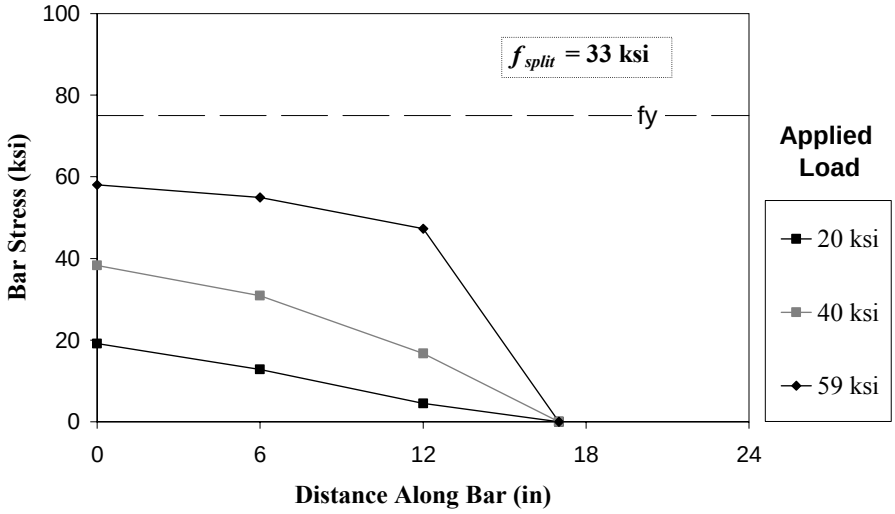

Figure 5.46 Stress Distribution along Connector Length (Test No. 17, Left Bar)

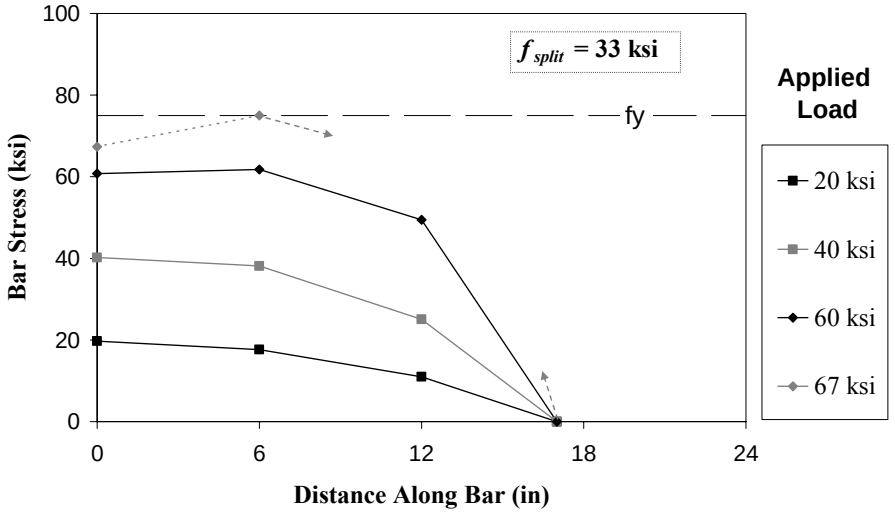

Figure 5.47 Stress Distribution along Connector Length (Test No. 7)

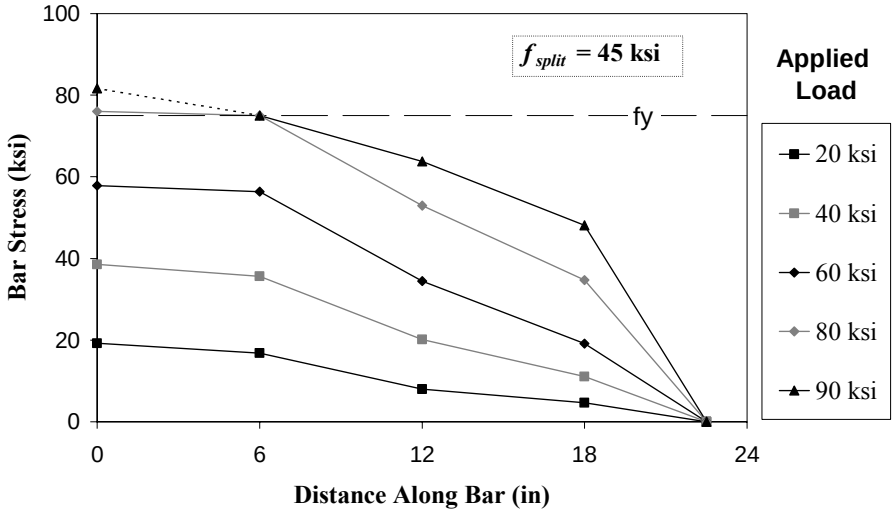

Figure 5.48 Stress Distribution along Connector Length (Test No. 22)

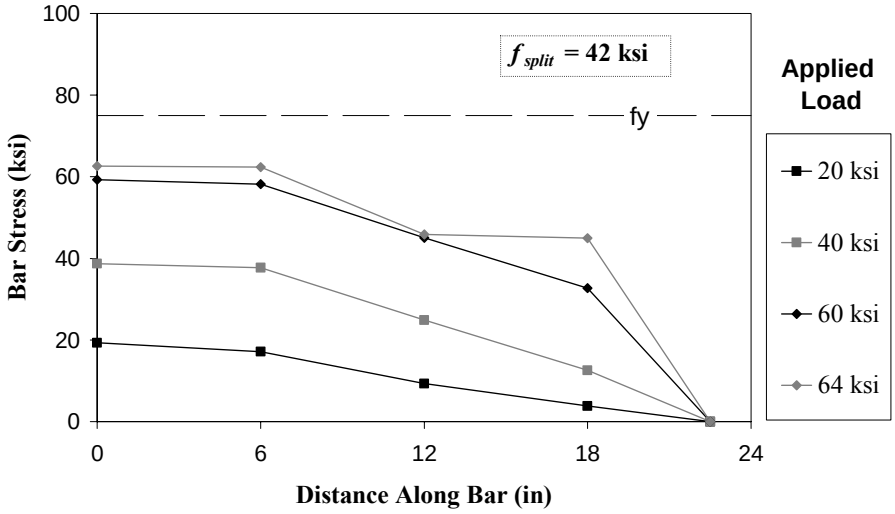

Figure 5.49 Stress Distribution along Connector Length (Test No. 14, Left Bar)

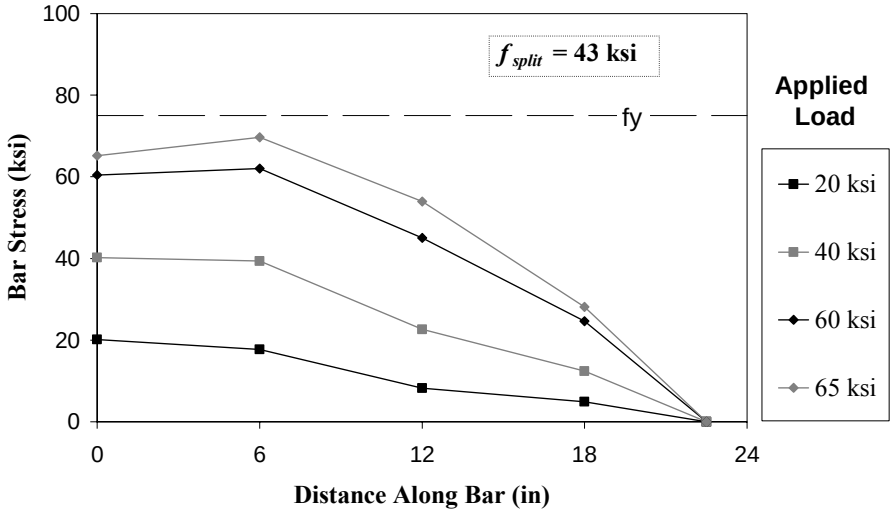

Figure 5.50 Stress Distribution along Connector Length (Test No. 24, Left Bar)

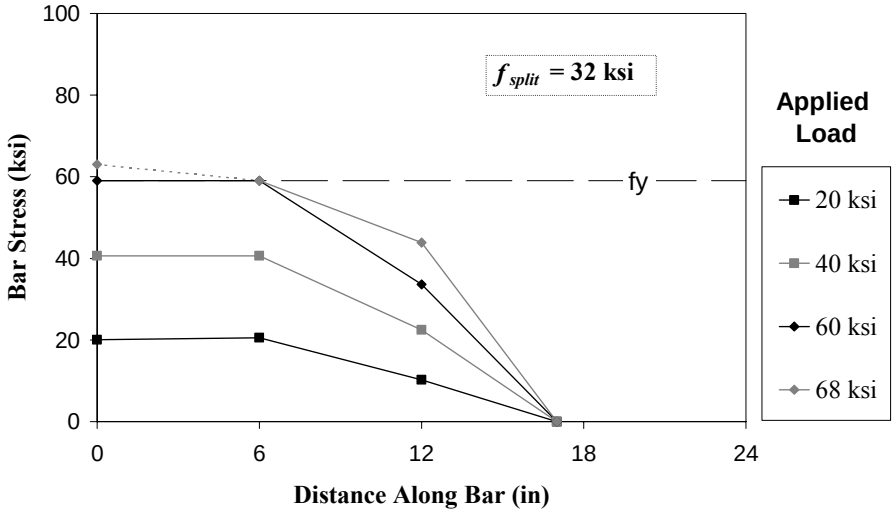

Figure 5.51 Stress Distribution along Connector Length (Test No. 30)

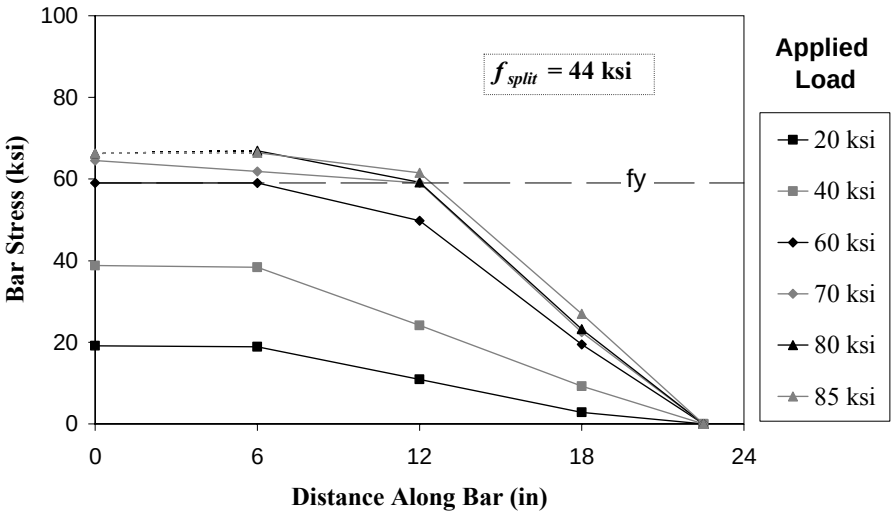

Figure 5.52 Stress Distribution along Connector Length (Test No. 28, Right Bar)

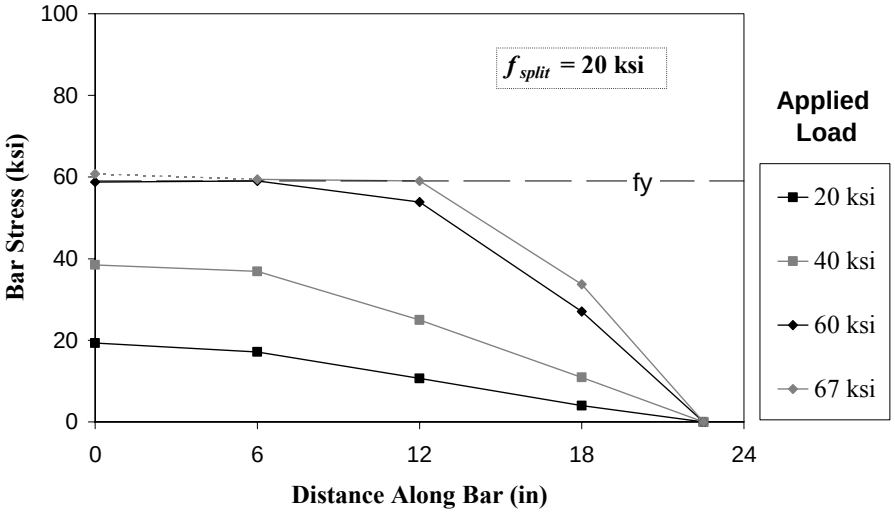

Figure 5.53 Stress Distribution along Connector Length (Test No. 32, Right Bar)

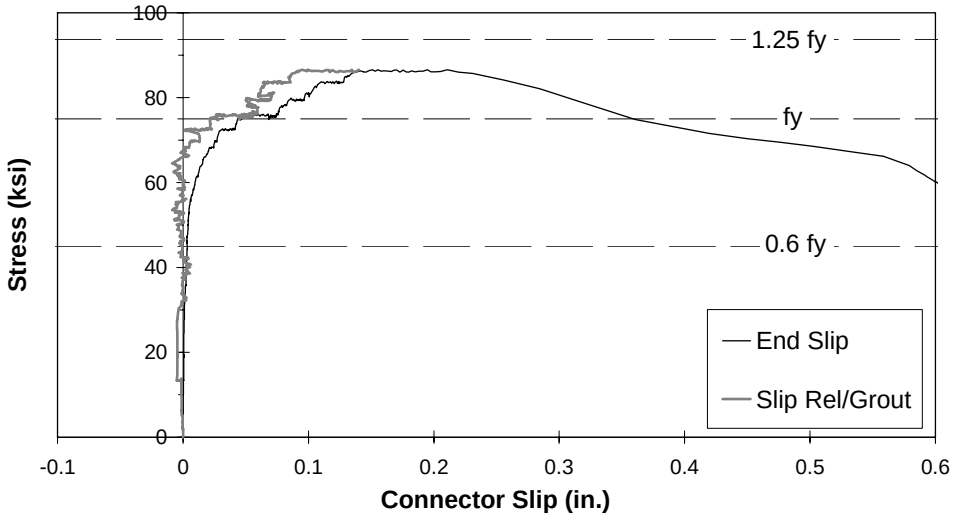

Figure 5.54 Stress vs. Connector Slip Relative to Grout (Test No. 3)

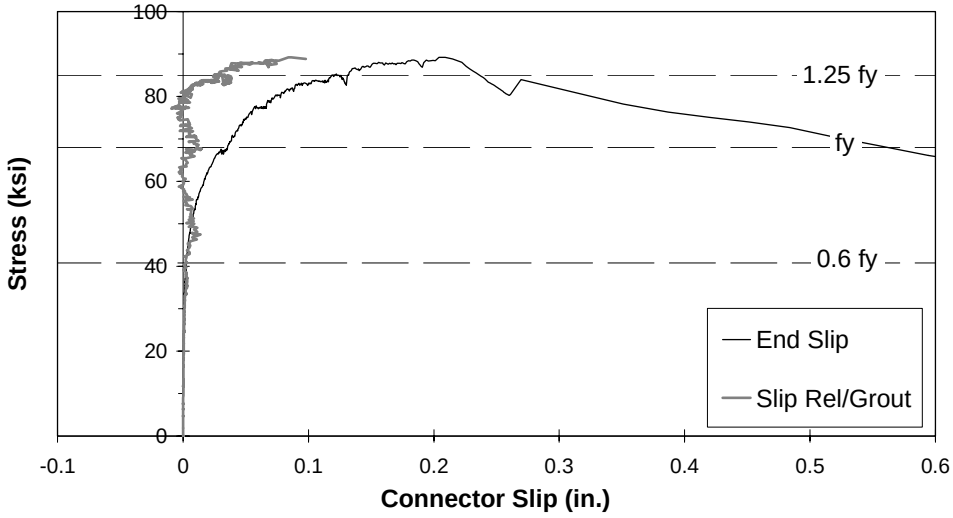

Figure 5.55 Stress vs. Connector Slip Relative to Grout (Test No. 4)

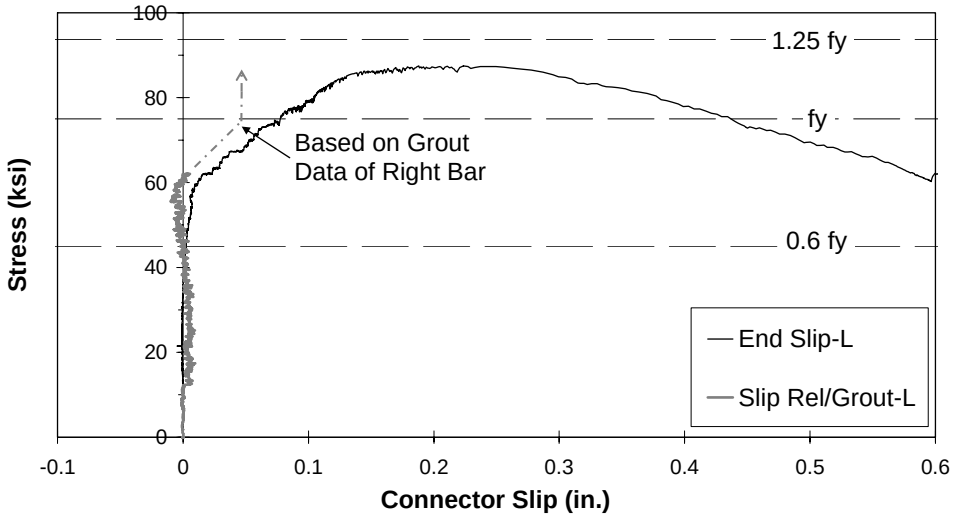

Figure 5.56 Stress vs. Connector Slip Relative to Grout (Test No. 13, Left Connector)

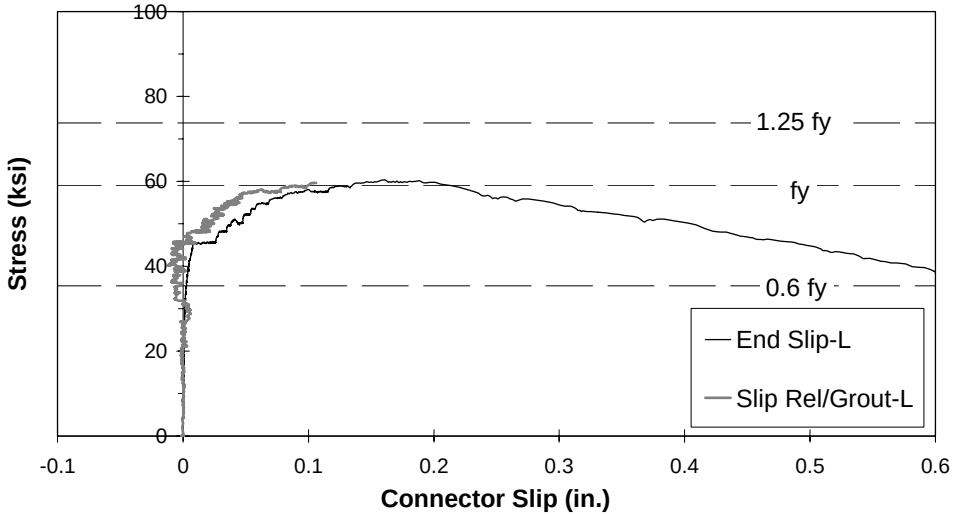

Figure 5.57 Stress vs. Connector Slip Relative to Grout (Test No. 17, Left Connector)

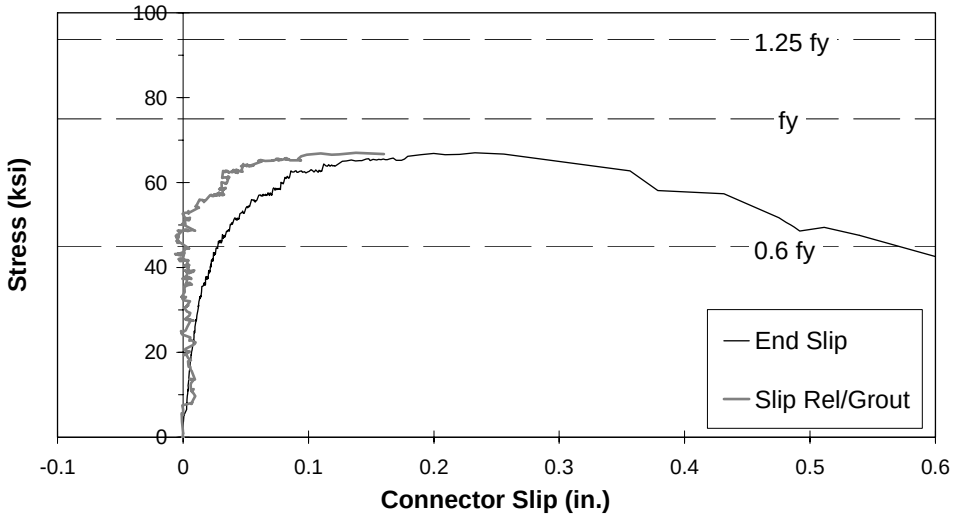

Figure 5.58 Stress vs. Connector Slip Relative to Grout (Test No. 7)

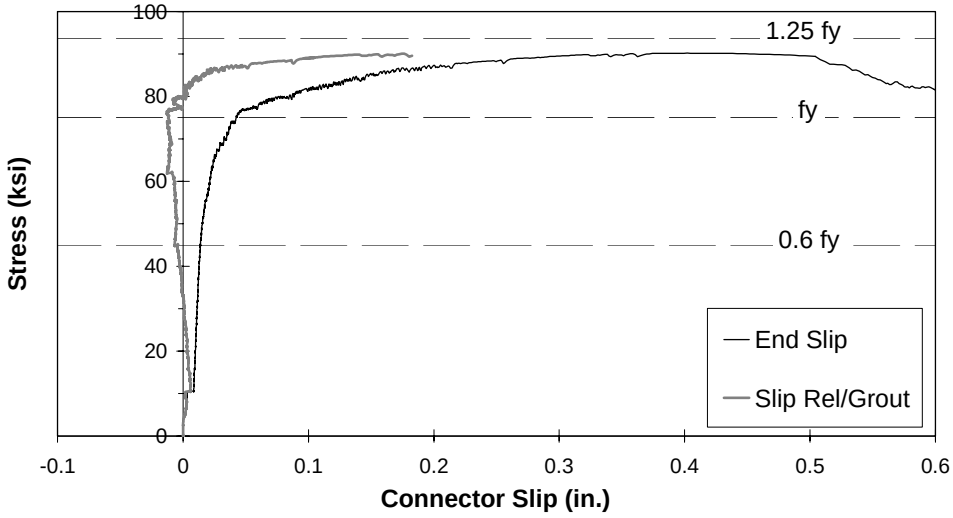

Figure 5.59 Stress vs. Connector Slip Relative to Grout (Test No. 22)

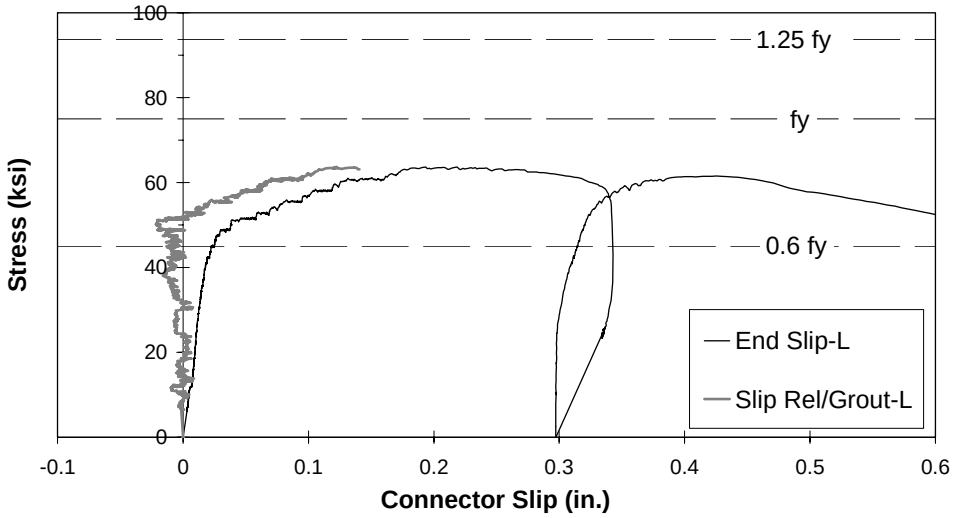

Figure 5.60 Stress vs. Connector Slip Relative to Grout (Test No. 14, Left Connector)

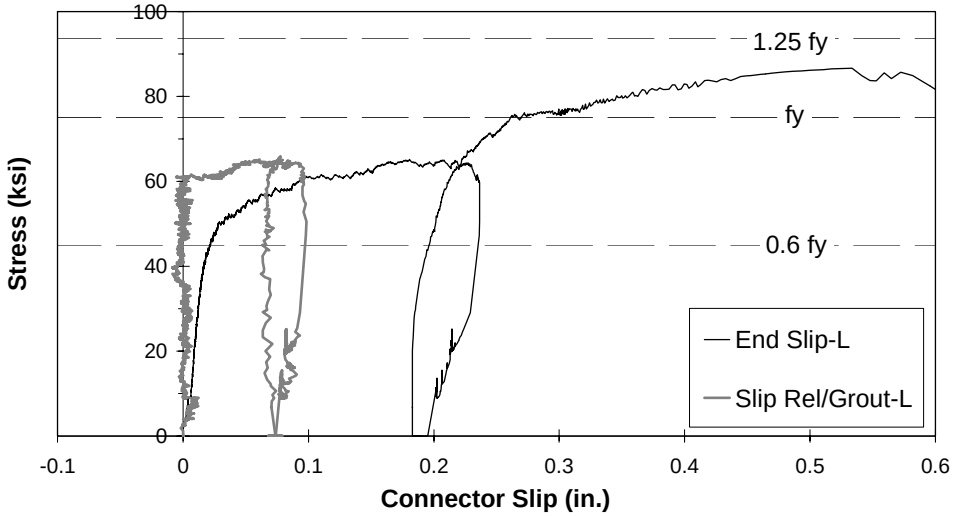

Figure 5.61 Stress vs. Connector Slip Relative to Grout (Test No. 24, Left Connector)

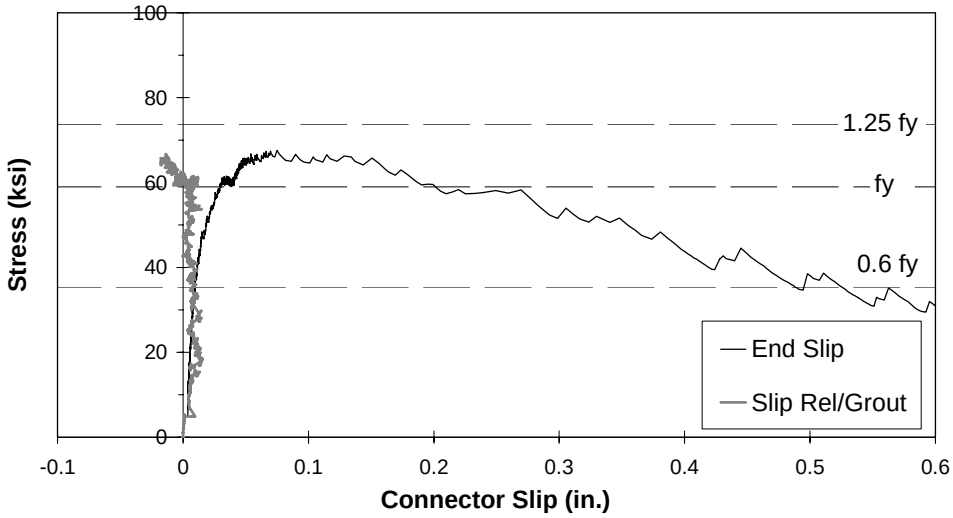

Figure 5.62 Stress vs. Connector Slip Relative to Grout (Test No. 30)

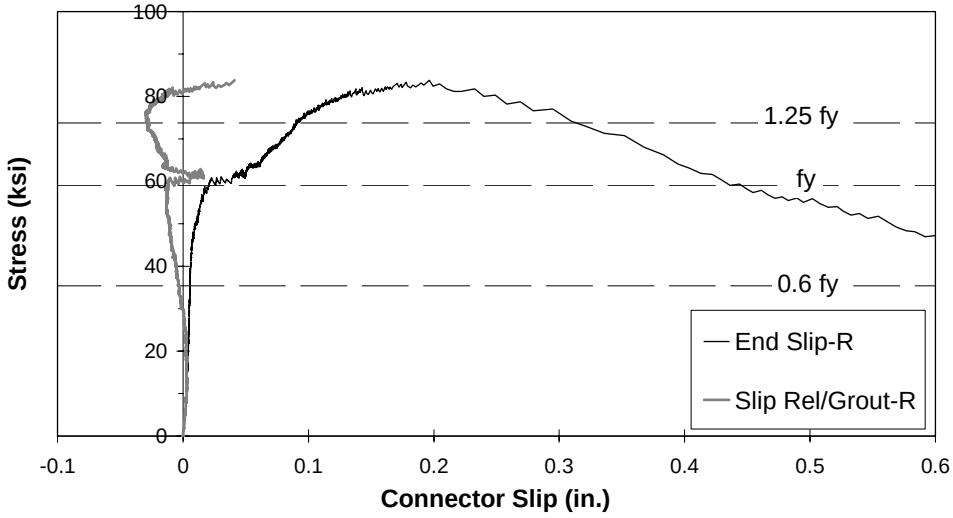

Figure 5.63 Stress vs. Connector Slip Relative to Grout (Test No. 28, Right Connector)

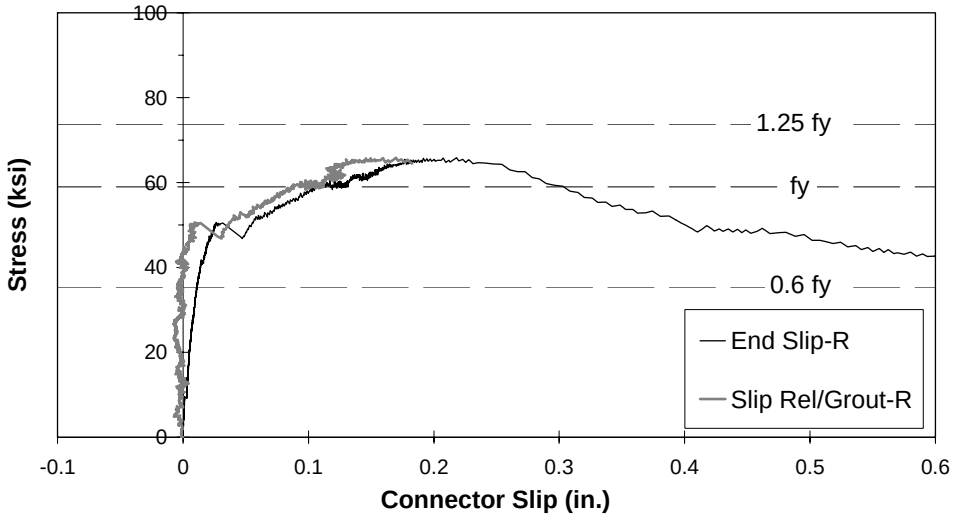

Figure 5.64 Stress vs. Connector Slip Relative to Grout (Test No. 32, Right Connector)

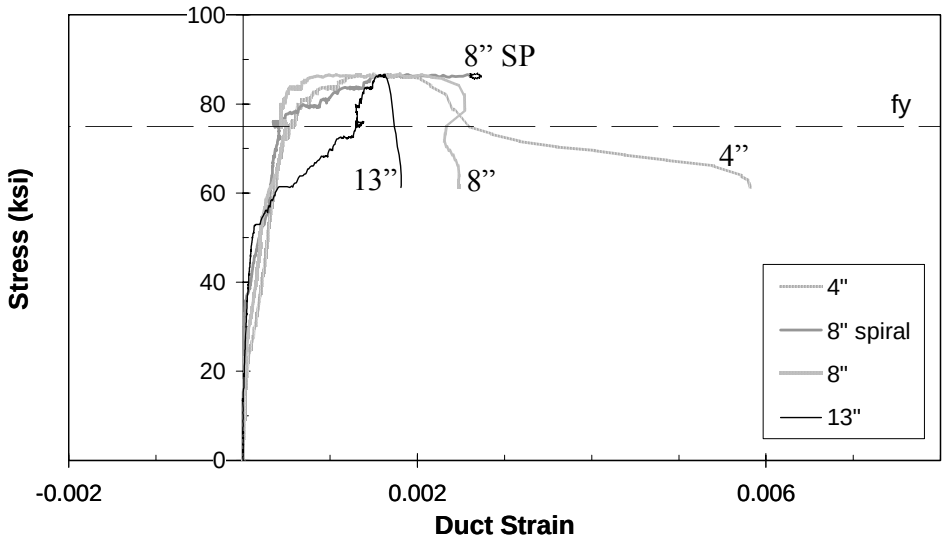

Figure 5.65 Stress vs. Duct Strain (Test No. 3)

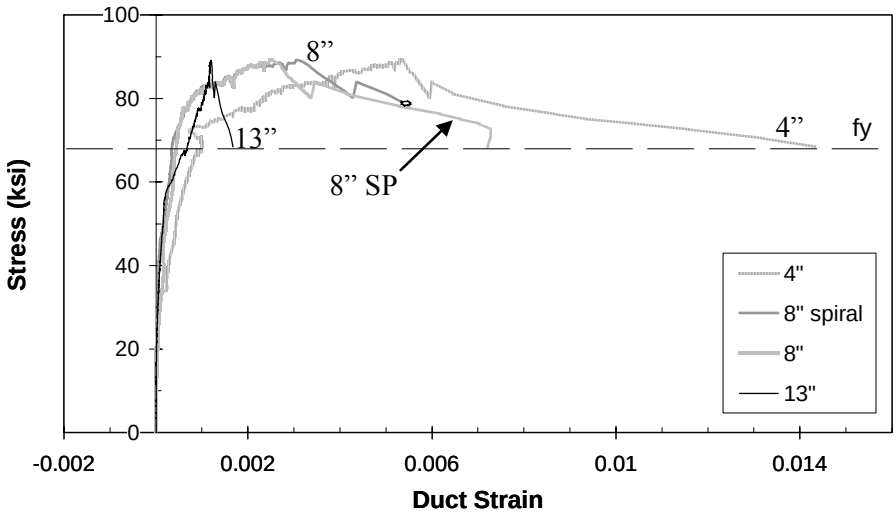

Figure 5.66 Stress vs. Duct Strain (Test No. 4)

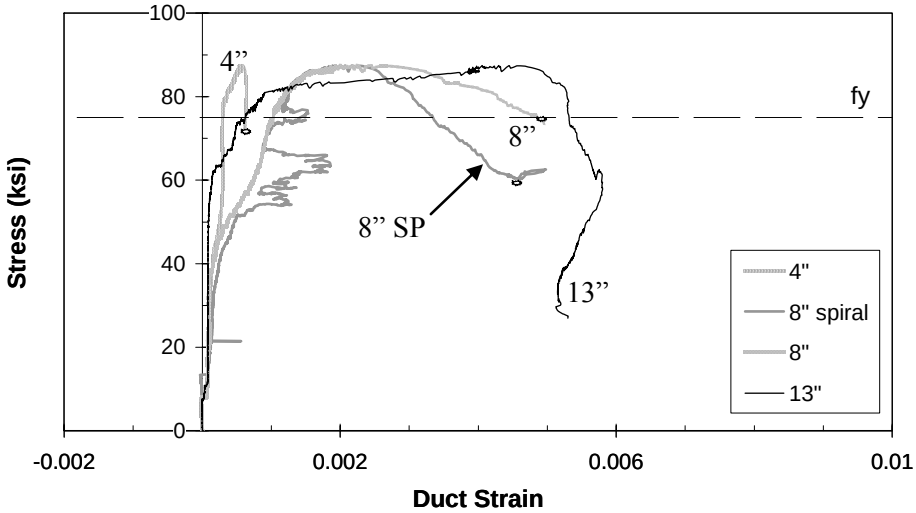

Figure 5.67 Stress vs. Duct Strain (Test No. 13, Left Connector)

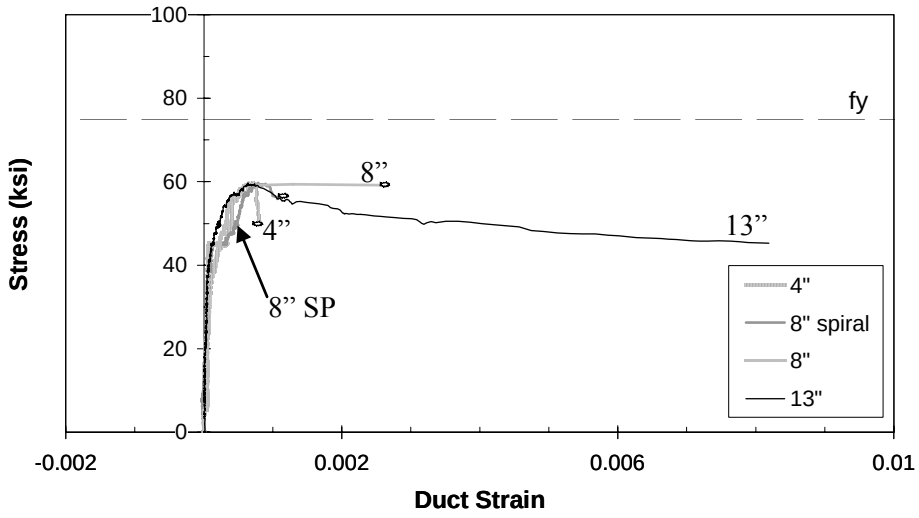

Figure 5.68 Stress vs. Duct Strain (Test No. 17, Left Connector)

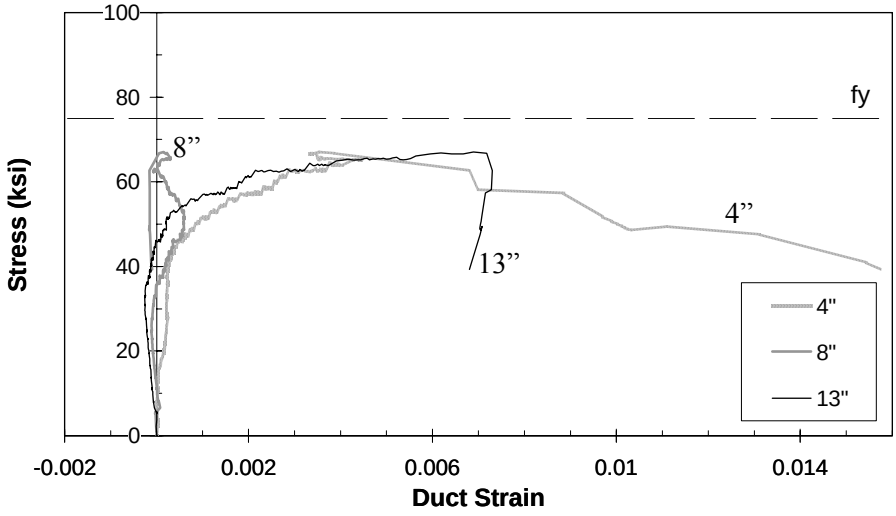

Figure 5.69 Stress vs. Duct Strain (Test No. 7)

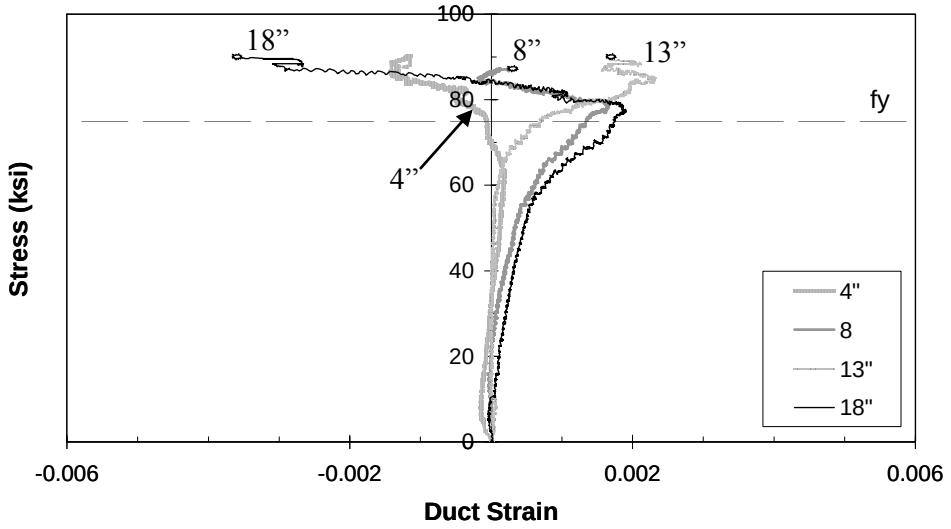

Figure 5.70 Stress vs. Duct Strain (Test No. 22)

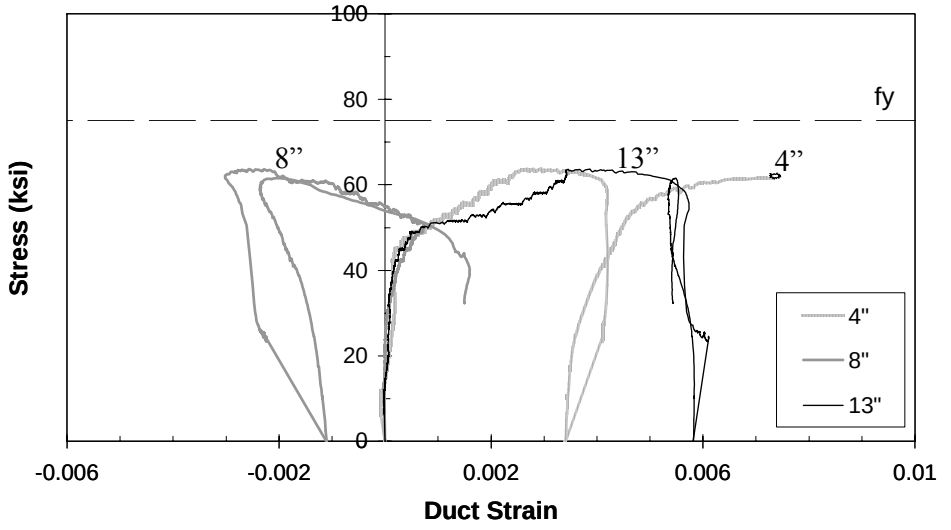

Figure 5.71 Stress vs. Duct Strain (Test No. 14, Left Connector)

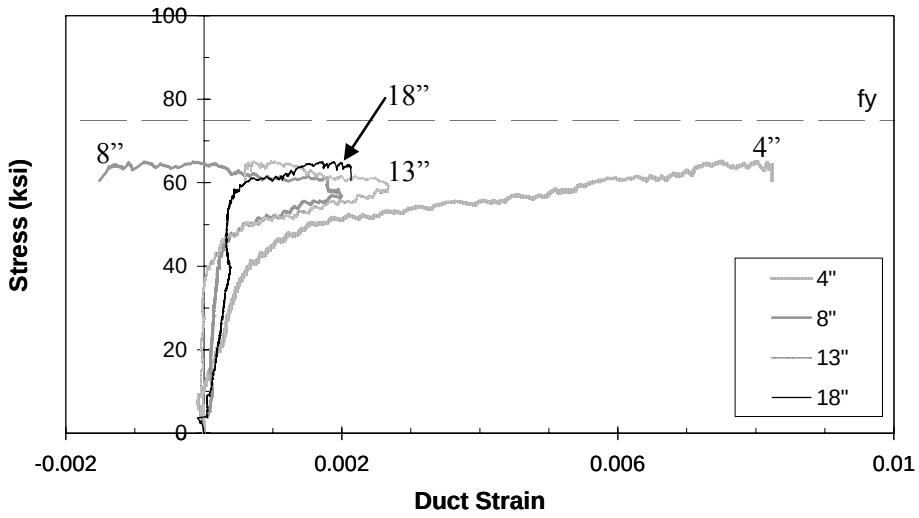

Figure 5.72 Stress vs. Duct Strain (Test No. 24, Left Connector)

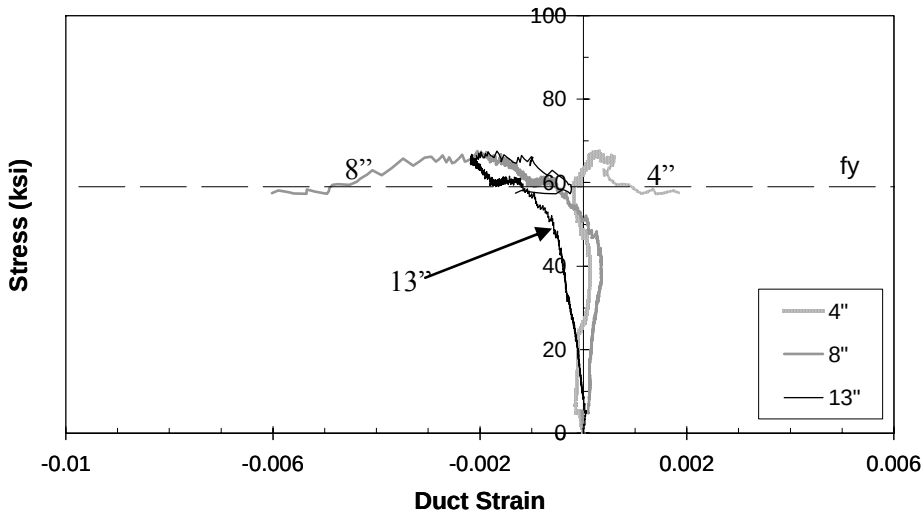

Figure 5.73 Stress vs. Duct Strain (Test No. 30)

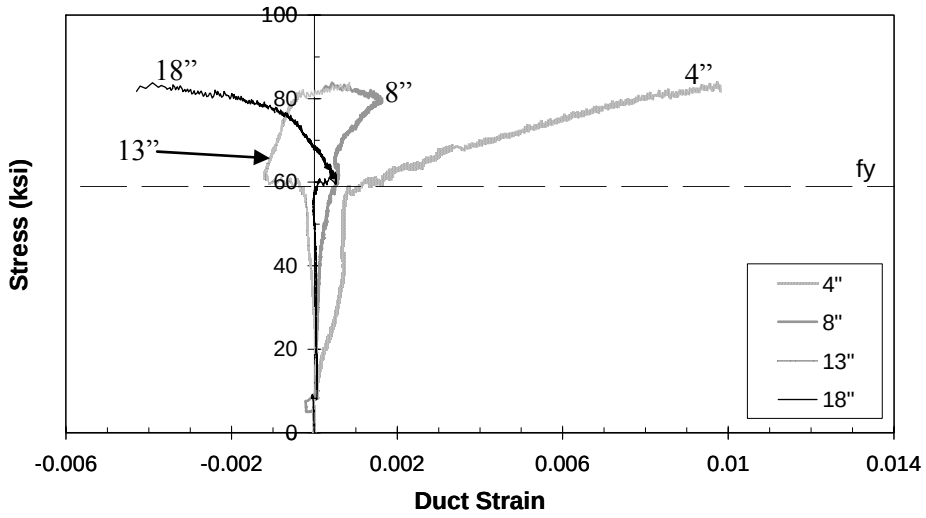

Figure 5.74 Stress vs. Duct Strain (Test No. 28, Right Connector)

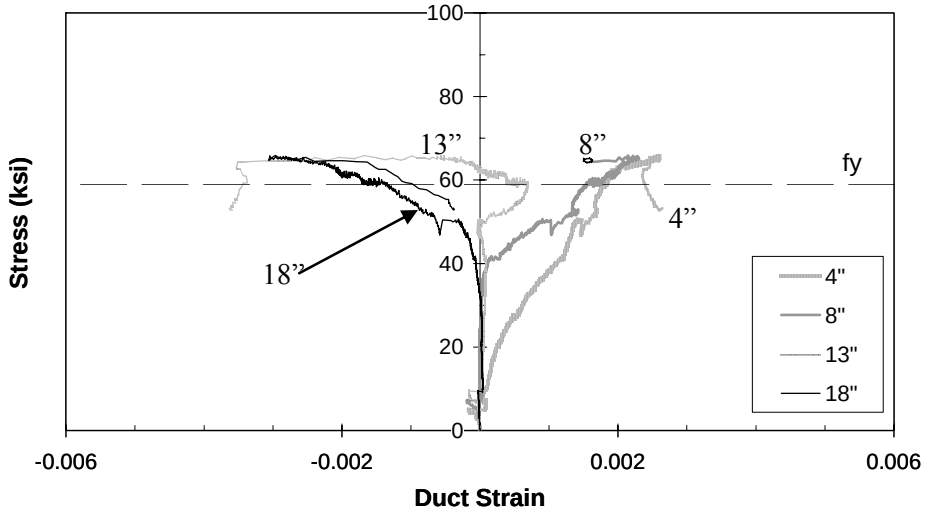

Figure 5.75 Stress vs. Duct Strain (Test No. 32, Right Connector)

Figure 5.76 Autopsy on Galvanized Steel Duct Specimen (Test No. 4)

Figure 5.77 Autopsy on Galvanized Steel Duct Specimen (Test No. 23, Left Connector)

Figure 5.78 Autopsy on Polyethylene Duct Specimen (Test No. 7)

Figure 5.79 Autopsy on Polyethylene Duct Specimen (Test No. 8)

Figure 5.80 Autopsy on Polypropylene Duct Specimen (Test No. 28)

Figure 5.81 Autopsy on Polypropylene Duct Specimen (Test No. 32)

CHAPTER 6
Evaluation of Test Results

6.1 INTRODUCTION

The measured response of connection specimens was presented in detail in Chapter 5. Test data were presented separately for specimens containing different duct materials. In this chapter, an attempt is made to evaluate the behavior of grouted vertical duct connections under the influence of the following parameters:

- Bar coating
- Duct material
- Embedment depth
- Number of connectors
- Duct clear spacing
- Bar eccentricity
- Transverse reinforcement

The compressive strengths of the concrete and grout were not selected as experimental parameters in this investigation. However, concrete compressive strengths varied between 4.5 and 6.1 ksi, and grout strength varied between 4.7 and 7.1 ksi. All conclusions discussed in this chapter are applicable only within the ranges of compressive strengths tested.

Average bond stress-slip relationships are used to evaluate differences in response among the specimens. To obtain these relationships, applied stresses on connectors were converted to bond stresses, u, using Equation 6-1:

$$u = \frac{f_s \, A_b}{\pi \, d_b \, l_e} \tag{6-1}$$

where f_s is the applied stress in the connector (psi), A_b is the area of the connector (in^2), $(\pi * d_b)$ is the connector perimeter (in.), and l_e the connector embedment depth (in.). Consideration of a uniform bond stress distribution along the embedment depth is an appropriate simplification, given the lack of information on the actual bond stress distribution.

Throughout the presentation of test data in Chapter 5, the development of splitting cracks in the concrete was considered to be a critical stage of response. Splitting occurs when the level of stress in the tension rings in the concrete surrounding the connectors exceeds the tensile capacity. Considerable changes in the stress distribution along connectors were observed immediately after the appearance of splitting cracks in the concrete. Moreover, passive confinement provided by ducts was mobilized following the formation of splitting cracks in the concrete.

The tensile strength of the grout is considered to play a secondary role with respect to the behavior of the connectors. Cracking of the grout was observed in the specimens during initial loading stages, but with minor effects on connection behavior. Splitting cracks in the grout are effectively restrained by the ducts. The connection stiffness was not observed to deteriorate until widespread splitting occurred in the concrete. In general, connection failures were related to cracking of the concrete and not cracking of the grout. Even in cases where the grout compressive strength was lower than the concrete strength by 800 psi (Test No. 5), no discernible negative effects were noted. In most tests, grout strength was either equal to or greater than the concrete strength. These conditions did not result in situations where connection failure was caused by a weakness in the grout material.

As described in Section 3.4.3, only one concrete mixture was used to construct the specimens. However, variability in material batches and the age of

the concrete at the time of testing led to small differences in the concrete strengths of the specimens. Similar levels of variability were also present in grout strength (Table 5.1). To account for this material variability, bond stress-slip relationships were normalized with respect to the strength of the concrete. Bond stresses were modified by the factor $(f'_c)^{-0.5}$ following the common assumption that the tensile strength of the concrete is approximately proportional to the square root of its compressive strength. As mentioned previously, the tensile strength of the concrete, rather than that of the grout, is considered to be the primary parameter that influences the response of the connection.

6.2 EFFECT OF TEST PARAMETERS ON BEHAVIOR

The sensitivity of the measured response to each of the experimental parameters is summarized in the following sections. The designations used in the plots of this section to identify test specimens are related to the individual connection tests in Table 6.1.

6.2.1 Bar Coating

The effect of bar coating on connection behavior is evaluated by comparing the normalized bond stress-end slip response of a group of single-connector specimens.

Figure 6.1 shows the bond stress-slip curve for connectors embedded $8d_b$ in galvanized steel ducts (GS) and polyethylene ducts (PE). A similar curve, but for connectors embedded $12d_b$, is shown in Figure 6.2. Very small differences in the initial stiffness (slope of the initial portion of the curve) can be observed for the connections. Figure 6.1 shows that at an embedment depth of $8d_b$, bar coating caused a reduction in bond strength. Reductions are 17% and 6% for connectors housed inside polyethylene ducts and galvanized steel ducts, respectively. No

differences in initial stiffness and bond strength are apparent when connectors are embedded $12d_b$ (Figure 6.2).

Figure 6.3 shows the effect of bar coating on the axial stress distribution along the length of the bar. Data are shown for bars embedded $12d_b$. Although the bond-slip curves for uncoated and epoxy-coated bars are similar, some differences exist regarding the stress distribution along the bar. As load is increased from 40 to 80 ksi, stresses at a depth of 12 in. do not increase in the uncoated connector as much as they do in the epoxy-coated connector. In a sense, the stresses are distributed more uniformly along the length of the epoxy-coated bar, and larger portions of the applied load are being anchored deep in the embedment. This difference in behavior can be attributed to the reduced frictional resistance of the epoxy coating.

Bar coating was one of the first parameters investigated experimentally. Because data showed negligible effects on connector behavior at an embedment depth of $12d_b$, no further tests were conducted. In actual connections, the connector embedment depth will likely be much larger than $12d_b$. Thus, for practical purposes, the effect of bar coating on connection behavior is considered to be insignificant.

6.2.2 Duct Material

The duct material has an important influence on connection behavior. In Chapter 5, it was shown that connection failure modes depend on the duct material. The effect of duct material on behavior is evaluated by comparing the normalized bond stress-end slip response of test specimens involving one, two, and three connectors. For multiple connector tests, the averages of the individual connector responses are shown.

In Figure 6.4, a comparison is made between specimens involving one connector embedded $8d_b$. The initial stiffness and strength of the specimen containing galvanized steel duct (GS) are superior to those of the other test specimens. Reductions in strength relative to the steel duct specimen are 18% and 37% for specimens with polyethylene (PE) and polypropylene (PP) ducts, respectively. The variation in stress distribution along the length of the connectors is shown in Figure 6.5. Stresses at a depth of 6 in. are smaller for the connector housed in galvanized steel duct. Polyethylene and polypropylene ducts are less effective at preventing slip of the connector, so high stresses propagate further down the connector.

Figure 6.6 shows the bond stress-slip response of single-connectors embedded $12d_b$. One of the curves plotted (ND) corresponds to a connector test where a steel duct was removed from the beam specimen prior to placement of the connector and grout. The initial stiffness is again higher for the test specimen containing galvanized steel ducts (GS). A slightly higher stiffness was observed for the specimen containing polypropylene (PP) with respect to the polyethylene (PE) duct specimen. The curve corresponding to the specimen with no duct presents a small kink at the beginning of loading, possible caused by instrumentation error or by sudden adjustment of the wedges that gripped the connector. Consideration of the portion of the curve above the kink shows that the initial stiffness for the specimen with no duct is comparable to that of the polyethylene duct specimen. The initial slope of the bond stress-slip curve is related directly to the degree of confinement surrounding the connector.

Comparison of the specimens in terms of bond strength leads to a surprising observation, where the bond strength of the specimen with no duct is actually higher than that of plastic duct specimens. Reductions in bond strength relative to the steel duct specimen are 17% for the specimen with no duct, 23%

for the specimen with polyethylene duct, and 27% for the specimen with polypropylene duct. Plastic ducts do not provide confinement to the connector and grout, and have a negative effect on the frictional resistance of the connection.

The variation in stress distribution along connectors embedded in different duct materials is shown in Figures 6.7a through 6.7c. The propagation of stress along connectors is directly related to the initial stiffness (or slip) of the connectors. At applied stress levels of 20 and 40 ksi, the connector with no duct has the highest stress at a depth of 12 in.; connectors housed inside both types of plastic duct follow. At an applied stress of 60 ksi, the stress at 12 in. in the connector housed inside the polyethylene duct is the highest.

When no duct is provided, cracks that form in the grout can propagate easier into the concrete. Ducts made of the plastic materials interrupt the cracks that form in the grout, but at higher load levels, slip of the grout/bar out of the duct becomes significant. Spacing between the ribs of the polyethylene ducts is larger than that of the polypropylene ducts. Shorter spacing between duct ribs increases the grout plug bond strength of the connection and has an effect on the initial stiffness of the connection. The geometrical properties of the ducts, namely the spacing between the ribs, and not the material properties (polyethylene and polypropylene have similar stiffness and strength) govern the behavior.

Figure 6.8 shows the bond-stress response of double-connector specimens with an embedment of $12d_b$. Comparison is made only between galvanized steel (GS) and polyethylene (PE) duct specimens. Higher initial stiffness and bond strength are again associated with steel duct specimens. The bond strength of the specimen containing polyethylene ducts is approximately 27% lower than that of the steel duct specimen. This reduction level is similar to that shown in Figure 6.6 for single connectors with the same embedment depth.

Figure 6.9 compares the bond stress-slip response of two connectors embedded $16d_b$. The steel duct specimen again has the highest initial stiffness, followed by the polypropylene duct specimen. With respect to bond strength relative to the steel duct specimen, a reduction of 27% was again observed in the specimen containing polyethylene ducts. The polypropylene duct specimen shows a smaller reduction in bond strength of 17%.

Figure 6.10 compares the bond stress-slip response of three connectors embedded $16d_b$. Only the response of galvanized steel (GS) and polypropylene (PP) duct specimens are compared. Following the established trend, initial stiffness and strength are higher for the galvanized steel duct specimen. With respect to strength relative to the steel duct specimen, a small reduction of 10% is observed for the polypropylene duct specimen.

6.2.3 Embedment Depth

The effect of embedment depth on connection behavior is evaluated by comparing the normalized bond stress-end slip response of test specimens involving one and two connectors. The comparisons are made separately for specimens containing different duct material. For multiple connector tests, the averages of the individual connector responses are shown.

Bond stress-slip data of single-connector specimens containing galvanized steel (GS) ducts are shown in Figure 6.11. Embedment depth appears to have a negligible effect on initial stiffness and connector strength. Figure 6.12 shows the effect of embedment depth on the bond stress-slip response of connection specimens involving two connectors each placed inside a galvanized steel duct. There is a reduction in bond strength of 14% for connectors that are embedded $12d_b$.

Figure 6.13 shows bond stress-slip data for single-connector specimens involving polyethylene (PE) ducts. Embedment depth appears to have a minor influence on initial stiffness and bond strength. Data for the connector embedded at $16d_b$ show an increase in toughness (area under the curve) with respect to the shorter embedment depths. Figure 6.14 shows the effect of embedment depth on the bond stress-slip response of connection specimens involving two connectors placed inside polyethylene ducts. Negligible differences in initial stiffness are observed, but there is a reduction in bond strength of 14% for connectors that are embedded at the shallower embedment of $12d_b$.

The effect of embedment depth on behavior of specimens containing polypropylene (PP) duct specimens is shown in Figure 6.15. A minor reduction in strength is observed in the response of the connector embedded at $8d_b$. The bond strength of the connector embedded at $8d_b$ is approximately 12% lower than that obtained at $12d_b$.

6.2.4 Number of Connectors

The effect of closely spaced connectors (approximately one duct diameter clear spacing between ducts) is evaluated separately for specimens containing different duct materials. For multiple connector tests, the averages of the individual connector responses are shown.

Figure 6.16 shows the bond stress-slip curves of two connection specimens involving galvanized steel ducts. One of these curves corresponds to a test involving two connectors. Whereas the initial stiffness is not affected by increasing the number of connectors from one to two, there is a substantial reduction in bond strength of approximately 23%. The reduction in bond strength is approximately 24% (Figure 6.17) when the number of connectors increases from two to three. Figure 6.18 shows the effect of increasing the number of

connectors from two to three on stress distribution along the connectors. At small loads, the shape of the stress distribution is independent of the number of connectors. At higher loads, increasing the number of connectors affects the stress distribution.

The effect of number of connectors on the behavior of connections containing polyethylene ducts is shown in Figures 6.19 and 6.20. The main effect that is observed in both plots is a reduction in bond strength with an increase in the number of connectors. Increasing the number of connectors from one to two leads to a decrease in bond strength of 29% and 24% for connectors embedded $12d_b$ and $16d_b$, respectively. The effect of increasing the number of connectors from one to two on the stress distribution along the length of connectors is shown in Figure 6.21. At low levels of applied load, the axial stress distribution along connectors is independent of the number of connectors. At high load levels (and after splitting of the concrete has occurred), increasing the number of connectors affects the stress distribution, and a larger portion of the load is anchored deep in the embedment.

Figure 6.22 shows the effect of number of connectors on behavior of connection specimens containing polypropylene ducts. An increase in the number of connectors from two to three leads to a decrease in bond strength of 21%. Initial connection stiffness is affected very little by an increase in number of connectors. The stress distribution along connectors in polypropylene ducts is affected by an increase in the number of connectors in a manner similar to that described for galvanized steel and polyethylene duct specimens (Figure 6.23).

6.2.5 Duct Clear Spacing

A limited number of tests were conducted to evaluate the effect of duct clear spacing. Duct clear spacing in double-connector tests was varied from one

duct diameter (1 D dia) to two duct diameters (2 D dia). The effect of duct clear spacing on galvanized steel duct specimen behavior is shown in Figure 6.24. A very small increase in bond strength is observed as duct clear spacing increases from one duct diameter to two duct diameters. It is possible that the small differences in behavior are related to experimental scatter. Figure 6.25 shows the effect of duct clear spacing on polyethylene duct specimen behavior. Unexpectedly, a reduction instead of an increase in bond strength was measured with an increase in duct clear spacing. Additional tests are required to explore this effect further; results seem to indicate that interaction between connectors is equally strong for duct clear spacing values of one and two duct diameters.

6.2.6 Bar Eccentricity

Eccentric placement of the connectors inside the duct was investigated to determine the corresponding effects on behavior. Figure 6.26 shows a series of bond stress-slip curves corresponding to test specimens involving single connectors embedded $8d_b$ inside galvanized steel and polyethylene ducts. Bar eccentricity affects primarily the bond strength of the connection; the reduction is approximately 17%. A small reduction in initial stiffness is also observable. Figure 6.27 compares the effect of bar eccentricity on galvanized steel duct specimens at an embedment of $12d_b$. A similar decrease in bond strength of 17% is observed at this deeper embedment.

Figure 6.28 shows the effect of bar eccentricity on the stress distribution along the connector. The stresses in the connector placed eccentrically inside the duct at depths of 6 and 12 in. are equal to or smaller than those of the connector placed concentrically. At high applied stresses, a larger portion of the load is anchored deep in the connector placed eccentrically.

6.2.7 Transverse Reinforcement

The presence of two types of transverse reinforcement (a large spiral around a group of ducts and smaller spirals around individual ducts) was evaluated. Tests were also conducted on specimens without any form of spiral reinforcement.

Figure 6.29 shows the bond stress-slip curves for tests involving two connectors, each housed inside galvanized steel ducts. One of the curves corresponds to a connection specimen with a large spiral around the connector group, whereas the other curve corresponds to a connection specimen without any form of transverse reinforcement. The effect of the transverse reinforcement (group spiral) is very minor, and does not appear to influence connection behavior.

The influence of transverse reinforcement on the behavior of connections containing polyethylene ducts is evaluated in Figures 6.30 and 6.31. Results from single-connector tests are shown in Figure 6.30; results show that the presence of individual spirals around ducts degraded the performance of the connection. Although the spiral reinforcement was somewhat effective in restraining the upward movement (slip) of the duct, failure occurred as the bar/grout slipped out of the polyethylene duct. The bond-slip curves of tests involving two connectors and a deeper embedment depth of $16d_b$ are shown in Figure 6.31. The test that used a large spiral around the connection group shows a slightly higher bond strength (less than 10%) compared with the test that had no transverse reinforcement. It is quite possible that this is due to random test variation and not due to the presence of the spiral. The use of small spirals around individual ducts did not lead to any improvements in performance; in fact, the lowest bond strength shown in the figure corresponds to the test involving these small spirals. The very small spacing of the coils of the individual spirals, and the small

clearance between spirals and the ducts probably interfere with the correct placement of the concrete, and gives rise to low strength concrete in the vicinity of the duct. This is an exploratory conclusion because an investigation of the concrete material surrounding the ducts and the individual spirals was not conducted.

The response of strain gages bonded to the spiral reinforcement is not presented because there is no meaningful data to report. Significant strains are possible only at locations where radial splitting cracks formed, and these did not coincide with the location of strain gages. Because crack widths were not measured, no evaluation is made of the effectiveness of the transverse reinforcement in controlling the opening of cracks.

6.3 DEVELOPMENT OF A PHENOMENOLOGICAL MODEL

6.3.1 Theory of Bond Mechanism

The bond mechanism of connectors placed inside grouted ducts is comparable to that of a connector anchored in well-confined concrete (Figure 1.28). After adhesion between grout and the connector is lost and ribs in the connector begin to bear on the grout, slip occurs by progressive crushing of the grout in front of the ribs (Figure 6.32a). Ducts constrain the splitting cracks that initiate in the grout. An increase in load distributes the bond stresses deeper along the connector engaging additional ribs to resist the additional load causing internal inclined cracks that continue to form along the connector.

The ducts act as a form of passive confinement that is engaged after splitting cracks form in the concrete (Figure 6.32b). Galvanized steel ducts provide confinement to the grout/bar unit. Growth of splitting cracks in the concrete is restrained more effectively when transverse reinforcement is placed close to the surface of the bar. In the case of galvanized steel duct connections,

the close proximity of the duct to the connectors provides a very efficient method of confinement. However, the presence of the duct isolates the connector from the concrete. After significant splitting in the concrete, the efficacy of the duct in providing confinement and in preventing slipping of the grout/bar unit determines the mode of failure of the connection. Experimental data (Section 5.8.2 and 5.8.3) show that plastic ducts experienced significant circumferential and axial strains. However, the low stiffness of plastic ducts makes any form of confinement to the grout/bar unit enclosed by these ducts impossible.

Connection specimens containing galvanized steel ducts failed by pullout of the connectors from the grout (Figure 6.32b). Splitting cracks propagated in the less confined areas near the surface of the beam specimens, and some inclined cracks that emanated from the perimeter of the duct reached the surface and formed a concrete break-out cone. In the confined region below, bond deterioration results from bearing failure, inelastic deformations of diagonal grout struts, and reductions in the effective shearing area of the grout between bar lugs. Failure occurs when the capacity provided by the interlocking of the steel ribs and the grout is reduced to zero.

Connection specimens using polypropylene ducts and many tests involving polyethylene ducts exhibited a pullout mode of failure where a large volume of the grout and the connector slipped out of the duct (Figure 6.32c). In some cases, the grout ribs (corresponding to corrugations of the duct) sheared off as the bar/grout plug slipped. All polypropylene duct specimens failed by plug pullout. Typically, the bar/grout plug and the duct pulled out of the concrete together. Polyethylene duct connection specimens failed by both connector pullout from the grout, and plug pullout. The shapes of the bond stress-slip curves corresponding to these two modes of failure are similar, as were the bond strengths.

6.3.2 Bond Stress-Slip Model

A bond stress-slip model was developed to reproduce the observed bond stress-slip curves. The main purpose of the model is to find similarities and establish characteristic bond strength, stiffness, and slip values for connections involving the different duct types. Model curves are developed by estimating the best fit to the experimental curves.

The model is based on the work of Ciampi et al. [6.1]. The original model was developed to study the anchorage of deformed bars in well-confined concrete blocks that were intended to represent beam-column connections in a moment-resisting frame. The generality and simplicity of the model make it attractive for use in this investigation. The model (Figure 6.33) consists of an initial non-linear relationship (initial stiffness), a plateau (representing the average peak bond strength), and a linear function that decreases to the value of the limiting frictional bond resistance:

$$u_a = u_1 \left(\frac{s}{s_1} \right)^{\beta} \qquad for\ s \le s_1 \tag{6-2}$$

$$u_a = u_1 \qquad for\ s_1 < s < s_2 \tag{6-3}$$

$$u_a = u_3 + \frac{(u_1 - u_3)(s_3 - s)}{(s_3 - s_2)} \qquad for\ s_2 \le s \le s_3 \tag{6-4}$$

where u_a is bond stress (psi), s is slip (in.), u_1 is the average peak bond strength (psi), u_3 is the limiting frictional bond resistance (psi), s_1 and s_2 are characteristic slip values (in.), s_3 is the slip at the limiting frictional bond resistance (in.), and β the stiffness coefficient.

Ciampi et al. [6.1] suggest that s_3 be taken as the clear distance between the ribs of the deformed bars. For the #11 bars considered in this investigation, the

clear distance between ribs was approximately 0.7 in., and this is the value taken for s_3. The values of s_1, s_2, u_1, u_3, and β are chosen to match the measured response.

Evaluation of the effects of the different test parameters on connection behavior made possible the identification of those that are most influential. The parameters of bar coating and the provision of transverse reinforcement around ducts are considered to have no effect on connection behavior.

A plot of average peak bond strength versus the ratio of embedment length to bar diameter (l_e/d_b) is shown in Figure 6.34. The plot includes all 32 tests, and bond strength values are normalized with respect to the square root of the concrete compressive strength. Tests were grouped in broad categories depending on duct material, number of connectors, clear spacing between ducts, presence of transverse reinforcement, and connector eccentricity. Trend lines are shown for those test categories that contain more than two tests. Figure 6.34 shows that there is little variation in the range of peak bond strengths as l_e/d_b increases, especially for tests involving only one connector. For tests involving two connectors, there seems to be a small increase in peak bond strength as l_e/d_b increases. Average peak bond strengths are shown in Table 6.2 normalized to the average test concrete strength of 5100 psi. Data for single epoxy-coated connectors with embedment depths of $8d_b$ are not included because bar coating reduced the connection capacity at that very short embedment. In the ensuing development of the basic curves, the peak bond strength is assumed to be independent of l_e/d_b. This simplification contradicts established theories for bond of reinforcement in concrete but appears to be valid for the specific connectors and range of parameters tested.

Figure 6.35 shows the relationship between normalized average bond strength versus duct material. The plot shows the effects of other test variables on

bond strength for each type of duct. The effect of duct material is taken into account in the basic model curves by estimating values of the average peak bond strength, u_1. Values listed in Table 6.2 were taken as a basis and modified accordingly to obtain a best fit with the measured response. Single connectors placed eccentrically, or with individual spirals around the ducts were not included in the development of the basic model curves because reductions in connection capacity were observed and the individual spirals would not be recommended for use in practice. In the case of tests with two connectors, there were very small differences in bond-slip response when the clear spacing between ducts varied from one to two duct diameters, and when individual spirals were provided around ducts. All tests involving two connectors are thus included in categories determined by the duct material. The fifteen test categories listed in Table 6.2 were reduced to nine for consideration:

- Single connectors in galvanized steel ducts (GS)
- Single connectors in polyethylene ducts (PE)
- Single connectors in polypropylene ducts (PP)
- Two connectors in galvanized steel ducts (2-GS)
- Two connectors in polyethylene ducts (2-PE)
- Two connectors in polypropylene ducts (2-PP)
- Three connectors in galvanized steel ducts (3-GS)
- Three connectors in polypropylene ducts (3-PP)

The model parameters s_1, s_2, u_3, and β were chosen to match the experimental curves by estimating the best fit to the data. Bond stress values are normalized to the average concrete compressive strength for the tests (5100 psi). Figures 6.36 through 6.43 show the nine curves that were developed independently for each set of parameters, and their comparison with experimental data. The values of the model parameters used in the basic curves are shown in

Table 6.3. The lower value of β for connections containing galvanized steel ducts reflects the higher initial stiffness values observed in these tests.

The limited number of tests that explored the parameter of clear spacing between ducts did not produce sufficient evidence to evaluate the effects of duct spacing on connection behavior. Any influence that this parameter may have on performance is included in the model together with the effect of number of connectors. Observations of the cracking patterns that developed in the test specimens, for example V-shaped cracks that formed on the sides (Section 5.3), indicate that the zone of influence around an individual connector may extend a radial distance, r, of approximately 11 in. from the axis of the connector (Figure 6.44). For a #11 bar, this corresponds to a radius of around $7.8d_b$. Measurements of the concrete cone breakout depths, d_c, ranged between 4 and 6 in. for single connector tests, and between 6 and 10 in. for multiple connector tests.

A modification factor, γ, is introduced to account for group effects:

$$\gamma = \frac{A_N}{nA_{No}} \leq 1.0 \tag{6-5}$$

where A_N is the projected failure surface of the group of connectors (in^2), A_{No} is the maximum projected failure surface of an individual connector (in^2), and n is the number of connectors. A similar modification factor is used by Miltenberger [6.2] to determine the nominal strength of grouted connectors (fasteners). This approach incorporates both the Concrete Capacity Design (CCD) model and the Uniform Bond Stress (UBS) model and was adopted in Appendix D of ACI 318-02 [6.3].

The projected failure surface of an individual connector, A_{No}, is defined as a square with sides equal to $15d_b$ (Figure 6.45). The failure surface is defined as square rather than a circle to simplify the calculations. The surface area proposed by Miltenberger [6.2] also considers a square surface, but the sides of the square

are $16d_b$ (shown in Figure 1.30). The projected failure surface of a group of connectors, A_N, is limited by the distance between the connectors and the nearest edge.

Table 6.4 shows a comparison of the average bond strengths achieved by single-connector tests modified by the group effect factor, γ, and bond strengths obtained in tests with multiple connectors. The mean value of the group effect modification factors calculated using Equation 6-5 for double-connector tests (1 D and 2 D clear spacing between ducts) is 0.72. The mean value of the ratios of average peak bond strength of double-connector tests to single-connector tests of steel and polyethylene duct specimens is 0.72. Agreement is good between calculated and experimental values for the triple-connector test with steel ducts. Very poor agreement is observed for specimens with polypropylene ducts. The average peak bond strength of single-connector polypropylene duct connection specimens was based on two tests (Tests No. 29 and No. 30). These tests involved connectors embedded $8d_b$ and $12d_b$, whereas multiple connector tests (Tests No. 28 and No. 32) involved two and three connectors embedded $16d_b$. Polypropylene duct specimens failed by plug pullout, and it is possible that the shallow embedment depths of 8 and $12d_b$ limited the capacity of the single connectors. Moreover, data were extremely limited for polypropylene duct specimens, and the comparison between tests involving single and multiple connectors may not be appropriate. Nonetheless, the ratio of average peak bond strength of the double-connector specimen with polypropylene duct to that of the triple-connector test is 0.79, which agrees favorably with the ratio obtained for tests with galvanized steel ducts.

An attempt to reduce the number of basic curves by incorporating the group effect modification produces curves that are reasonable. Figures 6.46 to 6.48 show comparisons between the basic model curves developed for tests with

multiple connectors and the single-connector model curves multiplied by the group effect factor γ. A value of γ equal to 0.72, which is the average value for clear spacing between ducts of one and two duct diameters, is used for the double-connector tests involving polyethylene and steel ducts. As the number of connectors increase, not only strength is affected, but also the values of the characteristic slip values, s_1 and s_2. Model curves modified by the group effect factor underestimate somewhat the average response of double-connector tests. There is better agreement between model curves for the polyethylene duct connections. The single-connector model curve modified by the group effect factor slightly overestimates the response of the triple-connector test involving galvanized steel ducts. No attempts were made to include the group effect factor in model curves for polypropylene duct connections because of the limited data available, and the uncertainties regarding peak bond strength of single connectors.

Tests involving connector eccentricity are not included in any of the test categories. No attempts were made to introduce this effect into the phenomenological model. Effects of this parameter on connection behavior can better be included later in the development of a design equation to estimate the required development length of connectors. The effect of connector eccentricity can be included in the derivation of a suitable equation by assuming that all connectors are located eccentrically and simply reducing the calculated capacity.

In the development of the bond stress-slip curves, the value of u_3 was assumed to depend only on the physical characteristics of the connector. The method of testing was force-controlled, which introduces a high degree of variability in the post-peak bond-slip behavior. Although connection specimens containing polyethylene duct had various types of pullout modes of failure, development of a single basic curve for all tests was considered adequate. Some differences were recognized, in particular regarding the value of limiting

frictional bond resistance; connection specimens exhibiting a plug pullout mode of failure (grout and connector slipping out of the duct as a unit), such as Test No. 8 and Test No. 22, were characterized by having a higher frictional resistance.

Reasonable agreement between estimated and experimental bond-slip curves indicates that the framework developed by Ciampi et al. [6.1] for anchorage of deformed bars in well-confined concrete can be used to describe the behavior of grouted vertical duct connections. In the phenomenological model described in this section, no attempts were made to determine model parameter values (s_1, s_2, u_1, u_3, and β) using physical properties of the connection system. Curve fitting was used to evaluate test results and establish characteristic bond strength, stiffness, and slip values for connections using the different duct materials. The anchorage design provisions that are developed in Chapter 7 are not based on the phenomenological bond stress-slip model.

6.4 REFERENCES

6.1. Ciampi, V., Eligehausen, R., Popov, E. P., and Bertero, V. V., "Analytical Model for Concrete Anchorages of Reinforcing Bars under Generalized Excitations," Report No. UCB/EERC-82/23, Earthquake Engineering Research Center, University of California, Berkeley, CA, November 1982.

6.2. Miltenberger, M., "Capacity Design of Grouted Anchors," *16th International Conference on Structural Mechanics in Reactor Technology (SMiRT 16) Transactions*, Washington D. C., August 2001.

6.3. ACI Committee 318, "Building Code Requirements for Structural Concrete and Commentary," *ACI 318-02/ACI 318R-02*, American Concrete Institute, Farmington Hills, MI, 2002.

Table 6.1 Designations Used to Identify Test Specimens

Figure	Label	Test No.	Label	Test No.	Label	Test No.	Label	Test No.
6.1	GS	1	GS (epoxy-coated)	2	PE	5	PE (epoxy-coated)	6
6.2	GS	3	GS (epoxy-coated)	4	PE	7	PE (epoxy-coated)	8
6.3	GS	3	GS (epoxy-coated)	4				
6.4	GS	1	PE	5	PP	29		
6.5	GS	1	PE	5	PP	29		
6.6	GS	3	PE	7	PP	30	ND	12
6.7a	GS	3	PE	7	PP	30	ND	12
6.7b	GS	3	PE	7	PP	30	ND	12
6.7c	GS	3	PE	7	PP	30	ND	12
6.8	GS	17	PE	18				
6.9	GS	13	PE	14	PP	28		
6.10	GS	31	PP	32				
6.11	GS-8	1	GS-12	3				
6.12	GS-16	13	GS-12	17				
6.13	PE-8	5	PE-12	7	PE-16	22		
6.14	PE-16	14	PE-12	18				
6.15	PP-8	29	PP-12	30				

Table 6.1 (continued) Designations Used to Identify Test Specimens

Figure	Label	Test No.	Label	Test No.	Label	Test No.	Label	Test No.
6.16	1	3	1	17				
6.17	2	13	3	31				
6.18	2	13	3	31				
6.19	1	7	2	18				
6.20	1	22	2	14				
6.21	1	22	2	14				
6.22	2	28	3	32				
6.23	2	28	3	32				
6.24	GS (2 Duct dia)	23	GS (1 Duct dia)	13				
6.25	GS (2 Duct dia)	23	GS (1 Duct dia)	13				
6.26	GS	1	GS (eccentric)	19	PE	5	PE (eccentric)	20
6.27	GS	3	GS (eccentric)	21				
6.28	GS	3	GS (eccentric)	21				
6.29	GS (no spiral)	15	GS (group spiral)	13				
6.30	PE-8	5	PE-8 (indiv. spiral)	25	PE-12	7	PE-12 (indiv. spiral)	27
6.31	PE (no spiral)	16	PE (group spiral)	14	PE (indiv. spiral)	26		

Table 6.2 Average Bond Strength of Broad Test Categories

Broad Test Category	Average Peak Bond Strength, $u_{f'c=5100}$ (psi)
1-GS[A]	1710
1-GS (eccentric)	1430
1-PE[A]	1290
1-PE (eccentric)	1180
1-PE (individual spiral)	960
1-PP	1160
1-ND	1420
2-GS (1 Duct diameter spacing)	1310
2-GS (2 Duct diameter spacing)	1190
2-PE (1 Duct diameter spacing)	930
2-PE (2 Duct diameter spacing)	910
2-PE (individual spiral)	870
2-PP (1 Duct diameter spacing)	1150
3-GS	1000
3-PP	910

GS: Galvanized Steel Duct, PE: Polyethylene Duct, PP: Polypropylene Duct, ND: No duct.

[A]Test data do not include epoxy-coated connector tests at $8d_b$ embedment.

Table 6.3 Values of Model Parameters used in Basic Bond-Slip Curves

Test Category	**s_1 (in.)**	**s_2 (in.)**	**u_1^C (psi)**	**u_3^C (psi)**	**β**
GS[A]	0.13	0.22	1690	900	0.14
PE[A]	0.13	0.26	1280	700	0.22
PP	0.05	0.14	1150	300	0.28
ND	0.11	0.18	1410	500	0.34
2-GS[B]	0.15	0.26	1270	700	0.15
2-PE[B]	0.14	0.29	910	560	0.19
2-PP	0.15	0.23	1130	500	0.20
3-GS	0.10	0.16	970	600	0.15
3-PP	0.17	0.24	880	500	0.18

[A]Data do not include epoxy-coated connector tests at $8d_b$ embedment, eccentrically placed connectors, and specimens with spiral reinforcement around individual ducts.

[B]Data include specimens with spiral reinforcement around individual ducts and specimens with both one and two duct diameter clear spacing between ducts.

[C]Average peak bond strength values are normalized to a concrete compressive strength of 5100 psi.

Table 6.4 Group Effect Modification Factor – Comparison with Test Data

		$r = \frac{Multiple\ Connector\ Test}{Single\ Connector\ Test}$		
Connector Arrangement	**γ Eq. (6-5)**	**GS**	**PE**	**PP**
Two Connectors (2 D dia)	0.77	0.70	0.71	-
Two Connectors (1 D dia)	0.68	0.77	0.72	0.99
Three Connectors (3)	0.60	0.58	-	0.78

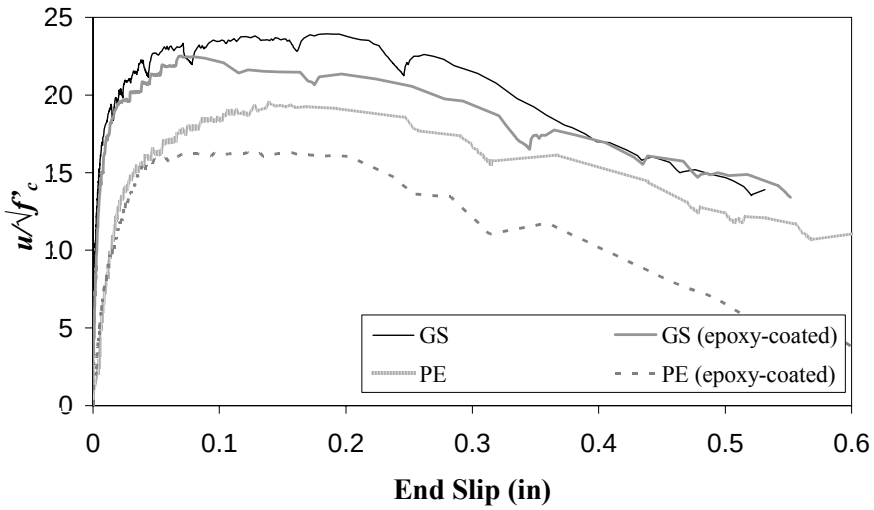

Figure 6.1 Effect of Bar Coating (8d_b Embedment)

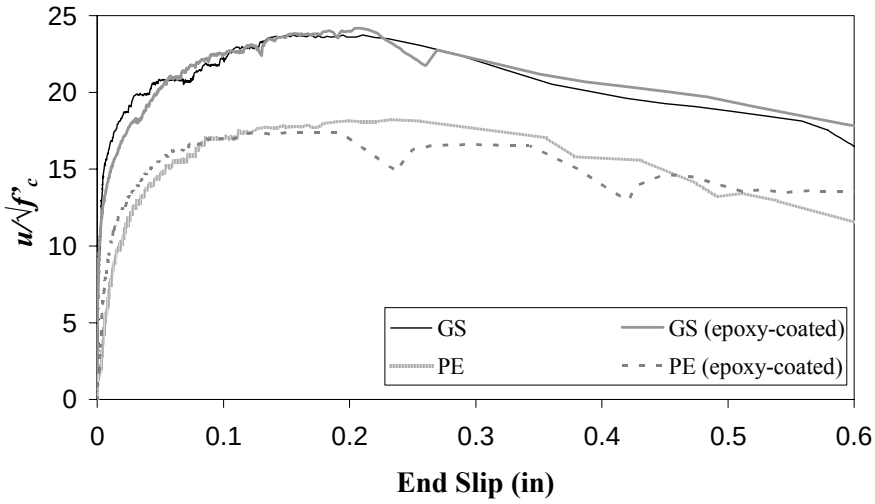

Figure 6.2 Effect of Bar Coating (12d_b Embedment)

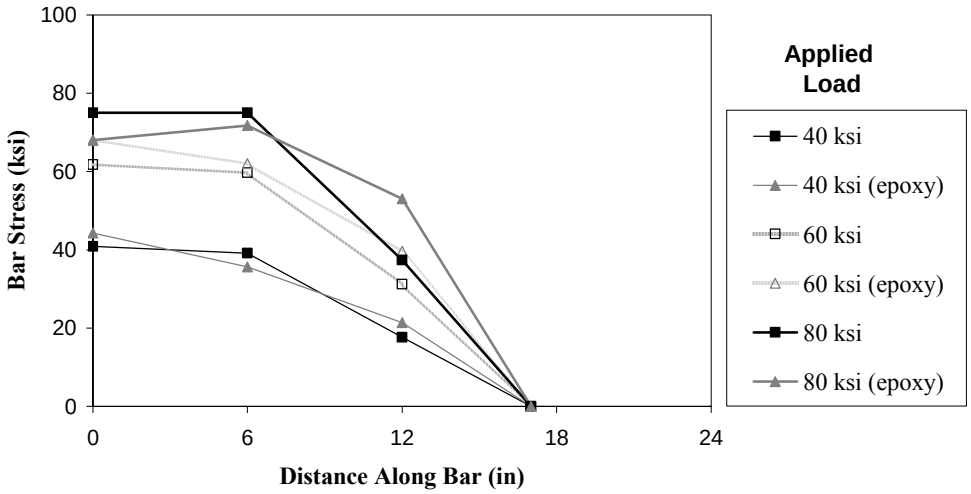

Figure 6.3 Effect of Bar Coating on Stress Distribution along Connector ($12d_b$)

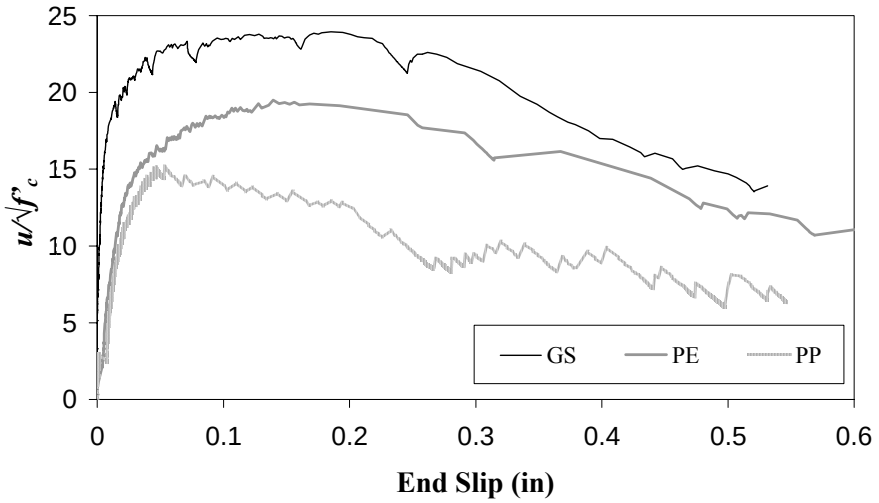

Figure 6.4 Effect of Duct Material (Single Connectors, $8d_b$ Embedment)

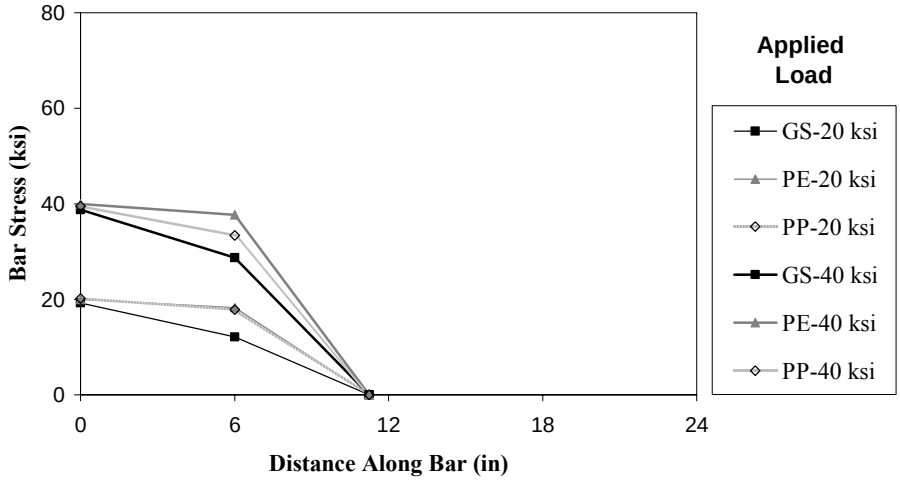

Figure 6.5 Effect of Duct Material on Stress Distribution along Connector (Single Connectors, 8d_b Embedment)

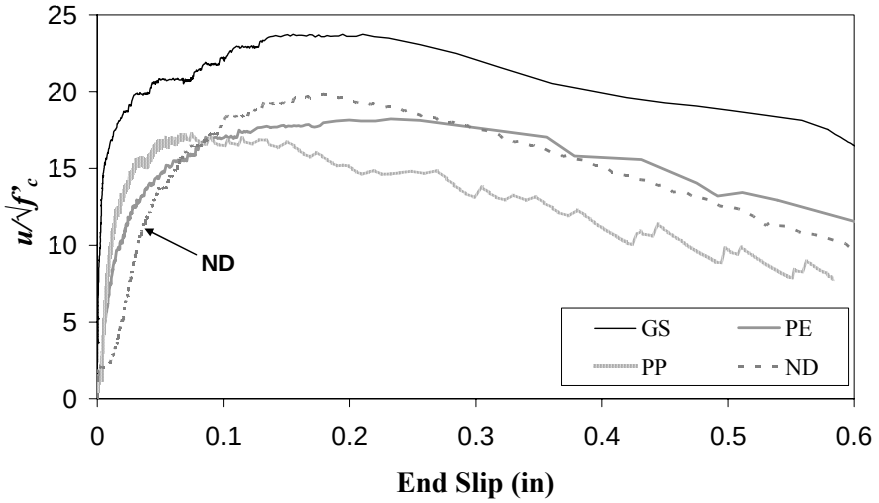

Figure 6.6 Effect of Duct Material (Single Connectors, 12d_b Embedment)

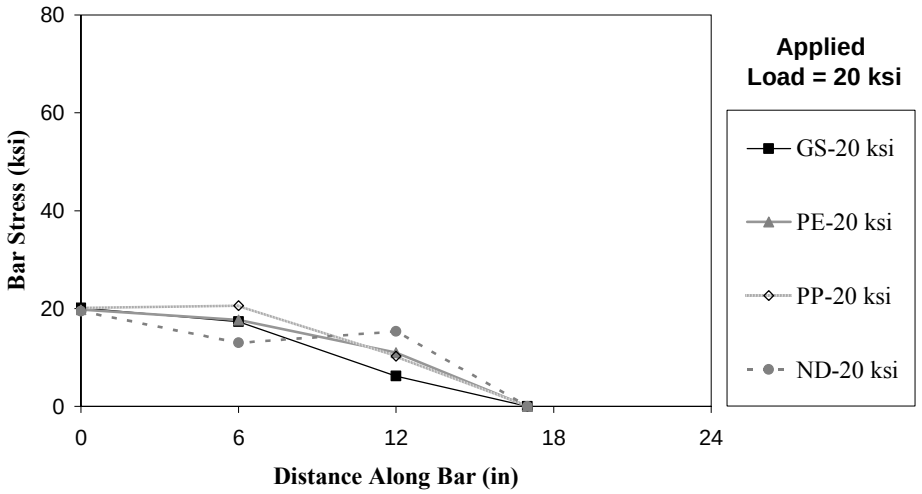

Figure 6.7a Effect of Duct Material on Stress Distribution along Connector (Single Connectors, 12d_b Embedment, and Applied Load 20 ksi)

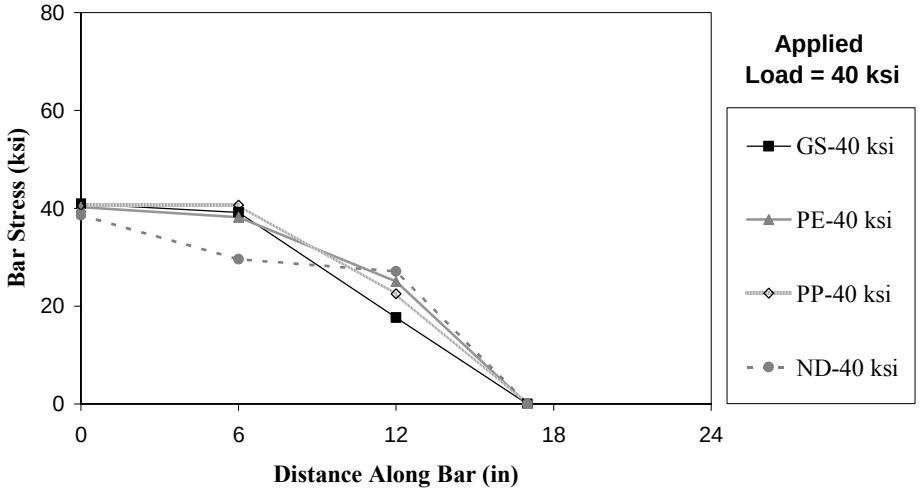

Figure 6.7b Effect of Duct Material on Stress Distribution along Connector (Single Connectors, 12d_b Embedment, and Applied Load 40 ksi)

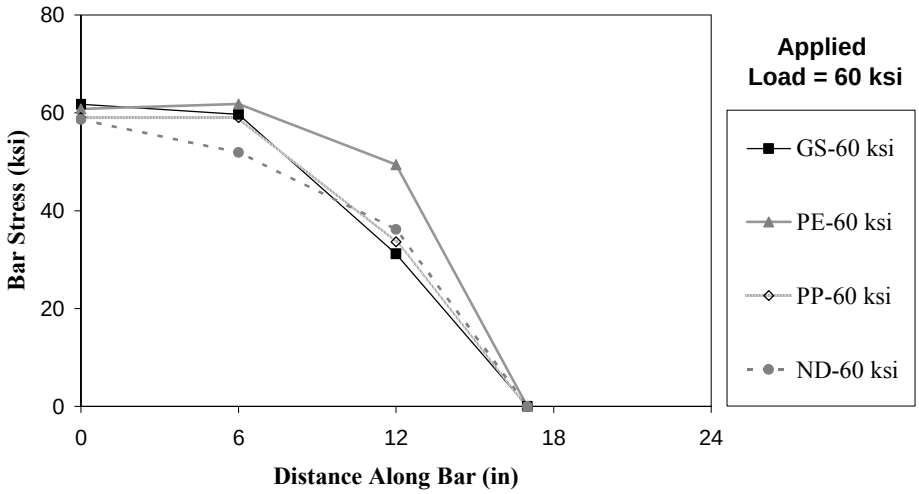

Figure 6.7c Effect of Duct Material on Stress Distribution along Connector (Single Connectors, 12d_b Embedment, and Applied Load 60 ksi)

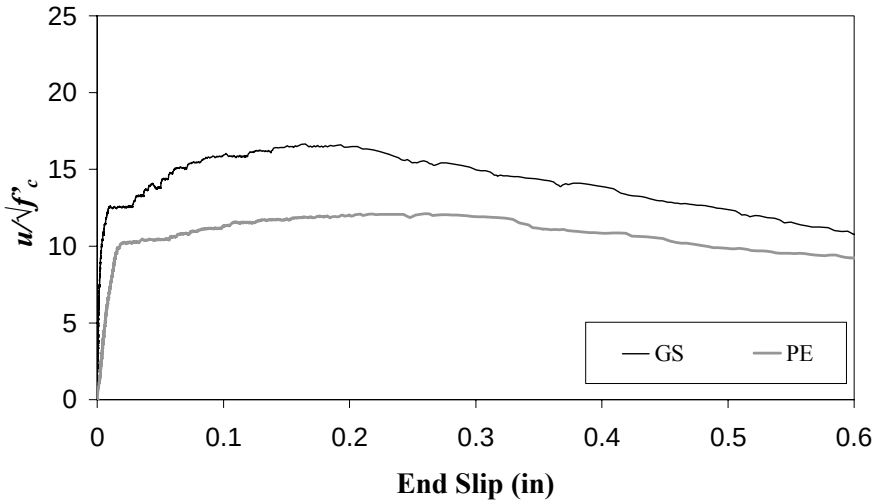

Figure 6.8 Effect of Duct Material at 12d_b (Double-Connector Tests)

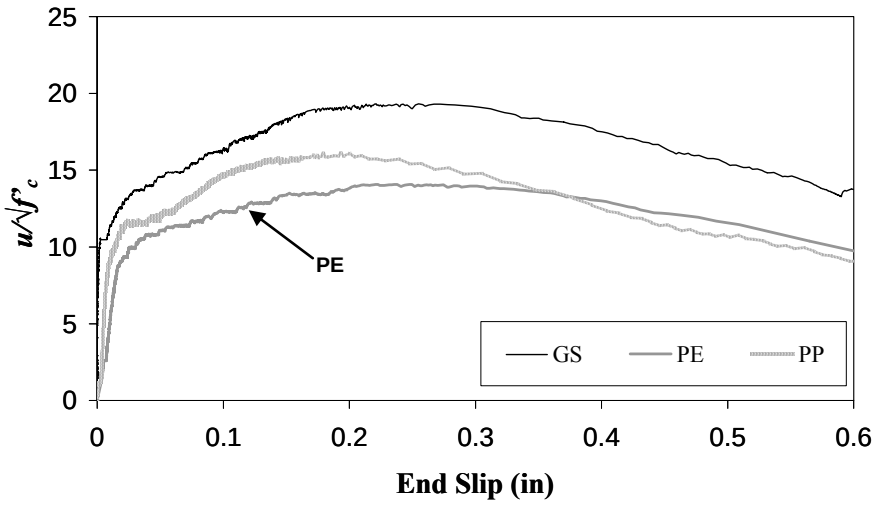

Figure 6.9 Effect of Duct Material at 16d_b (Double-Connector Tests)

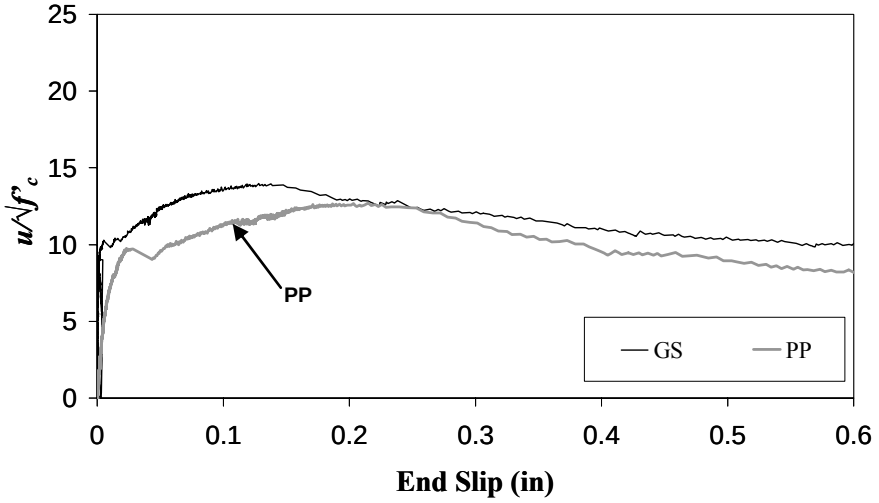

Figure 6.10 Effect of Duct Material at 16d_b (Triple-Connector Tests)

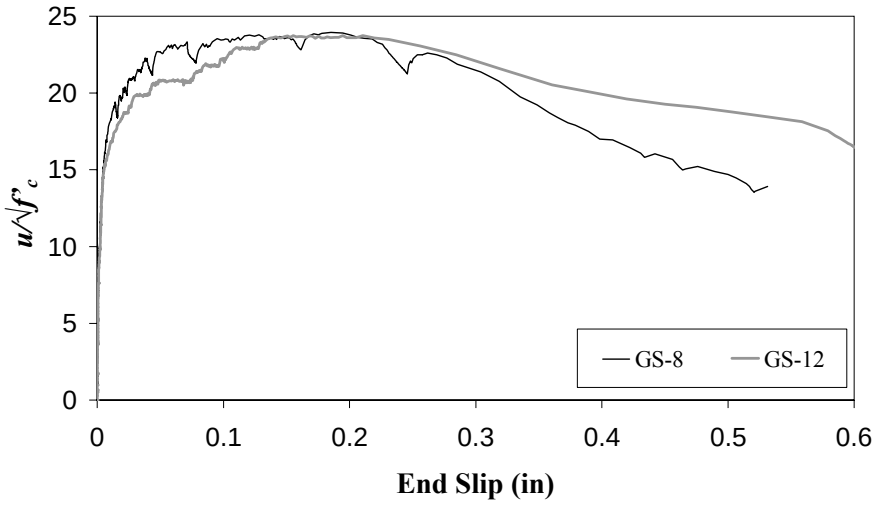

Figure 6.11 Effect of Embedment Depth (Single Connectors in Steel Duct)

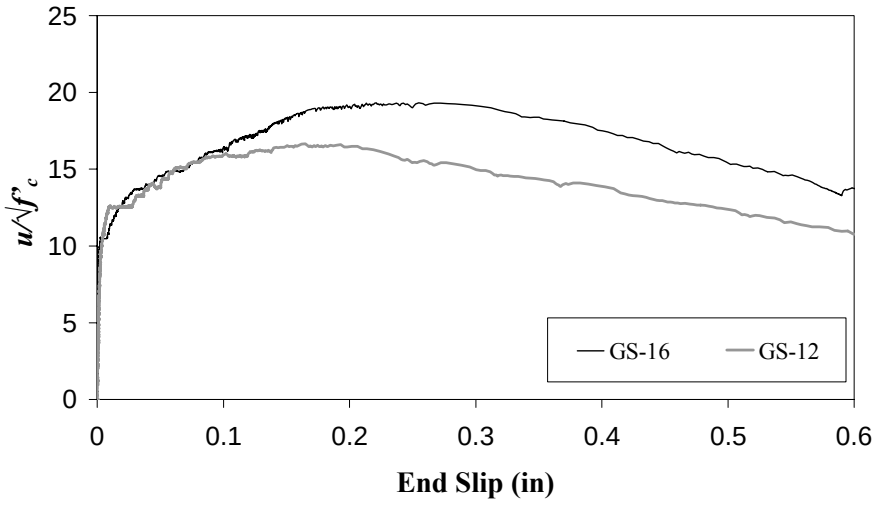

Figure 6.12 Effect of Embedment Depth (Double-Connector Tests, Steel Ducts)

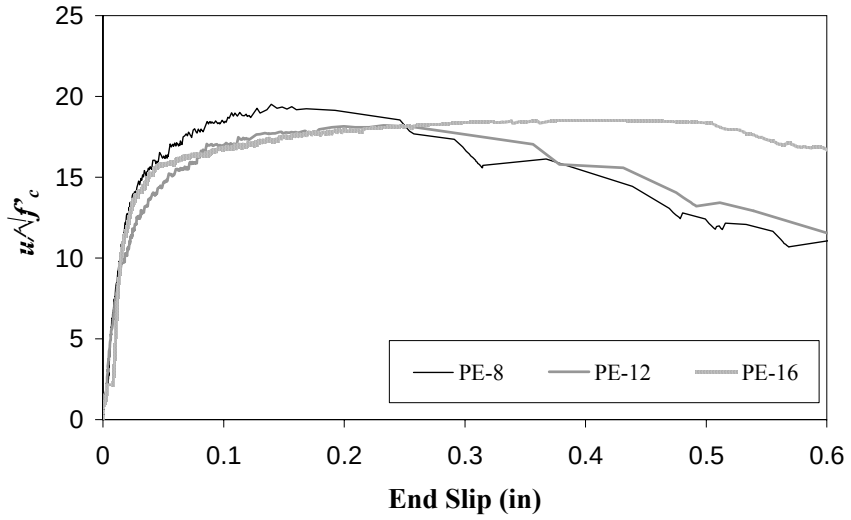

Figure 6.13 Effect of Embedment Depth (Single Connectors in Polyethylene Duct)

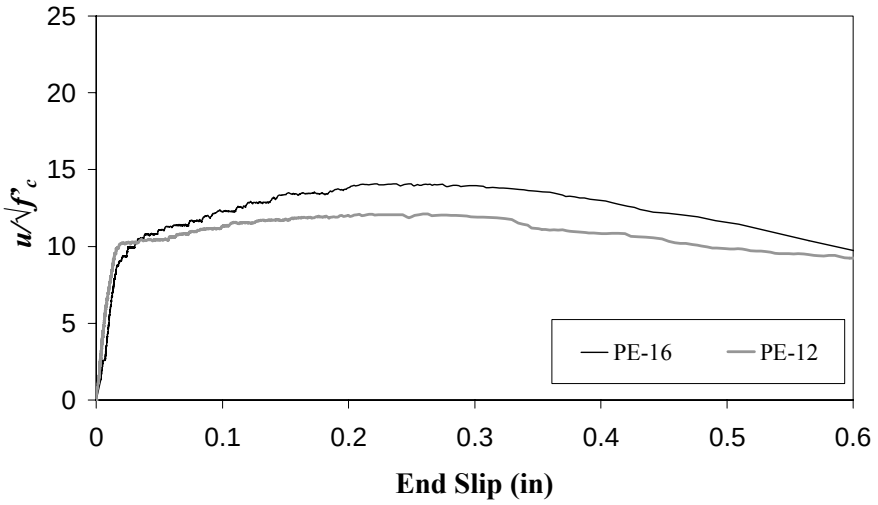

Figure 6.14 Effect of Embedment Depth (Double-Connector Tests, Polyethylene Duct)

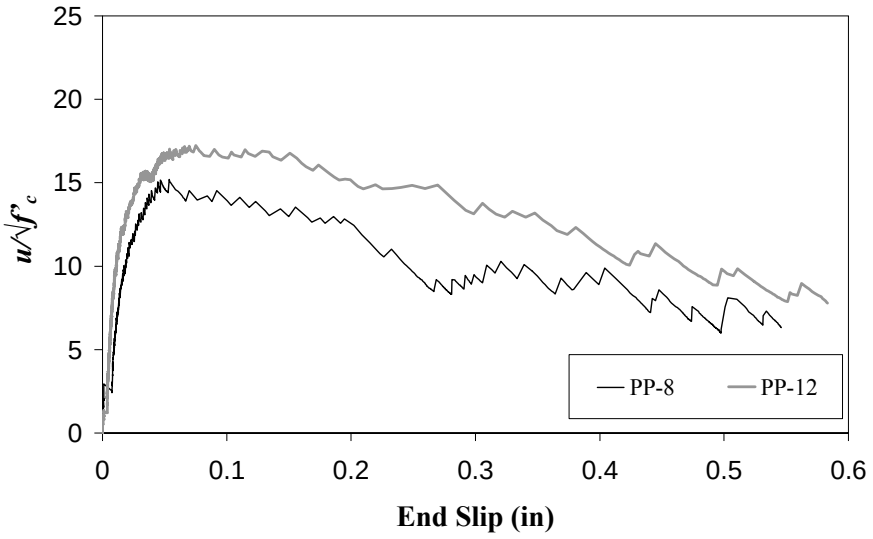

Figure 6.15 Effect of Embedment Depth (Single Connectors in Polypropylene Duct)

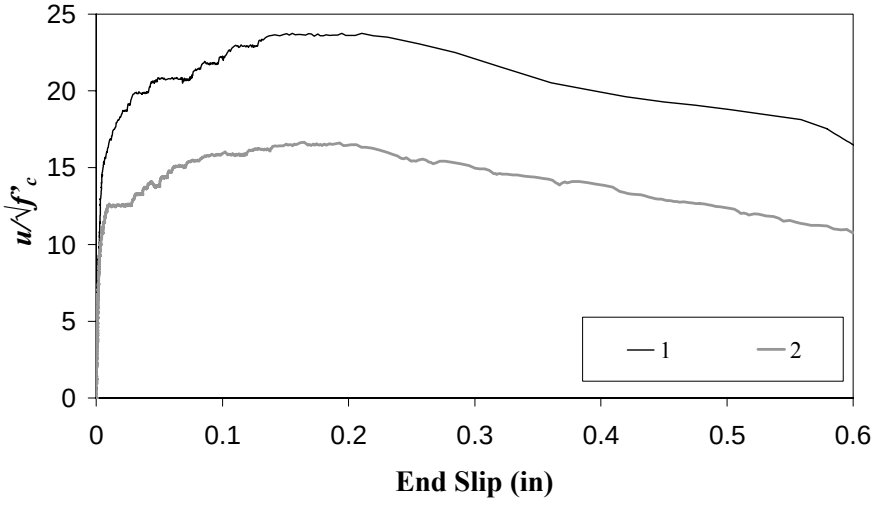

Figure 6.16 Effect of Number of Connectors (Steel Ducts, 12d_b Embedment)

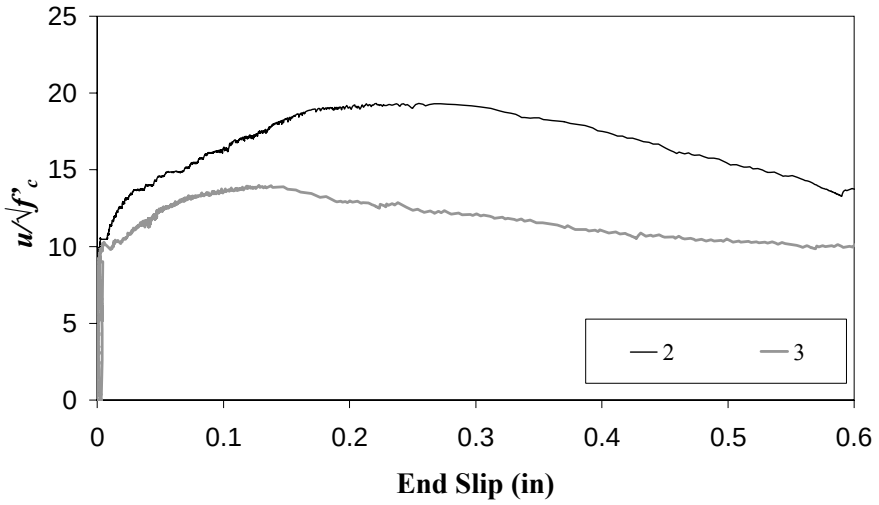

Figure 6.17 Effect of Number of Connectors (Steel Ducts, 16d_b Embedment)

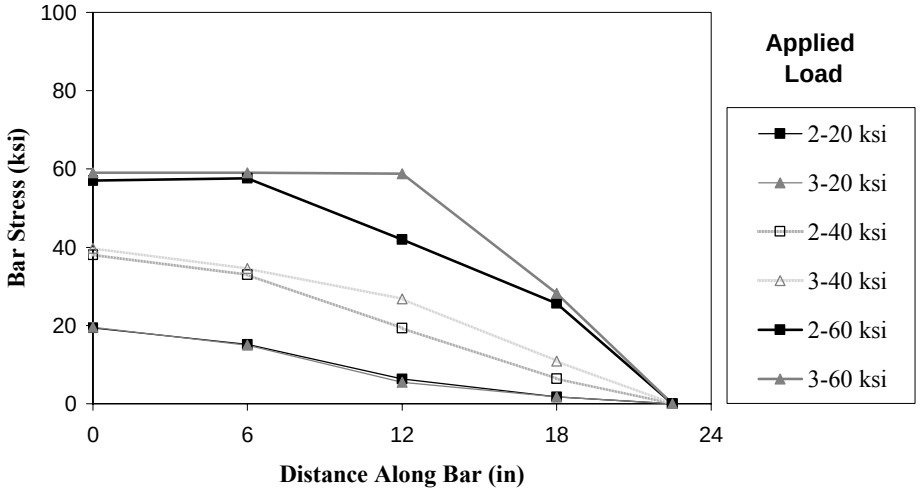

Figure 6.18 Effect of Number of Connectors on Stress Distribution along Connectors (Steel Ducts, 16d_b Embedment)

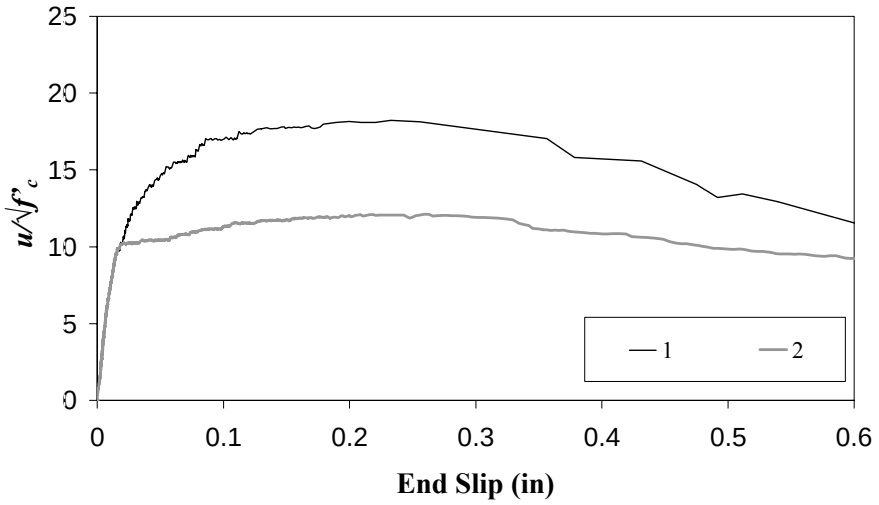

Figure 6.19 Effect of Number of Connectors (Polyethylene Ducts, 12d_b Embedment)

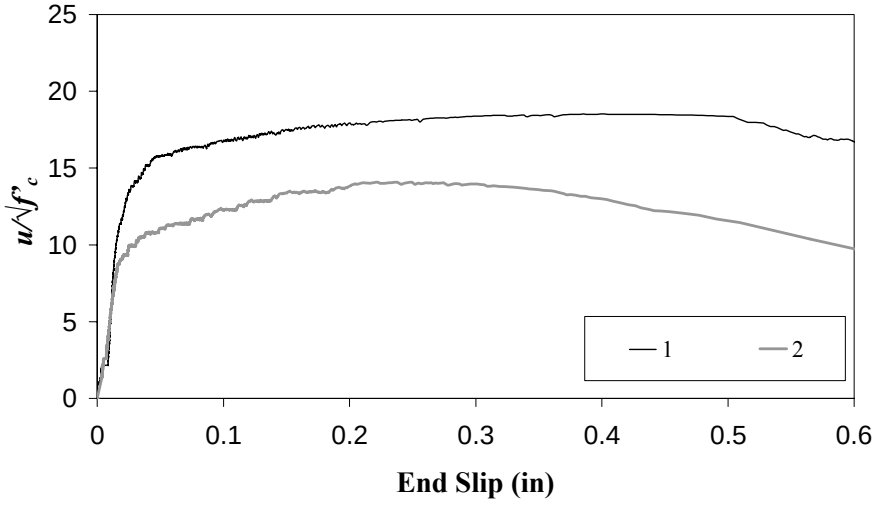

Figure 6.20 Effect of Number of Connectors (Polyethylene Ducts, 16d_b Embedment)

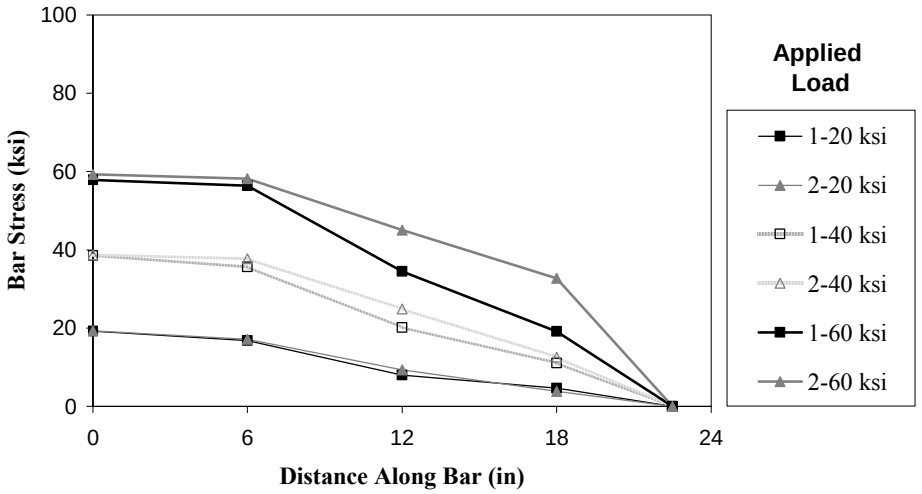

Figure 6.21 Effect of Number of Connectors on Stress Distribution along Connectors (Polyethylene Ducts, 16d_b Embedment)

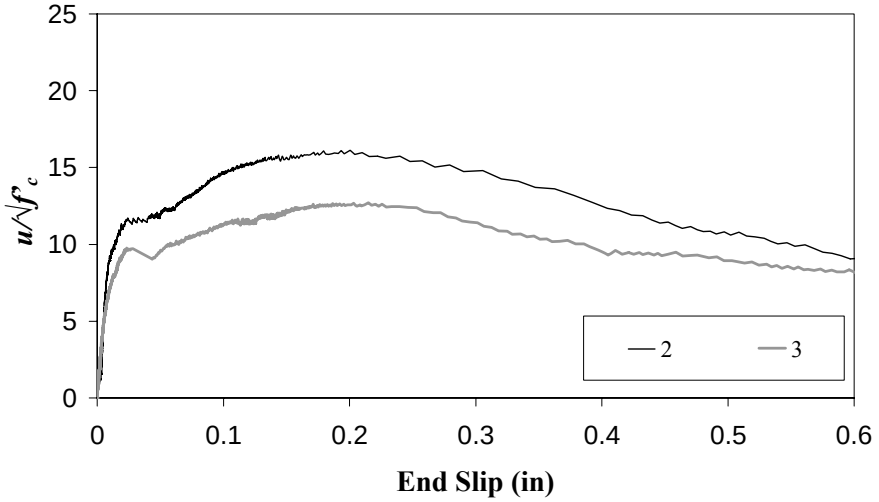

Figure 6.22 Effect of Number of Connectors (Polypropylene Ducts, 16d_b Embedment)

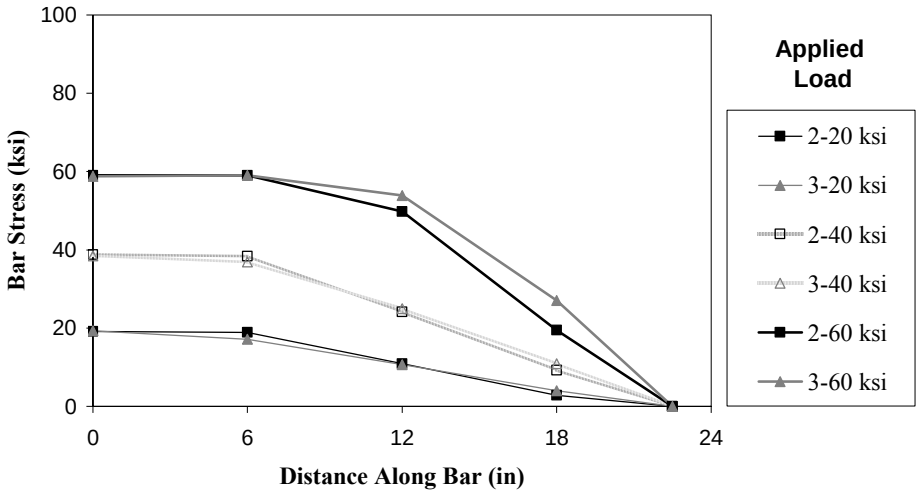

Figure 6.23 Effect of Number of Connectors on Stress Distribution along Connectors (Polypropylene Ducts, 16d_b Embedment)

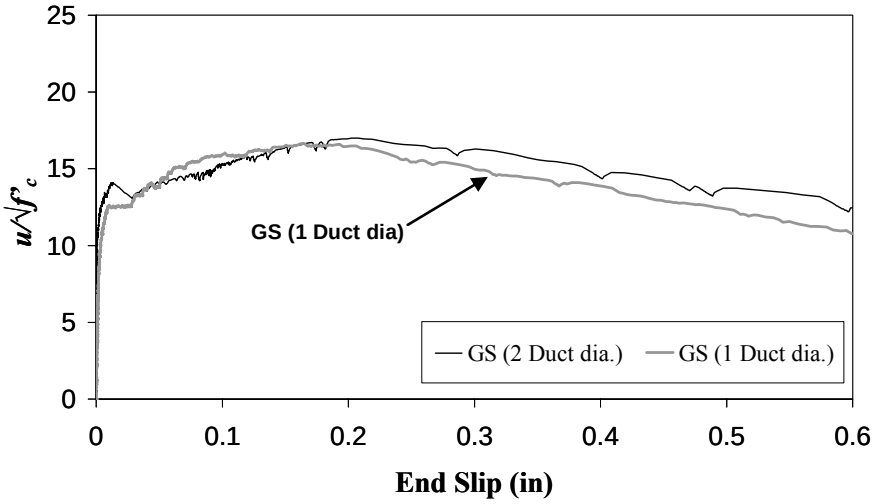

Figure 6.24 Effect of Duct Spacing (Steel Ducts, 12d_b Embedment)

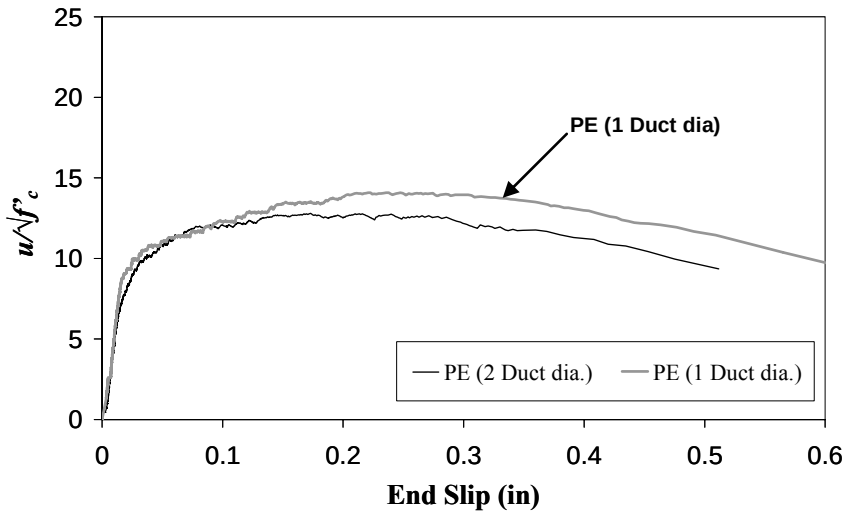

Figure 6.25 Effect of Duct Spacing (Polyethylene Ducts, 16d_b Embedment)

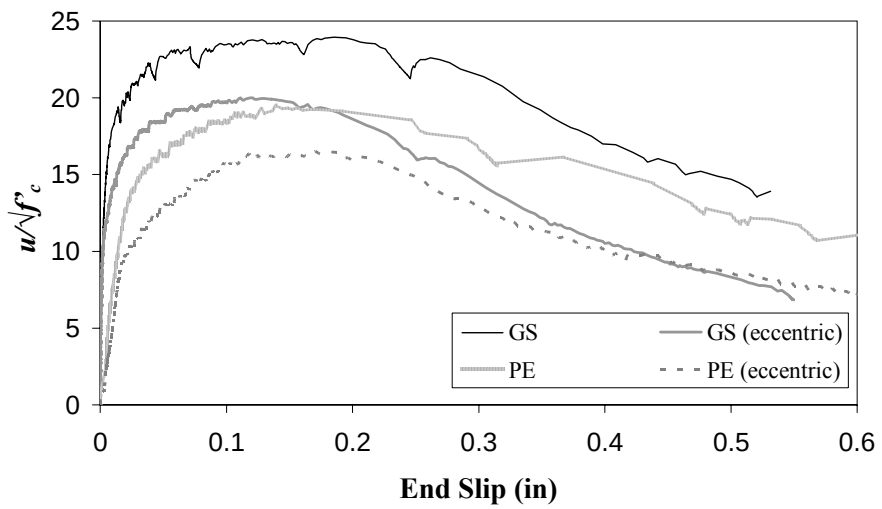

Figure 6.26 Effect of Connector Eccentricity (8d_b Embedment)

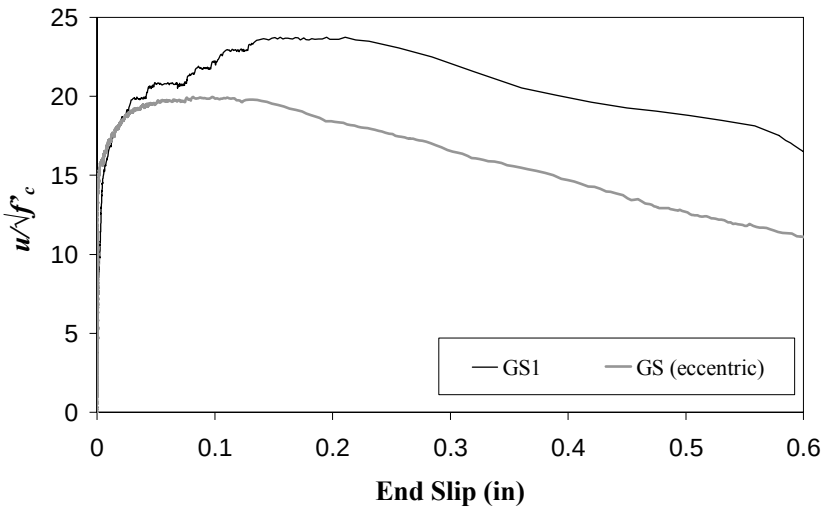

Figure 6.27 Effect of Connector Eccentricity (12d_b Embedment)

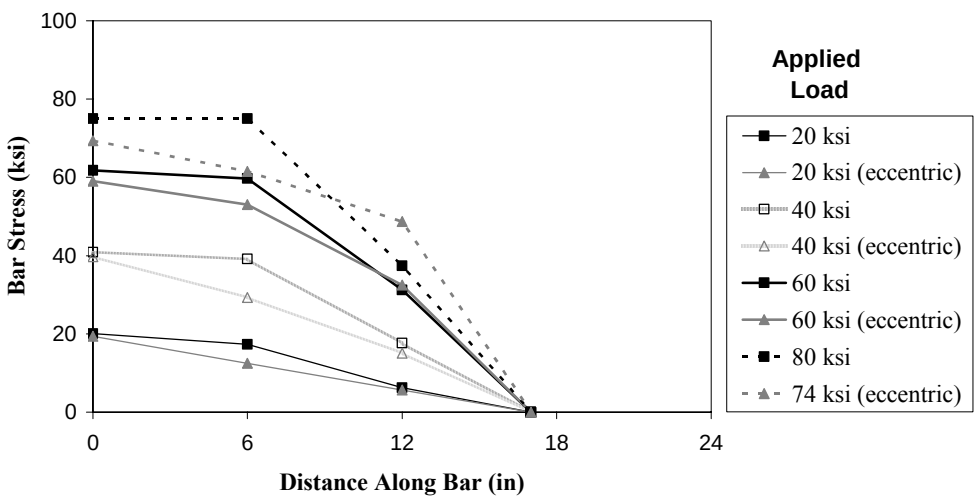

Figure 6.28 Effect of Bar Eccentricity on Stress Distribution along Connector (12d_b Embedment)

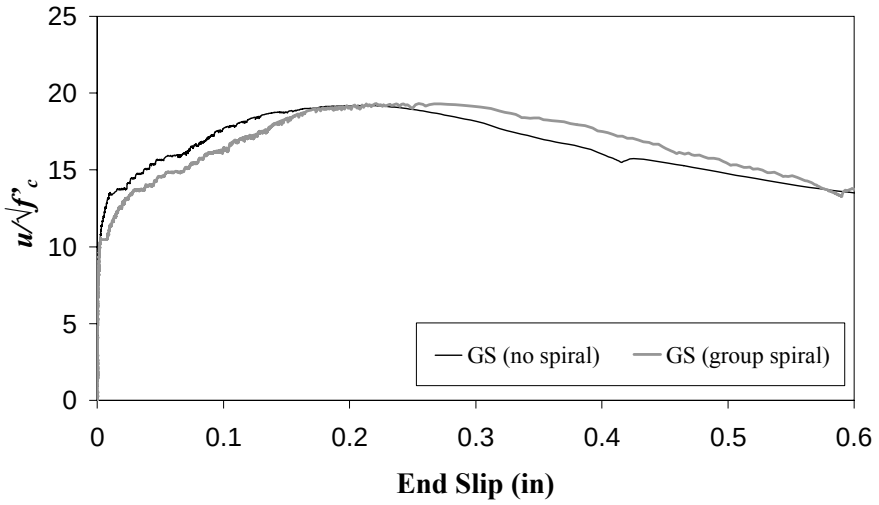

Figure 6.29 Effect of Transverse Reinforcement (Steel Ducts, 16d_b Embedment)

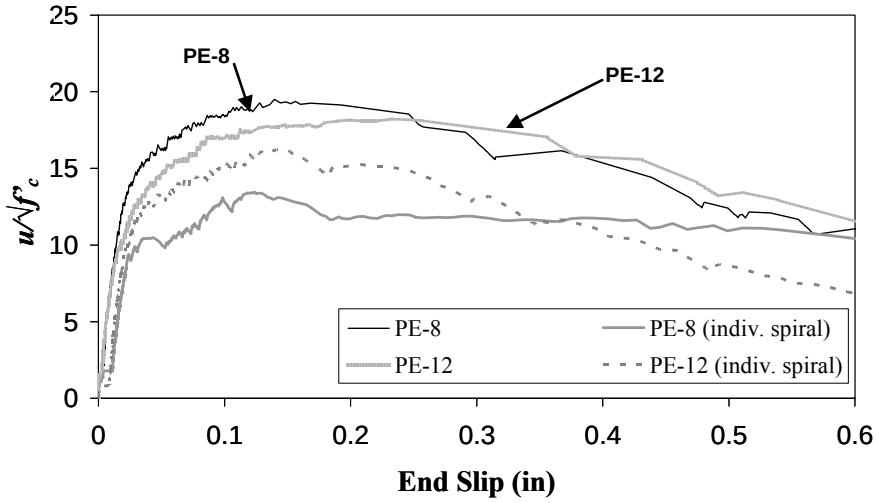

Figure 6.30 Effect of Transverse Reinforcement (Single Connectors in Polyethylene Duct)

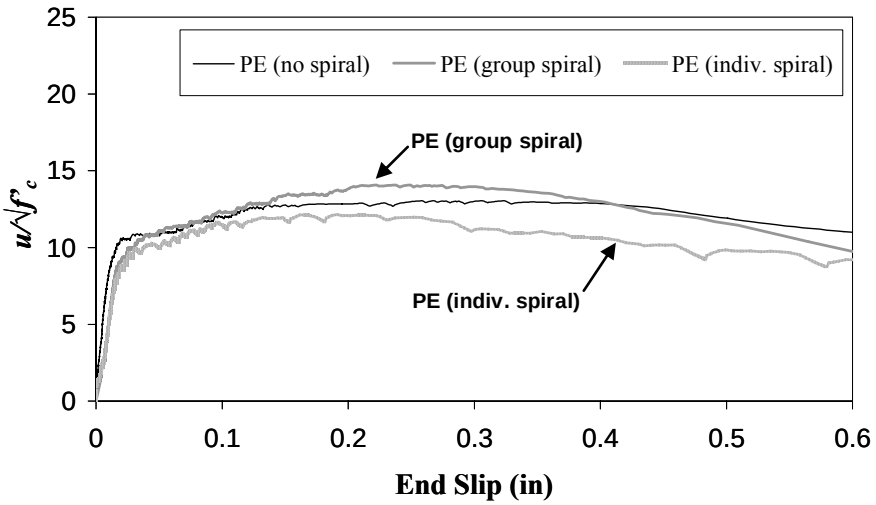

Figure 6.31 Effect of Transverse Reinforcement (Double-Connector Tests in Polyethylene Ducts, 16d_b Embedment)

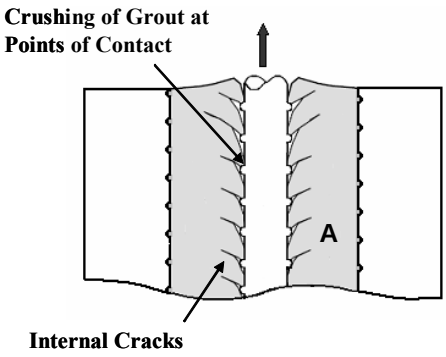

A. Initial Stages of Loading

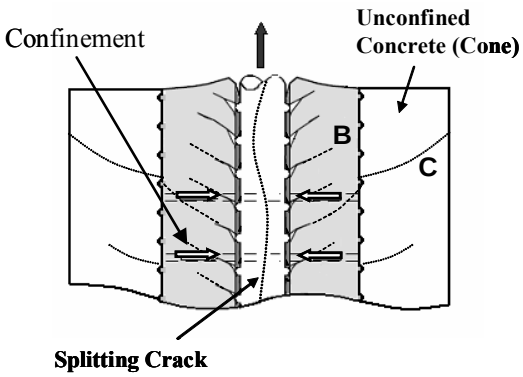

B. Connector Pullout Failure Mode

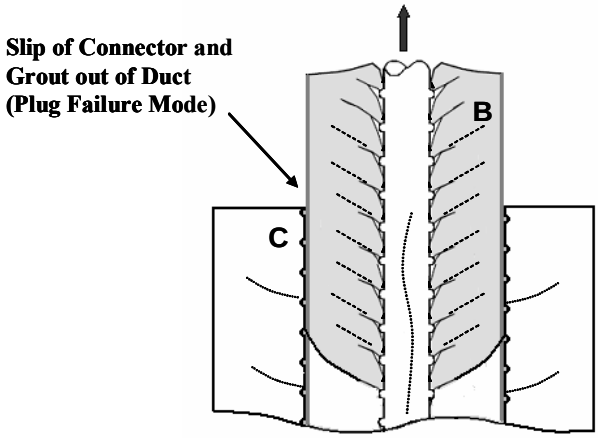

C. Plug Bond Failure Mode

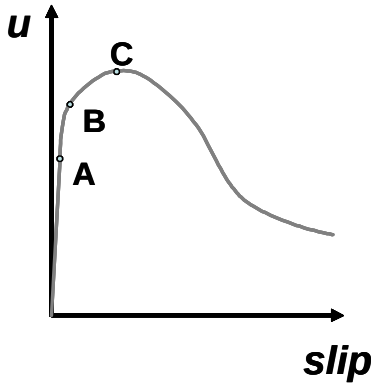

D. Bond Stress vs. Slip – Load Stages

Figure 6.32 Theory of Bond Mechanism

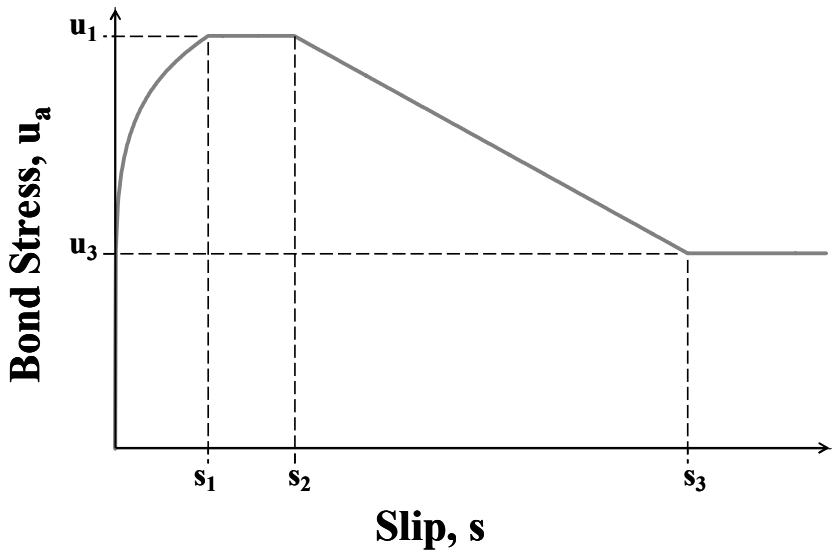

Figure 6.33 Bond Stress – Slip Model

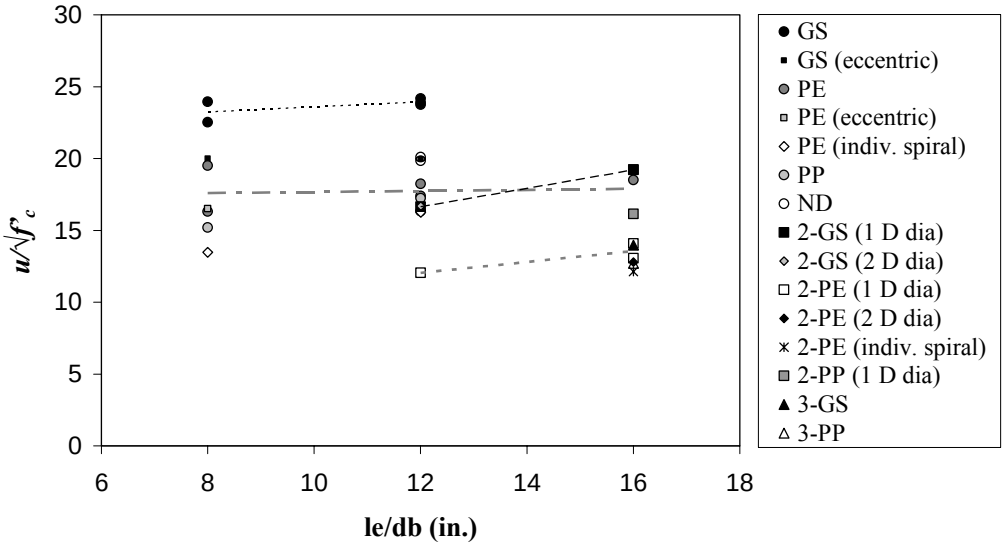

Figure 6.34 Effect of Embedment Depth on Average Peak Bond Strength

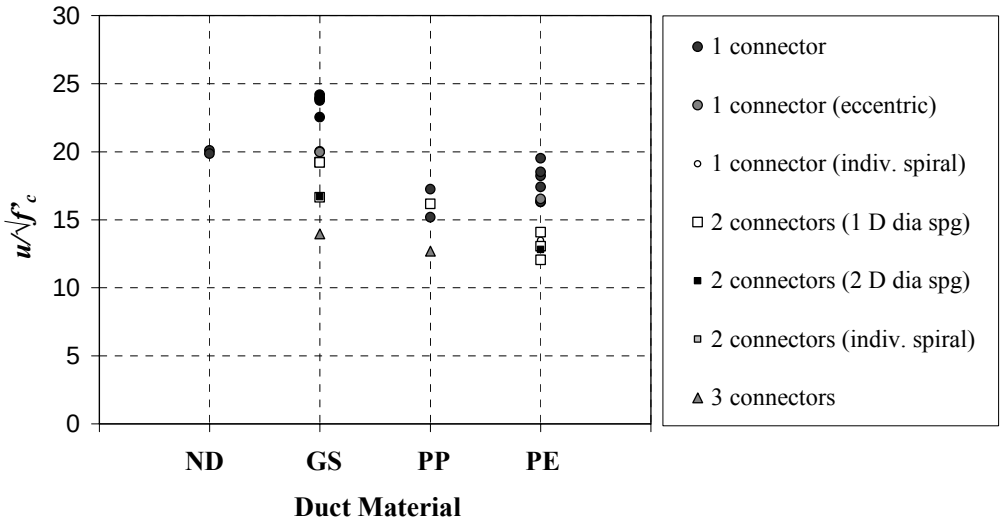

Figure 6.35 Effect of Duct Material on Average Peak Bond Strength

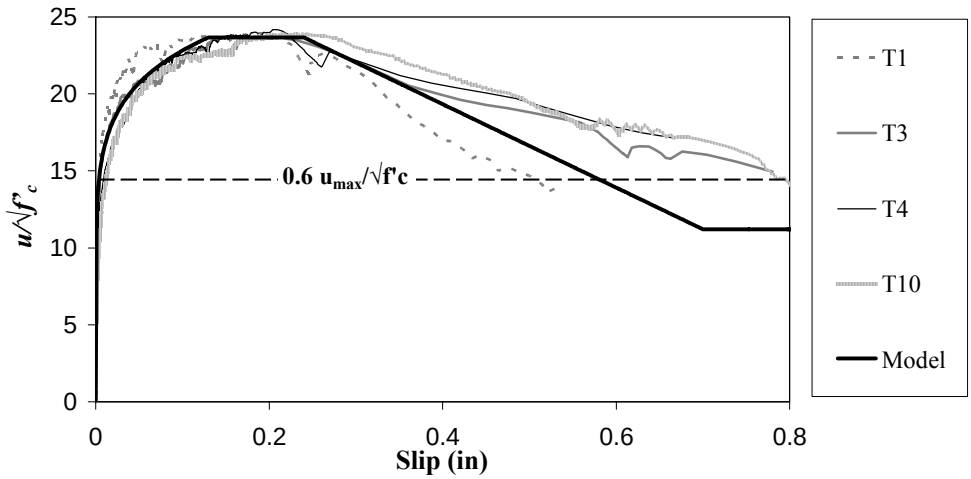

Figure 6.36 Idealized Curve for Single Connectors in Galvanized Steel Ducts

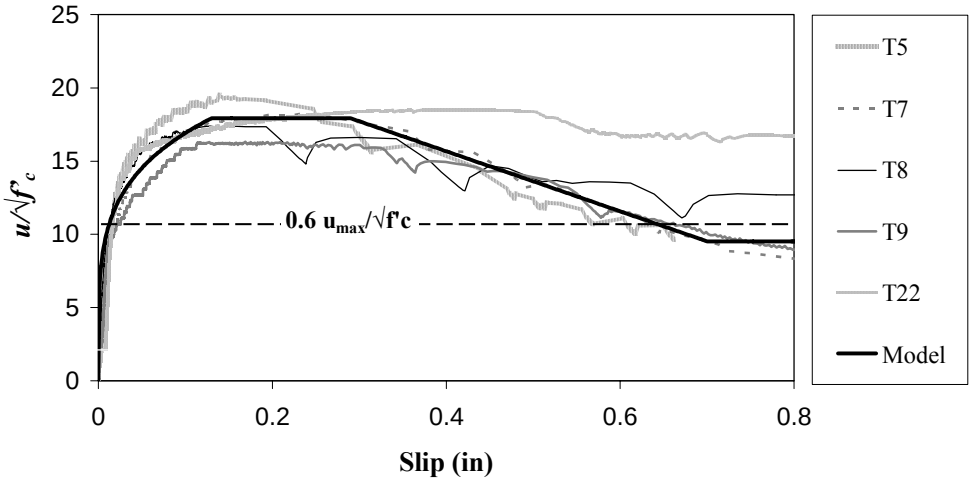

Figure 6.37 Idealized Curve for Single Connectors in Polyethylene Ducts

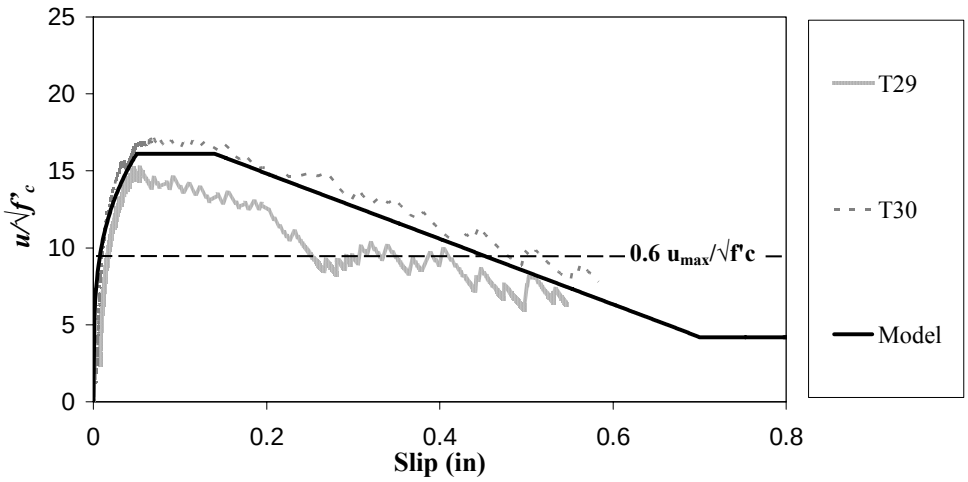

Figure 6.38 Idealized Curve for Single Connectors in Polypropylene Ducts

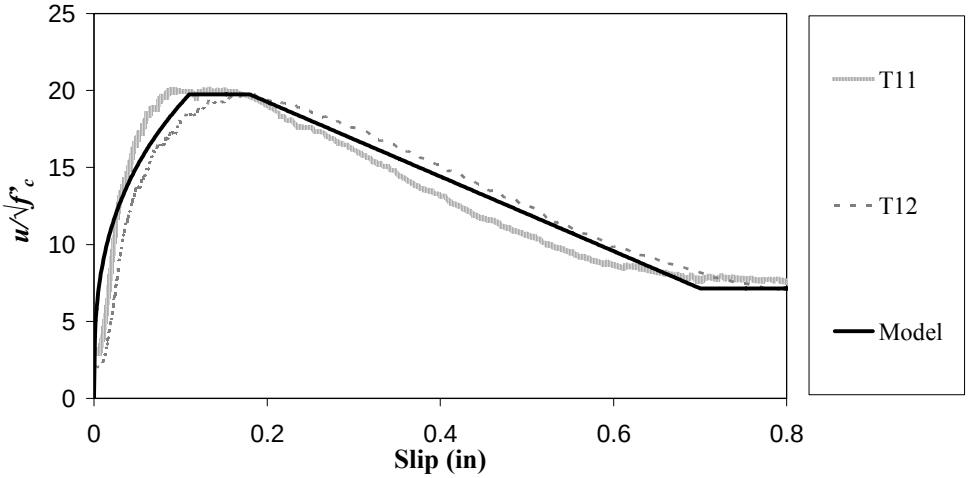

Figure 6.39 Idealized Curve for Single Connectors in Specimens without Ducts

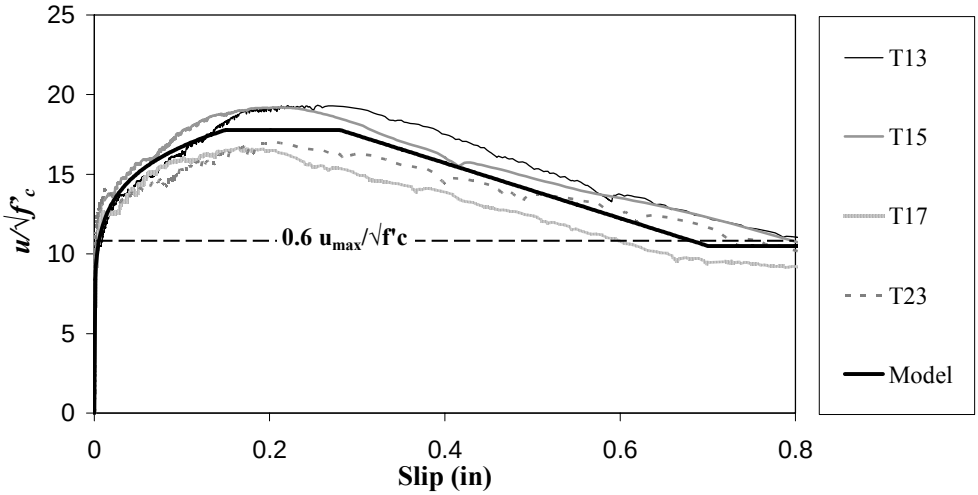

Figure 6.40 Idealized Curve for Two Connectors in Galvanized Steel Ducts

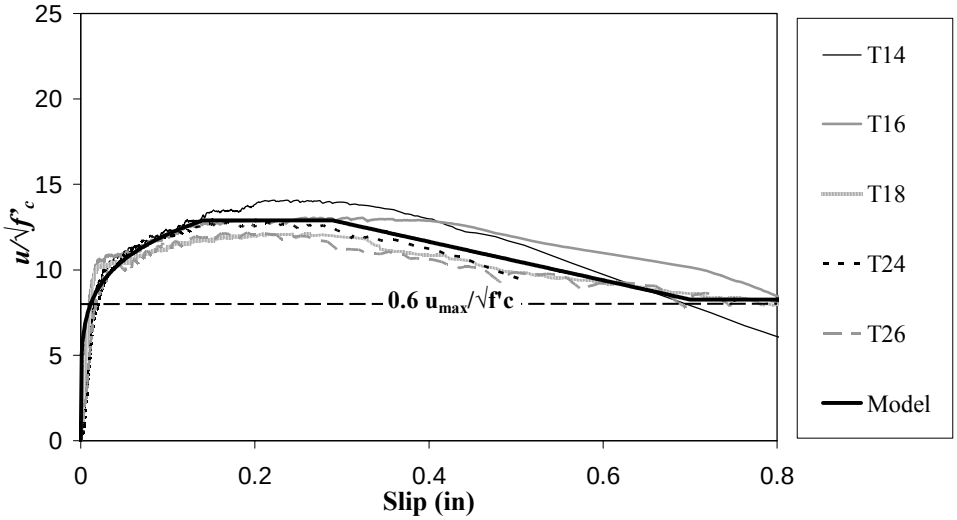

Figure 6.41 Idealized Curve for Two Connectors in Polyethylene Ducts

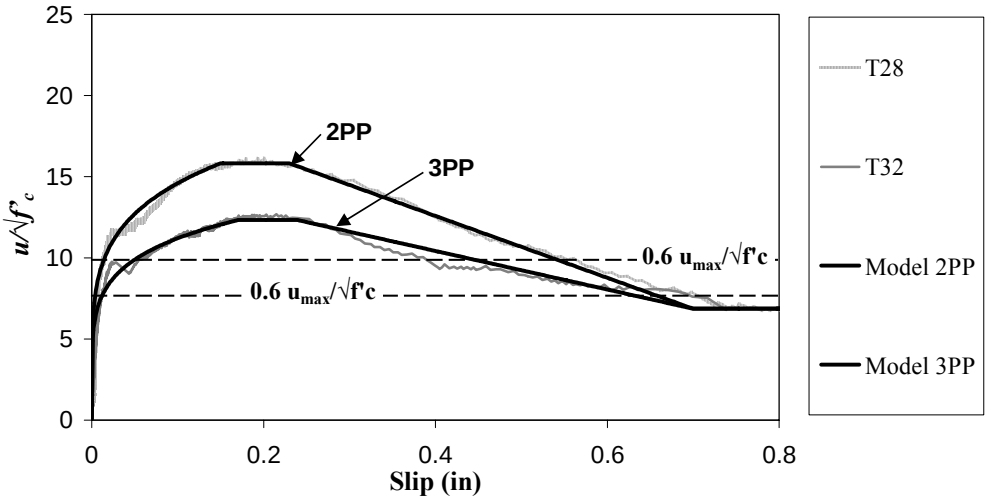

Figure 6.42 Idealized Curves for Two and Three Connectors in Polypropylene Ducts

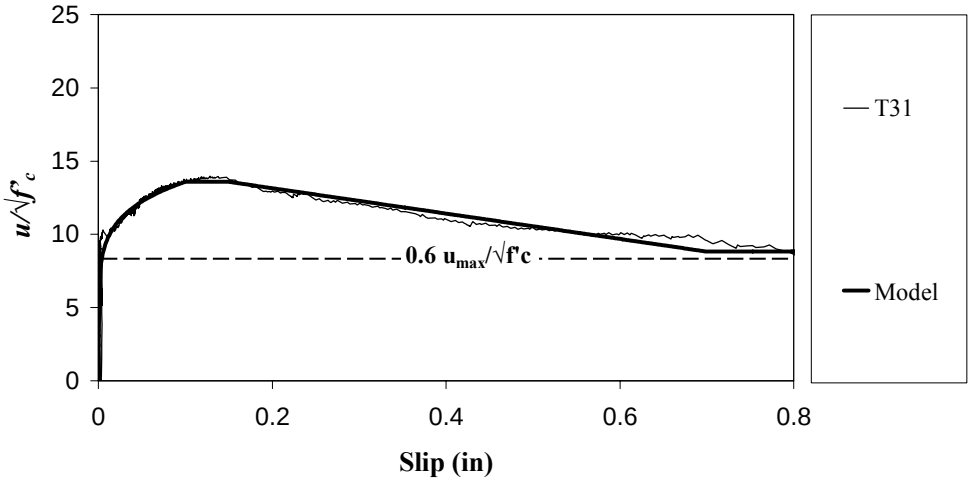

Figure 6.43 Idealized Curve for Three Connectors in Galvanized Steel Ducts

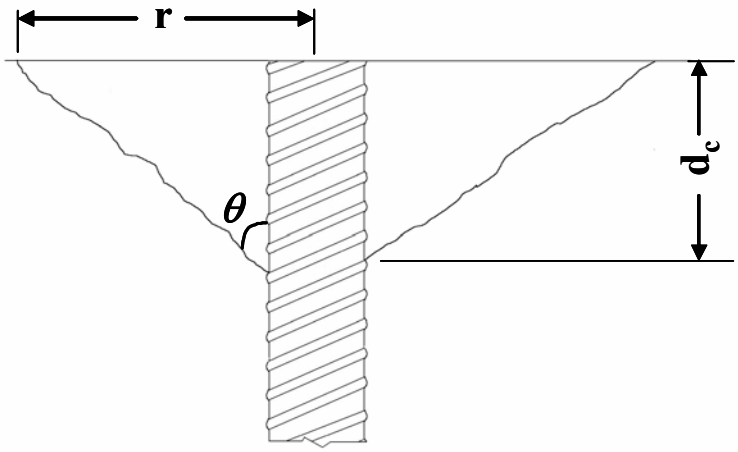

Figure 6.44 Concrete Cone-shaped Break-out

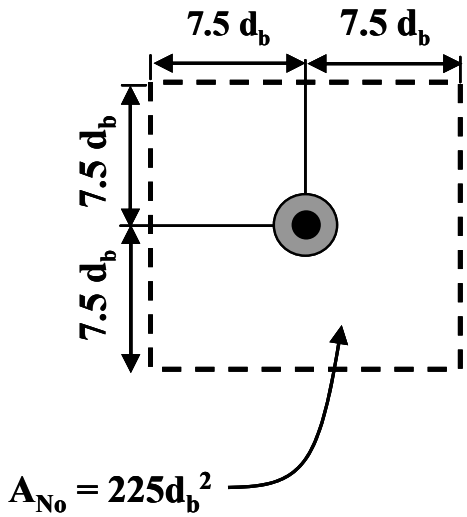

Figure 6.45 Projected Failure Surface for Individual Connector, A_{No}

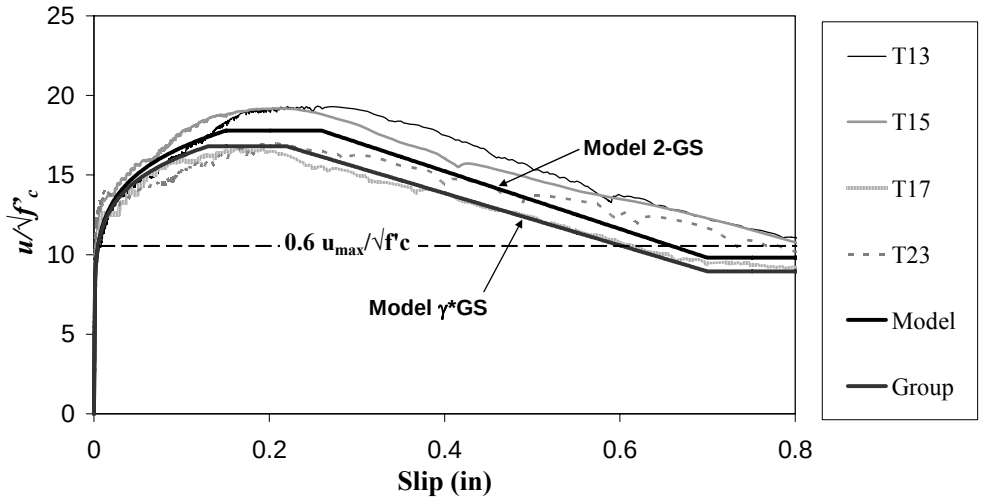

Figure 6.46 Comparison of Idealized Curves with Group Effect Modification Factor for Two Connectors in Galvanized Steel Ducts

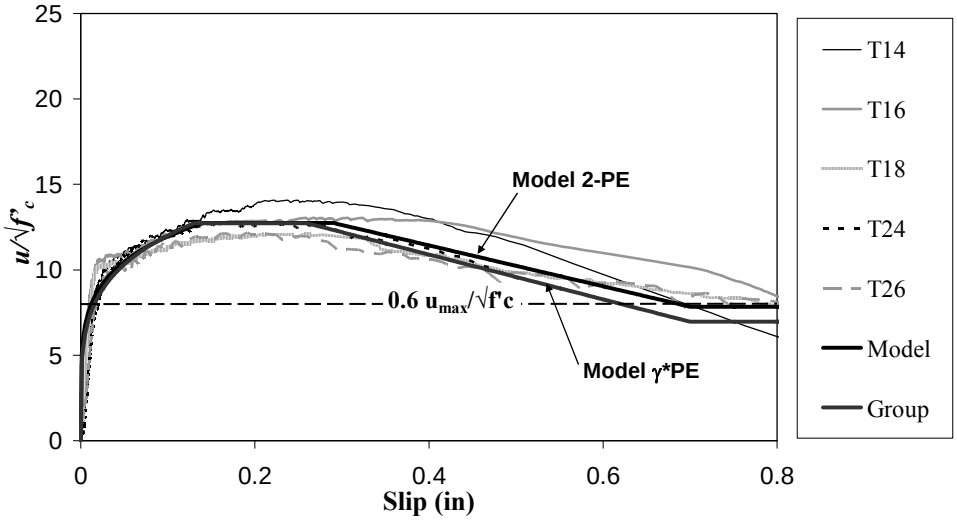

Figure 6.47 Comparison of Idealized Curves with Group Effect Modification Factor for Two Connectors in Polyethylene Ducts

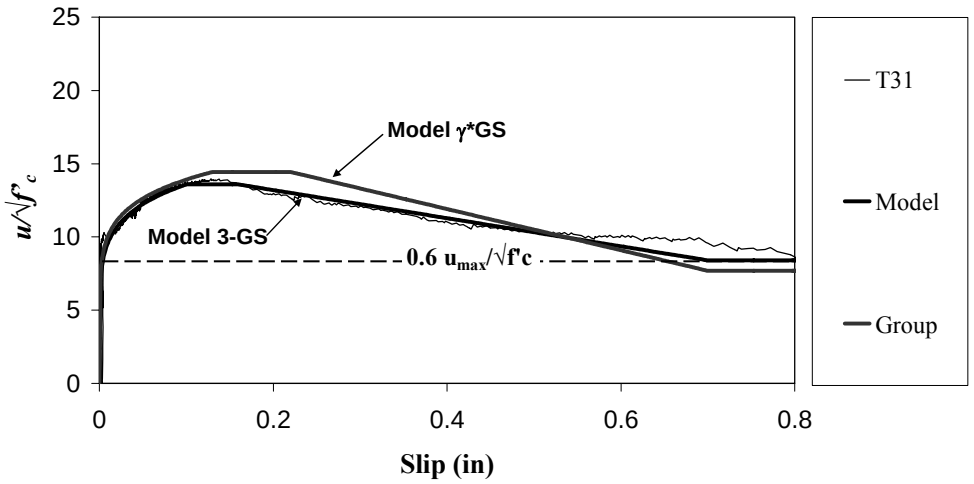

Figure 6.48 Comparison of Idealized Curves with Group Effect Modification Factor for Three Connectors in Galvanized Steel Ducts

CHAPTER 7
Design Recommendations

7.1 INTRODUCTION

The evaluation of test results in Chapter 6 made possible the identification of the test parameters that most influence the behavior of grouted vertical duct connections. In this chapter, connector anchorage design provisions are developed based on experimental results.

Generally, the dead load component dominates the design of bridge substructures. Design moments in the cap-to-column connections for typical multiple-column bents are usually small, and compression or low levels of tension are expected in the connectors. However, design moments may be large in cap-to-column connections of bents that do not have a symmetric configuration or that are formed by single columns. Tensile stresses may be induced in connectors during the construction stages of a bridge when dead loads are unbalanced, or when wind loads act on a tall-bent structure.

The stress in the connectors at service load levels is considered in the proposed design provisions. The connectors used in typical bent configurations generally experience compression or low levels of tension. Even at factored load levels, these connectors are not expected to yield in tension in most bent caps. Design provisions based on developing the yield strength of the connectors are therefore not appropriate for typical design situations. Design equations are instead based on a limiting serviceability stress related to the formation of widespread splitting cracks in the concrete. Nonetheless, significant tensile stresses may be induced in the connectors for certain bent configurations. For

these situations, design equations that ensure the yield strength of the connectors can be developed are also provided.

7.2 ANCHORAGE DESIGN PROVISIONS

Design provisions are developed for connectors that experience: (1) compression and low tension, and (2) significant tension. If the connector service load stress, $f_{service}$, is higher than $0.25f_y$, the connector is considered to experience significant tension. For these cases, the design procedure ensures that the connector can develop the yield strength. If connectors experience compression or low levels of tension ($f_{service} \leq 0.25f_y$), the design procedure is based on serviceability stress limits that correspond to the occurrence of widespread splitting in the concrete.

The limiting service load stress of $0.25f_y$ is intended to represent common design situations where the amount of reinforcement provided in the cap-to-column connection is dictated by minimum area of steel requirements, and not by the need to resist loads. For reinforcing steel with specified yield strength of 60 ksi, $0.25f_y$ equates to a stress of 15 ksi. In standard bridge design practice, service load stresses in the reinforcing bars are usually kept below 24 ksi ($0.40f_y$ for Grade 60 steel) to avoid cracking in members. A stress value of $0.25f_y$ is deemed a good intermediate value to distinguish design cases where the tension developed in the connectors can become a concern to the designer.

As was discussed in Chapter 5, slip of the connectors and bond degradation were directly related to the occurrence of widespread splitting in the concrete. As a result, the limiting stress in the connector that is used in the development of the design provisions corresponds to the formation of widespread splitting cracks, and not first cracking.

Table 7.1 shows values of connector stress at which widespread splitting occurred in the connection specimens. The definition of widespread splitting, as described throughout this dissertation, corresponds to the formation of a full complement of radial cracks around the connectors emanating from the surfaces of the ducts, as shown in Figure 5.5. Cracking patterns rather than crack widths were used to designate the occurrence of widespread splitting during the tests. Widespread splitting generally occurred at a higher stress relative to that corresponding to the formation of the first splitting crack in the specimens.

Figures 7.1 through 7.3 show the ratios of the stress in the connector at first splitting, f_{split}, the stress in the connector at widespread splitting, f_{ws}, and the stress in the connector at maximum stress, f_{max}, to the nominal yield strength of the connector (f_y of 60 ksi). The values of the stress ratios shown in the figures in some cases are an average for a group of tests. Experimental connector stress values are normalized to a concrete compressive strength of 5100 psi. Data in the figures are grouped by number of connectors (shown in parenthesis) present in the connection specimens. Stress ratios are shown for the three different duct materials.

The connector stress data shown in Figure 7.1 correspond to connection specimens involving galvanized steel ducts. Widespread splitting occurred at lower stresses for tests with shallow connector embedment depths and for tests involving multiple connectors. The relative increase in stress from f_{ws} to f_{max} depended on the length of embedment. In general, first splitting occurred in single-connector tests at stresses higher than $0.6f_y$. For the specimen involving three connectors, the ratios of f_{split} to f_y and f_{ws} to f_y were 0.32 and 0.70, respectively.

Figure 7.2 shows the connector stress data that correspond to connection specimens involving polyethylene ducts. Splitting occurred at lower stresses in

tests with shallow connector embedment depths and in tests that involved multiple connectors. In general, splitting cracks began to develop in single-connector test specimens at stresses higher than $0.45f_y$. Widespread splitting typically occurred at stresses higher than $0.6\,f_y$, for both single and multiple-connector specimens.

The connector stress data shown in Figure 7.3 correspond to connection specimens involving polypropylene ducts. Splitting occurred in the triple-connector test at a lower stress than it occurred in the double-connector test. Splitting cracks began to develop in single-connector test specimens at stresses higher than $0.45f_y$. In general, widespread splitting occurred at stresses higher than $0.6\,f_y$. For the specimen involving three connectors, the ratios of f_{split} to f_y and f_{ws} to f_y were 0.28 and 0.65, respectively.

Bar and plug pullout modes of failure should be prevented by incorporating adequate levels of safety in the development of the design recommendations. This can be done by selecting appropriate bond strength limits and capacity reduction factors.

7.2.1 Design Provisions for Connectors Experiencing Compression or Low Tension

Design bond strengths for connectors that experience compression or low levels of tension are based on the stress level at which widespread splitting occurred in the concrete during the connection tests. Figure 7.4 shows the stress in the connectors at the time of widespread splitting in the concrete as a function of duct material. Values of stress at widespread splitting for each of the tests were normalized with respect to the experimental concrete strengths in order to filter out differences in material strength. In general, widespread splitting occurred at higher stresses in specimens containing galvanized steel duct; this is attributed to the ability of the ducts to restrain splitting in the grout, which leads to slip of the

connector. Figures 7.5 through 7.7 show that there is a clear relationship between the stress in the connector when widespread splitting occurs in the concrete and the embedment depth of the connectors. Data for polyethylene and polypropylene duct specimens almost overlap each other. The trend lines shown in Figures 7.5 through 7.7 can be combined into a single relationship that takes into account the effects of number of connectors and duct material. The relationship that is developed to relate stress in the connector when widespread splitting occurs and embedment depth is:

$$\frac{f_{ws}}{\sqrt{f'_c}} = \gamma\left(60\frac{l_e}{d_b} + K\right) \tag{7-1}$$

where f_{ws} is the stress in the connector when widespread splitting occurs in the concrete (psi), f'_c is the specified compressive strength of the concrete (psi), γ is the group effect modification factor (shown in Equation 6-5), l_e is the embedment depth (in.), d_b is the bar diameter (in.), and K is the duct material modification factor. The value of K is taken as 190 for galvanized steel, and 60 for polyethylene and polypropylene ducts. One single value of K is assigned to both types of plastic duct for simplification reasons, and because differences in the data analyzed in its derivation are small and do not justify the use of two separate values.

To evaluate the accuracy of Equation 7-1 as it relates the stress in the connector at the onset of widespread splitting and the connector embedment depth, connector stresses are converted into average bond stresses by substituting f_s in Equation 6-1 by f_{ws}:

$$\frac{u_{ws}}{\sqrt{f'_c}} = \frac{\gamma\left(60\frac{l_e}{d_b} + K\right)\left(\frac{\pi d_b^{\,2}}{4}\right)}{\pi l_e d_b}$$

$$\frac{u_{ws}}{\sqrt{f'_c}} = \gamma\left(60\frac{l_e}{d_b} + K\right)\left(\frac{d_b}{4l_e}\right)$$

$$\frac{u_{ws}}{\sqrt{f'_c}} = \gamma\left(15 + 0.25\frac{d_b}{l_e}K\right) \qquad (7\text{-}2)$$

Table 7.2 shows values of $u_{ws}/\sqrt{f'_c}$ obtained using equation 7-2 for a series of connection configurations involving different duct materials, number of connectors, and embedment depths. There is very good agreement between calculated values and those obtained experimentally. Calculated values corresponding to the three-connector test containing steel ducts and the two-connector test involving polyethylene ducts with two duct-diameter clear spacing show some disagreement with the experimental values. These test categories consist of only one data point each.

The required embedment length for connectors that experience compression or low tension is calculated using the relationship shown in Equation 7-1. The limiting stress $0.25f_y$ is substituted for f_{ws}. A capacity reduction factor, ϕ, taken equal to 0.75 is included to account for deviations in material properties and uncertainties in the calculations involved. A connector eccentricity modification factor, ξ, taken equal to 0.8 is also included to account for reduction in capacity due to eccentric placement of the connectors in the ducts. The eccentricity modification factor is assigned a value of 0.8 because this was the approximate reduction in capacity that was measured in the three single-connector tests that

explored this parameter. The design embedment length l_d is substituted for the embedment length l_e. Solving Equation 7-1 for l_d provides the required embedment length equation for design:

$$\frac{0.25 f_y}{\sqrt{f'_c}} = \phi \xi \gamma \left(60 \frac{l_d}{d_b} + K \right)$$

$$l_d = \frac{\left(\frac{0.42 f_y}{\gamma \sqrt{f'_c}} - K \right)}{60} d_b . \qquad (7\text{-}3)$$

where l_d is given in inches, the group effect modification factor, γ, is calculated using Equation 6-5, values of K are the same as those described previously in the development of Equation 7-1, f_y (the specified yield strength of the connector) and f'_c (specified compressive strength of the concrete) are in psi, and the connector diameter, d_b, is in inches. The value of the group effect modification factor can be taken equal to 1.0 for connectors that are expected to experience no tension.

For connections that involve galvanized steel ducts, Equation 7-3 is used to calculate the required embedment length of connectors that experience compression or low tension levels. However, if plastic are going to be used in the connection, an additional design check must be made to prevent a plug pullout failure.

The average plug bond strength, u_{plug}, is calculated as follows:

$$u_{plug} = \frac{f_s A_b}{\pi D l_e} \qquad (7\text{-}4)$$

where f_s is the applied stress in the connector (psi), A_b is the area of the bar (in.^{2}), $(\pi*D)$ is the duct perimeter (in.), and l_e the connector embedment depth (in.).

Figure 7.8 shows the relationship between plug bond strength, normalized with respect to grout strength, and embedment depth for specimens containing polypropylene and polyethylene ducts that failed by plug pullout. The tensile strength of the grout is considered to be an important parameter when establishing the plug bond strength of a connector because plug pullout failures sometimes occurred before the onset of widespread splitting. There is some variation in plug strength as embedment depth increases, particularly in single-connector tests. The strengths of specimens with two connectors anchored in polyethylene ducts appear to be independent of the embedment depth. Average values of plug bond strength for the connection specimens included in Figure 7.8 are shown in Table 7.3. Based on single and multiple-connector test data, a single limiting value of $u_{plug}/\sqrt{f_g}$ equal to 4.0 is chosen as a lower bound for both polyethylene and polypropylene duct specimens in the development of design provisions to safeguard against this type of failure.

To develop a plug pullout design equation, Equation 7-4 is expressed in terms of normalized plug bond strength. The stress f_s is substituted by the limiting serviceability stress of $0.25f_y$. A capacity reduction factor, ϕ_{plug}, taken equal to 0.6 is included to account for deviations in material properties and uncertainties in the calculations involved. A capacity reduction factor of 0.6 was chosen instead of the larger factor of 0.75 used in the development of Equation 7-3 because there is a higher degree of uncertainty regarding the plug pullout mode of failure, and because the variability of the compressive strength of the grout can be higher than that of the concrete. Although only one type of grout was used in the tests, several proprietary grouts are available that meet the TxDOT grout performance standards. Some variability is expected between different proprietary brands of

grout, and use of the smaller capacity reduction factor of 0.6 is justified until further tests are conducted to assess the strength of different grouts. The required embedment length to preclude plug pullout of connectors, $l_{d,\,plug}$ is obtained:

$$\phi_{plug}\left(\frac{u_{plug}}{\sqrt{f_g}}\right)_{design} = \frac{0.25 f_y \left(\frac{\pi d_b^{\,2}}{4}\right)}{\pi D l_{d,plug}\sqrt{f_g}}$$

$$\phi_{plug}\left(\frac{u_{plug}}{\sqrt{f_g}}\right)_{design} = \frac{f_y\, d_b}{16\, l_{d,plug}\sqrt{f_g}}\left(\frac{d_b}{D}\right)$$

$$l_{d,plug} = \frac{f_y\, d_b}{9.6\left(\frac{u_{plug}}{\sqrt{f_g}}\right)_{design}\sqrt{f_g}}\left(\frac{d_b}{D}\right)$$

$$l_{d,plug} = \frac{0.026 f_y\, d_b}{\sqrt{f_g}}\left(\frac{d_b}{D}\right) \qquad (7\text{-}5)$$

where $l_{d,\,plug}$ is given in inches, f_y (the specified yield strength of the connector) and f_g (specified compressive strength of the grout) are in psi, the connector diameter, d_b, and the nominal duct diameter, D, are in inches.

The plug bond pullout strength is not modified to account for group effects because the limiting plug strength value of 4.0 was selected considering single and multiple connector tests. A connector eccentricity modification factor is not included because there is no information that indicates that eccentric placement of the connector inside the duct affects the plug bond strength.

The larger of the embedment length values calculated using Equations 7-3 and 7-5 is the design embedment length required for connectors anchored in polyethylene or polypropylene ducts that are expected to experience compression or low tension levels.

Table 7.4 shows embedment length requirements for single connectors (γ=1.0) that experience compression or low tension levels. Data are shown for #11 reinforcing bars placed inside galvanized steel (GS), and plastic ducts. Values are obtained using Equations 7-3 and 7-5. Embedment length values are calculated for a range of concrete and grout compressive strengths. In the calculation of the plug pullout design embedment length, $l_{d,\ plug}$, a nominal duct diameter of 4 in. is used corresponding to an ideal combination of duct and connector diameters (see Table 3.2). The specified yield strength of the connectors, f_y, is taken as 60,000 psi in all calculations.

The values of required embedment length shown in Table 7.4 are very small. For the cases shown, required lengths are smaller than 12 inches. Design embedment lengths should be greater than 12 in. or $8d_b$ because no test data are available to support the use of a shorter embedment. The following simplified expressions are suggested for use in design to calculate the design embedment length of connectors subjected to compression or low levels of tension:

galvanized steel duct connections,

$$l_d = \frac{4\,d_b}{\gamma} \geq \{8\,d_b \ or\ 12\ in.\} \tag{7-6}$$

plastic (PE and PP) duct connections,

$$l_d = \frac{6\,d_b}{\gamma} \geq \{8\,d_b \ or\ 12\ in.\} \tag{7-7}$$

For the case of connectors not expected to experience tension under service loads (γ=1.0), Equations 7-6 and 7-7 reduce to the same design provision requiring a minimum connector embedment of $8d_b$ or 12 inches. The simplified equations consider lower bound values of concrete and grout compressive strength (f'_c = 3600 psi and f_g = 5800 psi). As shown in Table 7.4, the embedment length required to preclude plug pullout of connectors in both polyethylene and polypropylene duct connections is approximately $8d_b$. The provision for a minimum embedment of $8d_b$ automatically guards against this type of failure.

7.2.2 Design Provisions for Connectors Experiencing Significant Tension

When the service load stress in connectors, $f_{service}$, is higher than $0.25f_y$, the connector is considered to experience significant tension. For these cases, the design procedure ensures that the connector can develop the yield strength. The normalized average peak bond strength values for single-connector specimens shown in Table 7.5 are used to develop design provisions for connectors that experience significant tension.

Table 7.6 shows a comparison between the normalized average bond strengths of Table 7.5 modified by the group effect factor and experimentally obtained values. Agreement is fair between modified and experimental values for specimens with steel and polyethylene ducts. It is believed that the shallow embedment provided to the single connectors anchored in polypropylene ducts ($8d_b$ and $12d_b$) led to a plug pullout failure mode with a reduced capacity, thus bond strengths may not be considered to be representative of a connector pullout (from the grout) failure mode. Because design bond strength values are based on single connector bond strengths, values corresponding to multiple connectors are much lower than the experimental.

With respect to the two types of plastic duct, there is not enough data to determine if it is the type of plastic or the rib geometry that is governing the response. The selection of two design bond strength values is not justified due to paucity in the data. A single value of $(u_{max}/\sqrt{f'_c})$ equal to 18.0 (which corresponds to polyethylene duct specimens) is deemed appropriate for use in the development of the anchorage design provisions for plastic ducts. The $(u_{max}/\sqrt{f'_c})$ value of 16.2 that was measured in single-connector polypropylene duct specimens appears to be too low when compared with measured values for multiple-connector tests using the same type of duct, and was thus disregarded as the appropriate lower bound.

The equation for obtaining the required development length for connectors that experience significant tension is based on Equation 6-1. In the development of the design equation, the bond stress, u, is normalized with respect to the square root of the compressive strength of the concrete. The stress in the connector f_s is substituted by f_y. A factor of 1.25 multiplies f_y to account for actual yield strengths of reinforcing steel (connectors) larger than 60 ksi. The design bond strength is based on the normalized average peak bond strength, u_{max}. A capacity reduction factor, ϕ, taken equal to 0.75 is included to account for deviations in material properties and uncertainties in the calculations involved. A connector eccentricity modification factor, ξ, taken equal to 0.8 is also included to account for reduction in capacity due to eccentric placement of the connectors in the ducts.

$$\left(\frac{u}{\sqrt{f'_c}}\right)_{design} = \frac{1.25 f_y d_b}{4 l_e \sqrt{f'_c}} \tag{7-8}$$

where:

$$\left(\frac{u}{\sqrt{f'_c}}\right)_{design} = \phi \xi \gamma \left(\frac{u_{\max}}{\sqrt{f'_c}}\right) \tag{7-9}$$

Combining Equations 7-8 and 7-9 and substituting l_d for l_e leads to:

$$\phi \xi \gamma \left(\frac{u_{\max}}{\sqrt{f'_c}} \right) = \frac{1.25 f_y d_b}{4 l_d \sqrt{f'_c}}$$

$$l_d = \frac{f_y d_b}{1.9 \left(\frac{u_{\max}}{\sqrt{f'_c}} \right) \gamma \sqrt{f'_c}}$$

(7-10)

where l_d is given in inches, f_y (specified yield strength of the connector) and f'_c (specified compressive strength of the concrete) are in psi, the group effect modification factor is calculated using Equation 6-5, d_b is in inches, and design values of $(u_{max}/\sqrt{f'_c})$ are 23.9 for galvanized steel ducts and 18.0 for plastic ducts.

Entering the design bond strength described above into Equation 7-10 yields two equations for determining the required development length:

galvanized steel duct connections, $$l_d = \frac{0.022 f_y d_b}{\gamma \sqrt{f'_c}} \quad (7\text{-}11)$$

plastic duct connections, $$l_d = \frac{0.029 f_y d_b}{\gamma \sqrt{f'_c}} \quad (7\text{-}12)$$

Equation 7-11 is used to calculate the development length required for connectors that experience significant tension and are housed inside galvanized steel ducts. If plastic ducts are going to be used, consideration of the pullout

strength of the grout plug inside polyethylene and polypropylene ducts is required.

The plug pullout design equation for connectors expected to experience significant tension is developed following the same procedure used to develop Equation 7-5 in Section 7.2.1. The stress $1.25f_y$, instead of $0.25f_y$, is substituted for f_s. The factor of 1.25 that multiplies f_y accounts for actual yield strengths of reinforcing steel larger than 60 ksi. A capacity reduction factor, ϕ_{plug}, taken equal to 0.6 is also included to account for deviations in material properties and uncertainties in the calculations involved. The required development length to preclude pullout of the grout plug, $l_{d,\,plug}$ is obtained:

$$\phi_{plug}\left(\frac{u_{plug}}{\sqrt{f_g}}\right)_{design} = \frac{1.25 f_y \left(\frac{\pi d_b^{\,2}}{4}\right)}{\pi D\, l_{d,plug}\sqrt{f_g}}$$

$$\phi_{plug}\left(\frac{u_{plug}}{\sqrt{f_g}}\right)_{design} = \frac{0.31 f_y\, d_b}{l_{d,plug}\sqrt{f_g}}\left(\frac{d_b}{D}\right)$$

$$l_{d,plug} = \frac{0.52 f_y\, d_b}{\left(\frac{u_{plug}}{\sqrt{f_g}}\right)_{design}\sqrt{f_g}}\left(\frac{d_b}{D}\right)$$

$$l_{d,plug} = \frac{0.13 f_y\, d_b}{\sqrt{f_g}}\left(\frac{d_b}{D}\right) \tag{7-13}$$

where $l_{d,\ plug}$ is given in inches, f_y (the specified yield strength of the connector) and f_g (specified compressive strength of the grout) are in psi, the connector diameter, d_b, and the nominal duct diameter, D, are in inches. The same limiting design value of $u_{plug}/\sqrt{f_g}$ of 4.0 used in the development of the design equations for connectors that experience compression or low tension is used.

The pullout strength of the grout plug is not modified to account for group effects because the limiting strength value was selected considering single and multiple connector tests. There is no information that indicates eccentric placement of the connector inside the duct affects the plug bond strength.

The larger of the development length values calculated by Equations 7-12 and Equations 7-13 is the required design development length for connectors anchored inside plastic ducts.

Table 7.7 shows development length requirements for single connectors (γ=1.0) that experience significant tension. Data are shown for #11 reinforcing bars placed inside galvanized steel and plastic (PE and PP) ducts. Values are obtained using Equations 7-11 through 7-13. Development length values are calculated for a range of concrete and grout strengths. In the calculation of the plug pullout development length, $l_{d,\ plug}$, a nominal duct diameter of 4 in. was used corresponding to an ideal combination of duct and connector diameters (see Table 3.2). The specified yield strength of the connectors, f_y, is taken as 60,000 psi in all calculations.

The following simplified expression is suggested for use in design to calculate the design embedment length of connectors subjected to significant tension:

$$l_d = \frac{0.022\,\Omega\, f_y\, d_b}{\gamma\sqrt{f'_c}} \tag{7-14}$$

The duct material modification factor, Ω, is taken as 1.0 for galvanized steel, and 1.3 for plastic (PE and PP) ducts. For design purposes, plug pullout failure is precluded by providing a minimum embedment length for connectors anchored in plastic ducts. Assuming a grout compressive strength of 5800 psi and using Equation 7-13, a minimum embedment length of $36d_b$ is required for connectors anchored in both polyethylene and polypropylene ducts.

7.3 COMPARISON OF ANCHORAGE DESIGN PROVISIONS WITH EXPERIMENTAL DATA

The embedment length requirements calculated using the design provisions of Section 7.2 are compared with experimental data to estimate the factor of safety built into the design equations.

7.3.1 Connectors Experiencing Compression or Low Tension

Design provisions developed for connectors subjected to compression or low tension levels are compared below with test results of single and multiple connectors. Factors of safety embedded in the design provisions are estimated by comparing stress levels in the connectors at the onset of widespread splitting in the concrete.

The connector in Test No. 1 represents single connectors anchored in galvanized steel ducts. The stress in the connector of at the onset of widespread splitting was 48 ksi (Table 7.1). This measured stress value is substantially higher than the serviceability stress of 15 ksi (48 ksi/15 ksi ≈ 3.2) set in the development of Equation 7-8. Although no multiple connector tests were conducted at the shallow embedment depth of $8d_b$, the stress in connectors at the occurrence of widespread splitting for a three connector configuration can be estimated by extrapolation, using Equation 7-1. Assuming a value of γ equal to 0.6 (configuration corresponding to Tests No. 31 and 32), a value of K equal to 190,

and a value of f'_c equal to 5100 psi, one obtains a corresponding stress in the connector at the onset of widespread splitting equal to 29 ksi. This value of 29 ksi divided by the serviceability stress of 15 ksi embedded in the design provisions yields a factor of safety of approximately 1.9.

With regards to plastic ducts (both polyethylene and polypropylene), the stresses in the single connectors of Tests No. 5 and No. 29 at the onset of widespread splitting were 41 ksi and 39 ksi, respectively. These measured stress values are again substantially higher than the serviceability stress of 15 ksi embedded in the design provisions. No multiple-connector tests involving plastic ducts were conducted at the shallow embedment depth of $8d_b$. Using Equation 7-1 with the same parameters used for galvanized steel ducts (but K taken equal to 60), one obtains a corresponding (extrapolated) stress in the connector at the occurrence of widespread splitting equal to 28 ksi for a three connector configuration. Note that the value of l_e/d_b entered in Equation 7-1 is 10 rather than 8, because the value of the group modification factor of 0.6 increases the required embedment length calculated using Equation 7-9 from $8d_b$ to $10d_b$. The extrapolated value of 28 ksi divided by the serviceability stress of 15 ksi set in the design provisions yields also a factor of safety of approximately 1.9.

7.3.2 Connectors Experiencing Significant Tension

Anchorage design provisions for connectors expected to experience significant tension are compared below with test results of single and multiple connectors. The factor of safety embedded in the design provisions is estimated by comparing design development lengths with experimental embedment depths that corresponded to observed yielding in the connectors.

The smallest design development lengths calculated using the provisions of Section 7.3.1 for connectors anchored in both galvanized steel ducts and plastic

ducts are $22d_b$ and $36d_b$, respectively. Direct comparison of design provisions with experimental data is not possible because the longest embedment depth that was explored in the test program was only $16d_b$. However, the test results provide valuable information about the embedment depth required for a given connection (having a specific configuration: duct material and number of connectors) to achieve the yield load.

Based on the observed capacities of Test No.1 (58 ksi), which involved a connector embedded $8d_b$, and Tests No. 3 (87 ksi) and No. 10 (80 ksi), which had connectors with an embedment of $12d_b$, it can be concluded that a single connector anchored in a galvanized steel duct is able to reach its yield stress at an embedment equal to or larger than $9d_b$. The design development length calculated using Equation 7-14, with a value of f'_c (specified value of concrete compressive strength) equal to 3600 psi and a value of γ equal to 1, is approximately $22d_b$. This means that the factor of safety for a single connector anchored in a steel duct experiencing significant tension is approximately 2.4 ($22d_b$ divided by $9d_b$).

Similarly, the factor of safety can be estimated for the case of two connectors anchored in steel ducts. Based on the capacities of Test No. 17 (59 ksi), which involved two connectors embedded $12d_b$, and Tests No. 13 (87 ksi) and No. 15 (86 ksi), which involved connectors embedded $16d_b$, it can be estimated that a connection consisting of two connectors with a duct clear spacing equal to one duct diameter is able to reach its yield load at an embedment equal to or larger than $13d_b$. The design development length calculated using Equation 7-14, with a value of f'_c (specified value of concrete compressive strength) equal to 3600 psi and a value of γ equal to 0.68, is approximately $33d_b$. The corresponding factor of safety for such a connection configuration is approximately 2.5 ($33d_b$ divided by $13d_b$).

The design provisions applicable to plastic duct connections are compared with experimental data using the same methodology just presented for steel ducts. Based on single-connector tests, it is estimated that single connectors anchored in the polyethylene ducts (plastic duct with large rib spacing) are able to reach their yield load when provided an embedment equal to or larger than $14d_b$. For polypropylene duct (plastic duct with small rib spacing) connections, an embedment depth equal to or larger than $11d_b$ is considered necessary for the connectors to develop yield. Corresponding factors of safety for single connectors are approximately 2.6 ($36d_b$ /$14d_b$) and 3.3 ($36d_b$ /$11d_b$) for polyethylene and polypropylene ducts, respectively.

Based on the capacities of Test No. 18 (44 ksi), which involved two connectors embedded $12d_b$, and Tests No. 14 (64 ksi) and No. 16 (59 ksi), which involved connectors embedded $16d_b$, it can be estimated that a connection consisting of two connectors anchored in polyethylene ducts and with a duct clear spacing equal to one duct diameter is able to reach its yield load when connectors are embedded a length equal to or larger than $16d_b$. The design development length calculated using Equation 7-14, with a value of f'_c (specified value of concrete compressive strength) equal to 3600 psi and a value of γ equal to 0.68, is approximately $42d_b$. The corresponding factor of safety for such a connection configuration is approximately 2.6 ($42d_b$ divided by $16d_b$). A higher safety factor is obtained for connections that use polypropylene duct.

Equation 7-14 includes a modification factor equal to 1.25 (1/0.8) to account for bar eccentricity. Only three of the 32 connections tested involved connectors placed eccentrically inside ducts. The estimated safety factors that are set in the design provisions were obtained through comparisons with experimental data assuming that connectors were placed eccentrically inside the duct. Actual safety factors incorporated into the design equation are actually smaller than those

reported in the previous paragraphs because most connectors were placed concentrically inside the ducts during the tests. This means that a safety factor of 2.6 obtained in the comparisons is in fairness equal to 2.1 (2.6/1.25) if the bar eccentricity modification factor is not included in the comparison. This is true whenever Equation 7-19 governs rather than minimum embedment required for precluding a plug pullout failure.

7.4 CONNECTION DESIGN

Connectors that are expected to experience tension under service loads are identified by performing a sectional analysis of the connection zone. These connectors are then used to calculate the projected failure surface of the connector group, A_N, used in the calculation of the group effect modification factor, γ. The connector that experiences the highest load (based on the analysis) controls the design of the connection group. If sectional analysis of a particular connection indicates that the connectors are not expected to experience tension, then the group modification factor, γ, is taken equal to 1.0.

The design embedment depth of connectors can be established by using the anchorage design provisions developed in Section 7.2. Regardless of which connectors are considered to be in tension for the calculation of the group effect modification factor, all connectors, if possible, should be provided with the same embedment depth in the final design to prevent mistakes from happening in the field.

7.5 GUIDELINES FOR APPLICATION OF THE ANCHORAGE DESIGN PROVISIONS

Because of limited test data, the specified compressive strength of the concrete, f'_c, used in the design equations should not exceed 6000 psi. Grout materials that do not satisfy the TxDOT Grout Performance Specification

requirements (shown in Table 3.3) should not be used in grouted vertical duct connections.

The design equations that were developed for connections having plastic ducts may apply to connections using similar ducts to those tested. Ducts made of similar plastic materials that have comparable wall thicknesses and corrugation patterns can be used. If geometric properties of the duct, such as wall thickness, spacing between ribs, and height of corrugations, differ significantly from those of the ducts tested, they should not be used in grouted vertical duct connections, unless demonstrated by tests that they can perform adequately. The spacing between ribs (or corrugations) is thought to be the primary feature that affects the performance of the connection.

Design equations are the same for uncoated and epoxy-coated connectors. No reduction in development length is recommended when transverse reinforcement is provided near or around the ducts. Use of spirals around individual ducts is discouraged.

Minimum clear spacing between ducts should be at least 2 in. to permit adequate placement of the concrete around ducts. It is recommended that clear spacing between ducts be kept equal to or greater than one duct diameter. Clear cover to the ducts housing the connectors tested was kept constant at approximately 8.25 inches. No information is available regarding the performance of connectors having smaller side cover. A minimum clear cover to ducts of 6 in. is suggested given the lack of test data available on anchorage of connectors having small concrete side cover. Regardless, a clear cover to ducts smaller than 6 in. is difficult to conceive after allowing for bent cap clear cover to reinforcement, placement of transverse steel, and corner bars in reinforcing steel cages.

Following standard practice in monolithic construction, straight dowels are terminated 6 in. from the top of the bent cap. Similarly, it is recommended that

the embedment length of the connectors be extended a distance of at least ¾ of the cap depth, even in cases where anchorage design provisions may indicate that a much shorter embedment length is acceptable. As long as this provision does not interfere with placement of bent cap reinforcement, it is considered to be a sound recommendation because it takes advantage of the depth of cap available. The minor increase in cost is vastly offset by improvements in structural redundancy and reserve capacity.

7.6 MODEL CODE PROVISIONS

The anchorage design provisions developed for grouted vertical duct connections are summarized in this section and presented in code format for practical use and clear interpretation by designers. Recommendations mainly concentrate on the design approach and the detailing of connections and are not intended to include all aspects of the design of precast bent caps.

1. Scope

1.1 The provisions in this section are applicable to the design of grouted vertical duct connections for precast bent caps. Equations for anchorage of connectors are developed based on experimental data. Practical details for connecting bent caps to columns and piles using grouted vertical duct connections are suggested.

1.2 Design recommendations presented herein are not intended for bent structures of unusual proportions, or bents subjected to seismic loads.

2. Definitions

Bent Cap – A concrete beam of rectangular or inverted-T cross-section that transfers loads from the bridge superstructure to columns or piles.

Bedding Layer – A thin layer of grout that is formed at the interface of the top of the column and the bottom of the bent cap.

Connector – A straight or headed reinforcing bar that is used to join together the bent cap to columns or piles.

Grouted Vertical Duct – Corrugated galvanized steel or plastic duct that is precast in the bent cap to serve later as a sleeve to house a connector, and then filled with grout.

Embedment Length – The length of reinforcement or anchor provided beyond a critical section over which transfer of force between concrete and reinforcement may occur.

Transverse Reinforcement – Reinforcement used to resist shear, torsion, or to confine concrete in a structural member.

3. Notation

A_N = the projected failure surface of a group of connectors (in.^{2}), which is limited by the distance between the connectors and the nearest edge.

A_{No} = the maximum projected failure surface of an individual connector (in.^{2}), defined as a square with sides equal to $15d_b$.

d_b = nominal diameter of the connector (in.)

f'_c = specified compressive strength of the concrete (psi)

$f_{service}$ = tensile stress in the connector at service loads (psi)

f_y = specified yield strength of reinforcing steel (psi)

γ = group effect modification factor

l_d = connector embedment length (in.)

n = number of connectors in the group

Ω = duct material modification factor, taken equal to 1.0 for galvanized steel ducts, and 1.3 for plastic ducts.

4. Material Properties

4.1 Concrete

4.1.1 Concrete used in precast bent caps shall be normal weight concrete with a 28-day compressive strength of at least 3600 psi.

4.1.2 The value of concrete compressive strength used in anchorage design equations shall not exceed 6000 psi, regardless of the specified compressive strength, f'_c.

4.2 Grout

4.2.1 Grout material used in grouted vertical duct connections must satisfy the TxDOT Grout Performance Specification.

4.2.2 No prepackaged grout material shall be used after the expiration date in grouted vertical duct connections.

4.3 Reinforcing Steel and Connectors

4.3.1 Use of both straight and headed connectors is permitted.

4.3.2 Reinforcing steel, also used as connectors, shall conform to ASTM A615 or A706. The specified yield strength for connectors shall be 60 ksi.

4.3.3 Epoxy-coated connectors shall conform to ASTM A775.

4.3.4 Plain bars may be used for transverse reinforcement in the form of spirals around the connector group.

4.4 Ducts

4.4.1 Ducts must be corrugated and shall provide sufficient bond transfer to the surrounding concrete as determined by Section 7.

4.4.2 Corrugated strip steel ducts shall be galvanized and conform to ASTM A653. The minimum wall thickness shall be 0.45 mm (26 gauge) for duct diameters up to 4 in., and at least 0.65 mm (24 gauge) for duct diameters larger than 4.5 inches. Corrugation (rib) height of steel ducts shall be at least 0.12 in.

4.4.3 Use of ducts made of high-density polyethylene and polypropylene is permitted. In lieu of a standard specification, plastic ducts shall comply

with fib technical bulletin 7: "Corrugated Plastic Ducts for Internal Bonded Post-Tensioning," [1] but their use is limited by the following restrictions:

- Minimum wall thickness of plastic ducts shall be 3 mm (0.118 in.).
- Corrugation (rib) height of plastic ducts shall be at least 0.2 in.
- Maximum spacing between ribs (corrugations) shall be 2.5 inches.

5. General Connection Design Approach

5.1 Determination of Connection Actions following AASHTO LRFD Specifications [2].

5.1.1 The forces acting on the connections are determined by frame analysis of the bent, considering the connection at the top of the columns to be capable of resisting moments. The load combination that controls the design consists of the most severe combination of simultaneous transverse and longitudinal actions.

5.2 Selection of Connector Configuration

5.2.1 The trial connector configuration is selected based on spacing and minimum connection reinforcement requirements.

5.2.2 Reinforcement crossing the joint must be at least 0.7% of the gross area of the column, or 1.0% of the gross area of the pile. To provide redundancy, a minimum of four connectors must be provided in columns, whereas a minimum of three connectors must be provided in trestle piles.

5.3 Analysis of Connector Configuration

5.3.1 The selected trial configuration shall be analyzed by evaluating strength and serviceability requirements.

5.3.2 Strength requirements shall include:

- Determination of the connector area of steel required to resist factored axial and flexural loads.
- Estimation of the shear friction at the bedding layer using the AASHTO LRFD Specification [2].

5.3.3 Serviceability checks shall include:

- Determination of potential opening at the bedding layer by estimating the location of the neutral axis.
- Control of concrete cracking in the connection area following the AASHTO LRFD [2, Section 5.7.3.4] provisions.
- Control of bent deflections.

5.3.4 Sectional analysis at the service limit state shall be employed to determine which connectors are expected to experience tension. These connectors are then used to calculate the projected failure surface of the connector group, A_N, used in the calculation of the group effect modification factor, γ. The connector experiencing the highest load controls the design of the connection group. If sectional analysis of a particular connection indicates that connectors are not expected to experience tension, then the group modification factor is taken equal to 1.0. The group modification factor, γ, is obtained:

$$\gamma = \frac{A_N}{nA_{No}} \leq 1.0 \qquad \text{(Eq-1)}$$

5.3.5 Determination of connector embedment

The required embedment length of connectors shall be determined using the provisions of Sections 7.1 and 7.2.

5.4 Selection of Transverse Reinforcement

5.4.1 Transverse reinforcement in the form of spirals can be provided around the connector group through the depth of the cap to control the expansion of splitting cracks in the connection region and prevent deterioration of the joint.

5.4.2 Use of small spirals around individual ducts is discouraged.

6. Detailing of Connections

6.1 The duct diameter shall be selected so that a horizontal clearance of at least 1 in. exists around the periphery of the connector. For connections involving more than six connectors, a minimum horizontal clearance of 1.5 in. should be provided.

6.2 Reinforcing bars used as connectors shall be no smaller than #9 and no larger than #14.

6.3 Minimum clear spacing between ducts shall be at least 2 in. to permit adequate placement of concrete around ducts. It is recommended that clear spacing between ducts be kept equal to or greater than one duct diameter.

6.4 Minimum clear cover to ducts should be 6 inches.

7. Embedment Length of Connectors

7.1 The design embedment length of connectors expected to experience compression or low levels of tension ($f_{service} \leq 0.25 f_y$) shall be calculated using Equations 2 and 3:

galvanized steel duct,

$$l_d = \frac{4 d_b}{\gamma} \geq \{8 d_b \ or \ 12 \ in.\} \qquad \text{(Eq-2)}$$

plastic (PE and PP) duct,

$$l_d = \frac{6 d_b}{\gamma} \geq \{8 d_b \ or \ 12 \ in.\} \qquad \text{(Eq-3)}$$

7.2 The design embedment length of connectors expected to experience significant tension ($f_{service} > 0.25 f_y$) shall be calculated using Eq-4:

$$l_d = \frac{0.022 \, \Omega \, f_y \, d_b}{\gamma \sqrt{f'_c}} \qquad \text{(Eq-4)}$$

For design purposes, plug pullout failure is precluded by providing a minimum embedment length for connectors anchored in plastic ducts. A minimum embedment length of $36d_b$, is required for connectors anchored in plastic ducts.

7.3 Regardless of which connectors are considered to be in tension for the calculation of the group effect modification factor, all connectors, when possible, should be provided with the same embedment length in the final design to prevent installation errors.

7.4 Design equations are the same for uncoated and epoxy-coated connectors.

7.5 No reduction in development length is permitted when transverse reinforcement is provided.

7.6 It is recommended that the embedment length of the connectors be extended a distance of at least ¾ of the cap depth, even for cases where anchorage design provisions may indicate that a much shorter embedment length is acceptable. As long as this provision does not interfere with placement of bent cap reinforcement, it is considered to be a sound recommendation because it takes advantage of the depth of cap available.

8. Durability

8.1 For designs where durability is a primary concern, such as in aggressive environments, the designer has the following options:

- Use of epoxy-coated connectors.
- Use of plastic ducts.
- Terminate the vertical ducts some small distance before reaching the top of the cap.
- Embedding the column (or pile) in the cap.
- Use of an external sealant.

9. References

1. Task Group 9.6 Plastic Ducts of fib Commission 9, "Corrugated Plastic Ducts for Internal Bonded Post-Tensioning," *Bulletin no. 7*, International Federation for Structural Concrete ***fib***, Lausanne, Switzerland, 2000.

2. Association of State Highway and Transportation Officials (AASHTO), *AASHTO LRFD Bridge Design Specifications*, 3rd ed., AASHTO, Washington, D.C., 2004.

Table 7.1 Connector Stress at Occurrence of Widespread Splitting

Test	Bars	Duct	l_e (d_b)	f_g (ksi)	f'_c (ksi)	f_y (ksi)	f_{split} (ksi)	f_{ws} (ksi)	f_{max} (ksi)
1	1-#11	GS	8	5.0	5.4	75	46	48	58
2	1-#11	GS	8	6.1	5.4	68	48	48	55
3	1-#11	GS	12	6.4	5.4	75	47	72	87
4	1-#11	GS	12	6.4	5.4	68	60	76	88
5	1-#11	PE	8	4.7	5.5	75	37	41	48
6	1-#11	PE	8	5.5	5.5	68	30	40	40
7	1-#11	PE	12	5.9	5.5	75	33	58	67
8	1-#11	PE	12	5.8	5.5	68	36	60	65
9	1-#11	PE	12	5.1	4.5	75	42	50	54
10	1-#11	GS	12	5.6	4.5	75	45	57	80
11	1-#11	None	12	5.1	4.6	68	45	56	68
12	1-#11	None	12	5.1	4.6	75	42	55	67
13	2-#11	GS	16	5.2	4.7	75	38	57	87
14	2-#11	PE	16	5.3	4.7	75	42	49	64
15	2-#11	GS	16	5.4	4.7	75	39	54	86
16	2-#11	PE	16	5.4	4.7	75	42	49	59
17	2-#11	GS	12	4.8	5.2	75	33	45	59
18	2-#11	PE	12	4.9	5.3	75	24	37	44
19	1-#11	GS	8	5.1	5.5	59	41	46	49
20	1-#11	PE	8	5.1	5.5	59	31	40	40
21	1-#11	GS	12	5.4	5.5	59	36	61	74
22	1-#11	PE	16	5.4	5.5	76	45	74	90

Table 7.1 Connector Stress at Occurrence of Widespread Splitting

Test	Bars	Duct	l_e (d_b)	f_g (ksi)	f'_c (ksi)	f_y (ksi)	f_{split} (ksi)	f_{ws} (ksi)	f_{max} (ksi)
23	2-#11	GS	12	6.0	6.1	59	48	53	68
24	2-#11	PE	16	6.3	6.1	75	43	52	65
25	1-#11	PE	8	6.5	6.1	75	34	34	34
26	2-#11	PE	16	6.5	6.1	75	39	48	62
27	1-#11	PE	12	6.5	6.1	75	49	54	63
28	2-#11	PP	16	6.8	6.1	59	44	53	85
29	1-#11	PP	8	7.1	6.1	59	39	39	40
30	1-#11	PP	12	7.1	6.1	59	32	60	68
31	3-#11	GS	16	5.8	6.1	59	23	50	73
32	3-#11	PP	16	5.8	6.1	59	20	47	67

Table 7.2 Values of $u_{ws}/\sqrt{f'_c}$ for a Series of Connector Configurations

			$u_{ws}/\sqrt{f'_c}$ (psi)								
			Measured			*Calculated (Equation 7.2)*			$\left(\frac{\text{Calculated}}{\text{Measured}}\right)$		
Number of Connectors	**γ**	**l_e/d_b**	**GS**	**PE**	**PP**	**GS**	**PE**	**PP**	**GS**	**PE**	**PP**
1	1.0	8	20.3	17.2	15.6	20.9	16.9	16.9	1.03	0.98	1.08
		12	19.8	16.2	16.0	18.9	16.2	16.2	0.95	1.0	1.01
		16	-	15.7	-	18.0	15.9	15.9	-	1.01	-
2 (1 D dia)	0.68	12	12.9	10.7	-	12.9	11.1	11.1	1.0	1.04	-
		16	12.6	11.3	10.6	12.2	10.9	10.9	0.97	0.96	1.03
2 (2 D dia)	0.77	12	14.1	-	-	14.6	12.5	12.5	1.04	-	-
		16	-	10.4	-	13.9	12.2	12.2	-	1.17	-
3	0.60	16	10.0	-	9.4	10.8	9.5	9.5	1.08	-	1.01

Table 7.3 Average Plug Bond Strength

Test Category	$u_{plug}/\sqrt{f_g}$
PE	5.72
PP	5.29
2-PE (1 D dia)	4.38
2-PP	5.40
3-PP	4.59

Table 7.4 Embedment Length Required for a Range of Concrete and Grout Compressive Strengths (#11 Bar, Compression or Low Tension, $\gamma = 1.0$)

		l_d (in.) (Equation 7-3)		$l_{d,\,plug}$ (in.) (Equations 7-5)		
		f'_c (psi)		f_g (psi)		
Duct Material	***K***	**3600**	**5000**	**4500**	**5800**	**7000**
GS	190	5.4	3.9	N/A		
Plastic	60	8.5	7.0	11.6	10.2	9.3

Table 7.5 Normalized Average Values of $u_{max}/\sqrt{f'_c}$ for Single-connector Tests

Duct Material	$u_{max}/\sqrt{f'_c}$
Galvanized Steel (GS)	23.9
Polyethylene (PE)	18.0
Polypropylene (PP)	16.2

Table 7.6 Comparison of Values of $u_{max}/\sqrt{f'_c}$ modified by the Group Effect Factor with Experimental Values

		$\gamma^*(u_{max}/\sqrt{f'_c})$ (Design)			$u_{max}/\sqrt{f'_c}$ (Experimental)			$\left(\frac{Design}{Experimental}\right)$		
Number of Connectors	**γ**	**GS**	**PE**	**PP**	**GS**	**PE**	**PP**	**GS**	**PE**	**PP**
1	1.0	23.9	18.0	16.2	23.9	18.0	16.2	1.0	1.0	1.0
2 (1 D dia)	0.68	16.3	12.2	11.1	18.3	13.0	16.2	0.89	0.94	0.69
2 (2 D dia)	0.77	18.4	13.9	12.5	16.7	12.7	-	1.10	1.09	-
3	0.60	14.3	10.8	9.7	14.0	-	12.7	1.02	-	0.76

Table 7.7 Development Length Required for a Range of Concrete and Grout Compressive Strengths (#11 Bar, Significant Tension, $\gamma = 1.0$)

	l_d *(in.)* *(Equations 7-11 through 7-12)*		$l_{d,\,plug}$ *(in.)* *(Equation 7-13)*		
	f'_c *(psi)*		f_g *(psi)*		
Duct Material	**3600**	**5000**	**4500**	**5800**	**7000**
GS	31	27	N/A		
Plastic	41	35	58	51	47

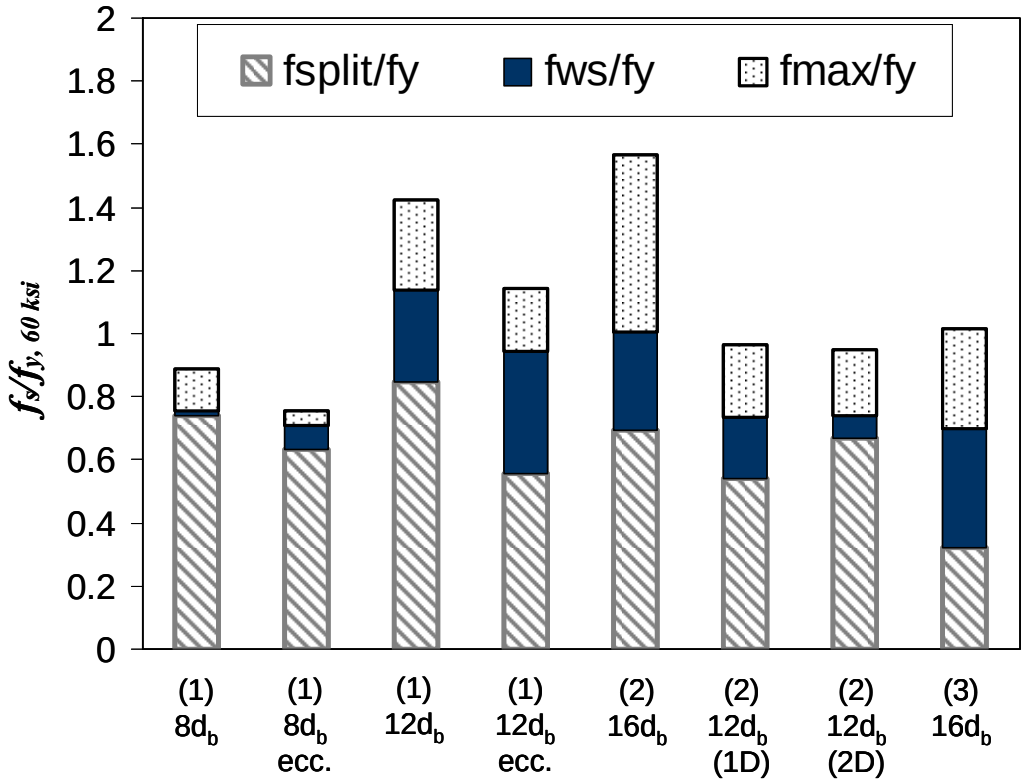

Figure 7.1 Connector Stress Ratios for Galvanized Steel Duct Specimens

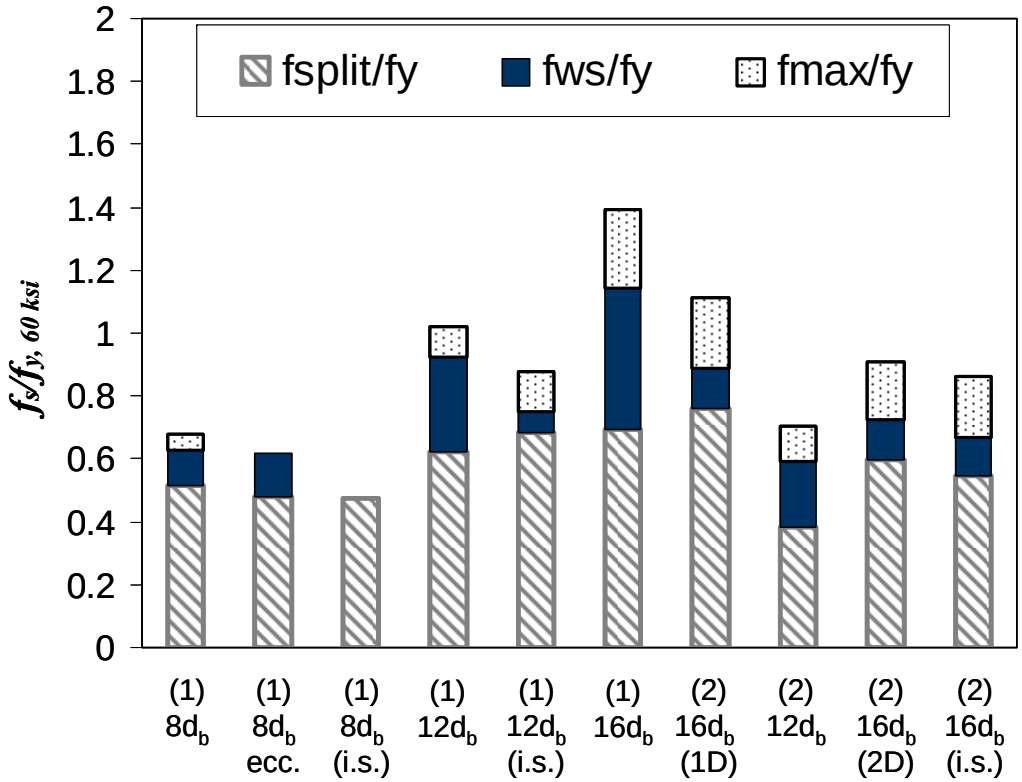

Figure 7.2 Connector Stress Ratios for Polyethylene Duct Specimens

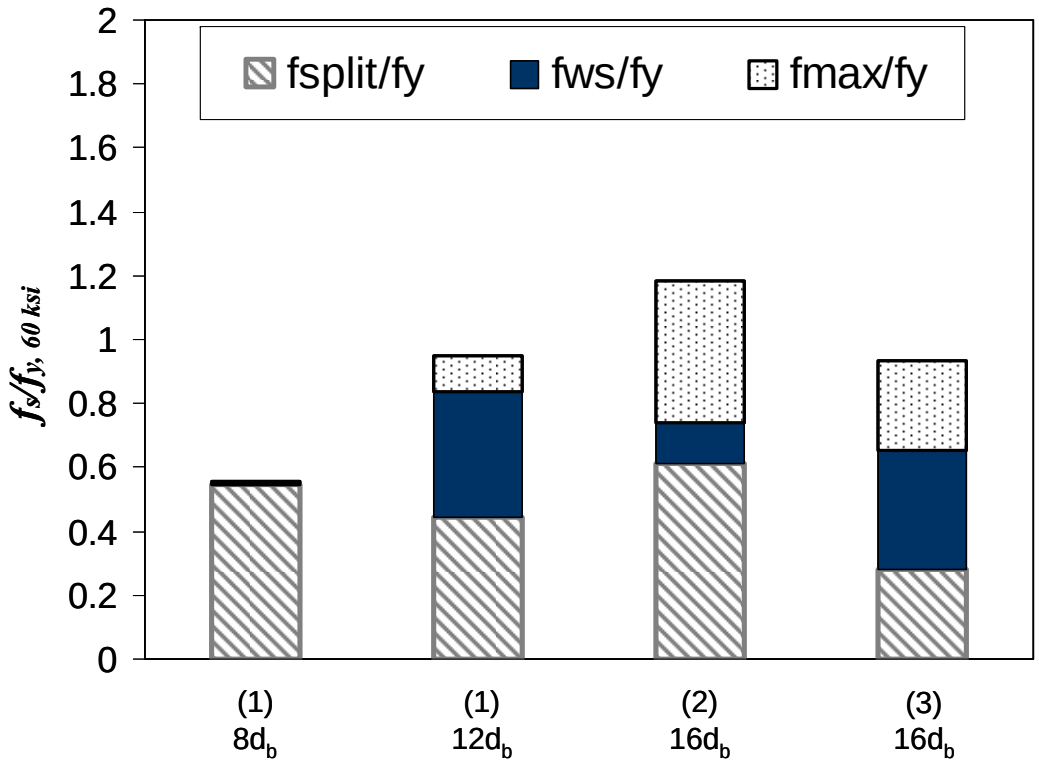

Figure 7.3 Connector Stress Ratios for Polypropylene Duct Specimens

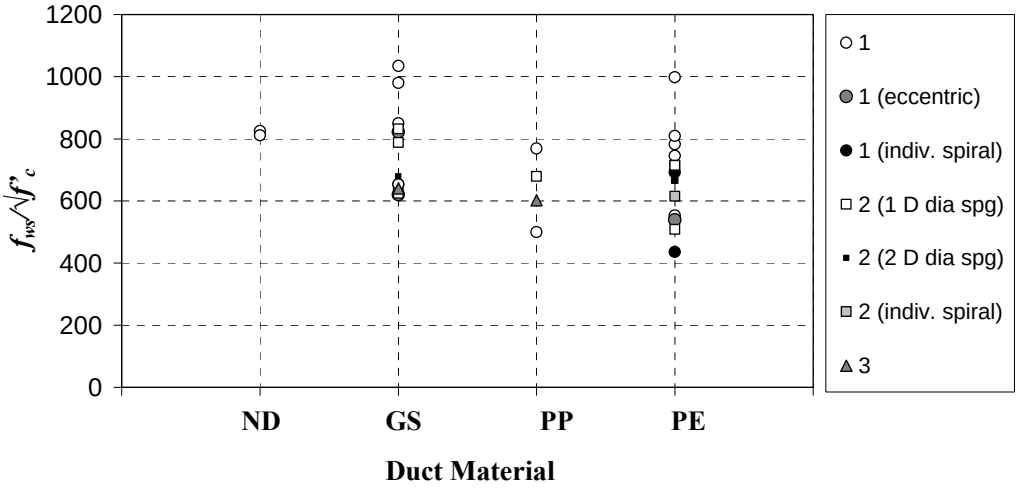

Figure 7.4 Influence of Duct Material on Connector Stress at Widespread Splitting in the Concrete

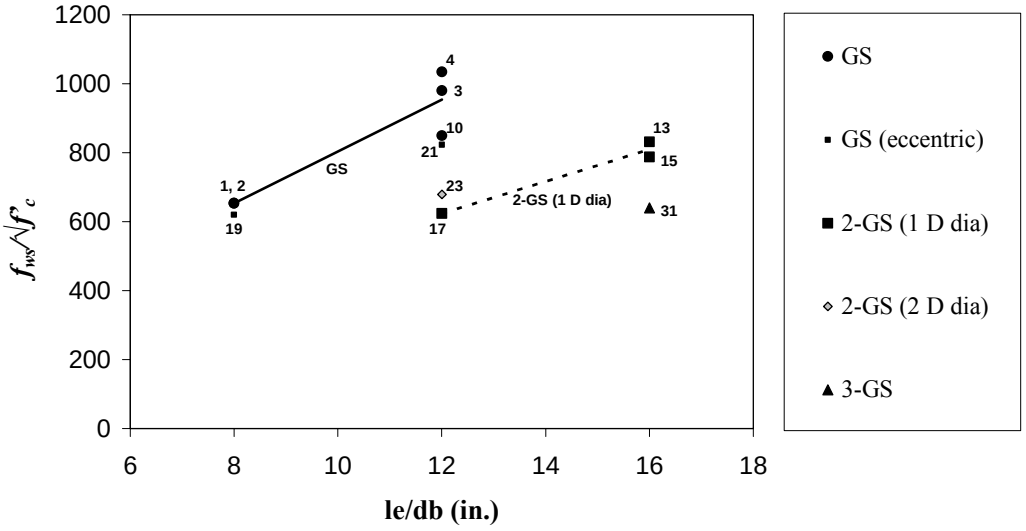

Figure 7.5 Influence of Embedment Depth on Connector Stress at Widespread Splitting in the Concrete (Galvanized Steel Ducts)

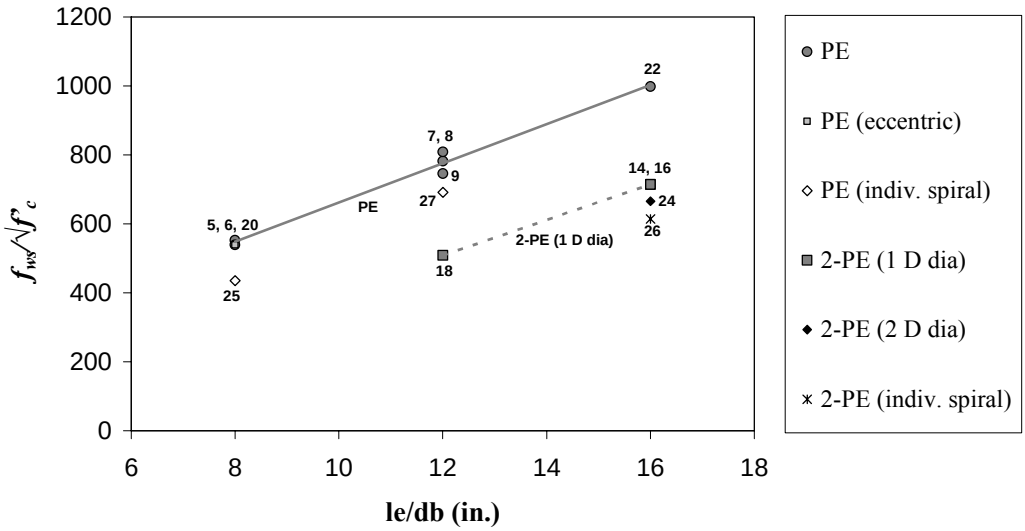

Figure 7.6 Influence of Embedment Depth on Connector Stress at Widespread Splitting in the Concrete (Polyethylene Ducts)

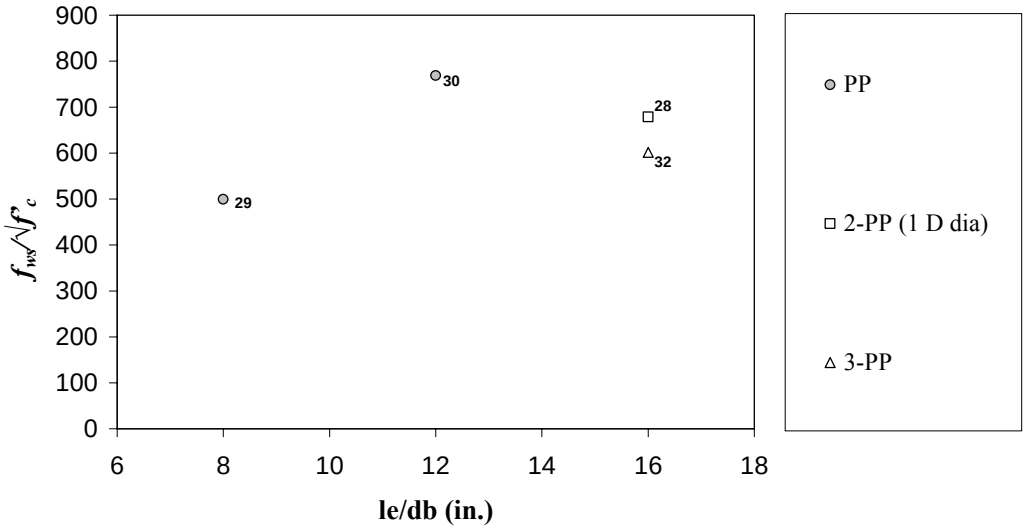

Figure 7.7 Influence of Embedment Depth on Connector Stress at Widespread Splitting in the Concrete (Polypropylene Ducts)

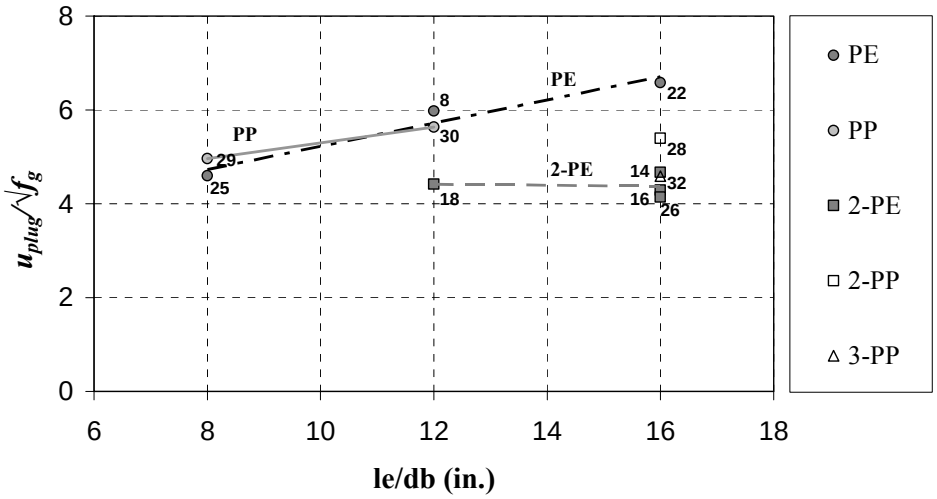

Figure 7.8 Influence of Embedment Depth on Plug Bond Strength

CHAPTER 8
Summary and Conclusions

8.1 SUMMARY

The Texas Department of Transportation (TxDOT) has used prefabricated bridge elements for many years. Prefabrication has provided efficiency by accelerating the construction schedule of bridges and has provided a safer working environment in congested urban areas and over water.

During the past five years, three bridge projects in Texas have incorporated precast bent caps. Grouted vertical ducts were used in the cap-to-column connections of all three of these bridges. Contractors and TxDOT engineers prefer this type of precast connection due to the simple geometry and because the volume of grout needed to complete the connections is minimized. Many uncertainties related to the configuration and details of grouted vertical connectors were identified during the design and construction of these bridges.

TxDOT Project 0-4176 was conducted at the University of Texas to accomplish the following objectives:

1. Understand the behavior of grouted vertical duct connections constructed using a variety of duct materials
2. Develop simple models to represent the observed connector behavior
3. Develop simple design expressions for grouted vertical connectors
4. Recommend practical details for connecting precast bent caps to columns and piles using grouted vertical duct connections

The following subsections provide a summary of the research program.

8.1.1 Experimental Program

The aim of the experimental program was to understand how different configurations and materials affect the behavior of precast bent cap connections constructed using grouted vertical ducts. The primary parameters selected for study were bar coating, duct material, connector embedment depth, number of connectors, bar eccentricity, and configuration of transverse reinforcement. Thirty-two large-scale connection specimens with single and multiple connectors were tested. Measured response was presented in the form of: (1) stress-end slip diagrams, (2) strain distribution along the connectors, (3) stress distribution along the connectors, (4) stress-slip of connectors relative to the grout diagrams, (5) stress-duct strain diagrams, (6) observed crack patterns, and (7) forensic examinations of pullout failures.

The observed modes of failure in the test specimens were sensitive to the choice of duct material and the embedment depth. The measured response was not sensitive to bar coating or the configuration of transverse reinforcement. Connector strength tended to decrease as the number of connectors increased and with increasing bar eccentricity.

8.1.2 Design Recommendations

Anchorage design provisions were developed for connectors based on the expected stresses in the connectors under service loads. Provisions are given for connectors that are expected to experience: (1) compressive and low tensile stresses and (2) significant tensile stresses ($f_{service} > 0.25f_y$). Serviceability limits were used to establish the design recommendations for connectors subjected to compressive and low tensile stresses. Cracking in the surrounding concrete would not be expected using the design provisions. Strength limits were used to establish the design recommendations for connectors subjected to significant

tensile stresses. The proposed development lengths were sufficient to achieve a stress of 1.25 f_y in the connectors.

8.2 CONCLUSIONS

Conclusions from this investigation on the behavior of grouted vertical duct connections are presented below:

1. *The duct material has an important influence on the behavior and mode of failure of connections.* The initial stiffness and strength of connection specimens constructed using galvanized steel ducts were higher than those of the test specimens constructed using plastic ducts. Reductions in strength relative to the specimens with galvanized steel duct specimens averaged 25% for single-connector specimens containing plastic ducts and 22% for specimens with two connectors and plastic ducts. In all cases, specimens constructed using galvanized steel ducts failed by pullout of the connector from the surrounding grout. In many instances, specimens constructed using plastic ducts failed by pullout of the connector and a grout plug.
2. *The development of splitting cracks in the concrete is considered to be a critical stage of response.* Considerable changes in the stress distribution along connectors were observed immediately after the appearance of splitting cracks in the concrete. The galvanized steel ducts provided passive confinement of the connector, which was mobilized after the formation of splitting cracks in the concrete, resulting in relatively stable bond stress–slip response. The plastic ducts did not provide confinement and capacity decreased rapidly after the formation of splitting cracks in the concrete.

3. *Increasing the number of connectors reduces the bond strength.* The magnitude of the stress in the connector at the onset of widespread splitting in the concrete was observed to decrease as the number of connectors increased. Reductions in bond strength averaged 28% when the number of connectors was increased from one to two. A reduction in bond strength of approximately 40% was observed for connectors anchored in steel ducts when the number of connectors was increased from one to three.
4. *Bar eccentricity causes a reduction in the bond strength of connectors.* Based on a limited number of single-connector tests, placement of the connector within the duct influenced the strength of the connector. The bond strengths were reduced an average of 17% when the connector was located near the duct, rather than centered within the duct.
5. *The presence of transverse reinforcement in the connection zone did not improve connection behavior.* The inclusion of a large spiral around a group of ducts did not influence connection behavior. Results indicated that the presence of individual spirals around polyethylene ducts degraded the performance of the connection. Although spirals were somewhat effective in restraining the upward movement of the duct, failure occurred as the connector/grout plug slipped out of the duct. Therefore, the use of small spirals around individual ducts is not recommended.

8.3 SUGGESTIONS FOR FURTHER RESEARCH

The demand for precast bent caps is expected to increase as TxDOT continues to incorporate rapid construction techniques as an option to conventional construction in upcoming bridge projects. This research has provided experimental data to clarify many of the uncertainties that had been

identified regarding the design of grouted vertical duct connections. Additional research is needed to extend the use of the anchorage design provisions to other design situations. Some suggestions for further research are given below:

1. *Duct materials and geometric properties* - Although two types of plastic ducts were included in this investigation, the available data were insufficient to determine if the type of plastic or the geometry of the ducts has a larger influence on the connector response. Additional tests are required to determine the influence of rib spacing, variations in duct wall thickness and rib height on connector behavior.
2. Grout materials – Other types of grout materials should also be investigated experimentally. Brands of prepackaged grout that meet the grout performance specifications should be identified and pullout tests should be conducted to assess variability in connection behavior. Durability properties of grout materials that are of interest to grouted vertical duct connections should also be investigated further.
3. Influence of a compressive stress field in the connection zone – The effects of varying the geometry of the compressive stress field in the connection zone should be studied to approximate different load conditions in the field. Tests of column-bent cap subassemblies and/or connector pullout tests that incorporate movable test frame reaction supports can be conducted to further evaluate serviceability stress limits, and differences in crack patterns and load resisting mechanisms of grouted vertical duct connections.
4. Ratio of duct to connector diameter - Plug bond strength is assumed to be inversely proportional to the ratio of duct to connector diameter. Anchorage design provisions developed in this investigation could be refined through an experimental investigation of variations in this test

parameter. Differences in bond behavior are possible between connectors having different diameters. Tests also need to evaluate the effect of connector diameter on connection behavior.

APPENDIX A

Bonding Strain Gages to Plastic

The heat generated within a strain gage must be transferred by conduction to the mounting surface. The heat flow through the specimen causes a temperature rise in the substrate, which is a function of its heat-sink capacity and the gage power level [A.1]. Strain measurement on plastic requires special consideration. Most plastics act as thermal insulators rather than heat sinks. Very low values of excitation are required to avoid serious self-heating effects.

The elastic moduli of common plastic materials are typically two or more orders of magnitude lower than those for metals [A.2]. Strains measured on plastics tend to be considerably larger than on metals, and can normally exceed 1 percent. The presence of the gage installation may reinforce the material locally, leading to large measurement errors. Gages having very flexible backing material should be used in plastic applications.

Strain gages used to measure strains on the polyethylene and polypropylene ducts had a larger resistance and a larger grid area because of the poor thermal conductivity of these materials. Based on recommendations given in Reference A.1, a value of power grid density, P_G, of 0.1 watts/in.^{2} was considered appropriate during the selection of the strain gage size. Based on an excitation voltage, E_B, of 2 volts, the gages selected for use on the plastic materials had a length of 6 mm (0.236 in.), a grid area, A_G, of 16.2 mm^2 (0.025 in.^{2}), and a resistance, R_G, of 350 ohm. The power grid density of the strain gages selected is determined by the following equation:

$$P_G = \frac{E_B^{\ 2}}{4 A_G R_G} \tag{A-1}$$

The value of power grid density calculated using Equation A-1 is 0.11 watt/in^2.

Gages having a larger area or a higher resistance could have been selected to obtain an even smaller value of power grid density in order to increase the accuracy of measurements. Increasing the resistance of the gage was not possible because of limitations in the electronic equipment available in the laboratory. Larger gage sizes were not desired because of possible fitting problems in the areas of gage installation in the ducts.

Surfaces of the plastic materials were carefully prepared and cleaned before strain gages were applied. The adhesive used to bond gages to the plastic surfaces was a cyanoacrylate-type adhesive, commonly used in structural experiments. Surfaces had to be pre-treated with a poly-primer compound before bonding the gage using the cyanoacrylate adhesive. After visually confirming that the bonding procedure was successful, a series of water-proofing and protective coatings was applied to the gages. A flexible water-proofing coating (silicone rubber compound) was used over the gages installed on plastic materials to minimize the restrain on the gage.

The degree of uncertainty involved in strain gage applications on plastic materials is rather high since very limited information is available. In this investigation, strain measurements in the ducts were required in order to assess the mobilization of confinement by the ducts. There is substantial variability in material properties for many common plastics. Reference A.2 is a very useful guide to be used in the process of selecting strain gages for applications involving plastic materials.

REFERENCES

A.1 Measurements Group, Inc., "Optimizing Strain Gage Excitation Levels," Tech Note TN-502, Raleigh, NC.

A.2 Measurements Group, Inc., "Strain Gage Measurements on Plastics and Composites," http://www.measurementsgroup.com/guide/ta/pc/pcindex.htm

APPENDIX B

Stress-Strain Model for Connectors

Strains in the connectors were measured during tests using strain gages. In order to obtain values for stress, strains were converted to stresses using the model described in this appendix. The model consists of three different stress-strain relationships, which correspond to the three different kinds of connectors used:

- Epoxy-coated (f_y = 68 ksi)
- Uncoated Type I (f_y = 75 ksi)
- Uncoated Type II (f_y = 59 ksi)

The model is based on the work of Viwathanatepa et al. [B.1] and is described in Figure B.1. In the post-yield range, curve BC is obtained from a cubic polynomial function:

$$f_s = \left[E_{sh} r - 2\left(f_{s\max} - f_y\right)\right]\left(\frac{s}{r}\right)^3 + 3\left[\left(f_{\max} - f_y\right) - \frac{2}{3} E_{sh} r\right]\left(\frac{s}{r}\right)^2 + E_{sh} s + f_y$$

where $r = \varepsilon_{s\max} - \varepsilon_{sh}$ *and* $s = \varepsilon_s - \varepsilon_{sh}$

At the onset of strain hardening, point B in Figure B.1,

$$f(\varepsilon_{sh}) = f_y$$

At point C,

$$f(\varepsilon_{s\max}) = f_{s\max}$$

E_{sh} is the tangent stiffness of strain hardening, ε_{sh} is the strain at the onset of strain hardening, f_y is the yield strength, and f_{smax} and ε_{smax} are the stress and strain at maximum stress. Table B.1 shows the values of E_{sh}, ε_{sh}, f_y, f_{smax}, and ε_{smax} for the three kinds of connectors used in the tests. The value of the elastic modulus, E, used was 29000 ksi.

The model was calibrated to tensile tests of actual connectors. Figures B.2 through B.4 show a comparison between the stress-strain curves obtained using the model and those obtained in connector tensile tests (gage length of 8 in.). As seen in Figure B.4, slight discrepancies between the measured stress-strain curve for a given connector and the idealized model used for converting strains to stresses can lead to some error. These discrepancies are relevant only at the strain-hardening region, and the margin of error is estimated to be plus or minus 5%.

REFERENCES

B.1 Viwathanatepa, S., Popov, E. P., and Bertero, V. V., "Effects of Generalized Loadings on Bond of Reinforcing Bars in Confined Concrete Blocks," Report No. UCB/EERC-79/22, Earthquake Engineering Research Center, University of California, Berkeley, CA, August 1979.

Table B.1 Parameters for Stress-Strain Idealized Model

Parameter	#11 Epoxy Coated	#11 Uncoated Type I	#11 Uncoated Type II
E_{sh} (ksi)	1150	1200	1200
ε_{sh}	0.011	0.012	0.0105
f_y (ksi)	68	75	59
f_{smax} (ksi)	102	106	95
ε_{smax}	0.09	0.10	0.10

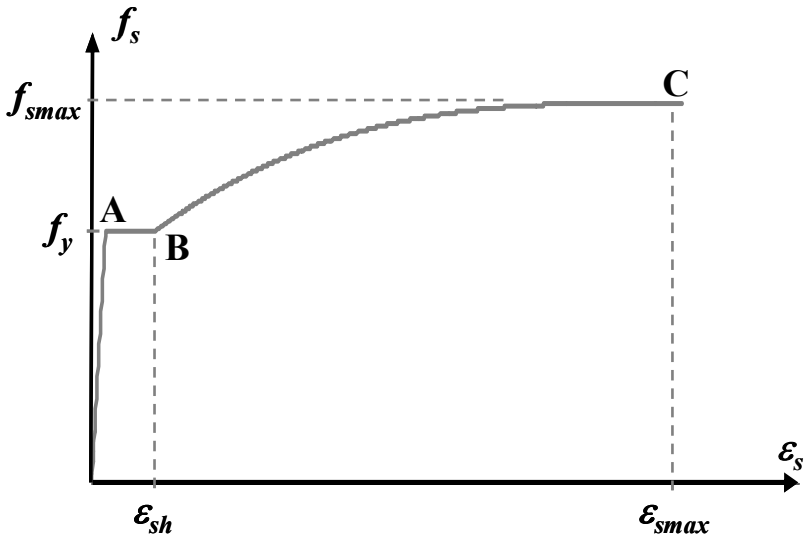

Figure B.1 Stress-Strain Idealized Model

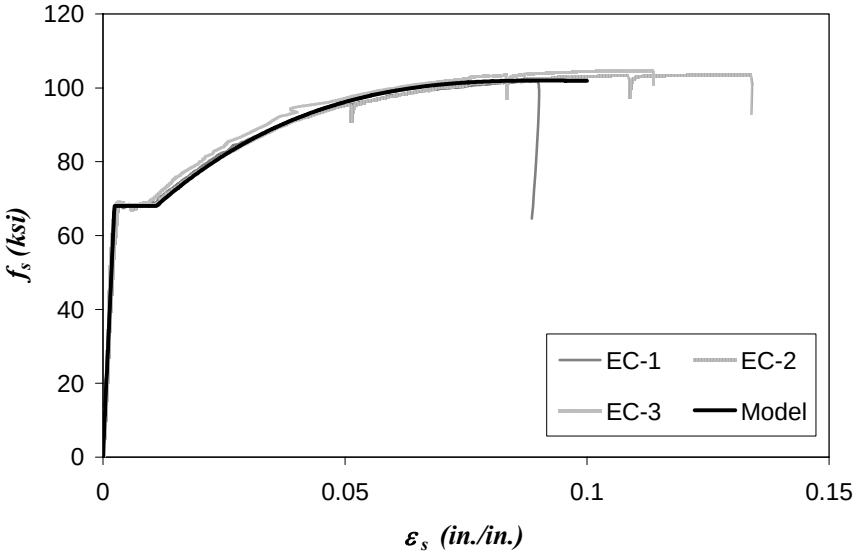

Figure B.2 Stress-Strain Curves for Epoxy-coated Connectors

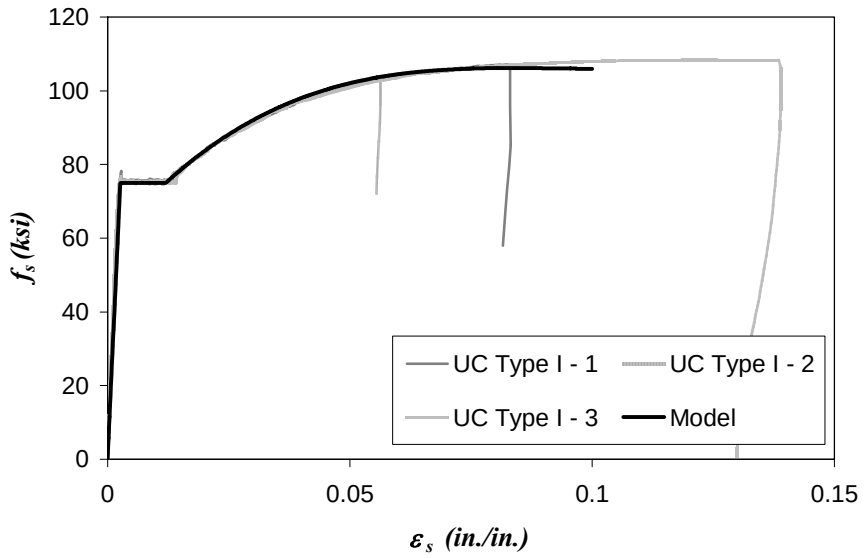

Figure B.3 Stress-Strain Curves for Uncoated Type I Connectors

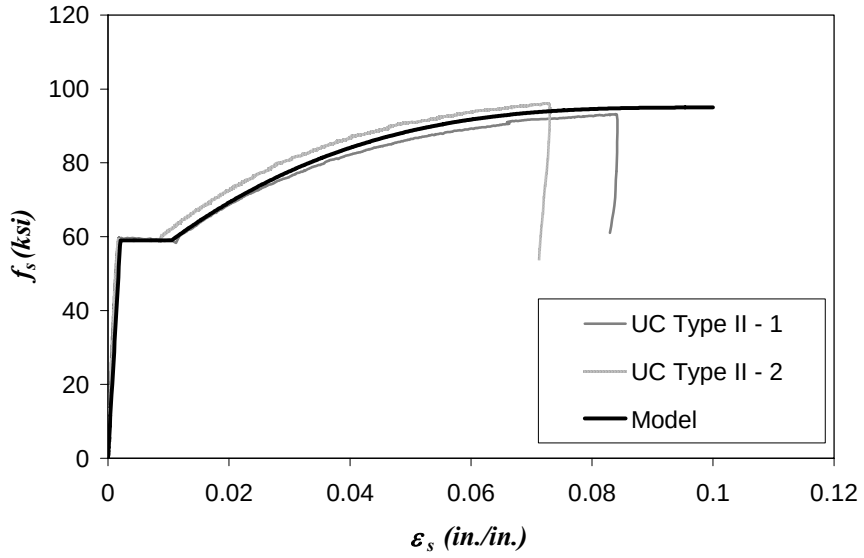

Figure B.4 Stress-Strain Curves for Uncoated Type II Connectors

APPENDIX C

Concrete and Grout Strength Data

The strength of the concrete and the grout in the beam specimens was monitored by way of cylinder and cube tests throughout the experimental program.

C.1 CONCRETE STRENGTH

Beam specimens were fabricated using the standard TxDOT Class C mixture, which has a minimum compressive strength of 3600 psi at 28 days. Six by twelve concrete cylinders were tested regularly to assess the strength of the concrete and to obtain an accurate value of concrete compressive strength associated with each of the connection tests. Table C.1 shows the age of test and corresponding concrete compressive strength for the beam specimens. The cylinder strength data are also shown in Figure C.1. It can be noticed from the figure that the average compressive strength at 28 days for the different batches of concrete was 5100 psi.

C.2 GROUT STRENGTH

The grout used in the experiments was Masterflow 928 (MF 928). This is a high precision, non-shrink natural aggregate grout that meets ASTM C 1107, Grades B and C, and satisfies the TxDOT Grout Performance Specification (Table 3.3). A series of trial batches were conducted to determine the optimal amount of water to be added per bag to obtain the fluidity necessary in the grout to complete the connections within the established working time of the mixture. Figures C.2 and C.3 show tests of the equipment to be used during the specimen grouting operations. The equipment included the mortar mixer, flow cone, funnels, plastic

hoses, and cube moulds. Figure C.4 shows strength data for the three trial batches conducted. Further information regarding the trial batches is presented in grout operations data sheets located at the end of this appendix.

For the grouting operations, the water amounts used varied between 1.27 to 1.37 gallons (10.45 to 11.25 lb) of water per 55 lb bag of grout material, which were within the fluid consistency range provided by the manufacturer that would produce an efflux time of 25 to 35 sec using the ASTM C 939 flow cone standard test. Water amounts were adjusted depending on the temperature at the time of grouting. Efflux times measured using the flow cone were generally inconsistent, when compared with the amount of water in the mix or the air temperature, and were always higher than 35 sec. Even when the efflux times were high, no re-mixing or tempering of the grout was made.

The compressive strength of the grout was inspected regularly by testing 2-in. grout cubes in accordance with ASTM C 109. Table C.2 shows the age of test and corresponding grout compressive strengths for the beam specimens. The strength data obtained from the cube tests are also shown in Figures C.5 through C.7. Further information regarding the specimen grouting operations is presented in the data sheets located at the end of this appendix.

Table C.1 Concrete Compressive Strengths for Beam Specimens and Age of Testing

Beam Specimen	**Test No.**	**Age at Testing (days)**	**f'_c (psi)**
1	1-4	90 (approx.)	5400
2	5-8	120 (approx.)	5500
3	9	42	4500
	10	49	4500
4	11-12	64 (approx.)	4600
5	13-14	48 (approx.)	4700
6	15-16	54 (approx.)	4700
7	17	34	5200
	18	41	5300
8	19-20	51	5500
	21-22	58	5500
9	23-24	58 (approx.)	6100
10	25-27	74 (approx.)	6100
11	28-30	36 (approx.)	6100
12	31-32	42 (approx.)	6100

Table C.2 Grout Compressive Strengths for Beam Specimens and Age of Testing

Beam Specimen	Test No.	Age at Testing (days)	f_g (psi)
1	1	14	5000
	2	21	6100
	3	27	6400
	4	31	6400
2	5	7	4700
	6	21	5500
	7	24	5900
	8	28	5800
3	9	13	5100
	10	20	5600
4	11	12	5100
	12	12	5100
5	13	13	5200
	14	14	5300
6	15	13	5400
	16	14	5400
7	17	14	4800
	18	21	4900

Table C.2 (continued) Grout Compressive Strengths for Beam Specimens and Age of Testing

Beam Specimen	Test No.	Age at Testing (days)	f_g (psi)
8	19	14	5100
	20	14	5100
	21	21	5400
	22	21	5400
9	23	27	6000
	24	33	6300
10	25	20	6500
	26	23	6500
	27	29	6500
11	28	14	6800
	29	16	7100
	30	16	7100
12	31	14	5800
	32	14	5800

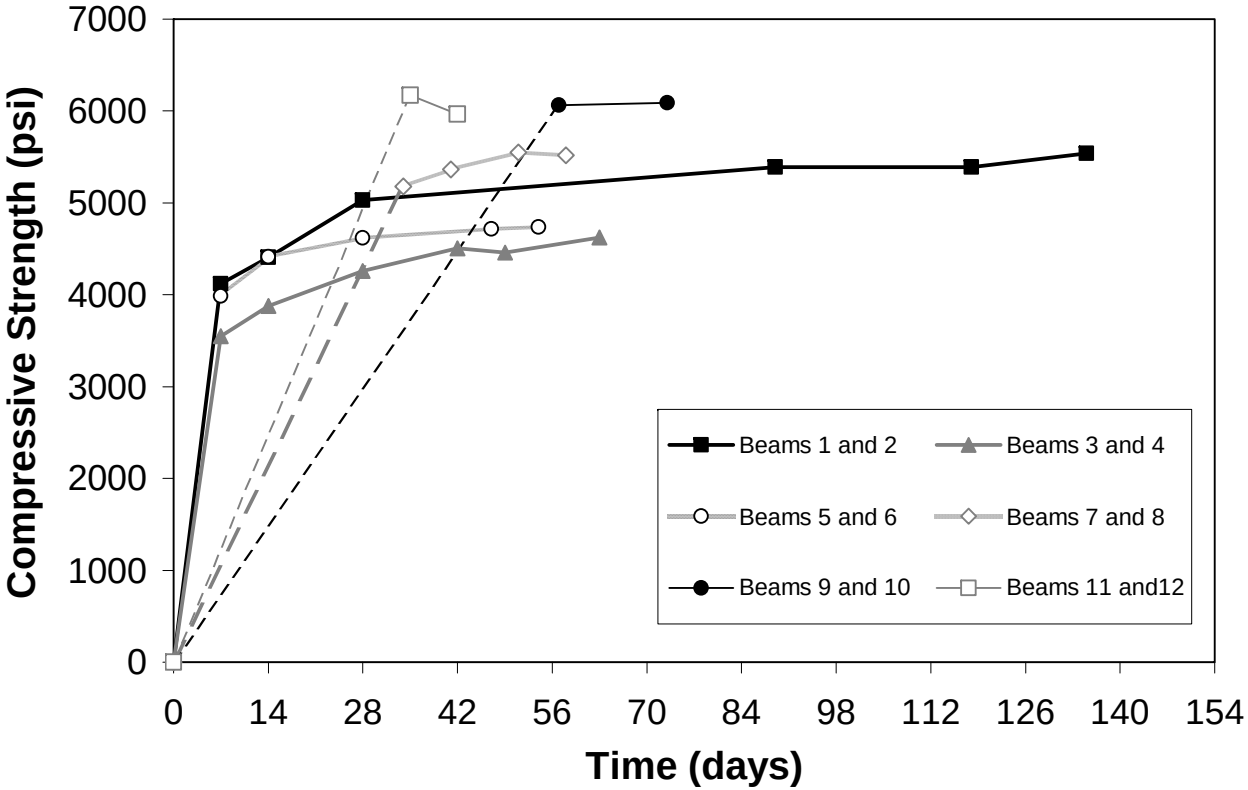

Figure C.1 Concrete Compressive Strengths for Beam Specimens

Figure C.2 Equipment used during Grout Operations

Figure C.3 Emptying of Grout Bags for Mixing

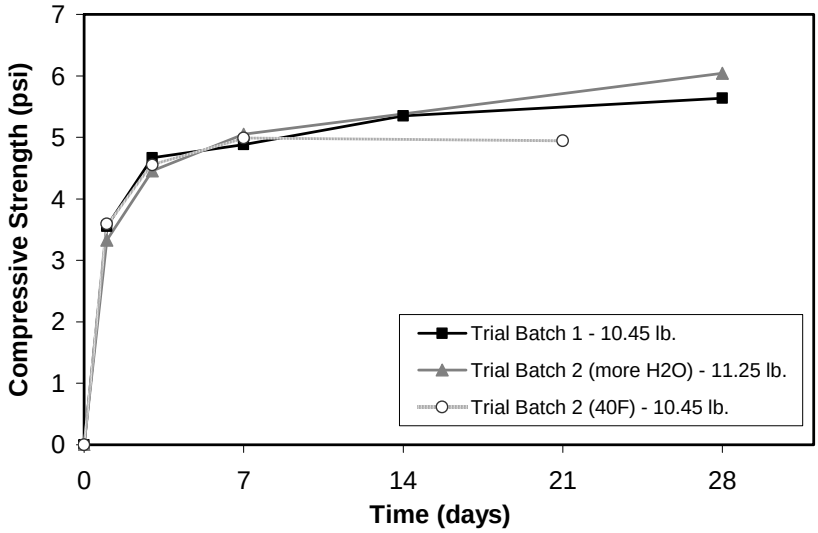

Figure C.4 Grout Strength – Trial Batches

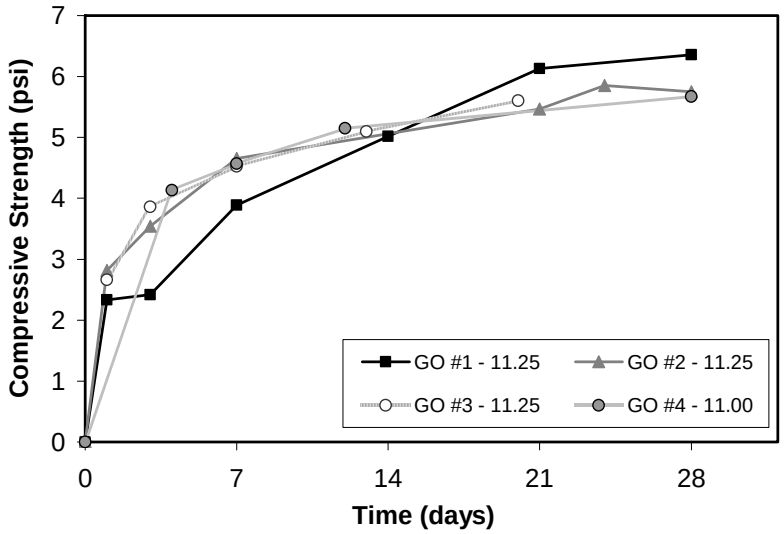

Figure C.5 Grout Strength – Beam Specimens 1 through 4

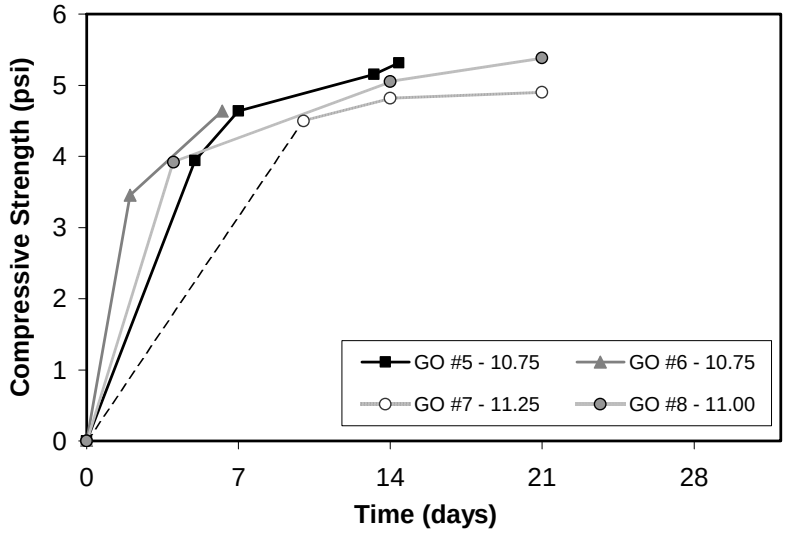

Figure C.6 Grout Strength – Beam Specimens 5 through 8

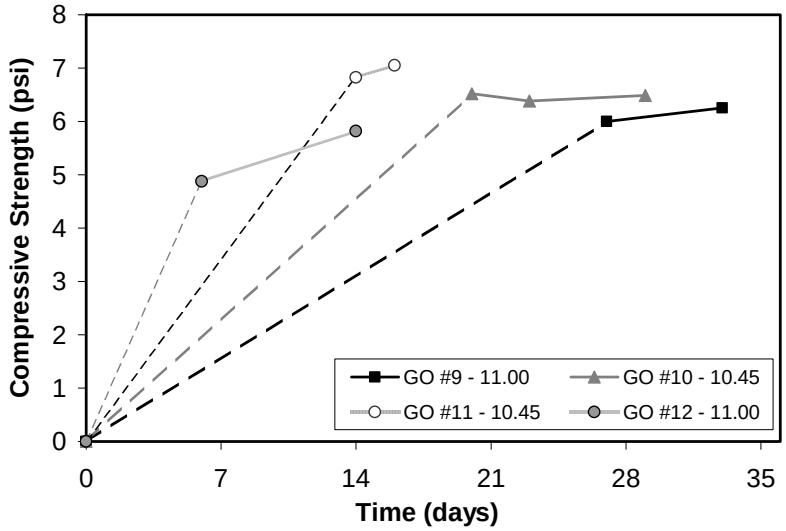

Figure C.7 Grout Strength – Beam Specimens 9 through 12

FERGUSON STRUCTURAL ENGINEERING LAB
Project 4176

Grout Operations Information Sheet Operation Label: **1**

1. Type of Grouting Operation:

☒ Trial Batch ☐ Specimen Grouting ☐ Other: _____

2. Date of Operation: 6/3/2003 Time of day: 2:00 PM

3. Number of Grout Bags to be mixed: 2

4. Amount of mixing water to be added per bag: 10.45 lb.

5. Temperature of mixing water: 87.5 ºF

6. Mixing Time : 4 minutes ☐ with stop ☒ without stop

7. Original temperature of mixer (pre-soaking water after 10 minutes): 88.5 °F

8. Flow Cone Test
   Efflux Time: 65 seconds
   Air Temperature: 92 °F
   Grout Temperature: 93 °F

9. Apparent working time of the mix: 45 minutes

10. Additional Notes: mix too stiff, but flowable.

FERGUSON STRUCTURAL ENGINEERING LAB
Project 4176

Grout Operations Information Sheet Operation Label: **more water**

1. Type of Grouting Operation:

☒ Trial Batch ☐ Specimen Grouting ☐ Other: _____

2. Date of Operation: 6/4/2003 Time of day: 12:30 PM

3. Number of Grout Bags to be mixed: 1

4. Amount of mixing water to be added per bag: 11.25 lb.

5. Temperature of mixing water: 81 ºF

6. Mixing Time : 5 minutes ☒ with stop ☐ without stop

7. Original temperature of mixer (pre-soaking water after 10 minutes): 80 °F

8. 1st Flow Cone Test
   Efflux Time: 28 seconds
   Air Temperature: 85.5 °F
   Grout Temperature: 84 °F

9. 2nd Flow Cone Test
   Time after conclusion of 1st Flow Cone Test: 36 minutes
   Efflux Time: 60 seconds
   Air Temperature: 87 °F
   Grout Temperature: 86 °F

10. Apparent working time of the mix: 35-40 minutes

11. Additional Notes: Filled a 4x8 and a 6x12 cylinders in 10 minutes, 20 minutes after mixing. No clumps observed on 1/4" mesh.

FERGUSON STRUCTURAL ENGINEERING LAB
Project 4176

Grout Operations Information Sheet Operation Label: **water 46 °F**

1. Type of Grouting Operation:

☒ Trial Batch ☐ Specimen Grouting ☐ Other: _____

2. Date of Operation: 6/4/2003 Time of day: 3:30 PM

3. Number of Grout Bags to be mixed: 1

4. Amount of mixing water to be added per bag: 10.45 lb.

5. Temperature of mixing water: 46 °F

6. Mixing Time : 5 minutes ☒ with stop ☐ without stop

7. Original temperature of mixer (pre-soaking water after 10 minutes): 84.5 °F

8. 1st Flow Cone Test
   Efflux Time: 37 seconds
   Air Temperature: 90 °F
   Grout Temperature: 79 °F

9. 2nd Flow Cone Test
   Time after conclusion of 1st Flow Cone Test: 41 minutes
   Efflux Time: 56 sec. (a substantial amount of grout never made it out of the cone)
   Air Temperature: 91 °F
   Grout Temperature: 86.5 °F

10. Apparent working time of the mix: 35 minutes

11. Additional Notes: Filled a 4x8 and a 6x12 cylinders in 20 minutes, 15 minutes after mixing. Some clumps observed in 1/4" mesh (like 40%).

FERGUSON STRUCTURAL ENGINEERING LAB
Project 4176

Grout Operations Information Sheet Operation Label: **GO #1**

1. Type of Grouting Operation:

☐ Trial Batch ☒ Specimen Grouting Specimen # 1 through 4

2. Date of Operation: 6/17/2003 Time of day: 11:45 AM

3. Number of Grout Bags to be mixed: 5

4. Amount of mixing water to be added per bag: 11.25 lb.

5. Temperature of mixing water: 83.5 °F

6. Mixing Time : 5 minutes ☒ with stop ☐ without stop

7. Original temperature of mixer (pre-soaking water after 10 minutes): 83.5 °F

8. Flow Cone Test
   Efflux Time: 44 seconds
   Air Temperature: 85 °F
   Grout Temperature: 88.5 °F

9. Apparent working time of the mix: 45-50 minutes

10. Additional Notes: Minimal clumps observed. Some bubbles observed rising on two ducts (minimal bleeding coupled with bubbling (picture available)). Approximate setting time 4-4.5 hours. Curing compound applied 4 hr after grouting, then rags applied for 24 hour moist curing. Next time could apply compound sooner, like one hour or 30 min after grouting.

FERGUSON STRUCTURAL ENGINEERING LAB
Project 4176

Grout Operations Information Sheet Operation Label: **GO #2**

1. Type of Grouting Operation:

☐ Trial Batch ☒ Specimen Grouting Specimen # 5 through 8

2. Date of Operation: 7/22/2003 Time of day: 9:15am

3. Number of Grout Bags to be mixed: 5

4. Amount of mixing water to be added per bag: 11.25 lb.

5. Temperature of mixing water: 84.5 °F

6. Mixing Time : 5 minutes ☒ with stop ☐ without stop

7. Original temperature of mixer (pre-soaking water after 10 minutes): 82.5 °F

8. Flow Cone Test
   Efflux Time: 65 seconds
   Air Temperature: 86.5 °F
   Grout Temperature: 88 °F

9. Apparent working time of the mix: 45-50 minutes

10. Additional Notes: No clumps observed. Some bubbles observed in ducts, air escaping, leaving superficial voids. Approximate setting time 4-4.5 hours. Curing compound applied 1:45 min. after grouting, then rags applied for 24 hours moist curing. First duct filled in 12 minutes; secnd duct filled in 14 minutes. Total time for grouting the beam was 40 minutes.

FERGUSON STRUCTURAL ENGINEERING LAB
Project 4176

Grout Operations Information Sheet Operation Label: **GO #3**

1. Type of Grouting Operation:

☐ Trial Batch ☒ Specimen Grouting Specimen # 9 and 10

2. Date of Operation: 10/17/2003 Time of day: 3:05 PM

3. Number of Grout Bags to be mixed: 5

4. Amount of mixing water to be added per bag: 11.25 lb.

5. Temperature of mixing water: 81.5 °F

6. Mixing Time : 5 minutes ☒ with stop ☐ without stop

7. Original temperature of mixer (pre-soaking water after 10 minutes): 79 °F

8. Flow Cone Test
   Efflux Time: 77 seconds
   Air Temperature: 80.9 °F
   Grout Temperature: 80.8 °F

9. Apparent working time of the mix: 45-50 minutes

10. Additional Notes: 9.5 minutes to fill first duct. Entire beam grouting operation was realized in 35 minutes. Curing compound applied 2 hr after grouting. Moist rags applied 3 hr after grouting. Very minimal clumps. No bubbles seen escaping on top.

FERGUSON STRUCTURAL ENGINEERING LAB
Project 4176

Grout Operations Information Sheet Operation Label: **GO #4**

1. Type of Grouting Operation:

☐ Trial Batch ☒ Specimen Grouting Specimen # 11 and 12

2. Date of Operation: 11/6/2003 Time of day: 12:15 PM

3. Number of Grout Bags to be mixed: 5

4. Amount of mixing water to be added per bag: 11.00 lb.

5. Temperature of mixing water: 68.0 °F

6. Mixing Time : 5 minutes ☒ with stop ☐ without stop

7. Original temperature of mixer (pre-soaking water after 10 minutes): 68.4 °F

8. Flow Cone Test
   Efflux Time: 60 seconds
   Air Temperature: 68.6 °F
   Grout Temperature: 71.4 °F

9. Apparent working time of the mix: 45-50 minutes

10. Additional Notes: Some clogs (3/8" to 1/2"). Entire beam grout operation performed in under 30 minutes. Compound applied 2:15hr after mixing. Moist rags applied 3:30hr after mixing. No bubbles seen.

FERGUSON STRUCTURAL ENGINEERING LAB
Project 4176

Grout Operations Information Sheet Operation Label: **GO #5**

1. Type of Grouting Operation:

☐ Trial Batch ☒ Specimen Grouting Specimen # 13 and 14

2. Date of Operation: 11/25/2003 Time of day: 10:45 AM

3. Number of Grout Bags to be mixed: 5

4. Amount of mixing water to be added per bag: 10.75 lb.

5. Temperature of mixing water: 64.4 °F

6. Mixing Time : 5 minutes ☒ with stop ☐ without stop

7. Original temperature of mixer (pre-soaking water after 10 minutes): 67.3 °F

8. Flow Cone Test
   Efflux Time: 81 seconds
   Air Temperature: 70 °F
   Grout Temperature: 68 °F

9. Apparent working time of the mix: 45-50 minutes

10. Additional Notes: Lots of clogs (3/8" to 1/2"). Entire beam grout operation performed in 40 minutes. Compound applied 2:20hr after mixing. Moist rags applied 3:30hr after mixing. No bubbles seen. Grout appeared a little thick.

FERGUSON STRUCTURAL ENGINEERING LAB
Project 4176

Grout Operations Information Sheet Operation Label: **GO #6**

1. Type of Grouting Operation:

☐ Trial Batch ☒ Specimen Grouting Specimen # 15 and 16

2. Date of Operation: 12/2/2003 Time of day: 10:10 AM

3. Number of Grout Bags to be mixed: 5

4. Amount of mixing water to be added per bag: 10.75 lb.

5. Temperature of mixing water: 70.8 ºF

6. Mixing Time : 5 minutes ☒ with stop ☐ without stop

7. Original temperature of mixer (pre-soaking water after 10 minutes): 68.4 °F

8. Flow Cone Test
   Efflux Time: 83 seconds
   Air Temperature: 69.5 °F
   Grout Temperature: 72.8 °F

9. Apparent working time of the mix: 50 minutes

10. Additional Notes: Lots of clogs (3/8" to 1/2"). One big one about 2" in diameter during the middle of the operartion. Entire beam grout operation performed in 50 minutes. Compound applied 3hr after mixing. Moist rags applied 4hr after mixing. Little bubbles seen when finishing the duct grouting. The grout seemed thicker than usual by the end of the operation.

FERGUSON STRUCTURAL ENGINEERING LAB
Project 4176

Grout Operations Information Sheet Operation Label: **GO #7**

1. Type of Grouting Operation:

☐ Trial Batch ☒ Specimen Grouting Specimen # 17 and 18

2. Date of Operation: 3/12/2004 Time of day: 2:25 PM

3. Number of Grout Bags to be mixed: 5

4. Amount of mixing water to be added per bag: 11.25 lb.

5. Temperature of mixing water: 66 ºF

6. Mixing Time : 5 minutes ☒ with stop ☐ without stop

7. Original temperature of mixer (pre-soaking water after 10 minutes): 68.8 °F

8. Flow Cone Test
   Efflux Time: 56 seconds
   Air Temperature: 66 °F
   Grout Temperature: 71 °F

9. Apparent working time of the mix: 50 minutes

10. Additional Notes: Some small 3/8" clumps. Operation concluded around 3:00 PM. Curing compound applied at 5:25 PM. Wet rags applied at 6:25 PM.

FERGUSON STRUCTURAL ENGINEERING LAB
Project 4176

Grout Operations Information Sheet Operation Label: **GO #8**

1. Type of Grouting Operation:

☐ Trial Batch ☒ Specimen Grouting Specimen # 19 through 22

2. Date of Operation: 3/29/2004 Time of day: 3:15 PM

3. Number of Grout Bags to be mixed: 5

4. Amount of mixing water to be added per bag: 11.00 lb.

5. Temperature of mixing water: 77.4 ºF

6. Mixing Time : 5 minutes ☒ with stop ☐ without stop

7. Original temperature of mixer (pre-soaking water after 10 minutes): 71.7 °F

8. Flow Cone Test
   Efflux Time: 86 seconds
   Air Temperature: 76 °F
   Grout Temperature: 78.2 °F

9. Apparent working time of the mix: 50 minutes

10. Additional Notes: Many clumps around 1/2". One big clump 1-1/2". Entire operation completed in around 45 minutes. Curing compound applied 2hr 30min after mixing. Moist rags applied 3hr 45min after mixing.

FERGUSON STRUCTURAL ENGINEERING LAB
Project 4176

Grout Operations Information Sheet Operation Label: **GO #9**

1. Type of Grouting Operation:

☐ Trial Batch ☒ Specimen Grouting Specimen # 23 and 24

2. Date of Operation: 8/19/2004 Time of day: 3:30 PM

3. Number of Grout Bags to be mixed: 5

4. Amount of mixing water to be added per bag: 11.00 lb.

5. Temperature of mixing water: 87.8 ºF

6. Mixing Time: 5 minutes ☒ with stop ☐ without stop

7. Original temperature of mixer (pre-soaking water after 10 minutes): N/A °F

8. Flow Cone Test
   Efflux Time: 68 seconds
   Air Temperature: 91 °F
   Grout Temperature: 89 °F

9. Apparent working time of the mix: 45 minutes

10. Additional Notes: Some clumps seen. One big clump 1". Curing compound applied 2hr 30min after mixing. Moist rags applied 3hr 15min after mixing.

FERGUSON STRUCTURAL ENGINEERING LAB
Project 4176

Grout Operations Information Sheet Operation Label: **GO #10**

1. Type of Grouting Operation:

☐ Trial Batch ☒ Specimen Grouting Specimen # 25 through 27

2. Date of Operation: 9/8/2004 Time of day: 2:20 PM

3. Number of Grout Bags to be mixed: 5

4. Amount of mixing water to be added per bag: 10.45 lb.

5. Temperature of mixing water: 83.6 ºF

6. Mixing Time : 5 minutes ☒ with stop ☐ without stop

7. Original temperature of mixer (pre-soaking water after 10 minutes): 87 °F

8. Flow Cone Test
   Efflux Time: 102 seconds
   Air Temperature: 85 °F
   Grout Temperature: 84 °F

9. Apparent working time of the mix: < 45 minutes

10. Additional Notes: Many small clumps. MIx was stiff and working time was less than usual. Curing compound applied 4hr after mixing. Moist rags applied 5hr after mixing.

FERGUSON STRUCTURAL ENGINEERING LAB
Project 4176

Grout Operations Information Sheet Operation Label: **GO #11**

1. Type of Grouting Operation:

☐ Trial Batch ☒ Specimen Grouting Specimen # 28 through 30

2. Date of Operation: 11/22/2004 Time of day: 4:00 PM

3. Number of Grout Bags to be mixed: 5

4. Amount of mixing water to be added per bag: 10.45 lb.

5. Temperature of mixing water: 76.1 ºF

6. Mixing Time : 5 minutes ☒ with stop ☐ without stop

7. Original temperature of mixer (pre-soaking water after 10 minutes): 75.2 °F

8. Flow Cone Test
   Efflux Time: 96 seconds
   Air Temperature: 77 °F
   Grout Temperature: 76 °F

9. Apparent working time of the mix: < 35 minutes

10. Additional Notes: Some problems with the grout. 2hr after grouting, grout level settled between 1 and 2 in. in ducts. No leaks in the formwork were observed. Bubbling and bleeding accompanied the decrease in volume of grout. Additional grout was added at a later time to reach the top of elevation of the specimen. These problems were attributed to reactivity in the grout due to storage time of around 5 months.

FERGUSON STRUCTURAL ENGINEERING LAB
Project 4176

Grout Operations Information Sheet Operation Label: **GO #12**

1. Type of Grouting Operation:

☐ Trial Batch ☒ Specimen Grouting Specimen # 31 and 32

2. Date of Operation: 11/30/2004 Time of day: 3:30 PM

3. Number of Grout Bags to be mixed: 5

4. Amount of mixing water to be added per bag: 11.00 lb.

5. Temperature of mixing water: 68.8 ºF

6. Mixing Time : 5 minutes ☒ with stop ☐ without stop

7. Original temperature of mixer (pre-soaking water after 10 minutes): 65.6 °F

8. Flow Cone Test
   Efflux Time: 81 seconds
   Air Temperature: 67.4 °F
   Grout Temperature: 67.7 °F

9. Apparent working time of the mix: < 45 minutes

10. Additional Notes: Some problems with the grout. 2hr after grouting, grout level settled between 1 and 2 in. in ducts. No leaks in the formwork were observed. Bubbling and bleeding accompanied the decrease in volume of grout. Additional grout was added at a later time to reach the top of elevation of the specimen. These problems were attributed to reactivity in the grout due to storage time of around 5 months.

BIBLIOGRAPHY

"Bridges: Precast Concrete Bridges Aid Environment, Seismic Design," Precast/Prestressed Concrete Institute website http://www.pci.org/markets/markets.cfm?path=bridges&id=wolf_river.cfm

"Prefabricated Bridge Elements and Systems: Beaufort and Morehead Railroad Trestle Bridge Project Photos," Federal Highway Administration website http://www.fhwa.dot.gov/bridge/prefab/beauphot.htm.

"Prefabricated Bridge Elements and Systems-Substructures: Bent Caps," Federal Highway Administration website http://www.fhwa.dot.gov/bridge/prefab/bentcaps.htm

ACI Committee 318, "Building Code Requirements for Reinforced Concrete," *ACI 318-71*, American Concrete Institute, Detroit, MI, 1971.

ACI Committee 318, "Building Code Requirements for Structural Concrete and Commentary," *ACI 318-02/ACI 318R-02*, American Concrete Institute, Farmington Hills, MI, 2002.

ACI Committee 318, "Building Code Requirements for Structural Concrete and Commentary," *ACI 318-05/ACI 318R-05*, American Concrete Institute, Farmington Hills, MI., 2005.

ACI Committee 550, "Emulating Cast-in-Place Detailing in Precast Concrete Structures," *ACI 550.1R-01*, American Concrete Institute, Farmington Hills, MI, 2001.

Association of State Highway and Transportation Officials (AASHTO), *AASHTO LRFD Bridge Design Specifications*, 3rd ed., AASHTO, Washington, D.C., 2004.

Astrova, T. I., Dmitriev, S. A., and Mulin, N. M., "The Anchorage of Deformed Reinforcing Bars in Ordinary and Prestressed Reinforced Concrete," Transactions of the Scientific-Research Institute of Concrete and

Reinforced Concrete of the Academy of Building and Architecture, issue 23, Moscow, 1961.

Ciampi, V., Eligehausen, R., Popov, E. P., and Bertero, V. V., "Analytical Model for Concrete Anchorages of Reinforcing Bars under Generalized Excitations," Report No. UCB/EERC-82/23, Earthquake Engineering Research Center, University of California, Berkeley, CA, November 1982.

Cook, R. A., "Grouted and Adhesive Anchor Tests of Master Builders Products," Structures and Materials Research Report No. 98-4, UF Project No. 4910 4504 640 12, University of Florida, December 1998.

Cook, R. A., Kunz, J., Fuchs, W., and Konz, R. C., "Behavior and Design of Single Adhesive Anchors Under Tensile Load in Uncracked Concrete," *ACI Structural Journal*, V. 95, No. 1, January-February 1998.

Darwin. D., and Zavaregh, S. S., "Bond Strength of Grouted Reinforcing Bars," *ACI Structural Journal*, V. 93, No. 4, July-August 1996.

Einea, A., Yamane, T., and Tadros, M. K., "Grout-Filled Pipe Splices for Precast Concrete Construction," PCI JOURNAL, V. 40, No. 1, Jan-Feb 1995.

Eligehausen, R., Popov, E. P., and Bertero, V. V., "Local Bond Stress-Slip Relationship of Deformed Bars Under Generalized Excitations," Report No. UCB/EERC-83/23, Earthquake Engineering Research Center, University of California, Berkeley, CA, October 1983.

Ferguson, P. M., Breen, J. E., and Jirsa, J. O., *Reinforced Concrete Fundamentals*, 5th edition, John Wiley & Sons, Inc., New York, 1988.

Freeby, G., Hyzak, M., Medlock, R. D., Ozuna, K., Vogel, J., and Wolf, L., "Design and Construction of Precast Bent Caps at TxDOT," *82nd TRB (Transportation Research Board) Annual Meeting*, Washington, D. C., January 2003.

Friggle, T., "State Highway 66 Lake Ray Hubbard Bridge Construction with Precast Bent Caps," *Lake Ray Hubbard Bridge-Precast Concrete Bent Cap*

Demonstration Workshop, *FHWA/AASHTO/TxDOT*, Mesquite, TX, March 2002.

Ganz, H. R., "PT-Plus Plastic Duct System," Report No. 241 e, VSL International Ltd, Berne, May 1991.

Goto, Y., "Cracks Formed in Concrete around Deformed Tension Bars," Journal of the American Concrete Institute, *Proceedings* V. 68, No. 4, April 1971.

Holt, J., and Medlock, R., "Standardized Concrete Bridges in Texas," Post-Tensioning Institute (PTI)/National Concrete Bridge Council Concrete Bridge Conference Proceedings, Charlotte, NC, May 2004.

Hyzak, M., "Lake Belton: Precast Bent Cap Design," Lake Belton Bridge-Precast Concrete Bent Cap Demonstration Workshop, FHWA/AASHTO/TxDOT, Temple, TX, July 2003.

Hyzak, M., "Lake Ray Hubbard Bridge: Structural Design," Lake Ray Hubbard Bridge-Precast Concrete Bent Cap Demonstration Workshop, FHWA/AASHTO/TxDOT, Mesquite, TX, March 2002.

Josten, M. G., Painter, W. L., and Guarre, J. S., "Precast Prestressed Concrete Structure Provides Solution for Getty Center Tram Guideway," PCI JOURNAL, V. 40, No. 3, May-June 1995.

LoBuono, Armstrong, and Associates, "Development of Precast Bridge Substructures," Report for the Florida Department of Transportation, May 1996.

Lutz, L. A., and Gergely, P., "Mechanics of Bond and Slip of Deformed Bars in Concrete," Journal of the American Concrete Institute, *Proceedings* V. 64, No. 11, November 1967.

Mandawe, J., Mislinski, S., and Matsumoto, E. E., "Reinforcement Anchorage in Grouted Duct Connections for a Precast Bent Cap System in Seismic Regions," *PCI/Federal Highway Administration/National Concrete Bridge*

Council Concrete Bridge Conference Proceedings, Nashville, TN, October, 2002.

Marti, P., "Pull-out Tests with PT-Plus Plastic Ducts," Report No. 92.205-1, VSL International Ltd., Berne, June 1993.

Matsumoto, E. E., "Development of a Precast Bent Cap System for Seismic Regions," *Lake Belton Bridge-Precast Concrete Bent Cap Demonstration Workshop*, *FHWA/AASHTO/TxDOT*, Temple, TX, July 2003.

Matsumoto, E. E., Waggoner, M. C., Sumen, G., Kreger, M. E., Wood, S. L., and Breen, J. E., "Development of a Precast Bent Cap System," Research Report 1748-2, Center for Transportation Research, University of Texas at Austin, January 2001.

Measurements Group, Inc., "Optimizing Strain Gage Excitation Levels," Tech Note TN-502, Raleigh, NC.

Measurements Group, Inc., "Strain Gage Measurements on Plastics and Composites," http://www.measurementsgroup.com/guide/ta/pc/pcindex.htm

Medlock, R., Hyzak, M., Wolf, L., "Innovative Prefabrication in Texas Bridges," *Proceedings of Texas Section, American Society of Civil Engineers, Spring Meeting 2002*, American Society of Civil Engineers, Texas Section, Austin, TX, March 2002.

Miltenberger, M., "Capacity Design of Grouted Anchors," *16th International Conference on Structural Mechanics in Reactor Technology (SMiRT 16) Transactions*, Washington D. C., August 2001.

Nicholas, D. G., Solis, P. M., and Brown, D. K., "Airport on the Move," Civil Engineering Magazine, American Society of Civil Engineers, September 2001.

NMB Splice-Sleeve Systems-Product Brochure, Splice Sleeve North America, Inc., Ontario, California.

Orangun, C. O., Jirsa, J. O., and Breen, J. E., "Reevaluation of Test Data on Development Length and Splices," Journal of the American Concrete Institute, *Proceedings* V. 74, No. 3, March 1977.

Park, R., "A Perspective on the Seismic Design of Precast Concrete Structures in New Zealand," PCI JOURNAL, V. 40, No. 3, May-June 1995.

PCI Design Handbook-Precast and Prestressed Concrete, 4th edition, Precast/Prestressed Concrete Institute, Chicago, IL, 1992.

PCI Design Handbook-Precast and Prestressed Concrete, 5th edition, Precast/Prestressed Concrete Institute, Chicago, IL, 1999.

PTI Committee on Grouting Specifications, "Specification for Grouting of Post-Tensioned Structures," Post-Tensioning Institute, First Edition, 2001.

Restrepo, J. I., Park, R., and Buchanan, A. H., "The Seismic Behavior of Connections Between Precast Concrete Elements," Research Report No. 93-3, Department of Civil Engineering, University of Canterbury, Christchurch, April 1993.

Salas, R. M., Kotys, A. L., West, J. S., Shocker, A. J., Breen, J. E., and Kreger, M. E., "Long-Term Post-Tensioned Beam Exposure Test Specimens: Final Evaluation," Research Report 0-1405-7, Center for Transportation Research, University of Texas at Austin, August 2003.

Stanton, J. F., Anderson, R. G., Dolan, C. W., and McCleary, D. E., "Moment Resistant Connections and Simple Connections," Research Project No. 1/4, Precast/Prestressed Concrete Institute, Chicago, IL, 1986.

Task Group 9.6 Plastic Ducts of fib Commission 9, "Corrugated Plastic Ducts for Internal Bonded Post-Tensioning," *Bulletin no. 7*, International Federation for Structural Concrete ***fib***, Lausanne, Switzerland, 2000.

Tepfers, R, "A Theory of Bond Applied to Overlapped Tensile Reinforcement Splices for Deformed Bars," Publication No. 73:2, Division of Concrete Structures, Chalmers University of Technology, Göteborg, 1973.

U.S. Department of Transportation, 2002 Study of the Nation's Highways, Bridges, and Transit: Conditions and Performance, (FHWA), 2003.

Untrauer, R. E., and Henry, R. L., "Influence of Normal Pressure on Bond Strength," Journal of the American Concrete institute, Proceedings V. 62, No. 5, May 1965.

Viwathanatepa, S., Popov, E. P., and Bertero, V. V., "Effects of Generalized Loadings on Bond of Reinforcing Bars in Confined Concrete Blocks," Report No. UCB/EERC-79/22, Earthquake Engineering Research Center, University of California, Berkeley, CA, August 1979.

Wigington, N., "Pierce Elevated Draws Rave Reviews," Transportation News, Texas Department of Transportation, Houston, TX, March 1997.

Wolf, L. M., and Friedman, N. K., "Redfish Bay and Morris & Cummings Cut: Innovations on Bridge Construction and Durability," Technical Quarterly, V. 9, No. 2, Texas Department of Transportation, Austin, TX, October 1994.

Wolf, L. M., and Hyzak, M. D., "Design of Precast Bent Cap to Column Connections," *Post-Tensioning Institute (PTI)/National Concrete Bridge Council Concrete Bridge Conference Proceedings*, Charlotte, NC, May 2004.

VITA

Francisco Javier Brenes was born in San José, Costa Rica on September 25, 1975, the son of Jose Francisco Brenes and Irene Barzuna. He attended Saint Paul's High School in Alajuela, Costa Rica, and was elected the first member of the schools' Honor Society. After graduating from high school in December 1992, he traveled to West Lafayette, Indiana, to begin studies at Purdue University in civil engineering. He received the degree of Bachelor of Science in Civil Engineering in May 1997. During the following six months, he returned to Costa Rica and worked as an engineering assistant for a small design firm. In January 1998, he returned to Purdue University to begin graduate studies in civil engineering. He was employed as a teaching assistant in the courses of architectural engineering and senior design in civil engineering. In December 1998, he received the degree of Master of Science in Civil Engineering. Upon his return to Costa Rica, he worked for ESCO Costa Rica S.A. and Grupo IECA S.A., where he was involved in structural design. In the Fall of 2000, he entered the Ph.D. program in civil engineering of the University of Texas at Austin.

Permanent Address: 2525 Old Farm Rd. 1013, Houston, Texas 77063

This dissertation was typed by the author.